INTEGRATED APPROACH TO SOLVING RESERVOIR PROBLEMS AND EVALUATIONS USING SEQUENCE STRATIGRAPHY, GEOLOGICAL STRUCTURES AND DIAGENESIS IN ORANGE BASIN, SOUTH AFRICA.

By

Solomon Adeniyi Adekola

B.Sc. Hons (Ado), M.Sc (Ibadan)

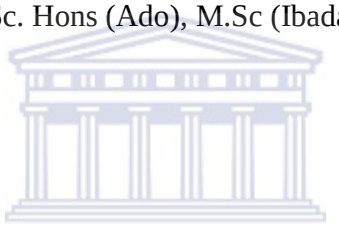

A Thesis submitted in fulfillment of the requirement for the Degree of Doctor of Philosophy in Earth Sciences of The University of the Western Cape.

Supervisor

Dr. A. Akinlua

May, 2010.

DECLARATION

I declare that “Integrated approach to solving reservoir problems and evaluations using Sequence Stratigraphy, Geological Structures and Diagenesis in Orange Basin, South Africa” is my own work, that it has not been submitted before for any degree or examination in any other university, and that all the sources I have used or quoted have been indicated and acknowledged by means of complete references.

Solomon Adeniyi Adekola May 2010

_____

Signature

ACKNOWLEDGEMENTS

I want to acknowledge the giver of life, God Almighty, who in His mercies made this dream a reality. I thank Him for protection, provision, presence, good health and sound mind to be able to complete this study.

My sincere appreciation goes to the University of Ado Ekiti, Nigeria for granting me a study leave for this programme. I am indebted to Petroleum Agency South Africa for the release of the data and samples for this study and permission to publish the findings. Appreciations are also due to Inkaba ye Africa for funding part of this research work by providing bursary and part of the cost of the analyses. I am very grateful to the Faculty of Natural Sciences of the University of the Western Cape for funding my trip to GeoForschungsZentrum (GFZ), Potsdam, Germany where some of the analyses were carried out. Special thanks to Prof. Jan van Bever Donker for his immeasurable assistance during the course of this study. I am indebted to many laboratories where some of the analyses were carried out; Prof. Roger M. Smith's laboratory, Department of Chemistry, Loughborough University, UK for the total organic carbon (TOC) determination of the rock samples. I am grateful to Humble Geochemical Laboratory, USA for the Rock – Eval pyrolysis of the rock samples. Dr. Arthur Kasson of Cornell University, USA for the stable isotope analysis. I am very grateful to my hosts at GFZ, Germany; Prof. B. Horsfield and Dr. K. Mangelsdorf for all their assistance during my stay in Germany. The assistance of Cornelia Karger, Kristin Günther and Anke Kaminski during instrumental analysis of my rock extracts is gratefully appreciated. Thanks to Dr. Remy Bucher of Itemba laboratories for the XRD analysis.

I want to appreciate the staff members of the Department of the Earth Science, UWC, both academic and non academic for a cordial working relationship during this programme. Your contributions, morally and financially will continue to be cherished. Thanks also go to my colleagues at lab 60, you are indeed an asset that will be remembered forever.

I also appreciate the church of God, which God used in nourishing my soul while here in South Africa, especially the prayer group, I am saying thank you for your prayer and love always. I know God will definitely reward your labour of love.

I want to thank my friends from UNAD, LASU, FUTA and every other places here in South Africa, thanks for being there always.

I want to gratefully thank my supervisor, Dr Akinsehinwa Akinlua for his invaluable criticism, insight and suggestions to work where others have not worked before in Orange Basin, am indeed very grateful. Your efforts made the extenuating task of PhD programme enjoyable. This success wouldn't have been achieved without your tireless efforts.

Lastly, I appreciate my parents, brothers, sisters, my wife, Billy and children, Siju and Toju for the love, support and encouragement.

Adekola S.A.

Dedication:

My loving wife

and children.

Table of content

	Page
Title page	i
Declaration	ii
Acknowledgements	iii-iv
Dedication	v
Table of content	vi-xi
List of figures	xii-xvii
List of tables	xviii-xvii
List of plates	xix
Key words	xx
Abstract	1-3
Chapter One	4
1.0 Introduction	4
1.1. Scientific Background and State-of-the-art	4
1.2. Location of the study area	9
1.3. Research objective	11
1.4. Scope of work	12
1.5. Review of previous work (General)	13
1.5.1. Basic sequence stratigraphic concepts	13
1.5.2. Evolution of sequence stratigraphy	13
1.5.3. Sequence stratigraphic elements	14
Sequence and Sequence boundary	14
Parasequences, parasequences set, and systems tract	16
Seismic and wireline log signatures of systems tract	20
Lowstand Systems Tract (LST)	20
Basin Floor Fan (BFF)	20
Slope Fan (SF)	21
Lowstand Prograding Wedge (PGC)	22
Transgressive Systems Tract (TST)	22
Highstand Systems Tract (HST)	22

1.5.4. Diagenesis, sequence stratigraphy and petroleum potential of the Orange Basin 23
1.5.5. Application of sequence stratigraphy in Orange basin 25
1.5.6. Diagenesis and sequence stratigraphy approach 29

Chapter Two 30

2.0. Geology of the Orange Basin 30
2.1. Regional geology of the Orange Basin 30
2.2. The Pay Zones of Orange Basin 34
2.2.1. Outcrops of the Cretaceous Orange Basin deposits 34
2.2.2. Stratigraphy 35
2.3. Orange Basin tectonic evolution 35

Chapter Three 37
3.1. Materials and methods 37
3.1.1. Materials 37
3.1.2. Methods
3.2. Digital data loading 38
3.2.1. Wireline logs data loading 38
3.2.2. Seismic section data loading 38
3.2.3. Seismic data interpretation (General principle) 40
Steps used in interpreting 40
Major seismic reflection termination patterns 41
Lapout 41
Baselap/downlap 41
Toplap 41
Erosional truncation 41
Apparent truncation 42
Onlap 42
Marine onlap 42
Coastal onlap 42
Fault truncation 42
Seismic facies 42

Factors that control interpretation of seismic facies 43
Major Seismic facies 43
Parallel/Divergent Seismic facies 43
Progradational Seismic facies 43
Recognition of Stratigraphic Surfaces from Seismic Data 44
Determination of Sequence Boundary 44
Determination of a Transgressive Surface 44
Determination of a Maximum Flooding Surface 44
Recognition of Systems Tract on Seismic Data 44
Recognition of Lowstand Systems Tract 44
Recognition Transgressive Systems Tract 45
Recognition of Highstand Systems Tract 45
3.2.4. Wireline log interpretation (General procedures) 45
Sequence Stratigraphy from Wireline Logs 46
The Cleaning up Trend 46
The Dirtying up Trend 47
Box Car Log Trends 47
The Bow Trend 48
Irregular Trends 48
The Log Response of Clinoforms 48
The Log Response of Parasequence 49
Log Responses from Basinal Environments 49
Estimation of depositional controls and sequence stratigraphy from log response 49
Key surfaces 50
Identification of systems tracts from log response 50
Log responses from Basinal Environments 50
Estimation of depositional controls and sequence stratigraphy from log response 50
3.3. Laboratory analyses procedures 51
3.3.1. Thin section procedure 51

3.3.2. XRD procedure 51
3.3.3. SEM/EDS procedure 52
3.3.4. Stable Carbon and Oxygen isotope geochemistry procedure 53
3.3.5. Rock-Eval pyrolysis and total organic carbon (TOC) determination 53
Total Organic Carbon 53
Rock-Eval (Programmed Pyrolysis) 53
Operating Conditions 54
3.3.5.1. Accelerated solvent extraction 54
3.3.5.2. Gas chromatography 55
3.3.5.3. Gas chromatography–mass spectrometry 56

Chapter Four 57

Results and Discussions

4.1. Introduction to interpretation of results 57
4.1.1. Wireline log interpretation 57
4.1.2. Sequence stratigraphic interpretation 58
4.2. Seismic interpretation 58
4.3. Lithostratigraphic interpretation 63
4.3.1. Lithostratigraphic of well succession 63
Bottom log-6At1 (reservoir zone) 65
The 6At-14At1 (reservoir zone) 65
Cycle frequency and stacking patterns 66
4.4. Petrography results 70
4.4.1. Thin section interpretation 70
LST 70
TST 73
HST 78
4.5. Mineralogical analyses results 84
4.5.1. The XRD interpretation 84
Diagenetic events in Lowstand Systems Tract (LST) 84
Diagenetic events in Transgressive Systems Tract (TST) 85

Diagenetic events in Highstand Systems Tract (HST) 86
4.5.2. The SEM interpretation 88
LST 88
TST 90
HST 93
4.5.3. The EDS interpretation 96
LST 96
TST 99
HST 104
4.5.4. Stable isotope analysis results 109
LST isotopic interpretation 113
TST isotopic interpretation 114
HST isotopic interpretation 115
4.6. Diagenetic alteration processes and reservoir environmental evolution in the basin 115
Compaction 116
Cementation/micitization 117
Dissolution 117
Silicification/quart growth 118
Fracturing 118
4.7. Diagenetic events within the depositional settings 118
4.8. Source Evaluation 121
4.8.1. Rock-Eval Pyrolysis 121
4.8.1.1. Source Rock Potential within LST 121
4.8.1.2. Source Rock Potential within TST 126
4.8.1.3. Source Rock Potential within HST 130
4.8.2. Organic geochemical evaluation of the shale samples 133
4.8.2.1. *n* – and *iso*-alkanes: provenance and thermal maturity 133
4.8.2.2. Biomarker geochemistry 143
Origin of the organic matter 143
4.8.3. Thermal maturity of the organic matter 149

Chapter Five 152

5.0. Conclusions and recommendations 152

5.1. Main scientific contributions of the dissertation 155

5.2. Recommendation for future work 156

References 157

List of Figures **Page**

Chapter One

Fig 1-1.	Map of South Africa showing the position of Orange Basin (Modified from Broad, 2004)	10
Fig 1-2.	Map of Orange Basin showing the distribution of the wells within the blocks.	11
Fig 1-3.	Typical Type-1 sequence adapted from Van Wagoner et al., (1990).	15
Fig 1-4.	Typical Type-2 sequence adapted from Van Wagoner et al., (1990).	15
Fig 1-5.	Typical Wave dominated-Parasequence	17
Fig 1-6.	Typical Tidal-parasequence	18
Fig 1-7.	Typical Progradational Parasequence Set adapted from Van Wagoner et al., 1990.	19
Fig 1-8.	Typical Aggradational Paresequence Set adapted from Van Wagoner et al., 1990.	19
Fig 1-9.	Typical Retrogradional Parasequence Set adapted from Van Wagoner et al., 1990.	20
Fig 1-10.	Well log Response character after Emery and Myers 1996	21

Fig 1-11. Orange Basin standard chronostratigraphy and 2nd and 3rd order unconformities (Brown et al., 1996) 26

Fig 1-12. Generalised Chronostratigraphy and sequence stratigraphy Of Orange Basin offshore Mesozoic basin, based on results of sequence stratigraphic studies (modified after Broad et al., 2006). 28

Chapter Two

Fig 2-1. Gondwana showing African and South American plates (Modified from Broad, 2004) 30

Fig 2-2. Gondwana map showing the different Earth crustal plates (www.parks.tas.gov.au, 2003). 32

Fig 2-3. Map of Western part of South Africa showing the Walvis Ridge (Macdonald et al., 2003). 33

Chapter Three

Fig 3-1. Flow chart of methods of analyses 37

Fig 3-2. The seismic lines acquired in the Orange Basin for interpretation in SMT showing their relationship to one another based on their positions to the globe 39

Chapter Four

Fig 4-1. Interpreted seismic section line A81-007 where yellow lines are sequence boundaries, green lines transgressive surfaces and black lines fault lines. 59

Fig 4-2. Interpreted seismic section line AM-53F where yellow lines are sequence boundaries, green line transgressive surfaces and black lines fault lines 60

Fig 4-3. Interpreted seismic section line A87-047 where yellow lines are sequence boundaries, green lines transgressive surfaces and black lines fault lines. 61

Fig 4-4. Interpreted seismic section line A81-061 where yellow lines are sequence boundaries, green line transgressive surfaces and black lines fault lines. 62

Fig 4-5. The correlation of the wells used in the study 64

Fig 4-6. The photomicrograph of samples taken within LST showing different minerals both plain (PPL) and cross polarised (XP): Micas (M), Quart (Qtz), Quartz overgrowth (Qtz-o) and Glauconite (G). The arrows: blue showing evidence of fracturing, white showing dense micritic calcite cement and black, filled fractured with quartz. 71-73

Fig 4-7. The photomicrograph of samples taken within TST showing different minerals both plain (PPL) and cross polarised (XP): Micas (M), Quart (Qtz), Quartz overgrowth (Qtz-o), Pyrite (Pry), Chlorite (Chl), Clay and Glauconite (G). The arrows: blue showing evidence of fracturing and white showing dense micritic calcite cement. 74-78

Fig 4-8. The photomicrograph of samples taken within HST showing different minerals both plain (PPL) and cross polarised (XP): Micas (M), Quart (Qtz), Quartz overgrowth (Qtz-o), Chlorite (Chl), Clay, Calcite cement (Cal) and Glauconite (G). The arrows: blue showing evidence of fracturing and white showing dense micritic calcite cement. 79-83

Fig 4-9. XRD results showing mineral peaks within the Lowstand System Tract (LST) across the studied wells 85

Fig 4-10. XRD results showing mineral peaks within the Transgressive Systems Tract (TST) across the studied wells 86

Fig 4-11. XRD results showing mineral peaks within the High Systems Tract (HST) across the studied wells 87

Fig 4-12. SEM imageries of samples within LST showing massive quartz overgrowth (Qtz-o), authigenic minerals montmorillonite (Mont) and chlorite (Chl) coating detrital grains, with some nodular pyrite and flattened/ fibre like hematite 89-90

Fig 4-13. SEM imageries of samples within TST showing massive quartz overgrowth (Qtz-o), authigenic minerals montmorillonite (Mont) and chlorite (Chl) coating detrital grains, with some nodular pyrite and flattened/ fibre like hematite 91-93

Fig 4-14. SEM imageries of samples within HST showing massive quartz overgrowth (Qtz-o), authigenic minerals montmorillonite (Mont) and chlorite (Chl) coating detrital grains, with some nodular/framboidal pyrite and flattened/ fibre like hematite 94-96

Fig 4-15. EDS elemental distribution of samples within LST 98-99

Fig 4-16. EDS elemental distribution of samples within TST 102-104

Fig 4-17. EDS elemental distribution of samples within HST 107-109

Fig 4-18. Comparison of $\delta^{18}0$ and $\delta^{13}C$ values within generic packages (System tracts) of calcite cemented sandstone with published stable isotope data of other carbonate cements. 113

Fig 4-19. Paragenetic sequence of the diagenetic alteration within

the stratigraphic settings of Orange Basin sandstones using XRD and thin section results. The boundary between Eodigenesis and mesodiagenesis is according to Morad et al., (2000). 116

Fig 4-20. The Plot of Remaining hydrocarbon potential against total organic carbon 125

Fig 4-21. The Plot of hydrogen index against oxygen index 125

Fig 4-22. Plot of Hydrogen Index against Tmax 126

Fig 4-23. The Plot of Production Index against Maturity 130

Fig 4-24. (a) A representative gas chromatogram of rock extracts of samples from the Orange Basin 140

(b) A typical mass fragmentogram (m/z = 191) terpanes in rock extracts of samples from the Orange Basin 140

(c) A typical mass fragmentogram (m/z = 217) of steranes in rock extracts of samples from the Orange Basin 141

Fig 4-25. The plot of CPI against Pr/Ph of shale samples from stratigraphic sequences of Orange Basin 142

Fig 4-26. The plot of Pr/C17 vs Ph/C18 142

Fig 4-27. The ternary plot of steranes inherited directly from higher plants, animals and algae the 20R epimers of C27, C28 and C29 steranes (Peters and Moldowan, 1993), all values in the axes per 100. 149

Fig 4-28. Cross plot of $C_{29\alpha\beta\beta 20}/(_{\alpha\alpha\alpha}+_{\alpha\beta\beta})$ vs $C_{29\alpha\alpha\alpha 20S}/(_{S}+_{R})$ steranes 151

List of Tables **Pages**

Chapter Four

Table 4.1. The reservoir rock samples positions within the parasequence setting and the sequences. 68

Table 4.2. The source rock samples positions within the parasequence setting and the sequences. 69

Table 4.3a Weight elemental composition from EDS analysis within LST (%) 97

Table 4.3b Atomic elemental composition from EDS analysis within LST (%) 97

Table 4.4a Weight elemental composition from EDS analysis within TST (%) 100

Table 4.4b Atomic elemental composition from EDS analysis within TST (%) 101

Table 4.5a Weight elemental composition from EDS analysis within HST (%) 105

Table 4.5b. Atomic elemental composition from EDS analysis within HST (%) 106

Table 4.6. Geochemical results including pore water data and stable isotopes data of samples from the LST 111

Table 4.7. Geochemical results including pore water data and stable isotopes data of samples from the TST 111

Table 4.8. Geochemical results including pore water data and stable isotopes data of samples from the HST 112

Table 4.9a Results of Rock-Eval analysis of samples sourced from wells within LST 123

Table 4.9b Results of Rock-Eval analysis of samples sourced from wells

	within LST	124
Table 4.10a	Results of Rock-Eval analysis of samples sourced from wells within TST	128
Table 4.10b	Results of Rock-Eval analysis of samples sourced from wells within TST	129
Table 4.11a	Results of Rock-Eval analysis of samples sourced from wells within HST	131
Table 4.11b	Results of Rock-Eval analysis of samples sourced from wells within HST	132
Table 4-12.	Gas chromatographic data of Orange Basin sediments within LST	136
Table 4-13.	Gas chromatographic data of Orange Basin sediments within TST	136
Table 4-14.	Gas chromatographic data of Orange Basin sediments within HST	137
Table 4.15.	Re-ordered gas chromatographic and rock eval pyrolysis results of samples collected based on wells, ages and sequences in Orange Basin	138
Table 4-16.	Biomarkers of data within the LST of Orange Basin sediments	145
Table 4-17.	Biomarkers of data within the TST of Orange Basin sediments	145
Table 4-18.	Biomarkers of data within the HST of Orange Basin sediments	146
Table 4.19.	Re-ordered biomarker results of samples collected based on wells, ages and sequences in Orange Basin	147

List of Plates **Page**

Chapter Four

Plate 1. XRD machine 52

Plate 2. Medium Pressure Liquid Chromatography equipment (MPLC) 55

INTEGRATED APPROACH TO SOLVING RESERVOIR PROBLEMS AND EVALUATIONS USING SEQUENCE STRATIGRAPHY, GEOLOGICAL STRUCTURES AND DIAGENESIS IN ORANGE BASIN, SOUTH AFRICA.

Key words:

unconformities,
Wireline logs,
stratigraphy,
reservoir,
seismic,
facies,
lithology,
faults,
sequence boundaries,
systems tract.

Abstract

The use of integrated approach to evaluate reservoir rock quality and source rock potential is becoming increasingly important in petroleum geology. This approach was employed to unravel the reason for variable reservoir quality of sandstones and evaluation of source rock potential of shale intervals of Orange Basin, SW, South Africa.

The data sets acquired for this study include 783.63 km digital 2D seismic lines cutting across the 5 blocks of the basin, digital wireline logs (gamma ray, resistivity, density and neutron), core (sidewall and core) and ditch cutting samples from 10 wells of interest. The digital seismic section and wireline logs were subjected to manual and computer interpretation using specialized softwares (FastTracker, PETREL 2008, and SMT 8.2). The wireline logs of the 10 wells were broken to depositional sequences and systems tracts: lowstand, transgressive and highstand systems tracts. The seismic section was analysed for depositional sequences, systems tracts and structures. Growth faults that are listric and normal were found localized in the basin. The faults are flank faults, crestal faults as well as antithetic faults.

Sandstone and shale samples were selected within the systems tracts for laboratory analyses. The sidewall and core samples were subjected to petrographic thin section analysis, mineralogical analyses which include x-ray diffraction (XRD), scanning electron microscopy (SEM), energy dispersive spectroscopy (EDS), and stable carbon and oxygen isotopes geochemistry to determine the diagenetic alteration at deposition and post deposition in the basin. The shale samples were subjected to Rock-Eval pyrolysis and accelerated solvent extraction (ASE) prior to gas chromatographic (GC) and gas chromatographic-mass spectrometric (GC-MS) analyses of the rock extracts, in order to determine the provenance, type and thermal maturity of organic matter present in sediments of the Orange Basin.

The results revealed a complex diagenetic history of sandstones in this basin, which includes compaction, cementation/micritization, dissolution, silicification/overgrowth of quartz, and fracturing. The Eh-pH shows that the cements in the area of the basin under

investigation were precipitated under weak acidic and slightly alkaline conditions. The $\delta^{18}O$ isotope values range from -1.648 to 10.054 %, -1.574 to 13.134 %, and -2.644 to 16.180 % in the LST, TST, and HST, respectively. While $\delta^{13}C$ isotope values range from -25.667 to -12.44 %, -27.862 to -6.954% and -27.407 to -19.935 % in the LST, TST, and HST, respectively. The plot of $\delta^{18}O$ versus $\delta^{13}C$ shows that the sediments were deposited in shallow marine temperate conditions. The consistency of abundance of $\delta^{13}C$ isotope across the stratigraphic sequences indicates that the burial diagenesis has no significant effect on geochemical pattern of occurrence of $\delta^{13}C$ isotope in the sandstones under investigation. The authigenic minerals precipitated blocked the grain interspaces and interlayers and with continued burial, compaction impeded the development of secondary porosity resulting in the poor reservoir quality. The origins of the cementing materials are both autochtonous and allochtonous.

The Rock-Eval pyroysis and TOC results of the shale samples revealed that LST is characterised by mainly marginally organic rich shale samples with a few organic rich rocks, variable organic matter types ranging from Type II to Type IV, and a few samples are thermally mature but have low organic matter quality. Four samples from two wells (A_F1 and O_A1) in the LST have good petroleum generative potential but not sufficiently mature for petroleum generation. TST is characterised with a few samples being marginally organic rich with only one being organic rich, mainly Type III kerogen with few Type IV kerogen, and only a few samples are thermally mature that has low organic matter quality. HST is characterised by many marginally organic rich rock samples, mainly Type III and a few mixed Type II/III kerogen, and only a few samples are thermally mature. The results of this study show that the LST has the best prospect in terms of petroleum generation potential, followed by HST and TST has least petroleum generation potential. The study also reveals that limited petroleum source rocks exist, which are also impacted by low thermal maturity levels. The basin is more gas prone than oil.

The shale samples were further analysed by Rock-Eval-Pyrolysis and for *n*-alkanes, aliphatic isoprenoid hydrocarbons and biomarkers (steranes and hopanes) by gas

chromatography (GC) and gas chromatography-mass spectrometry (GC-MS). For most of the shale samples from the different stratigraphic sequences from Aptian to Campanian age Rock-Eval data (hydrogen (HI) and oxygen index (OI)) and biomarker parameters (oleanane/hopane ratio, proportions of steranes, pristane/*n*-heptadecane vs. phytane/*n*-octadecane) point to mainly Typ III terrestrial organic matter. Only a few samples of Turonian age reveal a higher proportion of marine organic matter being classified as Typ II/III or Typ II. Biomarker parameters also suggest that the samples are deposited under suboxic to oxic environmental conditions. Rock-Eval data and biomarker maturity parameters assign for most of the samples a maturity level at the beginning of the oil window with some more mature samples of Aptian, Albian and Cenomanian age. The hydrocarbon generation potential is for most of the samples low as indicated by the S2/S3 ratio and HI values, exceptions are samples from Turonian and Aptian age.

Chapter One

1.0 Introduction

1.1 Scientific Background and State-of-the-art

Petroleum systems (reservoir rocks, source rocks, traps and seals) evaluation has shifted focus from single approach to integrated approach. This is becoming very important in petroleum geology because it has proved that it is worth it in solving exploration and production problems (Ketzer, 2002).

Orange Basin in the south western margin of the Atlantic Ocean showed variable reservoir rock qualities (Macdonald et al., 2003). These Cretaceous (Barremian-Santonian) clastic sediments marked by regional unconformities 6At1 to 15At1 (Brown et al., 1996) have not been widely studied to ascertain the reasons for the variable reservoir qualities as reported by Macdonald et al., (2003). This section of the basin is characterised by drifting and the resulting graben filled with predominantly siliciclastic continental and lacustrine rocks, with variable thicknesses of volcanic rocks (Brown et al., 1996). In the basin, a total of 34 wells have been drilled with only one oil discovery and a number of gas discoveries to date (PASA, 2003a).

There are many crucial unanswered questions, and more importantly, literatures about the events at deposition and post deposition of the sediments are scarce, which present study will attempt to investigate. The investigation will involve looking at the mode of deposition sediment on a regional scale within the genetically related packages and establishes its sources diagenetically. Diagenetic evolution of siliciclastic deposit is complex and controlled by several inter-related factors which include; changes in detrital composition in particular extrabasinal and intrabasinal grains (Garzanti, 1991; Zuffa et al., 1995; Ketzer et al., 2002), pore water chemistry (Mckay et al., 1995; Morad et al., 2000), residence time of sediment under certain geochemical conditions (Wilkinson, 1989; Taylor et al., 1995; Morad et al., 2000). All these complexities have been unravelled by sequence stratigraphic approach because variations in these factors are marked by sequence stratigraphic surfaces (such as parasequence boundaries,

transgressive surface and maximum flooding surfaces (El-ghali et al., 2009). The sequence stratigraphic tool has been widely used to correlate genetically related sedimentary successions bounded at top and base by unconformities or their strata patterns interpreted in response to interaction of eustatic change of sea level, compaction, sediment supply and tectonic subsidence (Van Wagoner et al., 1990).

Sequence stratigraphy has been widely employed in hydrocarbon exploration (Catuneanu and Eriksson, 2007). This tool using the understanding of sea level change has been used to understand the evolution of the sedimentary environments, distribution of sedimentary systems, and the effects on source, reservoir and seal rocks. The Orange Basin Deep Water Licence Area covers an area of about 43,000 km^2 (PASA, 2003b). Van der Spuy (2003) worked on the source rock in southern Africa basins. Three predominant source rock intervals have been identified in the basin, they are: Upper Jurassic-Necomanian lacustrine source rock (Paton et al., 2007), the Barremian-Lower Aptian marine transitional source rock (Jungslanger, 1999) and Cenomanian-Turonian marine maximum flooding surface source rock (Van der Spuy 2003). Van der Spuy (2003) said there is a strong case for the regional development of a good-quality source rock within the Early Aptian succession in the deeper parts of the Orange Basin. The hydrocarbon distribution in petroleum source rocks can give an insight into the origin, thermal maturity and paleoenvironmental history of petroleum which are essential elements in petroleum exploration (Akinlua and Smith, 2009).

Many workers have applied this concept to improve the understanding of source rocks potential within different stratigraphic settings in the late 80s' and 90s' (Vail, 1987; Cross, 1988; Arditto, 1991; Kosters and Suter, 1993; Pasley et al., 1993; Hart et al., 1994; Yancey, 1997; Petersen et al., 1998) in various basins of the world. Recently workers like Ryu (2008) used a stratigraphic framework and organic geochemistry of samples from southern Oregon Costal Range strata to propose petroleum systems for the basin. Akinlua et al. (2005) also used improved Rock-Eval pyrolysis to classify organic matter in the Niger Delta.

The understanding of petroleum system in any sedimentary basin remains a major key issue in the exploration of petroleum (Lopez et al., 1998). In petroleum exploration

activities both at initial and advanced stages organic geochemistry has become a vital tool for the identification of source rock and classification of crude oils into families (Ekweozor et al., 1979; Doust and Omatsola, 1990; Akinlua et al., 2007; Gulbay and Korkmaz, 2008). Source rock identification and classification is useful for the characterisation of an area and to address stratigraphic units of a basin to concentrate effort on during exploration and exploitation activities in order to reduce risk of blind zones target.

Understanding the composition of the source rock can provide detailed information on the original organic source material, the environmental conditions during time of deposition and the level of thermal maturation (Wang and Walters, 2007). Detailed geochemical analysis of source rock can give insight into the characteristics of the hydrocarbons they will generate.

Sequence stratigraphic study has been a useful tool in the prediction and choosing of oil and gas bodies as well as targets for drilling within a basin. There are many studies investigating organic matter deposition within a sequence stratigraphic framework (Pasley and Hazel, 1990; Bohacs and Isaken, 1991; Creaney et al., 1991; Pasley, 1991). In these studies it was indicated that the type and preservation of organic matter deposited in the marine realm is related to the stacking of the deposition systems and consequently, the depositional systems tract in which it is deposited. Hart et al., 1994 stated that during progradation in the lowstand and highstand systems tracts (LST and HST), organic matter is typically terrestrial in origin whereas mostly autochthonous (marine) organic matter is deposited on the shelf during an overall backstepping of depositional systems (transgressive systems tract, TST).

Previous workers like Jungslager (1999) and van der Spuy (2003) have carried out some studies on evaluation of the source rock potential of sediments from the Orange Basin. However, the determination of provenance and thermal maturity of the organic matter of the basin based on organic geochemistry of the rock extracts is not yet documented. Thus, the objectives of this study were to rank the organic matter and to determine its provenance and thermal maturity within the genetically related packages of the Orange Basin thereby suggesting the systems tract or the age penetrated by the wells that would most likely be the best candidate for hydrocarbon generation in the basin.

Catuneanu and Erikson (2007) said that the method of sequence stratigraphy requires the application of the same workflow and principles irrespective of the age of strata under analysis. In the Orange basin, there is possibility of diagenetic alteration related to sequence boundaries which includes mechanical clay infiltration and formation which can affect the reservoir properties in a basin. Siliciclastic reservoirs are known to be good reservoirs because they often have high porosity and permeability. The reverse is the case in most of the wells in the Orange Basin. Even if the petroleum potential of the source rock is not good it cannot affect reservoirs properties. This problem is common in major marginal fields of the world and with recent appraisal using diagenetic and sequence stratigraphic analyses, the one time abandoned, non producing fields are now producing due to better understanding of their reservoir qualities, for example, as in Niger Delta, Nigeria (Onuoha, 2000). The problem of reservoir in the Orange Basin might be as a result of clay infiltrations and formation which can only be studied by integrating sequence stratigraphy with diagenesis. Sand deposited below subaerially exposed sequence boundaries may also be subjected to percolation of meteoric water, which typically results in dissolution of unstable framework grains (e.g. mica and feldspar) and formation of intergranular porosity and kaolinite (De Ros et al., 1994) Favourable conditions for the formation of intergranular porosity and kaolinite occur below unconformities with much longer subaerially exposed time than sequence boundaries in the sequence stratigraphic of sand in humid climates (Van Wagoner et al., 1990). Over the years the use of diagenesis and sequence stratigraphy as a means of characterising reservoir in carbonate or clastic lithofacies has produced a better mode of reservoir construction and predicting the hydrocarbon plays accurately. This is because diagenetic changes affect porosity and thus now considered in petroleum exploration. Diagenesis can now be used based on the minerals and chemical composition to delineate the setting and environment of deposition and precipitation. Petrographic and diagenetic analyses of sandstone within a sequence stratigraphic framework provide a better understanding of the reservoir characteristics by comparison of relative abundance of major detrital framework grains in sandstone (Ryu and Niem, 1999).

As the exploration frontiers extend into progressively deeper waters where enormous capital expenditures and risk are involved, the exploration team is saddled with greater responsibilities necessitating the application of more accurate techniques for stratigraphic analysis. In recent times, sequence stratigraphy is used in reservoir characterization and hydrocarbon exploration in carbonate and/or clastic lithofacies. The technique, combined with seismic and well log interpretation makes the model built by reservoir geologists more accurate and reduces the risk associated with reserve estimation and secondary production. Without the application of sequence stratigraphy to carbonate and/or clastic reservoirs, the interpretation of seismic and well data can be flawed. This is because; the thickness of reservoir interval is often below the vertical resolution of wavelet and the lateral continuity of the reservoir lithologic layer tied between wells is often below the horizontal resolution of the well logs. Thus, predictions of the lateral and vertical reservoir properties have their risk reduced when sequence stratigraphy is applied as a tool to interpret seismic and well data.

Sequence stratigraphy proves to be more appropriate method to perform isochronous than lithological correlation. It has evolved as a branch of stratigraphy that subdivides the rock record using a succession of depositional sequence composed of genetically related strata as regional and interregional correlative units (Haq et al., 1988). Sequence stratigraphic analysis depends on the identification and correlation of major bounding surfaces (sequence boundaries and maximum flooding surfaces). It creates a framework for the subsurface called a sequence stratigraphic architecture, which is built from diagnostic sediments packages and key boundaries that are deposited as sea level falls, the shorelines shift basin ward and landward, while the cyclic patterns of the sediments in the subsurface form the sequence stratigraphic architecture. Elements of this architecture are revealed in subsurface data giving an insight into the subsurface to clarify principal features that operate on many scales from the regional basin scale, to individual prospect scale and the bed to bed scale reservoir characterization.

Vail's sequence stratigraphic model (Vail et al., 1977; Vail, 1987) recognizes sequences and systems tract boundaries as discontinuity surfaces of their correlative conformities

that bound stacks of strata units. The basin sequence stratigraphic unit is the depositional sequence bounded by regional unconformities or their correlative conformities. Internally, this depositional sequence consists of several key intervals such as the system tracts, parasequences, and surfaces (maximum flooding surfaces and transgressive surfaces). These intervals and surfaces form in response to cyclical changes in relative sea level and they create repetitive and predictable sequences (Brown and Fisher, 1977; Mitchum et al., 1977).

The greatest strength of sequence stratigraphic interpretation lies in its ability to generate a geological sound model consistent with all available multidisciplinary information. Each set of data (seismic section, well log data, and high resolution biostratigraphic data) contributes different piece of the puzzle. This ultimately aids in determination of the real-time line facies correlation with a high degree of certainty as opposed to the commonly recognized lithological correlation (Durand, 1995).

Today, this concept has been accepted and recognized by the oil industries as an effective tool for predicting stratigraphic traps, reservoir and source rocks continuity and quality (Patch et al., 1990; Vail and Wornardt, 1990; Posamentier et al., 1988), thereby helping to unfold the subsurface geology. This helps in reducing risks at exploration stage and improving correlation of reservoir units at exploitation stage.

1.2 Location of the study area

The largest river, in South Africa, Orange River drains the whole Orange Basin (Fig. 1-1). This river flows across almost the whole width of the country. It takes its source from the highland in the east through the Kalahari depression in the west and empties to the South Atlantic Ocean. The Orange Basin of South Africa Atlantic margin provides an ideal location to understand the entire processes of passive continental margin evolution, (Hirsch et al., 2006).

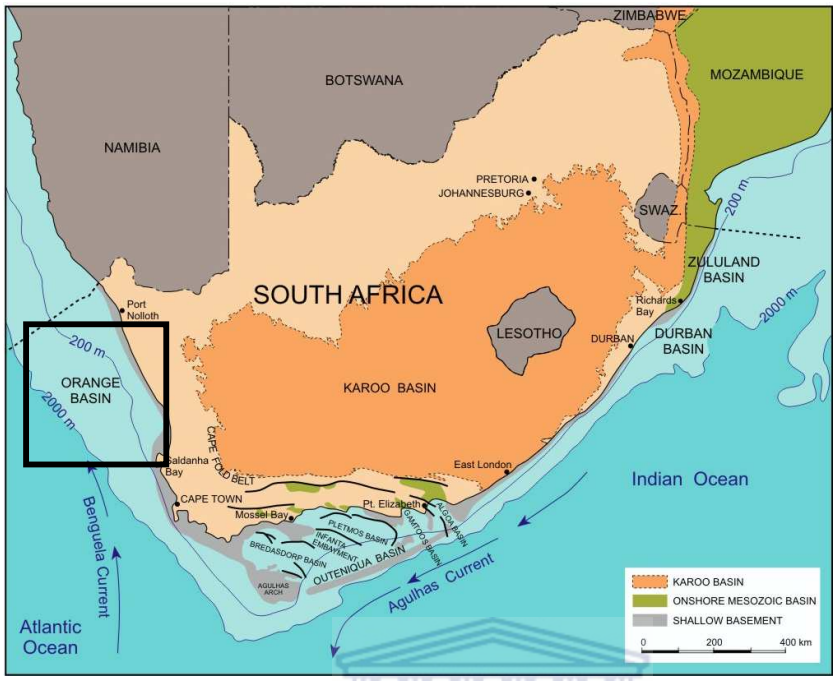

Fig. 1-1. Map of South Africa showing the position of Orange Basin (Modified from Broad, 2004)

The Orange basin is divided to five blocks, namely blocks 1, 2 3, 4 and 5. Ten wells across the basin were selected for this study. (Fig. 1-2).

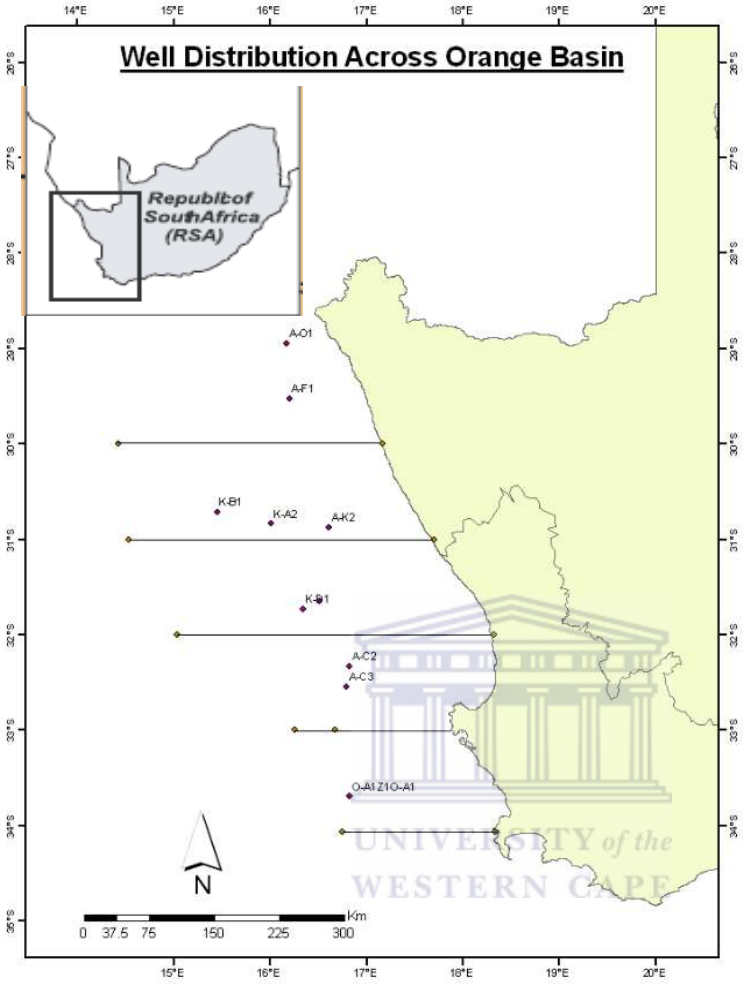

Fig 1-2. Map of Orange Basin showing the distribution of the wells within the blocks.

1.3 Research objectives

The objectives of this research work are to:

- Subdivide and interprete the stratigraphic columns of sediments penetrated by the wells into depositional sequences and systems tracts.
- Propose a sequence stratigraphic framework for the fields.
- Diagenetically investigate the basin to get clues to the events at deposition and post-deposition within the basin, whereby revealing the alterations at

burial and post-burial, which in any way must have affected the reservoir quality of the basin.

- Characterize the shale intervals in order to determine their source rock potential, origin, thermal maturity, and paleoenvironment and stratigraphic setting with the best source rock potential.

1.4 Scope of work

- Identification of major faults on seismic data
- Mapping of unconformities based on seismic reflection terminations and truncations.
- Interpretation of lithology from well log character
- Determination of the sequence boundaries on well logs provided
- Bridging the gap between well logs and seismic data in the study area.
- Identification of sequence boundaries and systems tracts on the well logs and seismic profiles.
- Correlation of wells in the study area based on depositonal sequences
- Reconstruction of sequence stratigraphic framework
- Comparing the geochemistry of the samples from the wells with the lithology of the wells. The geochemical analysis shall be conducted on the samples by carrying out multi mineral analysis, thin sectioning, SEM, X- Ray Diffraction (XRD) and stable carbon and oxygen isotopes analysis. The petrographic studies will look at the cementing materials and also through SEM.

- Shale samples shall be subjected to source rock evaluation using Rock-Eval pyrolysis, gas chromatography, and gas chromatography-mass-spectrometry.

1.5 Review of previous work and concepts (General)

1.5.1 Basic sequence stratigraphic concepts

Sequence stratigraphic is the study of rock relationships within a chronostratigraphic framework of repetitive, genetically related strata, bounded by surfaces of erosion or non-deposition, or their correlative conformities (Van Wagoner et al., 1988). A similar but more generic definition was however proposed by Posamentier et al., 1988, which did not specify the nature of the bounding surfaces.

1.5.2 Evolution of sequence stratigraphy

Sequence stratigraphy is the science of describing the vertical and lateral relationships of rocks. These relationships may be based on rock type, called lithostratigraphy, on age, called chronostratigraphy, on fossils, termed biostratigraphy, or on magnetic properties, named magnetostratigraphy. Stratigraphy has been in existence since 1600's with workers such as Nicholas Steno, James Hutton, and Charles Lyell. Sloss in 1948 (Sloss et al., 1949; Sloss, 1963) proposed the sequence as an unconformity-bounded strata unit.

Fairbridge (1961) summarised the main mechanism of sea level changes as tectono-eustacy and glacio-eustacy and stressed that the eustatic hypotheses apply worldwide while the tectonic hypotheses do not vary from region to region. Fairbridge (1961) summarised the perceived goal at the time: "we need therefore to keep all factors in mind and develop an integrated theory. Such an idea is not yet achieved and would involve studies of geophysics, stratigraphy, tectonics, and geochemistry, above sea level and below."

Another major development in the evolution of sequence stratigraphy took place in 1977, when Vail et al. (1977) published the first instalment of such an integrated theory. Through series of seminar articles, these authors presented the concepts of eustacy and resulting unconformity-bounded strata patterns applied to and documented with seismic data. This new approach of stratigraphy which is referred to as seismic stratigraphy was developed by Vail et al. (1977) based on the idea proposed by Sloss (1963) – the

grouping of layers into unconformity-bounded sequences based on lithology, and by Wheeler (1958) – the grouping of layers based on what has become known as chronostratigraphy (Sloss, 1963). Mitchum et al., (1977) sharpened and broadened the concept of the sequence by defining it as "a stratigraphic unit that composed of a relatively conformable succession of genetically related strata and bounded at its top and base by unconformities or their correlative conformities".

Subsequent seismic stratigraphic studies in basins around the world produced a set of charts showing the global distribution of major unconformities interpreted from seismic discontinuities for the past 250million years (Haq et al., 1987). The development of newer accommodation model by Jervey (1988) to explain seismically resolvable strata patterns led to the realisation that the sequence could be subdivided into smaller units, ultimately referred to as systems tract (Brown and Fisher, 1977).

Further studies on well logs, cores and outcrops by several stratigraphers concurrently with the development of the conceptual model revealed that the unconformities interpreted from seismic discontinuities were controlled by relative changes in sea level and that relative changes in sea level can be recognised on well logs and outcrops, with or without seismic sections. This led to the interdisciplinary concept of sequence stratigraphy- a linkage of seismic, wireline log, fossil and outcrop data at local, regional and global scales.

1.5.3 Sequence stratigraphic elements

Sequence and sequence boundary

The fundamental unit of sequence stratigraphy is the depositional sequence, which comprises of sediments deposited during one cycle of sea level fluctuation. By Exxon Convention, this starts at low sea level, goes high and returns to low. It was defined as a succession of relatively conformable, genetically related strata bounded at the top and base by unconformable surfaces or their landward or basinward correlative conformities (Van Wagoner et al., 1990). Basically, there are two types of sequences, which are Type-I (Fig. 1-3) and Type-II (Fig. 1-4) sequences. Based on the variations in the sea level

cycles there may be first order , second order, third order, fourth order, fifth order, or sixth order sequences.

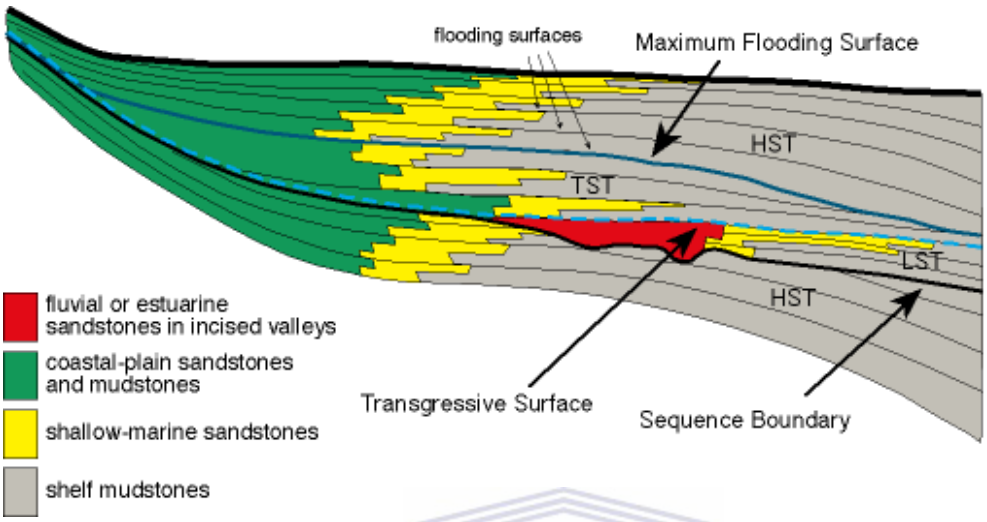

Figure 1-3. Typical Type-1 sequence (adapted from Van Wagoner et al., 1990).

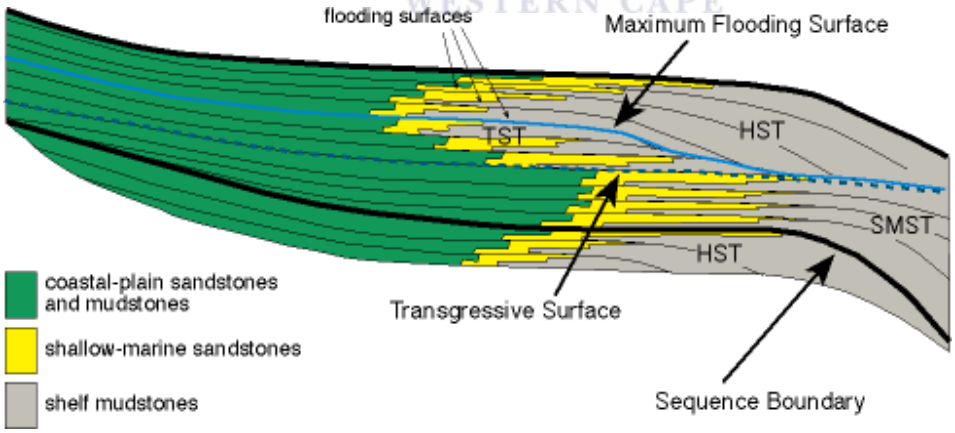

Figure 1-4. Typical Type-2 sequence (adapted from Van Wagoner et al., 1990).

Sequence boundaries are defined as unconformities or landward or basinward correlative conformities, that are laterally continuous over at least the basin scale and separating older underlying sediments from younger overlying sediments by a significant

depositional hiatus. Recognition of sequence boundaries is possible in well logs core, seismic sections and outcrops by one or more criteria:

- Subaerial erosional surfaces (developed paleosol profiles), and downdip submarine erosion
- Stratigraphic onlap unto a coast
- Changes from prograding parasequences set stacking pattern to retrograding parasequences set stacking pattern
- Downward shift in coastal onlap
- Basinward shift environments (landwards facies directly overlying basinward facies with no intermediate environments in between, (Van Wagoner et al., 1990)

On seismic profiles, the upper boundary may be recognised by erosional truncations or toplap while the lower boundary can be recognised by downlap and onlap.

Parasequences, parasequences set, and systems tract

The fundamental unit of the sequence is parasequence. Parasequence is simply a relatively conformable succession of genetically beds or bedsets bounded at the base and top by marine flooding surfaces or their correlative surfaces. Generally, a parasequence shows upward and typically the lower part of parasequence consisting of deeper water facies and its upper part shallower water facies (Fig 1-5).

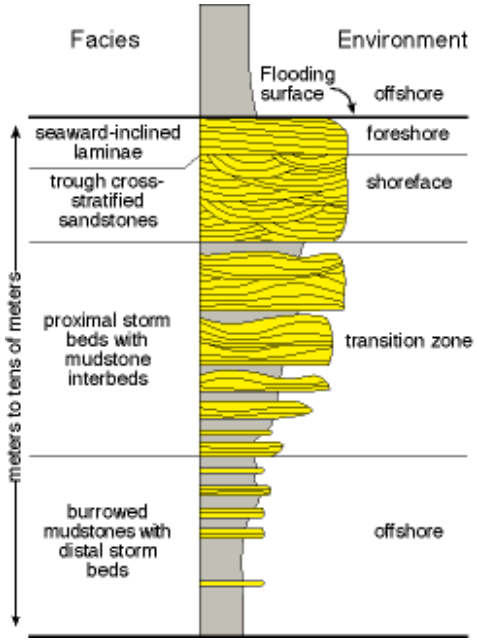

Fig 1-5. Typical wave dominated-parasequence (adapted from Van Wagoner et al., 1990).

Parasequence boundaries have correlative surfaces both on the coastal plains as an erosive surface, root horizon, or as localised erosion, and basinward as an upward succession of facies suggestive of deepening depositional surface (Fig 1-6). A flooding surface occurs over a paleosol, offshore transition, open marine limestone, or any depositional facies. At some points within the sequence, flooding surfaces reach a maximum landward position known as maximum transgression. The horizon of maximum transgression within a sequence is known as the maximum flooding surface (MFS) (Van Wagoner et al., 1990).

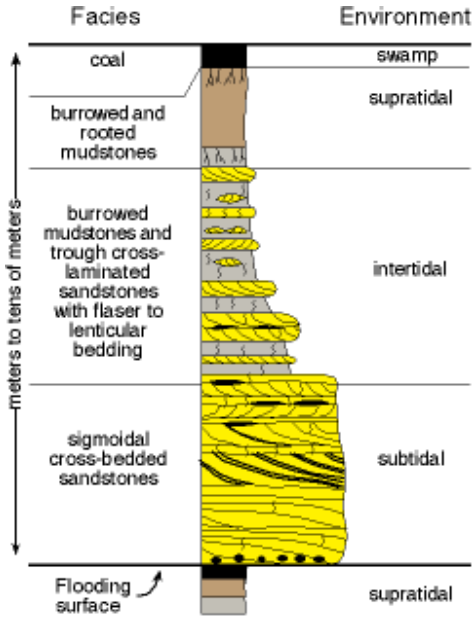

Fig 1-6. Typical tidal-parasequence (adapted from Van Wagoner et al., 1990).

Based on the predictive stacking patterns within a sequence, parasequences are classified into parasequence sets. Parasequence sets are simply a succession of genetically related paresequences forming distinctive stacking patterns typically bounded by major marine flooding surfaces and their correlative surfaces. These parasequence stacking patterns are responsive to variations in sediment supply and accommodation. Although, each parasequence shoals upward (progadational) (Fig. 1-7), represent relatively constant water depth (aggradational) (Fig. 1-8) or may dip upward- backstepping (retrogradational) (Fig. 1-9), all belonging to various forms of systems tract.

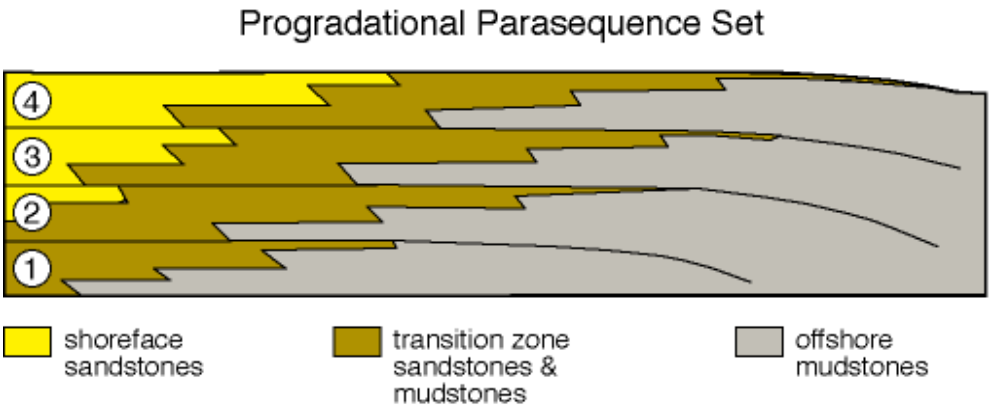

Fig. 1-7. Typical progradational parasequence set (adapted from Van Wagoner et al., 1990).

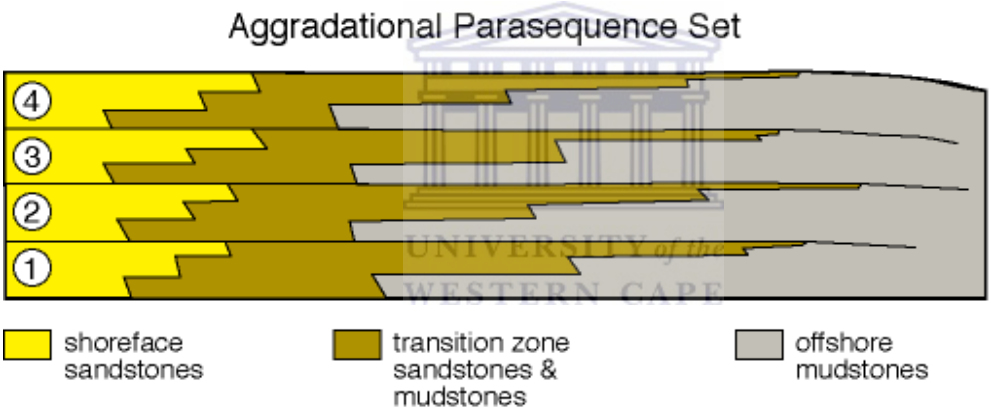

Fig 1-8. Typical aggradational paresequence set (adapted from Van Wagoner et al., 1990).

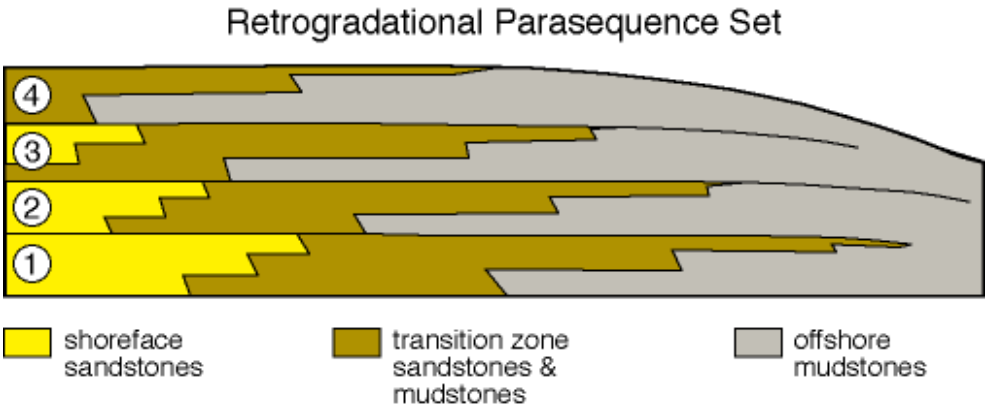

Fig 1-9. Typical retrogradional parasequence set (adapted from Van Wagoner et al., 1990).

The building blocks of systems tract are the parasequences and parasequence sets. The systems tracts are divided into three- lowstand systems tract (LST), transgressive systems tract (TST), and highstand systems tract (HST) - based on the internal parasequences and parasequence sets stacking pattern, strata geometry of their bounding surfaces and their position within a sequence.

Each systems tract exhibits a characteristic log response, seismic signature and paleontologic fingerprints, and performs a predictable role in oil and gas play-reservoir rock, source rock or seal.

Seismic and wireline log signatures of systems tract

Lowstand Systems Tract (LST): constitutes the oldest deposits in Type I depositional sequence. It is bounded at the base by Type-I sequence boundary and at top by transgressive surface. In a basin characterised by a shelf break, the LST may consist of three units namely the basin floor fan, slope fan complex, and the lowstand prograding wedge (Van Wagoner et al., 1990).

.

Basin Floor Fan (BFF): This is the earliest portion of the LST and is characterised by sand-rich submarine fan deposition on the basin floor or near the base of the lower slope. It is deposited during a relative sea level fall and its base is a Type-I sequence boundary

while its top is a surface on which overlying strata downlap. Minor condensed section may occur on the top of the basin floor.

On seismic sections it may exhibits relatively parallel and even high amplitude reflection with broad cycle breath and flat or slightly mounded top. On well log, especially gamma ray, they show a blocky character immediately above the sequence boundary (Emery and Myers, 1996) (Fig. 1-10).

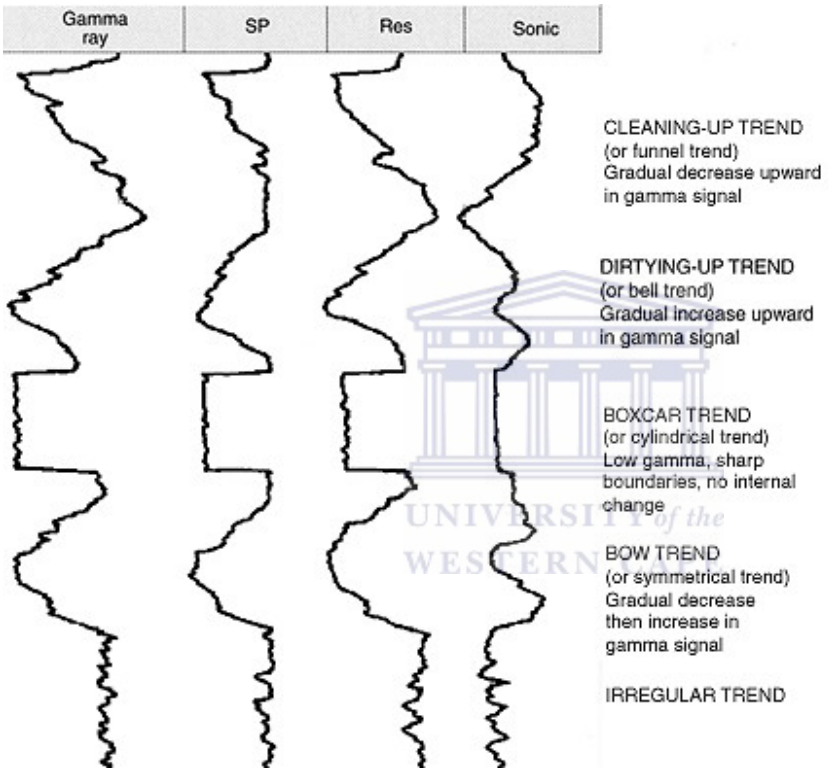

Fig. 1-10 Well log response character (after Emery and Myers, 1996)

Slope Fan (SF): This is the portion of the LST characterised mainly by the deposition of turbidites and debris flows on the lower slope and the basin floor during a relative sea level fall. The slope fan develops the basin floor fan or the sequence boundary. On seismic sections they exhibit a hummocky to mounded character and on gamma ray well log they display a crescentic shape. Minor condensed section may also occur on top of the slope fan complex. Sometimes this unit appear to be a highly variable mixture of thin

to moderately thick sand within a mud background that may produce a wide variety of log character (Emery and Myers, 1996).

Lowstand Prograding Wedge (PGC): This is the latter part of LST and is characterised by progradational or aggradational parasequences that form sedimentary wedges basinward of the shelf break and incised valley fill on the shelf and upper slope. The lowstand prograding wedge and incised valley fill are deposited during late relative sea level fall to early relative sea level rise (Emery and Myers, 1996).

On seismic section they show aggradational offlap seaward of the shelf break and a coarsening upward on well logs.

Transgressive Systems Tract (TST): This is the middle systems tract in an ideal depositional sequence and is deposited during a relative rise in sea level. It is bounded at its base by transgressive surface and at the top by maximum flooding surface (MFS), and contains backstepping or landward stepping parasequences.

On seismic section the TST shows characteristic seismic configuration including apparent truncation and continuous reflection at MFS.

The TST commonly onlaps the sequence boundary in a landward direction from the shelf break and can be recognized on the well logs by fining upward sequence using the maximum gamma ray and shaliest SP and resistivity logs. From biostratigraphic data, the MFS has peak abundance and diversity of microfossil (Emery and Myers 1996).

Highstand Systems Tract (HST): consists of the youngest strata within the depositional sequence and is commonly widespread on the shelf. It is bounded at its base by MFS and at its top by a sequence boundary. The HST is deposited during the late stages of relative rise in sea level to the early stages of relative fall in sea level.

Landward of the shelf break, the HST progresses from aggradational to progradational parasequences representing shallower water facies, whereas in the basin, it consists predominantly of the condensed section.

On seismic section, the HST is recognized by downlap unto the MFS condensed section. The Early HST is characterised predominantly by progradational offlap whereas the Late

HST is characterised by oblique offlap. On well log (GR), they exhibit a coarsening upward sequence (Emery and Myers 1996) (Fig. 1-10).

Integration of diagenesis and sequence stratigraphy helps to unravel and discuss the spatial and temporal distribution of diagenetic alteration in sandstone and source rocks evaluation. Diagenetic alterations in a sequence stratigraphic framework can be discussed based on the following sequence stratigraphic entities; sequence stratigraphy, parasequence boundaries, transgressive surface and maximum flooding surface and systems tract. Diagenetic alterations related to sequence boundaries including mechanical clay infiltration and formation of kaolinite and intergranular porosity below sequence boundaries due to percolation of muddy water below incised and by crevassing and flooding of interflusive area. Usually, mechanical clays infiltration is low below sequence boundary where sequence boundaries coincide with ravinement surfaces. Though the relationships between diagenetic alterations and changes in the relative sea level in clastic rocks are gaining increasing attention (Taylor et al., 1995, 2000; Loomis and Crossey, 1996; South and Talbot, 2000; Ketzer et al., 2002; Al-Ramadan et al., 2005), the links are less straightforward, and thus not fully explored yet (Ketzer et al., 2003). Diagenetic alterations in clastic rocks that are relatively well constrained within sequence stratigraphy include the distribution of carbonate cements and clay minerals (Taylor et al., 1995; Morad et al., 2000; Ketzer et al., 2002; 2003a; Al-Ramadan et al., 2005).

1.5.4 Diagenesis, sequence stratigraphy and petroleum potential of the Orange Basin

Muntingh et al., (1991) worked on sequence stratigraphic framework for the west coast of South Africa by applying sequence-stratigraphic concepts developed by Exxon to interpret 10,000 km of seismic data within an area of 90,000 km^2. The sequence-stratigraphic framework and depositional model generated were tested against geophysical log, core, and paleontological data of 31 wells, which showed good correlations. They said the interaction of the sequence-stratigraphic model and substantive, paleontological, source bed, and lithological information lead to a more reliable and refined geological model of the evolution of the Orange Basin.

Ben-Avraham et al., (2002) worked on Orange River delta and they established widespread occurrence of bottom-simulating reflectors (BSRs) in the multichannel seismic profiles on the upper continental slope in the southern periphery of the delta. Their work showed the presence of BSRs on seismic records on the southwest African continental margin south of the Walvis Ridge and also, occurrence of a large number of mud volcanoes. The two are controlled by active faults in the basin. They said the gas hydrate in this region may consist of a mixture of microbial and thermogenic gas, whereas much of the gas flowing through the mud volcanoes probably originated from deep-seated Aptian source shales.

Van Der Spuy, (2003) worked on the source rock samples within the Orange Basin. His finding showed that the source rock of the Aptian played an important role in petroleum systems operating off the west coast of Africa. He said there is strong case for regional development of a good-quality source within the Early Aptian succession in the deeper part of the Orange Basin. This study showed that Aptian sediments should be in the oil window in the large areas to the west of the basin centre.

Paton et al., (2008) worked on structural modeling of the southern part of the Orange Basin passive margin, South Africa using seismic-stratigraphic investigation approach. They predicted that margins alteration has a significant effect on the hydrocarbon system of the area and its potentials. They divided the phase margins evolution into two: the one comprising aggradational shelf margin with little or no deformation during the Cretaceous. The second phase of deposition, during the Tertiary, occurred to the west of the Cretaceous shelf margin and was characterized by significant margin instability and the development of a coupled of growth faults and toe-thrust system. They said the change in passive-margin configuration and the associated switch in the location of overburden accumulation is likely to have increased the petroleum prospectivity of the deep-water part of the margin. They predicted that the rapid western (seaward) migration of sediment accumulation resulted in the maturation of the high-quality distal source

interval, whereas the resulting toe-thrust geometry provides suitable structural traps for the hydrocarbons.

Kuhlmann et al., (2010) used 2D seismic data set that covers part of the Southern Orange Basin offshore to reconstruct the geological evolution of the basin. They used evolutionary model to investigate the occurrence of natural gas within the sedimentary column and the distribution of gas leakage features in relation to sedimentary and tectonic structure developed in the post-rift succession since the Early Cretaceous. They were able to subdivide the Cretaceous succession into five units with Barremian/Aptian and Turonian/Coniacian ages as the highest sedimentation rates in the basin. They concluded that the generated thermogenic gas does not migrate directly through the gravitational faults but driven up-dip along stratigraphical layers, to escape through the sediments to the sea-floor in the inner shelf area.

1.5.5 Application of sequence stratigraphy in Orange basin

Brown et al., (1996) worked on the sequence stratigraphy in offshore South Africa divergent basins. They were able to divide the basins into unconformity-bounded sedimentary sequences (Fig 1-11). They said each sequence is interpreted to have been deposited in response to world-wide (eustatic) relative changes in sea level and is defined at its base by type 1 unconformity as defined by Van Wagoner et al., (1987). Each sequence is associated by a sea-level lowstand followed by highstand flooding events. Their conclusions on the sequence stratigraphy of Orange Basin are as follows;

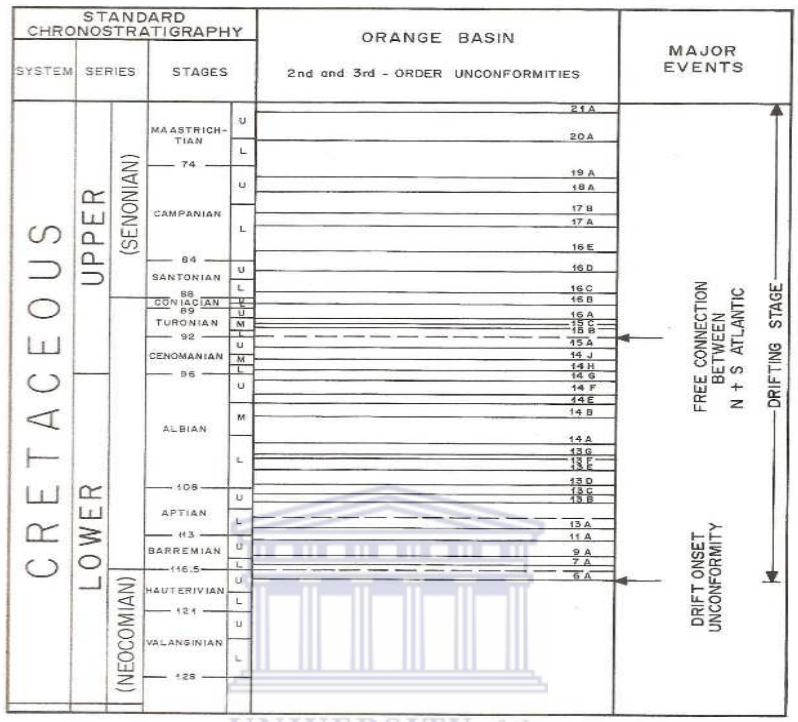

Fig 1-11. Orange Basin standard chronostratigraphy and 2nd and 3rd order unconformities (Brown et al., 1996)

- Understanding distribution of sand-rich highstand coastal, fluvial and deltaic systems provides an important key to predicting siliciclastic reservoir potential in subsequent lowstand systems tract.
- In the Orange Basin the stacking patterns exhibited by 3rd order sequence are also keys for predicting quality and deep basin delivery of lowstand sands.
- The composition and paleogeography of its depositional systems and their stacking geometries may be used to forecast the location and quality of subsequent lowstand systems
- Construction of regional sequence framework is an important step in preparing to explore for stratigraphic or combination traps

- The framework helps to constrain the areal and stratigraphic boundaries of lowstand fairways having favourable reservoir potential on the shelf and within and basinward of the gravity fault zone.
- All the sequences exhibit incised valley systems updip of shelf wedges, and this play has been verified within sequence 14A LST in borehole 4.
- The incised valley fill displays an excellent seals by the superimposed TST, fault traps, and migration pathways that are either vertically upward along faults or updip via prograding wedges from underlying marine condensed sections.
- The location where each incised valley entered the fault complex marks a point source where sandy sediment may have been introduced to the to lowstand systems before faulting.
- Optimum petroleum fairways can be predicted down dip of these incised valleys point sources.

The chronostratigraphic correlation chart produced (Fig 1-12) was based on sequence stratigraphic studies and utilises the time scale of Haq et al., (1988) to provide a geological framework, which is useful for understanding of the distribution of lithofacies through time and space, (Broad et al., 2006).

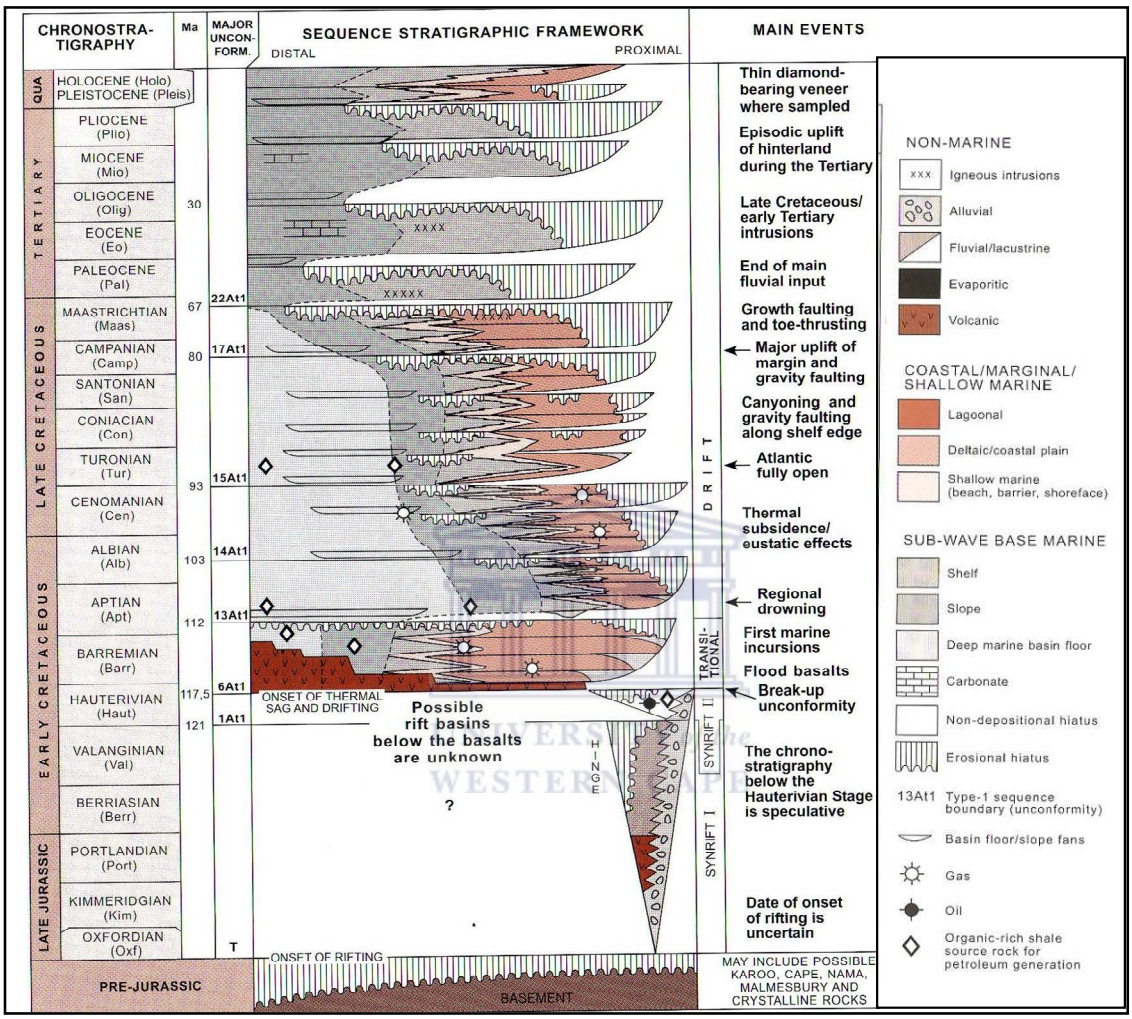

Fig. 1-12 Generalised chronostratigraphy and sequence stratigraphy of Orange Basin offshore Mesozoic basin, based on results of sequence stratigraphic studies (modified from Broad et al., 2006).

1.5.6 Diagenesis and sequence stratigraphy approach

The combination of diagenesis and sequence stratigraphy over the years has shown its usefulness in accessing reservoirs qualities. Mineralogical, textural, cementation and dissolution changes can be used to study diagenesis. These alterations occur at any time from initial deposition to deep burial, and, most of it occurs at the sequence boundary (Taylor et al., 1995; Morad et al., 2000; Ketzer et al., 2002; 2003a; Al-Ramadan et al., 2005). Minerals and chemical composition can be used to assess diagenesis, which is useful to delineate the setting/environment of precipitation. With the use of trace elements such as strontium, manganese, and iron, information can be obtained on interpretation of cement origin (Scholle, 1978). Stable isotopes can also be used to unravel diagenetic history. The two of most common isotopes are ^{18}O and ^{16}O, which always have different compositional ratios depending on the diagenetic environments. The lighter ^{16}O is common in cements precipitated by fresh water or surface water with elevated temperature; it is rare in marine associated cements (Morad et al., 2000). Other common isotopes are ^{13}C and ^{12}C which shows similar relationship. Lighter associated with fresh water and deep burial. Some of the light carbon may be derived from organic carbon associated with migrating hydrocarbon. In all, the precipitation of clay at or beneath the sequence boundary can be studied only by diagenetic analysis. The clays exhibit different properties that can affect reservoir quality, Scholle, (1978).

Chapter Two

2.0 Geology of the Orange Basin

2.1 Regional geology of the Orange Basin

The Orange Basin offshore Southwest Africa is located within the passive continental margin (Jungslager, 1999) of the South Atlantic between 31° and 33.3° latitude. It was formed as a result of the break-up of South America and Africa in the Late Jurassic, which was followed by seafloor spreading and the opening of the South Atlantic Ocean in the Early Cretaceous around 136 Ma (Brown et al., 1996; Reeves and Wit, 2000; Macdonald et al., 2003). It was formed within divergent plate boundary settings in the response to the lithologic extension related to the break-up.

Three major tectonic phases can be recognized in the area (Gerrard and Smith, 1982). On regional terms they are referred to as pre-, syn- and post-rifts. During the pre-rift time (until the Late Triassic), the area was dominated by compressional tectonism and formed part of the Gondwana foreland (Fig 2-1).

Fig 2-1. Gondwana showing African and South American plates (Modified from Broad, 2004)

The Falkland/Malvinas Islands lay east of Africa, the Falkland/Malvinas Plateau was 33% shorter and Patagonia was displaced east with respect to the rest of South America, in part along the line of the Gastre Fault System. Potential source facies are dominantly postglacial black shales of Late Permian age deposited in lacustrine or hyposaline marine environments; these rocks could also act as an effective regional seal. Sandstones deposited in the Late Permian were dominantly volcaniclastic with poor reservoir qualities; Triassic sandstones tend to be more mature. There was significant extension from about 210 Ma (end-Triassic) until the South Atlantic opened at about 130 Ma (Early Cretaceous). In the early syn-rift phase, extensions were accompanied by strike-slip faulting and block rotation; later extension was accompanied by extrusion of large volumes of lava. Early opening of the South Atlantic was oblique, which created basins at high angle to the trend of the ocean on the Argentine margin, and resulted in microplate rotation in NE Brazil. Intermittent physical barriers controlled deposition of Upper Jurassic–Cretaceous anoxic sediments during breakup; some of these mudrock units are effective seals with likely regional extent. During crustal reorganization, clastic sediments changed from a uniform volcaniclastic provenance to local derivation, with variable reservoir quality, (Macdonald et al., 2003). The South Atlantic continental passive margins of Africa comprise the major depocentres on the African plate. They reach 15km in thickness off Angola and extend hundreds of kilometres across the continent-ocean transition. Accumulation of sediments not only records the evolution from the continental rifting and break-up of Gondwana during latest Jurassic-Early Cretaceous, but also provides a complete record of the post-rift evolution of the margin and of the adjacent continent Africa (Fig. 2-2).

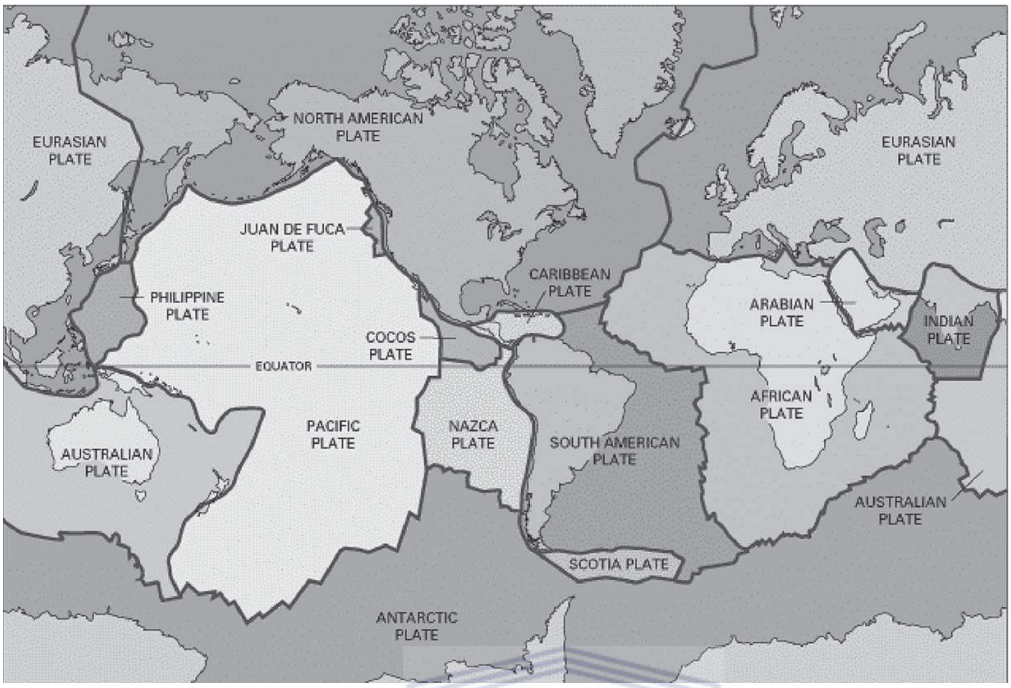

Fig.2-2.Gondwana map showing the different Earth crustal plates (www.parks.tas.gov.au, 2003).

Early Cretaceous active rifting south of the Wavis Ridge (Fig. 2-3) resulted in the formation of the SW Africa volcanic margin that displays thick and wide intermediate igneous crust adjacent to thick unstreched continental crust (Gerrard and Smith, 1982). The non-volcanic mode of rifting north of the Walvis ridge, led to the formation of equatorial western Africa margin, characterised by a wide zone of crustal stretching and thinning, and thick, extensive, syn-rift basin. Contrasting lithologies of the early post-rift (salt vs. shale) determined the style of gravitational deformation, whilst periods of activity of the decollements were controlled by period sedimentation rates. Regressive erosion across the prominent shoulder uplift of SW Africa account for high clastic sedimentation rates during the Late-Cretaceous to Eocene. Dominant carbonate production on equatorial western African shelf suggests very little erosion of a low hinterland.

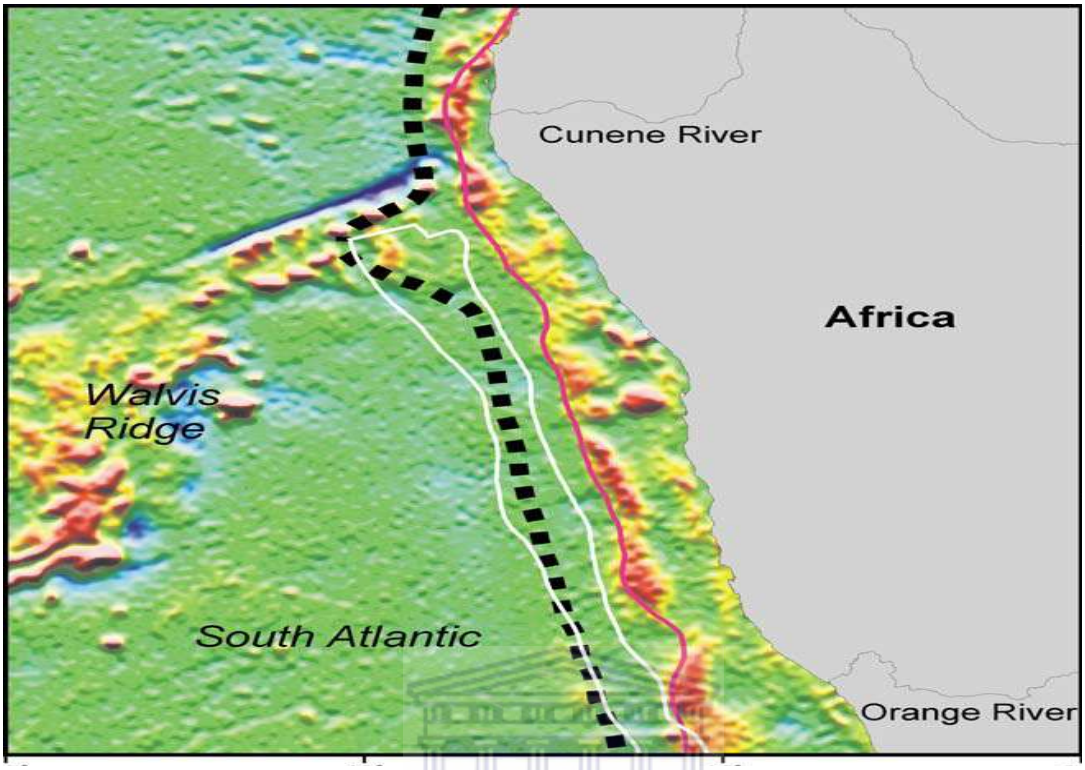

Fig 2-3. Map of western part of South Africa showing the Walvis Ridge (Macdonald et al., 2003).

The arid climate in the south indicates a drastic decrease of denudation rate, and thus reduced sedimentation on the margin (Seranne and Anka, 2005). Neogene emplacement of the African super well beneath Southern Africa was responsible for renewal onshore uplift on the margin. Neogene high sedimentation rate reactivated gravitational tectonic activities that had remained quiescent since late Cretaceous. Intercontinental rifting leading to the opening of the future South Atlantic occurred during Late Jurassic-Early Cretaceous. It was accommodated to the south by right-lateral motion on the Agulhas-Falkland fracture zone. However, this rifting was preceded by a "basin and Range type", late-orogenic extension of a Pan African tectonically thickened crust (Light et al., 1993). This phase allowed deposition of the extensive Permian-Jurassic Karoo continental formation and the development of a shallow marine embayment in the post subsiding axis, localised between the two future continents (Light et al., 1993. Clemson et al., 1997, 1999), recognised an early Triassic syn-rift and late Triassic-Middle Jurassic post rift

sequences, bounded by reactivated Damara (Pan African) fold belt structure, which later controlled the segmentation of South Atlantic rifting. Fault bounded sequences related to South-Atlantic rifting are divided into syn-rift I and syn-rift II in all SW African basins: Orange Basin (Gerrard and Smith, 1982; Jungslager, 1999), Luderitz and Walvis Basin (Maslanyl et al., 1982, Light et al., 1993) are separated by angular unconformities "R"of Valanginian age (Gerrard and Smith, 1982). The age of rift onset marked by "T" unconformity of Gerrard and Smith, (1982) is correlated with Late Jurassic. Syn-rift sequences are characterised by continental "red-bed" and volcanic rocks with rare lacustrine shale occurrences (Jungslager, 1999).

2.2 The Pay Zones of Orange Basin

2.2.1 Outcrops of the Cretaceous Orange Basin deposits

South Africa's western margin in which the Orange Basin is located comprises of three major groups of source rocks. The source rock from syn-rift, upper Jurassic-Neocomian which is generally lacustrine source rock pods, those sourced from Barrenian-Lower Aptian, generally marine, transitional succession source pods and those possibly sourced from Cenomanian-Turonian boundary, generally marine, drift succession source pods (Jungslager, 1999). The groups are further subdivided to individual petroleum systems in terms of: specific individual source rocks, level of maturity, type of organic matter and extent, and individual exploration play in terms of stratigraphic level of the reservoir and trap type. The predominantly gas bearing areas coincide with the main depocentre of the basin where the lower Aptian source rock is the window. The oil-bearing are predicted outside the depocentre, in the deepwaters, where the Lower Aptian source rock may become more oil prone and are possibly located in the oil window (Van der Spuy, 2003). The source rocks are mainly the shales and claystones. Reservoir rocks are clastic with poor characteristics across the basin.

2.2.2 Stratigraphy

The Orange Basin contains the stratigraphic record from lithospheric extension and rift tectonics throughout a fully evolved post-break-up setting, and thus provides an ideal area to study the evolution of a "passive" continental margin. The stratigraphy comprises a pre-rift successions (older than Late Jurassic, >130 Ma), that is overlain by syn-rift deposits of Late Jurassic to Hauterivian age (121 to 116.5 Ma) and in turn, by sediments of early drift stages up to Aptian age (113 to 108 Ma). Non-restricted marine deposits of an Aptian to present day age overly the Pre-Aptian successions. The rift stage basin was characterized by the development of north to south oriented grabens and half-grabens trending approximately parallel to the rift axis, from near Walvis Bay to south of Cape Town (Gerrard and Smith, 1982). These graben structures were filled predominantly with siliciclastic continental and lacustrine rocks, and variable thicknesses of volcanic rocks (Brown et al., 1996). The syn-rift sequences rest unconformably on the Precambrian or Paleozoic basement and are unconformably overlain by Early Cretaceous to present post-rift successions. Lithologically the early post-rift successions comprise sandstone and shales, and the majority of the post-rift successions are claystones

2.3. Orange Basin Tectonic Evolution

The Orange Basin of southwestern margin of South Africa is a divergent plate margin that is underlain by synrift graben basin and post-rift or passive margin. The rifting system was as a result of break up of South American and African continental plates which started during the Late Jurassic in response to extensional stress generated. There are several graben formed by rifting of continental crust along a sub parallel to the present coastline. Lower Cretaceous siliciclastic continental and lacustrine sediments filled the rift basin, but with some volcanic rocks present. The pre-rift basement of Precambrian or Palaeozoic is overlain by synrift strata resting unconformably (Jungslanger, 1999).

The drifting of the South American and African continental plates and emplacement of oceanic crustal rocks showed the Early Cretaceous onset of the South Atlantic drifting

phase comprising ~10 ma. long subsidence episodes as documented by geohistory curves. The drift onset occurred at ~117.5 Ma in Southern margin of African plate. The early drift siliciclastic sequences in the southern proto-Atlantic ocean contain evaporates, evidence that partially restricted marine environments existed in the basin before the main drifting phase began at 112Ma. A restricted post siliciclastic Cretaceous strata of maximum height of 220m, aged 112Ma occur within the elongated depocentre of the basin, followed by more than 500m open marine post passive margin Cretaceous rocks (Brown et al., 1996). The Orange River was responsible for the deposition of sand-rich sediments at high rates in the northern part of the region after 103Ma. The Olifants drainage system to the south (near Lamberts Bay) also contributed sediments along the Agulhas-Columbine Arch, between 117.5 and 103 Ma. The principal passive margin drifting phase in the southern proto-Atlantic ocean was restricted in the basin by open marine conditions at 112Ma. The main drift phase begins and recorded by the unconformity (112Ma). There was deposition of at least 30 third-order postrift sequences during the Cretaceous (Brown et al., 1996). The total thickness of drift sequence is at least 8000 m within the Orange Basin depocentre.

Chapter Three

3.1 Materials and methods

3.1.1 Materials

The data set for this study was obtained from the Petroleum Agency of South Africa (PASA). These include 783.63 km seismic reflection sections (2D) digital and hard copies, digital wireline logs (gamma ray, resistivity, density, neutron and sonic), Basemap showing the distributions of the wells in the blocks, ditch cuttings, sidewall core and core samples acquired from different stratigraphic sequences in the wells from the area under investigation.

3.1.2 Methods

The flow chart of the methods used in this study is presented below.

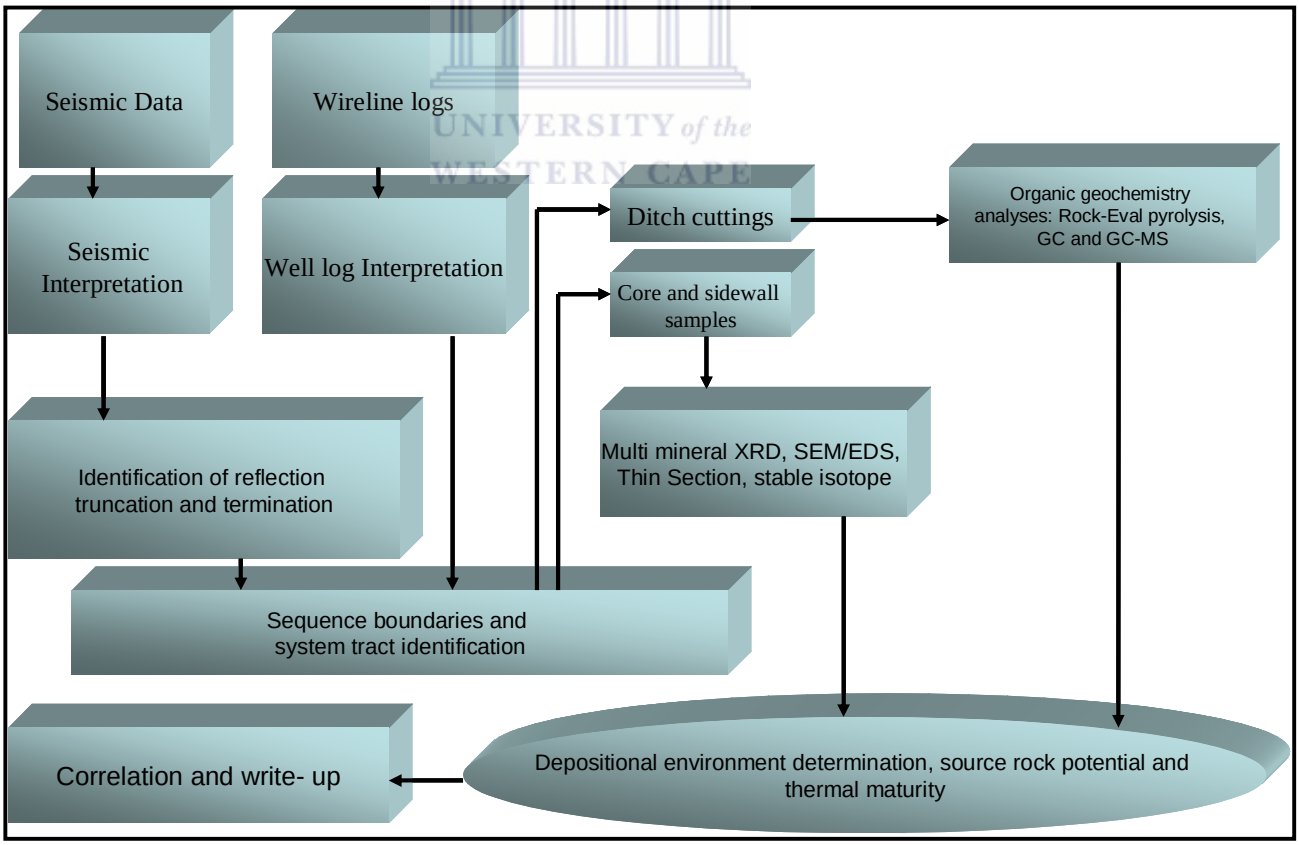

Fig. 3-1 Flow chart of methods of analyses.

3.2 Digital data loading

3.2.1 Wireline logs data loading

The data sets obtained from Petroleum Agency of South Africa (PASA) were prepared in LAS format showing different runs in each well. In order to obtain a continuous run for each well the data files were opened using, FastTracker, PETREL 2008 and seismic micro-technology (SMT 8.2) to check the files to see the depth available. The continuous depths were then extracted, meaning joining the runs to make a complete run for each well. As the extract from the files was being taken it was saved in excel spreadsheet to get lithology from top to bottom. When the extraction was completed the file was saved as text file (txt). The position of the wells to the globe was also obtained in Universal Transverse Mercator (UTM) format and it was also saved as text file in excel spread sheet. The UTM text file was first loaded before loading the well extract in text format, which then showed the complete run for each well. The signature obtained from each well was then studied to prepare for data editing. The editing involved checking the minimum and maximum values on gamma ray log to remove null values and arbitrary values were also removed. This was done for each well in conjunction with calliper log and other log types available. At the end of the editing the log is ready for interpretation.

3.2.2 Seismic section data loading

The data sets obtained were prepared in SEGY format for each of the lines picked. The cross line A87-047 controlled wells K_D1 and A_U1, in-line A81-061 controlled wells A_C2 and A_C3, the cross line AM-53 controlled wells K_B1, K_A2 and A_K2, and in-line A81-007 controlled wells A_F1 and A_O1 (Fig 3-2).

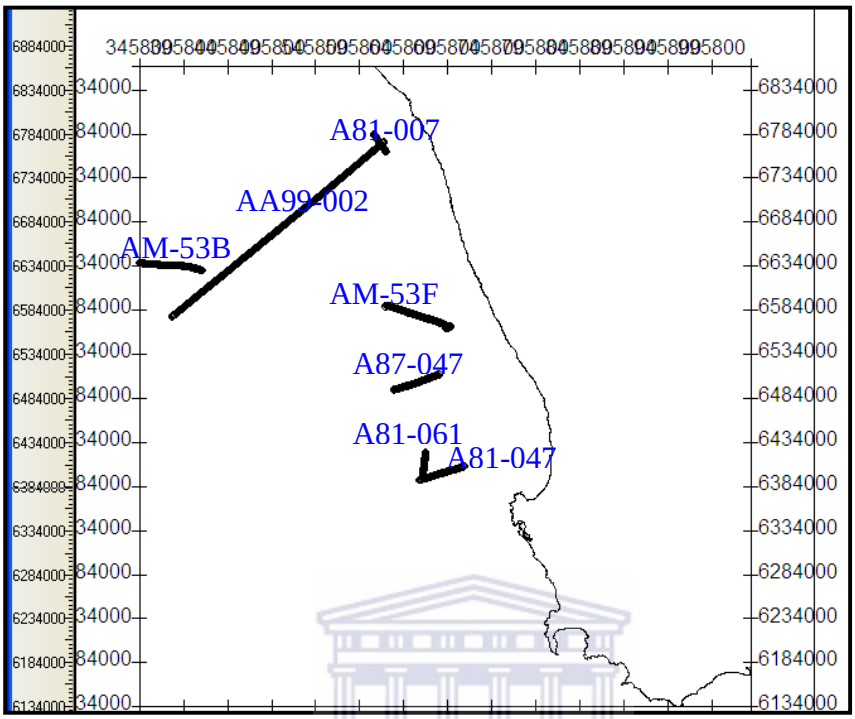

Fig 3-2. The seismic lines acquired in the Orange Basin for interpretation in SMT showing their relationship to one another based on their positions to the globe

The digital SEGY files were opened in SMT 8.2. The data are in two way travelled time (TWT) format. The navigation data for each of the line were first loaded in the SMT 8.2 software to know their positions relative to one another. After which the seismic data was loaded to get the visual expression of the seismic section. The image format in TIF format was also obtained to get the image look so as to make comparison with the digital seismic section. The well positions were located on the seismic section based on the shot point values as obtained from the well reports from PASA. The seismic sections were subjected to analyses by looking for the reflection termination and truncation, structural features, and studying the unconformities patterns as regard to periods of non-deposition and erosional effects.

3.2.3 Seismic data interpretation (General principle)

The seismic data acquired for this study are 2D seismic sections and were used for structural and sequence stratigraphic analyses. Structural analysis involved the identification and mapping of faults. The seismic sequence stratigraphic analysis procedure entails the following:

- Identifying the unconformities in the area of interest. These generally occur at an angle to underlying and/or overlying strata surfaces.
- Drawing the unconformity surface between the onlapping and downlapping reflections above and the truncating and toplapping reflections below.
- Extending the unconformity surface over the complete section. Where the boundary become conformable, its position was traced across the seismic section by visually correlating the reflections.

This process of identifying the bounding unconformities was carried out on all the seismic profiles provided in the fields of interest and the interpretation was done to tie correctly along all correlation loops throughout the grid.

Having identified the sequence boundary, the systems tracts (LST, TST, and HST) within each sequence were recognized based on the aforementioned characteristic seismic and log signatures. Primary seismic reflections are generated in response to significant impedance changes along stratal surfaces or unconformities. The seismic stratigraphy technique was employed in interpreting the stratigraphic information from seismic data. The fundamental principle of seismic stratigraphy is that within the resolution of the seismic method, seismic reflections follow gross bedding patterns are presented in time lines. A key message in seismic is that in which the correlative impedance contrasts are represented on seismic data from bedding interfaces but not lateral facies changes.

Steps used in interpreting

- First, determined the horizontal and vertical scale of the section and read trace headers and other data information.
- Looked for ways of determining the major multiples.

- Divided the seismic data into the discrete natural stratigraphic packages by marking reflection terminations.
- After marking all the seismic surfaces a similar exercise was performed on other lines.

Major Seismic Reflection Termination Patterns

The reflections terminations were characterized by the geometric relationship between the reflection and the seismic surface against which they terminates. The following terms introduced by Mitchum et al. (1977) were mapped:

Lapout was mapped between the lateral terminations of a reflector (generally a bedding plane) at its depositional limit.

Baselap/downlap - lapout of reflectors was mapped against an underlying seismic surface. Baselap which consist of downlap, where the dip of the surface is greater, and downlap, seen at the base of the prograding clinoforms representing the progradation of a basin margin slope system into deep water, were also mapped.

Toplap - a termination of inclined reflections (clinoforms) against an overlying lower angle surface believed to represent the proximal depositional limit. An apparent toplap in which clinoforms pass upwards into topsets that are too thin to resolve seismically were also encountered.

Erosional Truncation - is a termination of strata against an overlying erosional surface, in which toplap developed into erosional surface, but truncations are more extreme than toplap and led to development of erosional relief and the development of angular unconformity. The erosional surface in marine such as the base of a canyon, channel or major scour surface, or of non-marine erosional surface developed in a sequence boundary also mapped.

Apparent Truncation - is a termination of relatively low angle seismic reflectors beneath a dipping seismic surface in which the surface represents a marine condensation where termination process represents a distal depositional limit (or thinning) below seismic resolution, generally within topset strata, but sometimes also within submarine fan also mapped.

Onlap is recognized on seismic data by the truncation of low-angle reflection against a steeper seismic surface. Two types of onlap were recognized in this study, namely marine and coastal:

Marine onlap represents a change from marine deposition to non marine deposition or condensation. Marine onlap reflects a submarine facies change from significant rates of deposition to a much lower energy pelagic drape. The seismic surface of marine onlap was mapped as marine hiatus or condensed interval.

Coastal onlap, an onlap of non-marine, paralic, or marginal marine strata was mapped at a zone of deposition between basin margin (subaerial or shelf) erosion and non deposition.

Fault Truncation marked the termination of reflections against a syn or post depositional fault, slump, glide or intrusion plane.

Seismic Facies

Further geological interpretations are done by interpreting seismic facies and attributes once the seismic data has been divided into its component depositional packages. Seismic facies an aerially definable 3-dimensional unit composed of seismic reflections whose elements, such as reflection configuration, amplitude, continuity, frequency and interval velocity differ from the elements of adjacent facies unit. A seismic facies was interpreted to express certain lithologies, stratification and depositional features of the deposits that generate the reflections in the study area.

Factors that control interpretation of Seismic facies include:

- Internal reflection composition and configuration: Continuity, amplitude/ frequency, interval velocity
- Boundary Relationship: Terminational and Transitional
- External Geometry
- Lateral facies relationship

Major Seismic Facies

Parallel/Divergent Seismic facies: They are the most common reflections within the basin they are parallel or sub-parallel or divergent in configuration. Parallel reflections suggests uniform deposition in a stable or uniformly subsiding surface whereas, divergent reflections indicate variation in the rate of deposition from one area to another or else gradual tilting (Mitchum et al., 1977). Because of wide, relatively uniform lateral extent in the basin it can be inferred that these facies were deposited on a broad, relatively stable shelf, delta platform or, even if less likely, on a broad basinal plain.

Progradational seismic facies: In dip sections, reflections were found inclined relative to underlying and overlying reflections and were called offlap reflections. This facies always deposited within prodelta and, or slope environments during basinward shifting of shelf/platform or delta systems, were also mapped. A variety of progradational configurations are possible: oblique, sigmoid singled complex/composition. Among them two types encountered are oblique and sigmoid. They occur in some progradational system. Oblique configuration was distinguished by toplap termination of clinoform reflections. They are found associated with deltaic progradation or with neritic shelf/ platform environments in the basin. Consequently, they consist of terrigenous clastic sediments and these clinoforms are indication of higher sand content up/dip in shallow – marine delta and fan-delta facies.

.

Recognition of Stratigraphic Surfaces from Seismic Data

Determination of Sequence Boundary

Development of a high relief truncation surface; particularly one which erodes the topsets of older units indicates a sequence boundary. The downward shift in coastal onlap across the boundary was also used in the sequence boundary determination.

Determination of a Transgressive Surface

A transgressive surface marks the end of lowstand progradation and the onset of transgression. It was found associated with reflection terminations, and marks the boundary between a topset clinoform and the topsets interval.

Determination of a Maximum Flooding Surface

A maximum flooding surface was recognized on seismic data as a surface where clinoforms downlap onto underlying topsets, thereby displaying backstepping and apparent truncation.

Recognition of Systems Tracts on Seismic Data

The principle applied to recognise the system tracts from seismic data (systems Tracts) was based on the nature of their boundaries, and by the stacking pattern of their internal stratigraphy.

Recognition of Lowstand Systems Tract:

A lowstand systems tract is bounded below by a sequence boundary, and above by a transgressive surface it is also overlain by a transgressive surface (a transition to a retrograding topset unit and it contains a basinal fan unit), it was recognised as a mounded unit of a couple of reflection lower and more distal from the clinoform. The lowstand systems tract were divided into two parts; a lowstand fan and a younger lowstand wedge in which the fan was the most dominant in the basin.

Recognition Transgressive Systems Tract:

Transgressive systems tract are bounded below by a transgressive surface and above by a maximum flooding surface. It was recognised on seismic section by retrograding topset parasequences. Transgressive systems tract often very thin, and consist of no more than one reflection as seen in this study. It is recognised as a transgressive systems tract as its base marks the transition from an underlying interval of mainly clinoforms, to an interval of mostly or entirely topsets. It also clearly showed internal retrogradational geometries. The transgressive systems tract overlain by a maximum flooding surface was recognized by the downlap of overlying clinoforms.

Recognition of Highstand Systems Tract

Highstand systems tract are bounded below by a maximum flooding surface and above by sequence boundary and exhibits progradational geometries. It consists of prograding topsets and clinoforms representing progradation and it overlies a maximum flooding surface, clinoforms within the system tract downlap topsets of the underlying systems tract. Apparent transactions were seen beneath the surface and the underlying systems tract infill erosional relief on an older sequence boundary

3.2.4 Wireline log interpretation (General procedures)

Van Wagoner et al., (1990) dealt specifically with high resolution sequence stratigraphy from outcrop, core and wireline log data. Their work on high resolution sequence stratigraphy has reached wider audience and much progress has been made in the last few years. The most important wireline logs utilized in well logs sequence stratigraphic analysis are the gamma ray and resistivity logs with respect to overall log response or characters. These log shapes and overall log responses are initially used in identifying, matching and tying sequence stratigraphic surfaces (sequence boundary, SB, maximum flooding surface (MFS), and transgressive surface (TS) and subsequently in interpreting the stacking patterns of the vertical sedimentary sequences.

This application of sequence stratigraphic principles to well logs allowed resolving genetically and chronostratigraphically related packages of strata that are too thin to recognise within seismic reflection data alone.

In this study, gamma ray and resistivity logs were analysed using the criteria for well logs sequence stratigraphic interpretation discussed by Emery and Myers (1996) (Fig 1-10) and Vail and Wornardt (1991).

At the inception of the well logs sequence stratigraphic analysis, the predominance of sequence stratigraphic surfaces was first identified. After establishing the sequence boundary and trangressive surfaces, the parasequences stacking pattern and their position within the parasequence was used in determining the systems tracts that are enveloped by the sequence boundaries. Having established the systems tracts and the sequence stratigraphic surfaces from each well log, correlation of the well was carried out using sequence stratigraphic concepts. The general principles and procedures of wireline logs are hereby presented and employed in the data analyses.

Sequence Stratigraphy from Wireline Logs:

Wireline log data provides a better tool of analysing subsurface conditions. Log data provides information on lithology and depositional environment of a particular borehole and but when tied with seismic sections or correlated with other wells it can provide better subsurface understanding. Trends in log response may equate with trends in depositional energy and thus can infer basin infill history. A number of distinct log trends can be recognized on wireline logs. Of all of them, the gamma ray log infers a good response for identifying lithology. The major log trends used in this study, that is the Cleaning up trend, Dirtying up trend, Boxcar trend, Bow trend and Irregular trend, are discussed below.

The Cleaning up Trend

The cleaning-up trend showed a progressive upward decrease in the gamma reading representing a gradual upward change in clay-mineral content. In shallow marine settings the cleaning-up motif is usually related to an upward transition from shale-rich to shale-free lithologies, owing to upward increases in depositional energy, upward

shallowing and upward coarsening. Occasionally, cleaning up units were seen as a result of a gradual change from clastic to carbonate deposition of a gradual decrease in anoxicity, neither of which need be necessarily related to upward shallowing or propagation of a depositional system.

The Dirtying up Trend:

The dirtying up trend showed a progressive upward increase in the gamma reading related to a gradual upward change in the clay-mineral component. This is a lithology change from sand to shale or an upward thinning of sand beds in a thinly interbedded sand-shale unit. Both imply decrease in depositional energy. Upward fining predominates within meandering or tidal channel deposits, in which it represents an upward decrease in fluid velocity and energy within the channel. The largest fining up units was found in coarse fluvial succession and in estuarine fills. Channel deposits have a basal lag which affects the gamma response when the lag contains shale clasts or heavy minerals. In shallow marine settings the dirtying-up trend reflected the retreat or abandonment of shoreline-shelf systems, resulting in upward deepening and decrease in depositional energy. The dirtying up trend results also as a result of gradual increase in anoxicity or gradual change from carbonate to clastic deposition.

Box Car Log Trends

This is also known as a cylindrical motif. Box car trends were recognised by sharp-based low gamma units with an internally relatively constant gamma reading, set within a higher gamma background unit. The boundaries with the overlying and underlying shales were abrupt. The sonic readings from the sands had higher and lower transit time for the shales, depending on cementation and compaction. Turbidite boxcar units generally showed a much greater range of thickness than boxcar fluvial channel units. Shallow marine sand bodies had truncated bases due to faulting or sharp bases as a result of falls in a relative sea level or other factors.

The Bow Trend

It is also known as barrel or symmetric trend. The bow trend consists of a cleaning up trend, overlain by a dirtying up trend of similar thickness and with no sharp break between the two. A bow trend, formed from the waxing and waning of clastic sedimentation rate in a basinal setting where the sediments are unconstrained by base level, was encountered. The bow trends were found developed in shallow marine settings, where base level constraints led to thicker progradational and thinner transgressive units.

Irregular Trends

Irregular trends were found to have no systematic change in either baseline or lack the clean character of the boxcar trend. They represent aggradation of a shaly or silty lithology, typical of shelfal settings; a lacustrine succession or muddy alluvial overbank facies. There is evidence of a subtle and systematic shift in the base line which appears to be an irregular trend. Irregular log trends were not recognised in shelfal or paralic facies because cyclic changes in water depth are likely recognised as cyclic log trends and identified as parasequences.

The Log Response of Clinoforms:

On well logs, the clinoform unit had a cleaning upward pattern that reflects upward shallowing. The base of the cleaning up trend was equivalent to a downlap surface. Confirmation that this log response represents a prograding clinoform pattern supporting upward shallowing because upward shallowing in clastic systems occur through progradation. The base of a clinoform unit was reported as a downlap horizon. This was recognized as a distinct base to the cleaning-up unit, with a log facies diagnostic of marine condensation, with high-gamma shale and a cemented horizon. The top of a cleaning-up clinoform trend was marked by an abrupt increase in shale content (gamma reading) resulting from abrupt deepening across the transgressive surface and overlain by topsets. An abrupt increase in the shale content within the clinoform trend implies an abrupt jump to a deeper facies, resulting from lobe switching or transgressions, during relative sea level rise. Similarly, an abrupt decrease in the gamma response implies an

abrupt jump to shallower facies, identified as sequence boundary, a normal fault or slump.

The Log Response of Parasequence

Topset parasequence were recognised by repeated cycles of filling of accommodation space between the offlap break and the coastal onlap point, and seen as small scale cycles on the logs interpreted. The most common cleaning-up motif recognized in parasequence is an evidence of marine settings. In the cleaning up motif the shale content decreases upwards whereas primary porosity and bed thickness increases upward. The marine flooding surfaces were recognized as abrupt upward increases in shale content. The parasequences are small-scale upward cleaning log units and the marine flooding surfaces showed abrupt increase in gamma reading.

Log Responses from Basinal Environments

Mud-rich basinal units show a symmetrical bow response whereas sand-prone systems tend to show a box-car or cylindrical log trend. Log trends were separated by log markers that represent background pelagic sedimentation, uninterrupted by sediment gravity flows from the basin margin. These markers showed thin shales with little or no silt and sand. They also showed anomalously high gamma response, low density, low resistivity and low sonic velocity.

Estimation of depositional controls and sequence stratigraphy from log response

Periods of basin-margin progradation and retrogradation, and the recognition of variations of relative sea-level from a well-log suite were used for sequence analysis. Progradation was recognised from a clinoform log response (large-scale cleaning and shallowing-up unit). Retrogradation of the basin margin showed significant upward-deepening units marked by upward deepening. The response of accelerating relative sea-level rise was suggested by a thinning-up stack of parasequences.

Key surfaces:

A maximum flooding surface was marked by log response in between a dirtying-up and cleaning-up trend. The maximum flooding surfaces pass laterally into shelfal, a condensed interval which showed a gamma peak, a resistivity trough, density maximum or minimum. A maximum progradation surface represented a surface between a prograding unit and an overlying retrograding unit, marked by cleaning-up and dirtying-up trends respectively. A marine condensed interval in the basin was recognized as the shale-break between basinal log motifs. A downlap surface represents a large scale cleaning-up motif. On the clinoform slope, a sequence boundary results in a jump to a significantly cleaner log response within the cleaning-up motif. Sequence boundaries were marked by an abrupt upward change from a progradational (cleaning-up) log motif to an aggradational or retrogradational log motif.

Identification of systems tracts from log response:

A lowstand fan was recognized as fan unit bounded by marine condensed intervals. A transgressive systems tract was recognized as a retrogradational parasequence set. It was bounded below by a maximum progradational surface (often coincident with the sequence boundary) and above by a maximum flooding surface or its correlative condensed interval. A highstand systems tract was recognized as a prograding basin-margin unit bounded below by a maximum flooding surface and above by a sequence boundary.

Log Responses from Basinal Environments:

Estimation of depositional controls and sequence stratigraphy from log response:

Progradation was recognised by a clinoform log response (large scale cleaning and shallowing up unit) and the progradational stacking of topset parasequences. Evidence of Basin margin progradation was found only within basin margin units (topsets, clinoform, and lowsets)

3.3 Laboratory analyses procedures

3.3.1 Thin section procedure

Thin section involves laying samples set in open sample trays with clean glass slides. Sample numbers were marked on the glass slide with diamond scriber. Samples number checked against the marked number on the glass slides to ensure the sample identity is correct. The samples were ground to a flat surface using only diamond abrasive with distilled water. Sample grinding was done by hand on a flat plate for the core samples. Samples that required stabilization (the side wall core samples) prior to grinding, were stabilized. Epoxy stabilization was done in a plastic using Epon 815-diethylene-triamine. The glass slide tray was ensured to be next to the samples. The sample was allowed to cure at room temperature. Final grinding of the surface to be mounted on the glass slide was done using 400-mesh diamond plate. Lapping was done using glass impregnated plate. 10 X-power magnification microscopes were used in observing the progress of the grinding. The prepared slides were analysed using petrographic microscope.

3.3.2 XRD technique

The core and side wall core samples collected at various stratigraphic sequences were analysed by XRD to assess any mineralogical changes. The samples were pulverised. A Bruker D8 Advance instrument with a pw3830 x-ray generator operated at 40 kV per 25mA was used and a scan speed of 4° (2 theta) mins. (Plate 1). The samples were oven-dried at 100°C for 12 hours to remove the adsorbed water. The samples were pressed into rectangular aluminium sample holders using an alcohol wiped spatula and then clipped into the instrument sample holder. The samples were step-scanned from 5 to 100 degrees 2 theta at intervals of 0.02 and counted for 0.5 seconds per step, later probe to less than 2 microns metre for authigenic minerals identification.

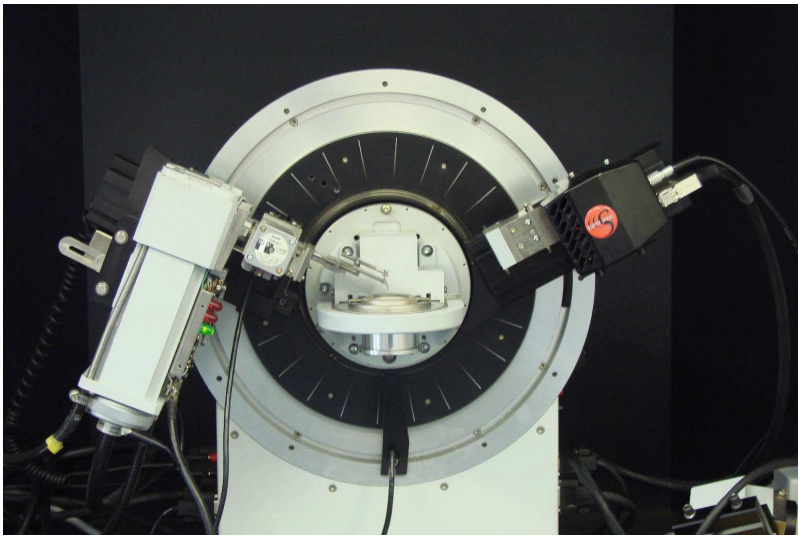

Plate 1. XRD machine

3.3.3 SEM/EDS Method

The SEM/EDS analyses involve each samples coated with gold palladium for about 30 minutes. This was done to make the samples conductive. The coated sample was put on a palette-like stand which was placed under an electron beam. SEM analysis was performed using a LEO Stereoscan 440 which is a high vacuum microscope. It has a stereo workstation attached to the instrument which enables the image taken by the electron microscope to be viewed on the computer. There is an allowance for magnification adjustment of the view in order to have a better and accurate view of the image. Freezing the view enables the image to be taken and snapshot of the desired image (s) can be taken for analysis. A dispersive X-ray spectrometer (EDS) coupled with a computer based multichannel analyzer (MCA) was used for this analysis. The SEM and the EDS were done simultaneously. A conventional Be window, Si (Li) detector with a 1024 channel MCA set to 10eV per channel was employed. Picoammeter was attached to measure beam and or specimen current. Samples were metallographically polished starting with 6 micron to 3 micron and ending with 1 micron grit with diamond paste to make them conductive. The detrital and authigenic minerals identification in the samples was carried out using X-ray diffraction.

3.3.4 Stable Carbon and Oxygen isotope geochemistry procedure:

Oxygen and carbon isotopes data were obtained from bulk-rock samples. Roasting of the samples were done for 40 min at 430 °C in high vacuum glass followed by dissolution in 100 % hydrochloric acid at 25 °C under high vacuum for 12 hours. The evolving CO_2 was cryogenetically separated from other gases and measured with a Finnigan Delta S mass spectrometer. The isotopic results were reported in the usual δ notation versus the sea mean ocean water (SMOW) for oxygen and Vienna PeeDee Belemnite (PDB) standards for carbon.

3.3.5 Rock-Eval pyrolysis and total organic carbon (TOC) determination

Sample Preparation: Samples for TOC and Rock-Eval were ground, and material passing through a 60 mesh (250 micron) sieve was used for analysis.

Total Organic Carbon: Approximately 0.10 g of ground rock was accurately weighed and then treated with concentrated hydrochloric acid to remove carbonates. The samples were left in acid for a minimum of two hours. The acid was removed from the sample with a filtration apparatus fitted with a glass microfiber filter. The filter was placed in a LECO crucible and dried at 110 ºC for a minimum of one hour. After drying the sample was analyzed with a LECO 600 Carbon Analyzer.

Rock-Eval (Programmed Pyrolysis): In Rock-Eval pyrolysis, ground samples were heated in an inert environment to measure yields in three portions (S1, S2 and S3), measured as three peaks on a pyrogram. Sample heating at 300 ºC for 3 min produced the S1 peak by vaporizing the free (unbound) hydrocarbons. High S1 values indicate either large amounts of kerogen-derived bitumen (as in an active source rock) or the presence of migrated hydrocarbons or components of the drilling mud system. The oven then increased in temperature by 25 ºC per minute to 600 ºC and the S2 and S3 peaks were measured from the pyrolytic degradation of the kerogen in the sample. The S2 peak is proportional to the amount of hydrogen-rich kerogen in the rock, and the S3 peak measures the carbon dioxide released (to 390 ºC) providing an assessment of the oxygen content of the organic portion of the rock. The temperature at which the S2 peak reaches a maximum, “Tmax”, is a measure of the source rock maturity. Rock-Eval II instrument

was used for the Rock-Eval pyrolysis and a summary of operating conditions is as follows:

Operating Conditions:

S1: 300 ºC for 3 minutes

S2: 300 ºC to 600 ºC at 25 ºC/min; held at 600 ºC for 1 minute

S3: CO2 trapped between 300 to 390 ºC

3.3.5.1 Accelerated solvent extraction

The samples were powdered using mortal and pestle. 20 g of each sample and 4 spoons of pre-extracted diatomaceous earth were thoroughly mixed. For extraction the metal tube of an Accelerated Solvent Extractor (ASE) system was filled with the sample material with filter paper placed at both ends of the tube before tightly sealed to avoid leakage. The tube was placed in an ASE 200 (DIONEX) extraction system using dichloromethane: methanol (99:1) as extraction solvents. Each extraction was carried out for 20 min at 75 °C and pressure of 50 bar. The extracts were concentrated using a Turbo Vap 500 closed cell concentrator and further concentrated by evaporating the solvent in a stream of nitrogen gas. After the addition of internal standards (ISTD: 5α-androstan, ethylpyren, 5α-androstan-17-on, erucic acid) the extracts were fractionated by medium-pressure liquid chromatography (MPLC) (Radke et al, 1980) into fractions of aliphatic/alicyclic hydrocarbons, aromatic hydrocarbons and polar hetero-components (nitrogen, sulphur and oxygen containing compounds, NSO) using *n*-hexane and methanol as eluents. Each fraction was concentrated prior to GC and GC-MS analyses.

Plate 2. Medium Pressure Liquid Chromatography equipment (MPLC) used at GeoForschungsZentrum (GFZ), Potsdam, Germany

3.3.5.2 Gas chromatography

Gas chromatography (GC) and gas chromatography-mass spectrometry (GC-MS) was performed on the saturated hydrocarbon fraction in order to determine the *n*-alkanes and isoprenoid hydrocarbons. GC-analysis was conducted on a Hewlett Packard 5890 series II gas chromatograph equipped with a Agilent Ultra 1 capillary column (50 m length, 0.22 mm inner diameter, 0.33 µm film thickness) linked with PTV splitless injector and a flame ionisation detector (FID). The GC oven was programmed from 40 °C (hold time 2 min) to 300 °C (hold time 60 min) at 5 °C/min. The carrier gas was helium. The peak areas were electronically detected and identification was based on the retention times and comparison with standard. The peak integration was achieved using the Agilent ChemStation software**.**

3.3.5.3 Gas chromatography–mass spectrometry

GC-MS analysis was performed on Thermo Trace GC Ultra coupled to a Thermo Trace DSQ mass spectrometer. The GC was equipped with a PTV injection system operating in the splitless mode and a SGE BPX 5 fused silica capillary column (50 m length, 0.22 mm inner diameter, 0.25 µm film thickness) using the following temperature program: initial temperature 50 °C, heating rate 3 °C/min to 310 °C, held isothermal for 30 min. The MS operated in the electron impact mode at 70 eV and Helium was used as a carrier gas. To improve the signal to noise ratio hopanes and steranes were measured in the single ion monitoring (SIM) mode using *m/z* 191 for hopanes and *m/z* 217, 218, 372, 386, 400 and 414 for steranes at a scan rate of 0.8 s per scan. The peak integration was achieved using the Xcalibur software**.**

Chapter Four

4.0 Results and Discussions

4.1 Introduction to interpretation of results

4.1.1 Wireline log interpretation

Wireline log is the main source of accurate information on the depths as well as apparent and real thickness of beds. They yield information on the subsurface geology including formation boundaries, lithology, fluid content, and porosity amongst others. The wireline log suite obtained for this study includes Gamma ray, Sonic, Resistivity, Neutron and Density which were used in lithostratigraphic and sequence stratigraphic analyses of the wells in the basin.

The Gamma ray log is used in measurement of natural radioactivity of the formation. It reflects the shale content since radioactive elements tends to concentrate in shale and clays and low in sand bodies. Clean formations tend to have very low level of radioactivity unless radioactive contaminants are present or the formation contains dissolved radioactive sediments. With increase in the shale content, the level of radioactivity increases.

Resistivity logs measure formation resistivity which is a reciprocal of conductivity. Formation resistivity depends on the resistivity of formation water, amount of water present and the pore structure geometry.

Neutron log is a radioactive log, can give an indication of amount of hydrogen present in a sedimentary sequence, which is an indication of the fluid porosity. Neutron logs are used primarily for delineation of porous formation and determination of their porosity. When combined with another porosity log or core analysis, it can yield more accurate porosity value and identification, including evaluation of shale content.

Sonic log is simply a recording versus depth of the time (ΔT) required for a compressional sound wave to traverse one foot of formation known as interval transit time. ΔT is the reciprocal of the velocity of the compressional sound wave. The interval transit time for a given formation depends on lithology and porosity.

Formation density log is a radioactive log. It measures the electron density of the formation. This is related to the true bulk density, which in turn depends on the density of the rock matrix material, formation porosity and the density of the fluid filling the pores.

4.1.2 Sequence stratigraphic interpretation

The wireline logs were broken down to parasequence sets using the log signatures. The coarsening and fining upward sequences were mainly used for the interpretation. This approach is a function of the lithologies encountered. The gamma ray was used in all the wells for the systems tracts delineation. This is because of the definite break between the sand and shale using the shale line and GR values in the software. The textural parameter of the lithology was used, studying the fining and coarsening upward sequence for sand to shale and vice versa for shale and sand. These two events signify progradation, retrogradation and aggradation which are products of sea level rise and fall. The rise and fall of sea level determines the type of sediment that will be deposited. The sharp break between the events is denoting episodes of deposition. Where there is two distinct break exist they are termed as sequence boundary. Sequence stratigraphic analysis is useful in the determination of the stratal pattern of depositional sequences and their constituent systems tract.

4.2 Seismic interpretation

Primary seismic reflections are generated in response to significant impedance changes along stratal surfaces or unconformities. The fundamental principle that seismic reflection follows is gross bedding and therefore approximate time lines are the basis for seismic sequence stratigraphy. Detailed study of seismic profile for faults identification was done on the dip section (cross lines) since faults are easily recognised on dip section than on strike sections. Though fault zone is normally too thin to be imaged on seismic data, but can easily be identified as line-ups of reflection discontinuities on vertical seismic sections (Loseth, et al., 2009). Series of faults, which are listric and normal, were picked on the section profiles. The seismic database of the area consists of 783.63km of

migrated stack 2D data on Seg-Y format. The in-line A81-007 controlled by wells A_O1 and A_F1 (Fig. 4-1) was interpreted based on sequence packages.

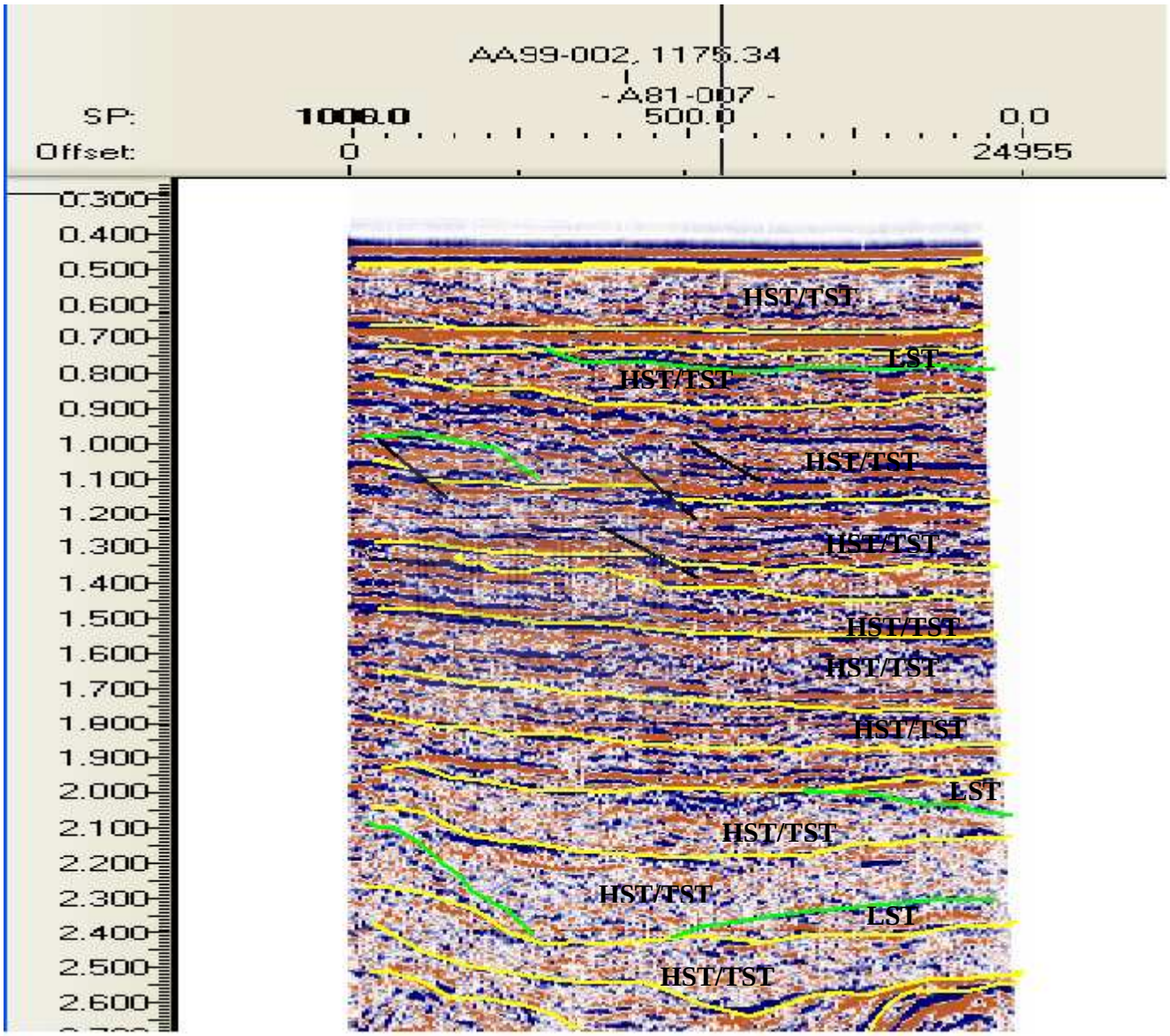

Fig. 4-1. Interpreted seismic section line A81-007 where yellow lines are sequence boundaries, green lines transgressive surfaces and black lines fault lines.

The interpretation was done based on 4 terminations: onlap, downlap, toplap and truncation. The sediments are Upper Cretaceous basin floor fan deposited in regular orders. At the southern part of the section at depth 2.300sec and below is Rift/Drift

unconformity marked by onlap in the south-western and downlap in the southeastern part of the section. The line AM-53F (Fig. 4-2) that controlled wells A_K2, K_A2, and K_B1 in block 2 of the basin shows Late Cretaceous growth-fault rollover as seen in the entire section area.

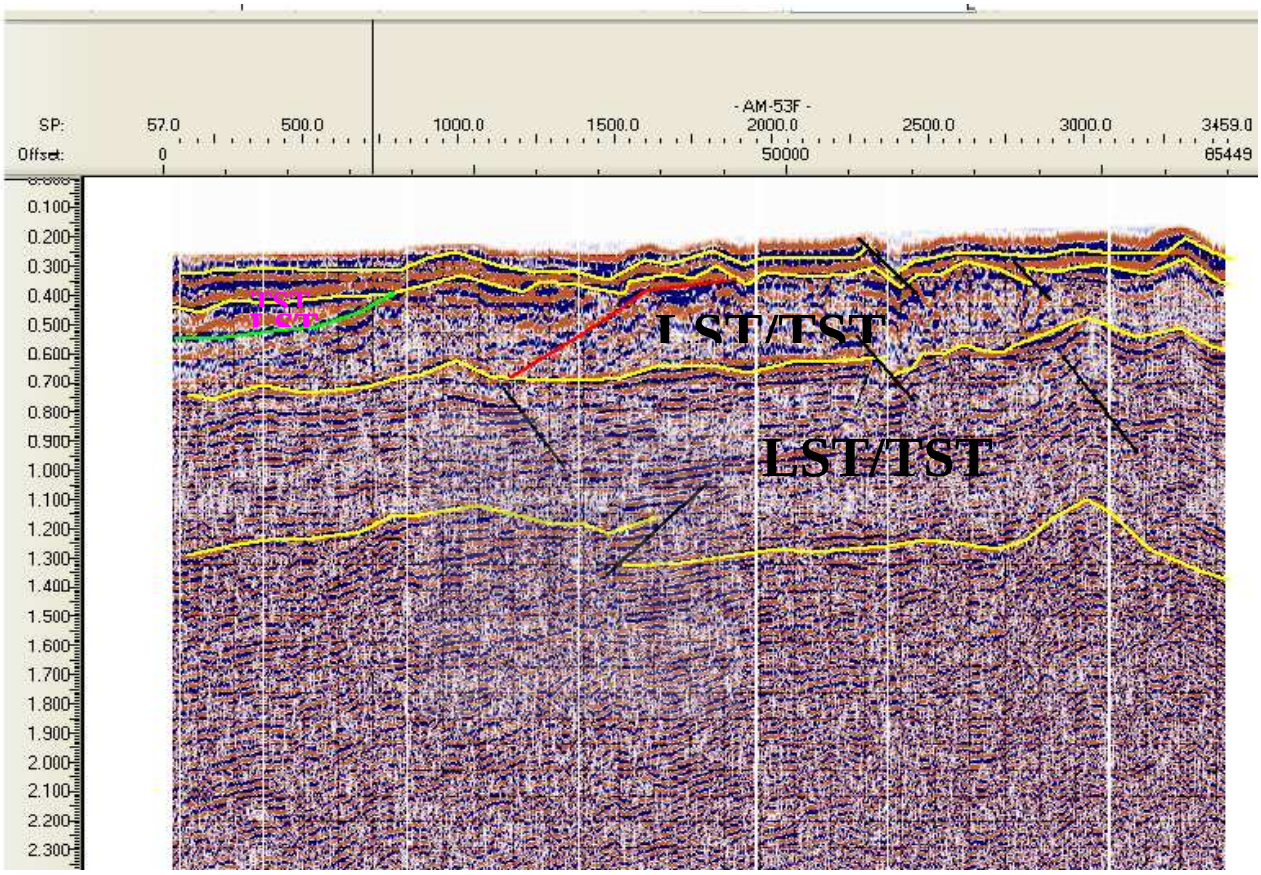

Fig. 4-2. Interpreted seismic section line AM-53F where yellow lines are sequence boundaries, green line transgressive surfaces and black lines fault lines.

Also there is Cretaceous/Tertiary unconformity at depth 0.500-0.800sec at the north-eastern part of the section. The basement rocks start to show at depth 1.600sec downwards. There are several toplapping at the middle of the section at Shot Point (SP) 1250 at depth 0.800sec of the Cretaceous/Tertiary unconformity which is rolling over to growth fault and faulted at SP 1950. The faulting trend is regular though faulted in opposite directions but of the same trend. The line A87-047 (Fig. 4-3) controlled by wells

K_D1 and A_U1 in block 3 on the top showing regular deposition of Tertiary sequences. There is rifting between SPs 1150 and 1300 just below the Tertiary sequences.

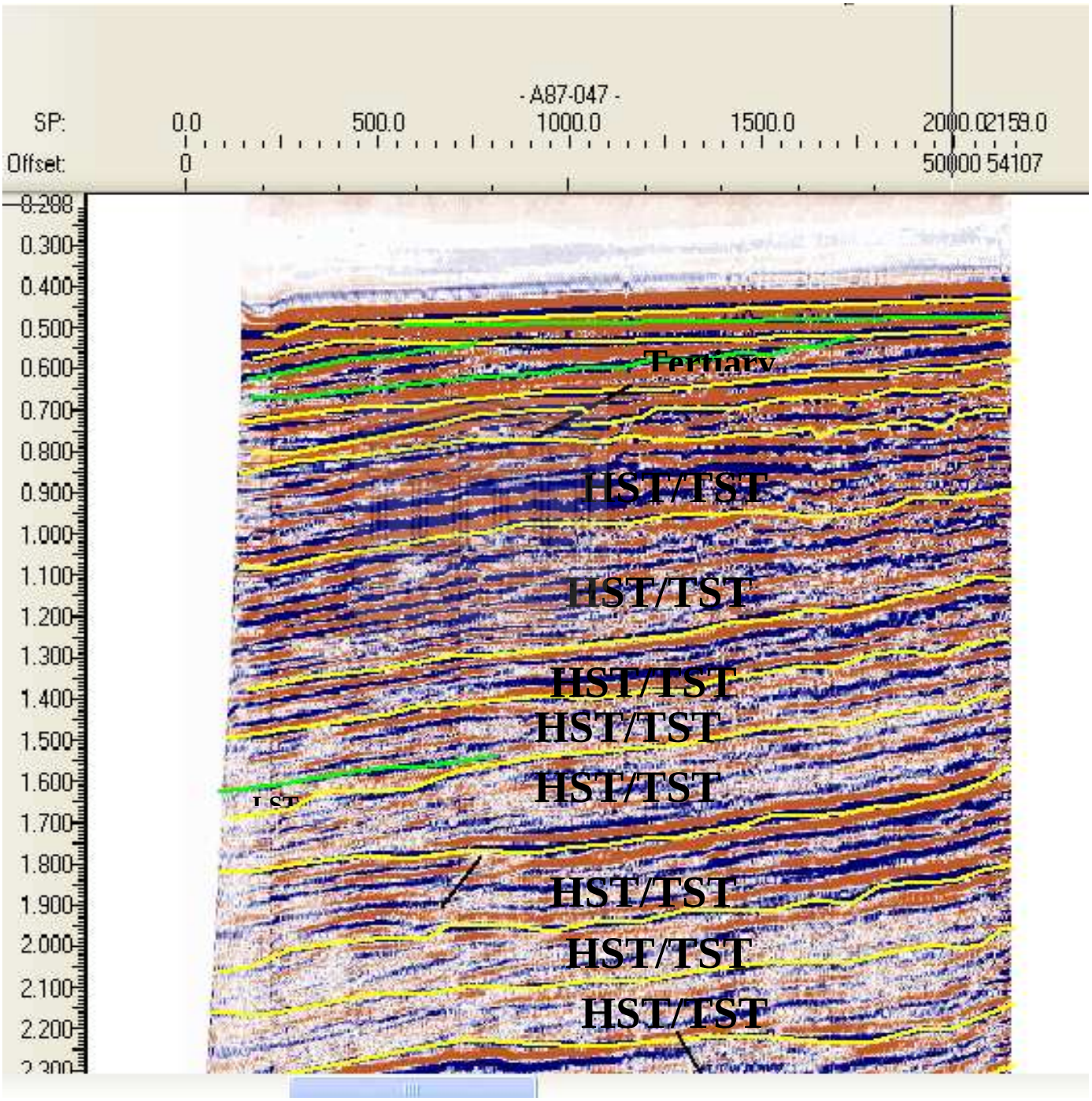

Fig. 4-3 Interpreted seismic section line A87-047 where yellow lines are sequence boundaries, green lines transgressive surfaces and black lines fault lines.

The Tertiary/Cretaceous unconformity separates the Tertiary sequences from the Cretaceous sequences. The faulting is in the same direction as seen in SPs 600 and 780 at depths 1.500 and 1.900sec respectively. The sediments are deposited regularly in Upper Cretaceous basin floor as fan. Line A81-061 (Fig. 4-4) controls wells A_C2 and A_C3 in block 4.

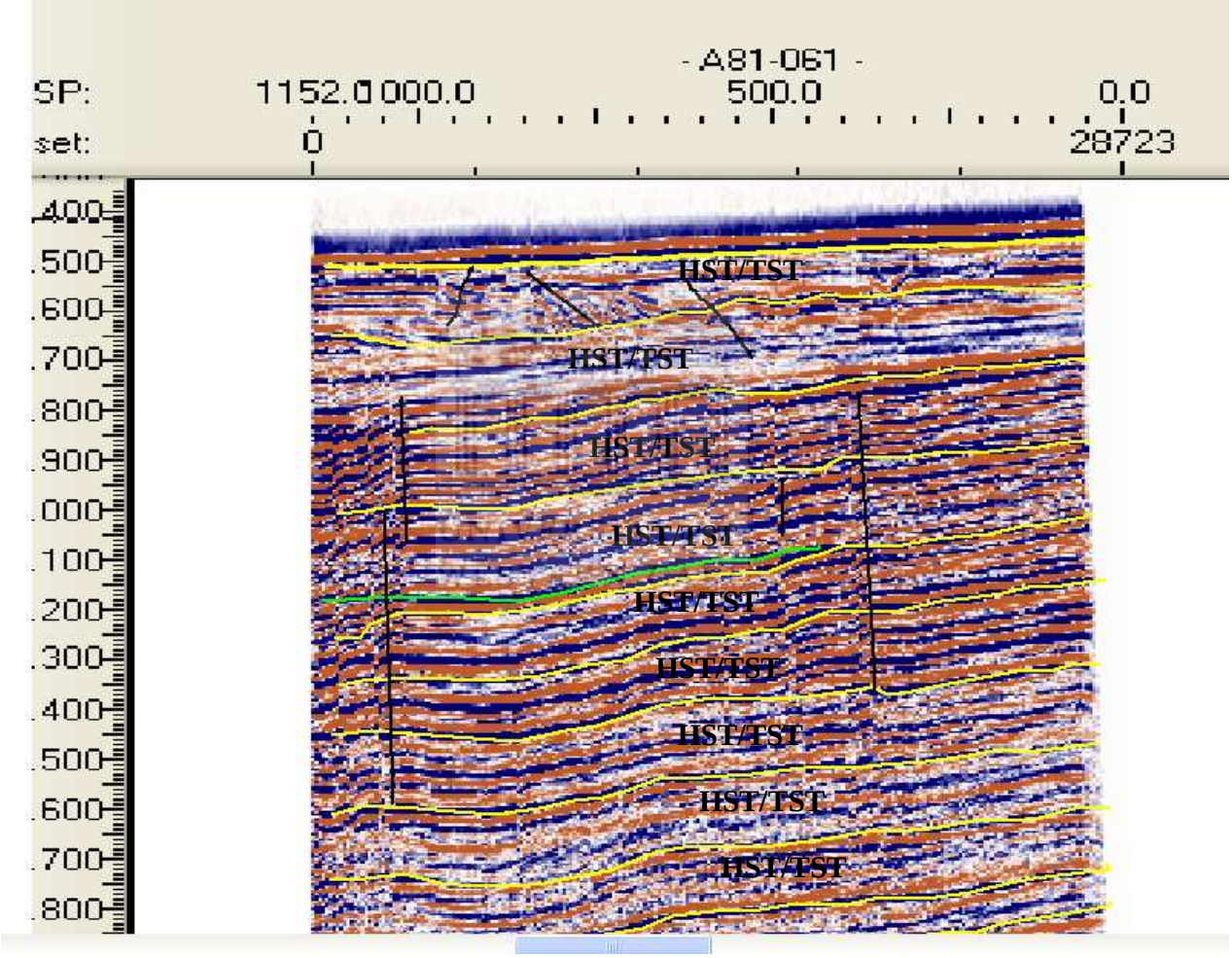

Fig. 4-4. Interpreted seismic section line A81-061 where yellow lines are sequence boundaries, green line transgressive surfaces and black lines fault lines.

The sediments are Upper Cretaceous basin floor fan. Within the section there is rifting between SP 25 and 75 at depth 0.600sec. There is toplapping between SPs 150 and 200 on the surface at depth 0.600sec. The faulting trend is in the same direction at the western

part of the section. Towards the east the trending is same but different from the one at SP 600.

4.3 Lithostratigraphic interpretation

Detailed qualitative interpretation of wireline log suite was carried out, thus allowing lithology and depositional patterns to be inferred from the well succession cross examined. This was based on the well log response of the sedimentary deposits which may equate to trends in depositional energy and hence the sedimentary infill pattern. The Gamma ray log shale reference line of 50 % API was chosen for all the API value range in this study. Deflection to the left and right to this reference line indicate sand and shale respectively.

Much emphasis was placed on the Gamma ray log as a tool for lithologic interpretation. The interpretation was cross examined with the available log in order to confirm that they corroborate the same interpretation. This interpretation which requires that certain characteristics of the open-hole tool be known and a systematic approach be followed was utilised in this study by comparing the logs horizontally starting with Gamma ray log to their other available logs.

Broad classification of litholgy into sand, claystone and shale using characteristics log motifs of these lithological indicators were used in identification and delineation of the logged interval.

4.3.1 Lithostratigraphic interpretation of well succession

Lithostratigraphic interpretation was based on the relative percentage of sand and shale and the presence of shale intercalation. Two major lithostratigraphic units encountered are ones between bottom log and 6At1 and those above 6At1 and 14J1 unconformities in the correlated wells (Fig. 4-5).

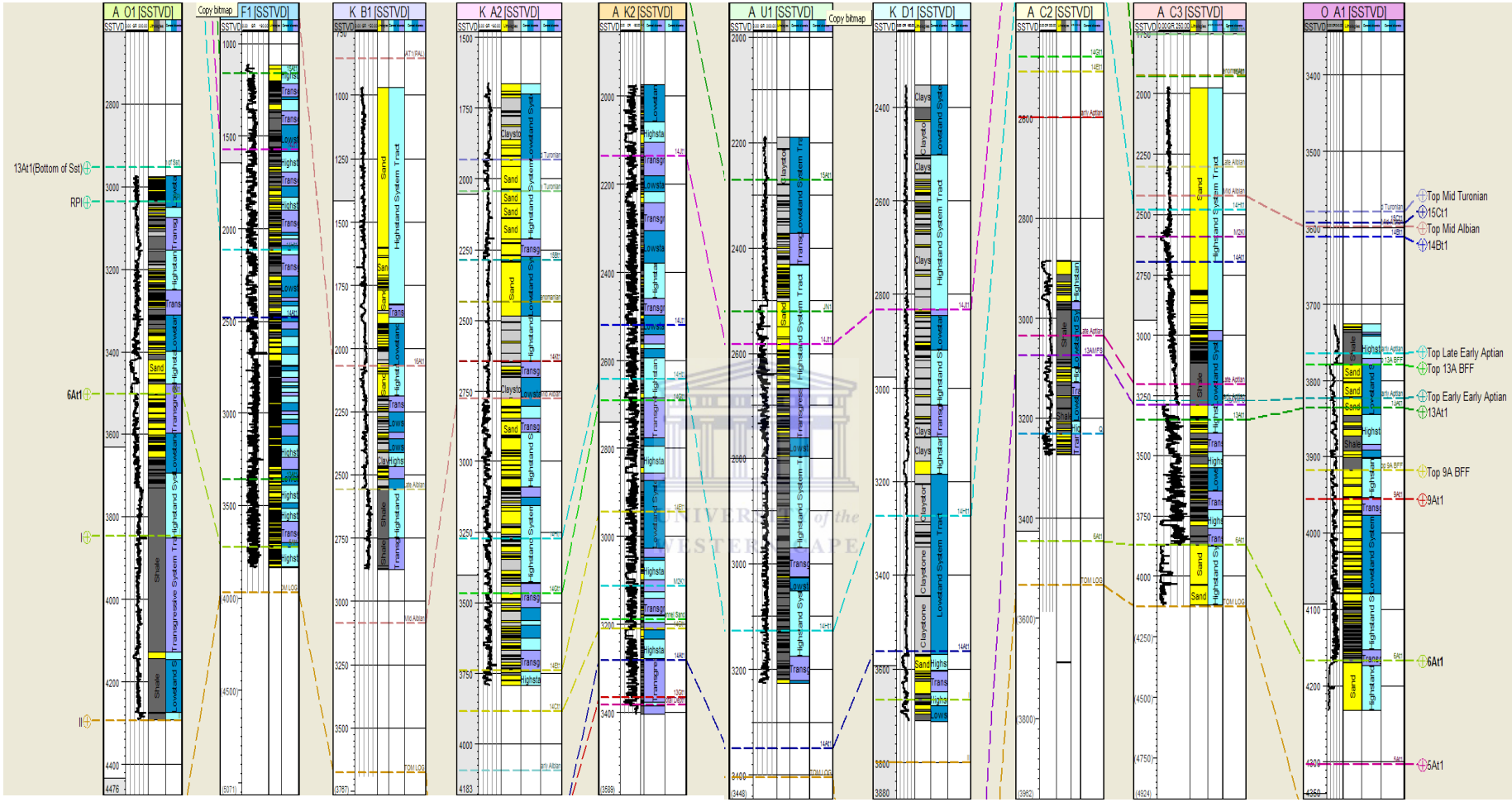

Fig. 4-5. The correlation of the wells used in the study

Bottom log-6At1 (reservoir zone)

These consist of sand predominantly sandy with little or no shale intercalation. The predominantly sandy nature of the deposit suggests deposition in high energy depositional environments, probably during the progradational phase of the basin (Fig. 4-5).

The 6At-14At1 (reservoir zone)

These consist of thick succession of sands and shale intercalations with sands (upper paralic), upper marine and lower paralic. Members consist of alternation of sand and shale sections subdivided into three lithofacies units as follows:

1. The ones consist of predominantly sands interbeded with shales, thickness varies between 3500.38 m and 3656.28 m in well A_O1. The serrate cylinder upward fining and occasional upward coarsening motif of the gamma ray (GR) log probably represents subaqueous channel and subaqueous mouth bar deposits (Fig. 4-5).
2. Monotonously shaly except for minor serrate cylinder shaped subaqueous channel sands noted over intervals 3550 m to 3872 m in well A_C3. The predominantly shaly character of this sub unit suggests deposition in low energy probably deep marine setting.
3. Predominantly sandy with alternating shale and sands observed on the GR log, with the shaly beds usually thinner than sandy one. Shale beds become progressively thicker at depth with shallower portion becoming sandy (Fig. 4-5).

The sands show hybrid unit consisting of a build up of multi-serrate cylinder-shaped, upward fining, as well as upward coarsening units, probably of subaqueous channel and barrier bar deposits in shallow water setting. The sand thickness varies between 21 m and 70 m in wells A_K2 and A_U1 in sequence IV marked by 14JTI unconformities.

The upper marine stands out amongst local members in the regional study. On the GR log studied it occurs in depth 968 m to 1723.43 m in well K_B1. It lower limit is defined by a sharp deflection from sand to claystone. It is predominantly shaly in character with minor sandy portion. The predominantly shaly base in well A_U1 is indicative of deposition in a low energy depositional environment well. The sands grade vertically upwards into the transitional shallow marine sand as observed in the well (Fig. 4-5).

Cycle frequency and stacking patterns

Eight depositional sequences bounded by nine sequence boundaries have been delineated in the area of study. Each of these sequences is produced by one cycle of sea level fluctuation and have been designated sequences I, II, III, IV, V, VI, VII and VIII from base to top of the study area.

Close examination of these eight sequences revealed that all sequences occur regionally throughout the study area and are underlain by Type 1 sequence boundaries. Sequence stratigraphic analysis of the wells and the subsequent comparison with seismic reflection permitted the delineation of the sequence stratigraphic elements of the depositional sequences (Fig. 4-5).

Lowstand systems tract (LST) occurs in some of the sequences represented by slope complex. In some instances the prograding complex overlies it. The basin floor fan is absent in some cases while recognition of the slope fan is a pointer to deposition on the continental slope or shelf edge.

Slope fan deposition occurred as sea level bottoms out and begins to rise and has seismic impression of gull-wing shape with an indication of channelization and some chaotic flows. Some of the slope fan complex show evidence of sharp base and slightly blocky pattern suggestive of basin floor fan but with fining upward sequence pattern. This slightly blocky pattern was interpreted to be that the well penetrated the channel centre. The sharp base within the crescent is indicative of sand in channel, while the bell shaped fining upward pattern suggests channel abandonment (Fig. 4-5 in well A_U1).

Deposition of transgressive systems tract resulted from a rapid rise in sea level above the relic shelf break causing sandiest sediments to be moved landward. Its top which is the maximum flooding surface is represented by laterally extensive and thick sometimes doublet seismic reflection while on well logs it is identified as clay rich layer with high gamma ray and low resistivity values.

Highstand systems tract recognized are laterally extensive and are associated generally with a of period stand still sea level as represented by the aggradational pattern as sand build basinward. However, the stand still aggradational pattern was dominant suggesting cessation of sediments supply in Fig. 4-5 well A_O1.

The age of the eight sequences (I-VIII) ranged from Barremian to Campanian (6At1 and 17At1; the marked major unconformities in the basin). None of the 33 sandstone samples collected for this study intersected sequence VI (Table 4.1). 40 shale samples were collected for this study (Table 4.2). The source shale samples intersect sequences II to VIII. None of the samples intersected the first sequence of Barremian age.

Table 4.1. The reservoir rock samples positions within the systems tracts and the sequences.

Reservoir rock samples	Age	Systems tracts	Sequences
K_B1 (1350 m)		HST	
K_B1 (1910 m)	Campanian	TST	VIII
		HST	
K_B1 (1950 m), K_B1 (2060 m)	Santonian	LST	VII
		HST	
	Coniacian	TST	VI
A_F1 (1178 m), A_F1 (1179 m), A_F1 (1180 m), (K_A2 (1690 m)		HST	
K_A2 (1963 m), K_A2 (2215 m)		TST	
	Turonian	LST	V
		HST	
A_U1 (2688 m), A_U1 (2694 m), A_U1 (2697 m)		TST	
	Cenomanian	LST	IV
K_D1 (3652 m), K_D1 (3174 m), K_A2 (2765 m)		HST	
		TST	
K_D1 (3272 m), K_A2 (2795 m), A_C3 (3597 m)	Albian	LST	III
		HST	
A_C2 (3245 m), A_C2 (3246 m), A_C3 (3670 m), A_C3 (3675 m)		TST	
K_D1 (3692 m)	Aptian	LST	II
A_O1 (3940 m), (3950 m), (3242 m), (3175 m), A_C3 (3727 m)		HST	
A_O1 (3305 m), (3493 m)		TST	
A_O1 (3601 m), (3679 m)	Barremian	LST	I

Table 4.2. The source rock samples positions within the systems tracts and the sequences.

Source rock samples	Age	Systems tracts	Sequences
		HST	
K_B1 (1855 m)	Campanian	TST	VIII
K_B1 (2084 m)		HST	
	Santonian	LST	VII
K_B1 (2423 m), K_B1 (2718 m), K_B1 (2721 m), K_B1 (2808 m)		HST	
K_B1 (2742 m)	Coniacian	TST	VI
A-F1 (1270 m), A-F1 (1290 m),		HST	
A_F1 (1300 m), A_F1 (1320 m)		TST	
A_F1 (1430 m), K_A2 (1855 m)	Turonian	LST	V
A_K2 (2405 m), K_A2 (2572 m)		HST	
A_F1 (1700 m), (1980 m), (1990 m), K_A2 (2655 m) A_K2 (2525 m), (2530 m)		TST	
A_F1 (1780 m), A_U1 (2210 m), (2220 m), A_K2 (2540 m), (2545 m)	Cenomanian	LST	IV
K_D1 (2947 m), (2979 m), (2988 m), (3008 m)		HST	
A_U1 (3068 m), K_D1 (2997 m)		TST	
	Albian	LST	III
O_A1 (3741 m), (3756 m), (3741 m)		HST	
		TST	
K_D1 (3447 m), A_C3 (3129 m), O_A1 (3771 m), (3789 m), (3792 m)	Aptian	LST	II
		HST	
		TST	
	Barremian	LST	I

4.4 Petrography results

4.4.1 Thin section interpretation

LST

The thin sections at depths 3679 m and 3601 m in well A_O1 (Fig. 4-6) under cross polarised light (XP) shows ductile mineral mica in spec scattered within the entire mass which is deformed by looking at the shape. In well K_B1 at depth 2060 m the mica is flattened or platy which can be as a result of severe compaction and it is embedded within quartz. There is also presence of glauconite at this depth, which is shown by green colour in both plane (PL) and cross polarised lights. The glauconite is diagnostic of the continental shelf marine depositional environment which might have been formed due to diagenetic alterations of mica under a reducing condition (Odin and Matter, 1981). There are evidences of fracturing denoted by the blue arrows (Fig. 4-6) in wells K_A2 (2795 m); K_B1 (2060 m); K_D1 (3692.5 m, 3272 m) and A_C3 (3597.5 m). The cementing material within the setting is micritic calcite. The cementing material might have filled the pore spaces before quartz cement could grow. The porosity within the setting is being controlled by lithic grains of detrital ductile minerals. There is evidence of healing of the fracture as shown by sample from well K_B1 (1950 m) by quartz. There must have been injection of magma rich in quartz to be able to crystallise in the fracture created as a result of deformation. The feldspar which is one of the major mineralogical compositions of sandstone is seen to have been altered to clay. The sandstone is polycrystalline in nature. Porosity within the setting is generally poor because of feldspar conversion to clay. The micas are angular to sub-angular meaning that they might not have travelled far from their source to place of deposition. The grain contacts are concave-convex surface that may have likely resulted from compaction. There is evidence of clay variation with depth.

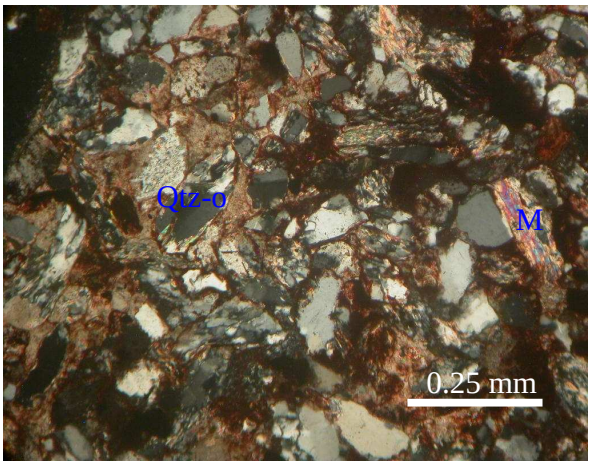

A_O1 (3679m) XP

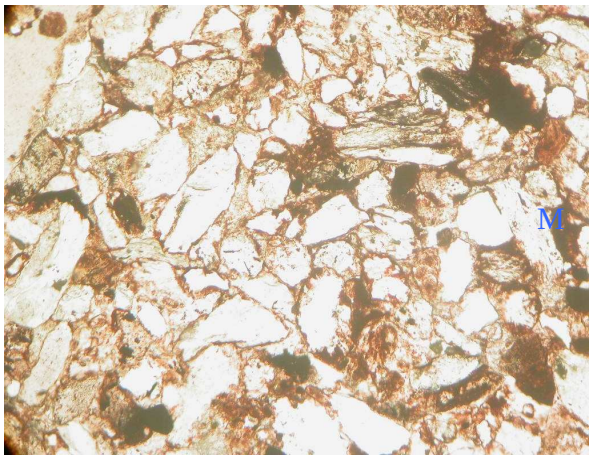

A_O1 (3679m) PPL

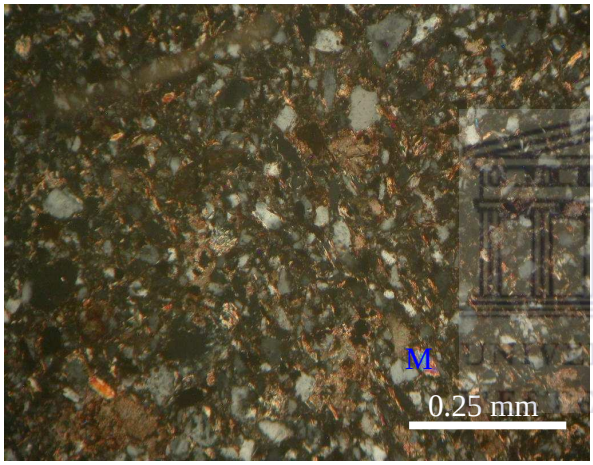

A_O1 (3601m) XP

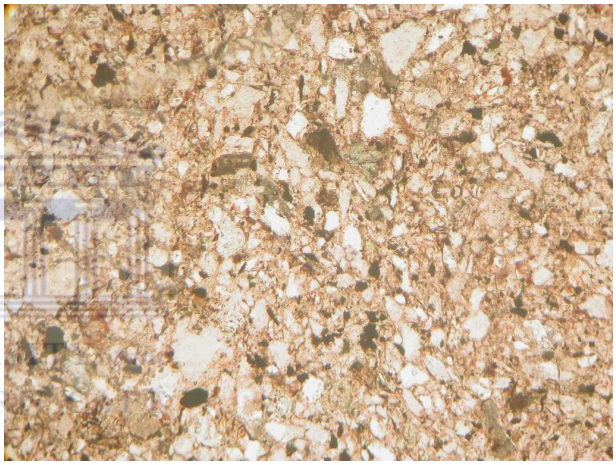

A_O1 (3601m) PPL

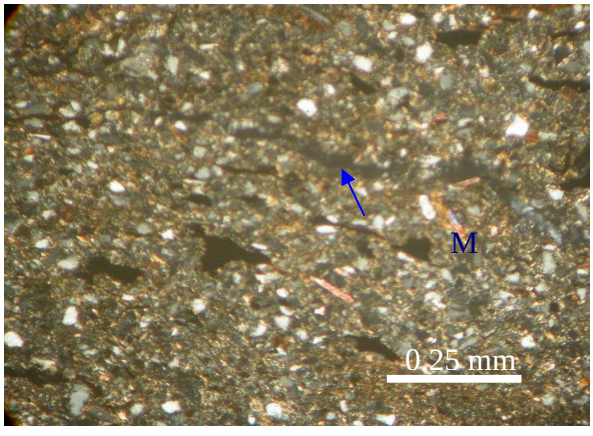

K_A2 (2795m) XP

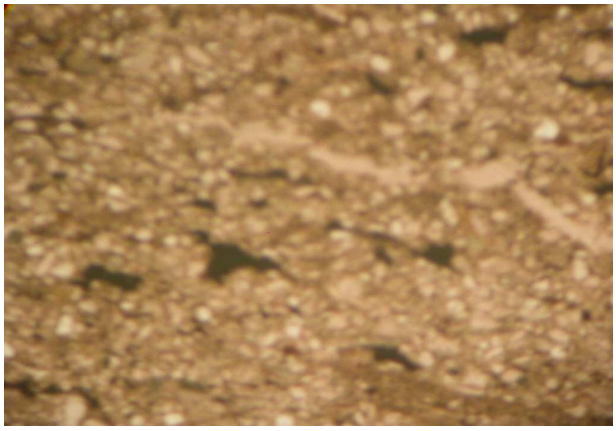

K_A2 (2795m) PPL

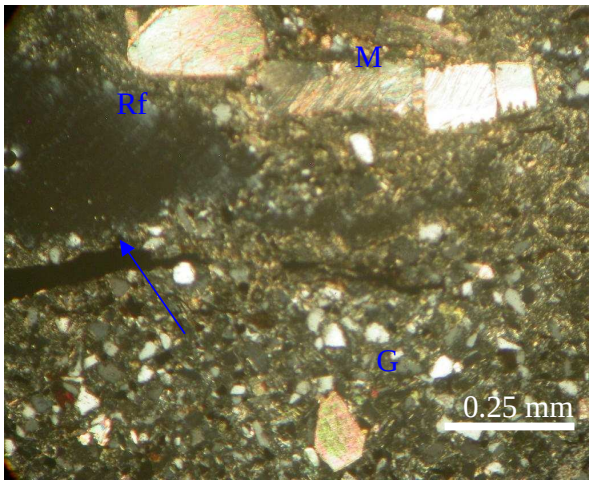

K_B1 (2060m) XP

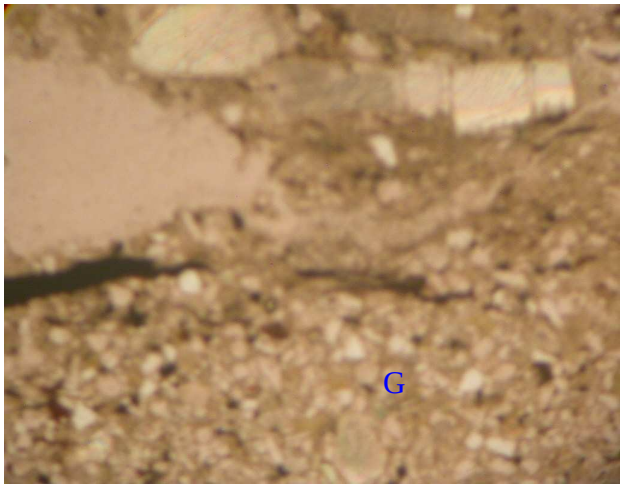

K_B1 (2060m) PPL

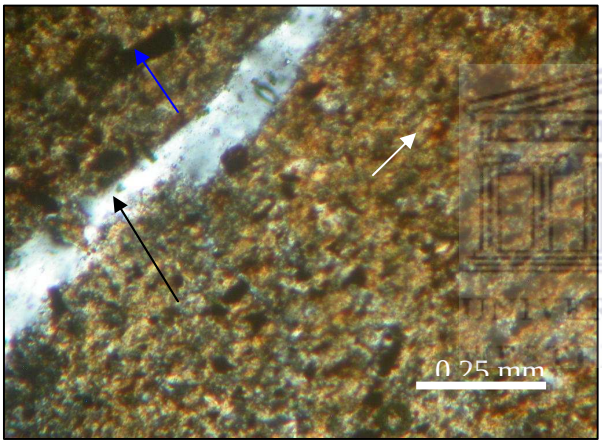

K_B1 (1950m) XP

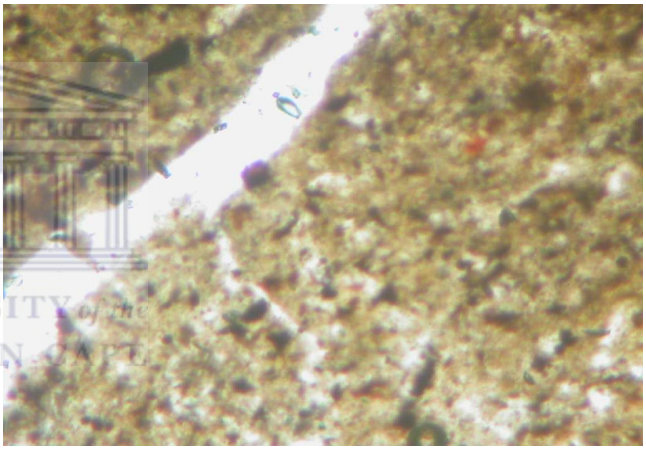

K_B1 (1950m) PPL

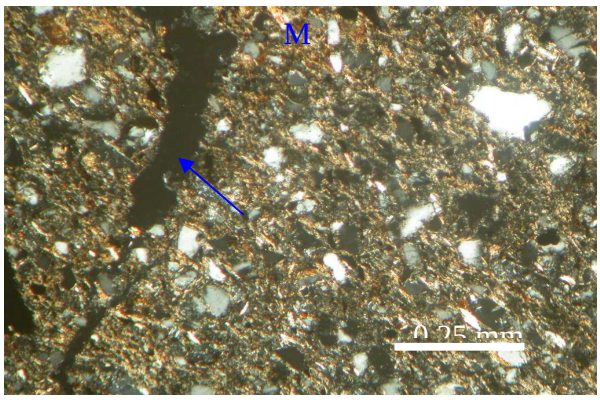

K_D1 (3692.5m) XP

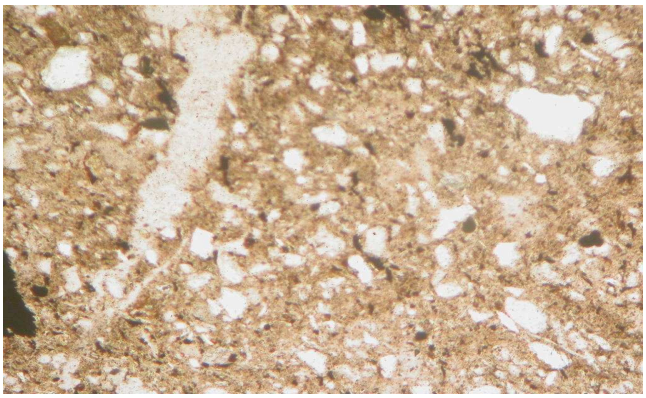

K_D1 (3692.5m) PPL

K_D1 (3272m) XP

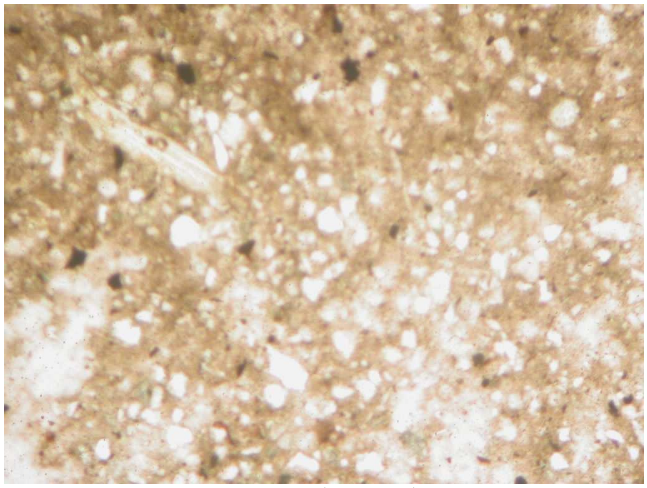

K_D1 (3272m) PPL

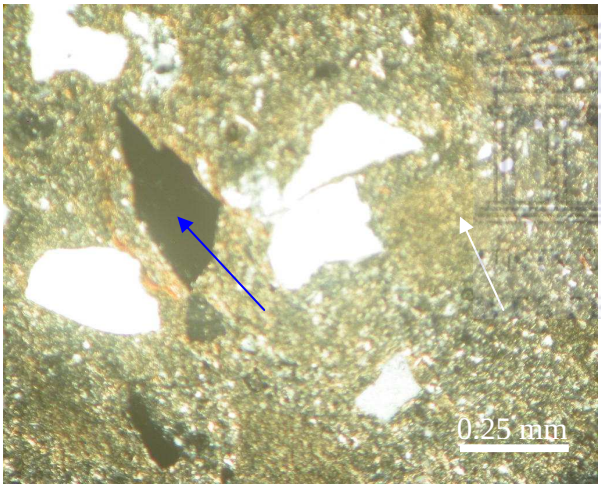

A_C3 (3597.5m) XP

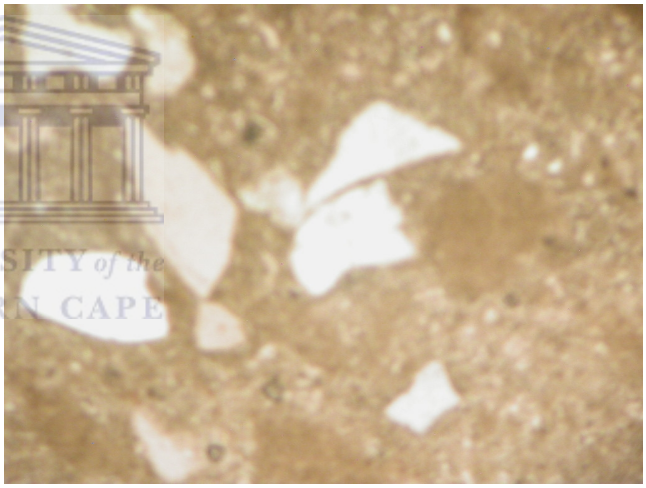

A_C3 (3597.5m) PPL

Fig. 4-6. The photomicrograph of samples collected within LST showing different minerals both in plain (PPL) and cross polarised (XP): Micas (M), Quart (Qtz), Quartz overgrowth (Qtz-o) and Glauconite (G). The arrows: blue showing evidence of fracturing, white showing dense micritic calcite cement and black, filled fractured with quartz.

TST

The sample at depth 3305 m in well A_O1 (Fig. 4-7) shows a good attribute of well sorted sandstone. The clay, chlorite and mica are completely mixed within the matrix indicating a severe diagenetic event. The detrital grains are coated by clay and mica, at

depth 3493 m in the same well, the micritic calcite holds the grains acting as a cementing material. Evidence of fracturing is seen in wells, K_A2 at depths 2215 m, and 1963 m; A_U1 (2688.1 m); A_C2 (3246.32 m) and A_C3 (3670 m). The presence of glauconite in well A_C3 at depth 3675 m is an indication of shallow marine deposition (Odin and Matter, 1981). In well A_C2 at 3245.16 m depth there is presence of pyrite. The framboidal pyrite in the setting is confirming the marine sedimentary environment deposition in reducing conditions within the TST (Sauer et al., 1992). There are over growth of quartz within the setting as shown in wells A_O1 (3601m); A_U1 (2694.05m); A_C2 (3245.16 m); A_C3 (3675 m) and A_C3 (3670 m). There are specs of mica as seen in A_O1 (3305 m); A_U1 (2694.05 m) and A_U1 (2688.1 m). They appear as specs except in A_C2 (3245.16 m) which shows complete alteration and grading. There is alot of chloritization within the setting. This must have been the one of the reasons why the porosity quality is generally poor. The fracturing and the pores are not linked hence the poor permeability characteristics within the setting (Fig. 4-7 in A_C2 (3245.16m). The clay clusters seen in the photomicrograph A_U1 (2697.55 m); A_U1 (2694.05 m); A_U1 (2688.1 m) and A_C3 (3670 m) must have resulted from alteration of feldspar due to diagenetic events. These series of diagenetic and post-depostional events must have been responsible for the poor porosity and permeability within the setting.

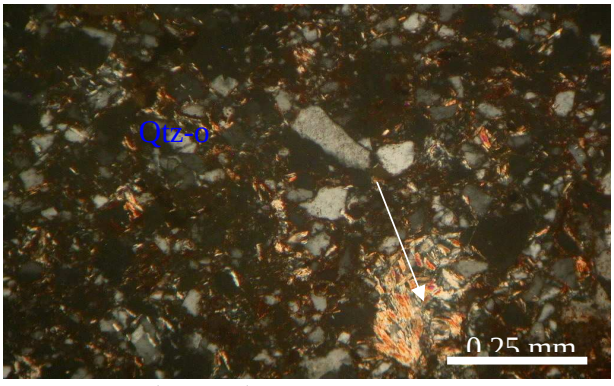

A_O1 (3493m) XP

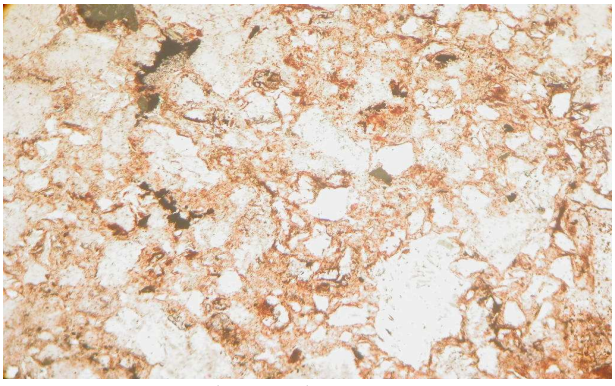
A_O1 (3493m) PPL

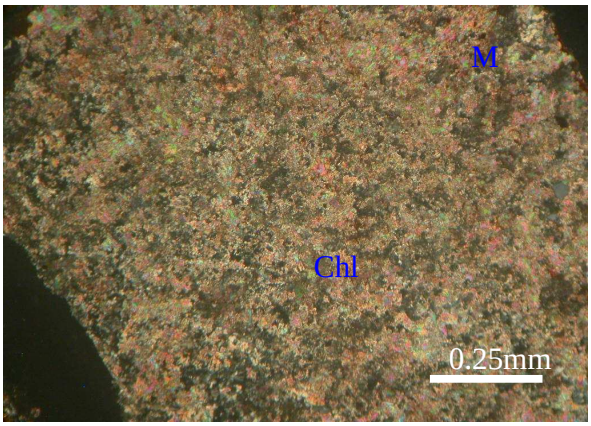

A_O1 (3305m) XP

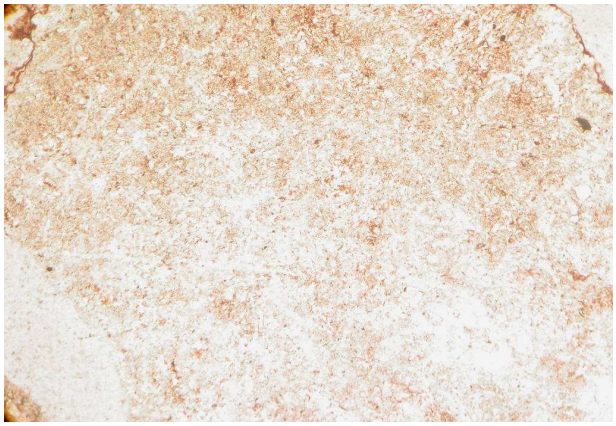

A_O1 (3305m) PPL

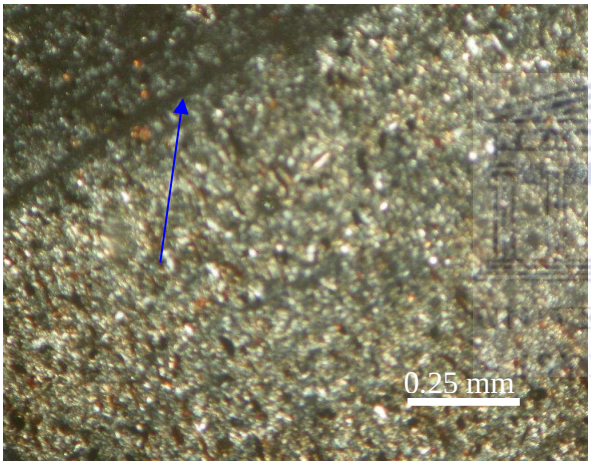

K_A2 (2215m) XP

K_A2 (2215m) PPL

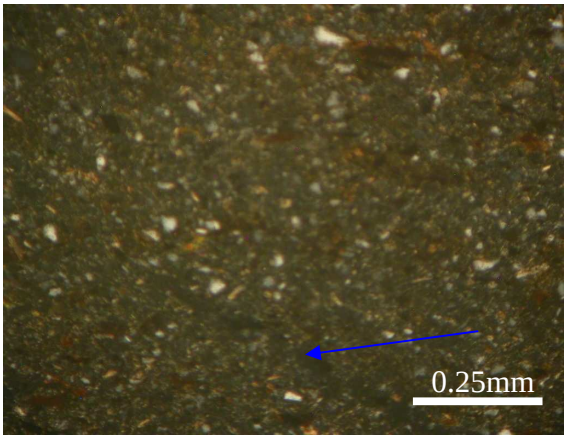

K_A2 (1963m) XP

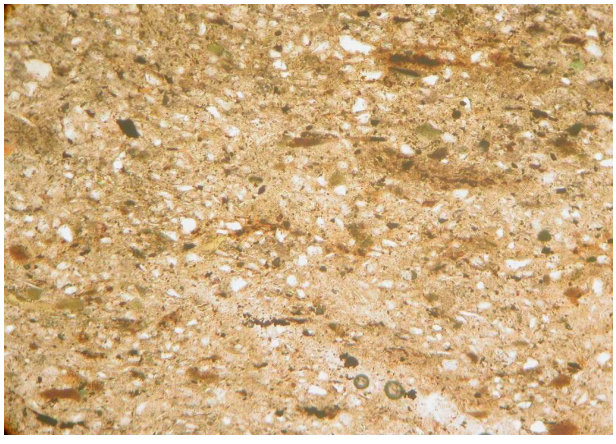

K_A2 (1963m) PPL

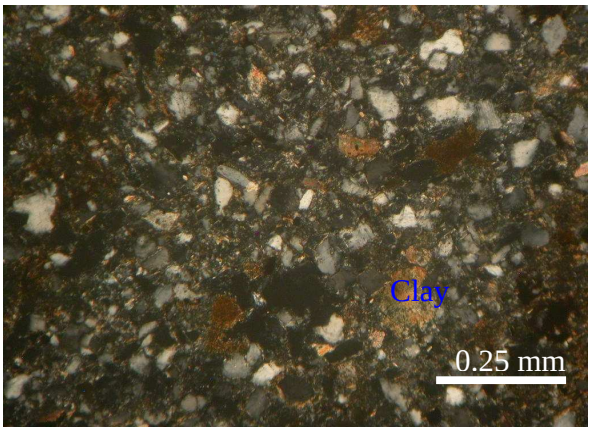

A_U1 (2697.55m) XP

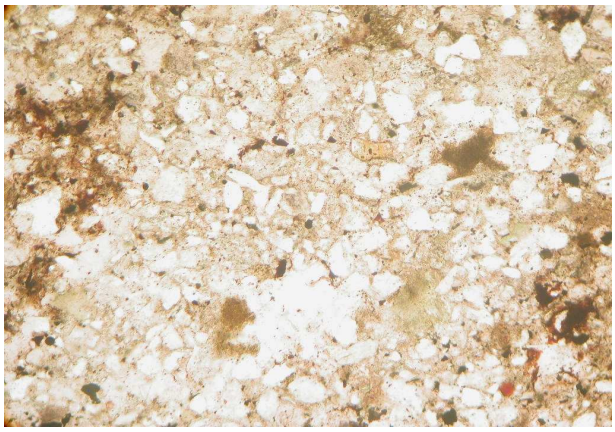

A_U1 (2697.55m) PPL

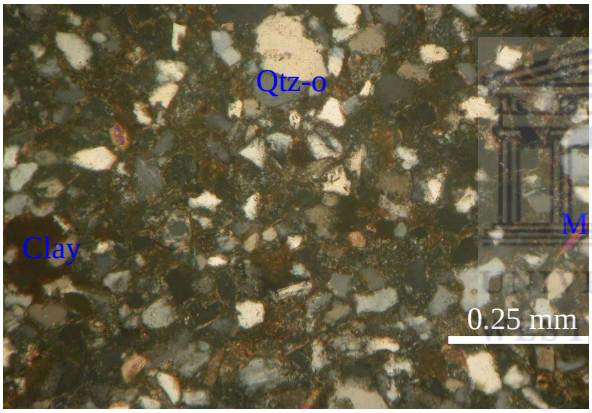

A_U1 (2694.05m) XP

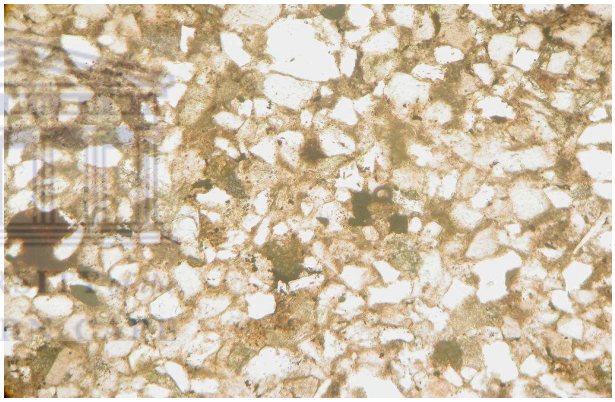

A_U1 (2696.05m) PPL

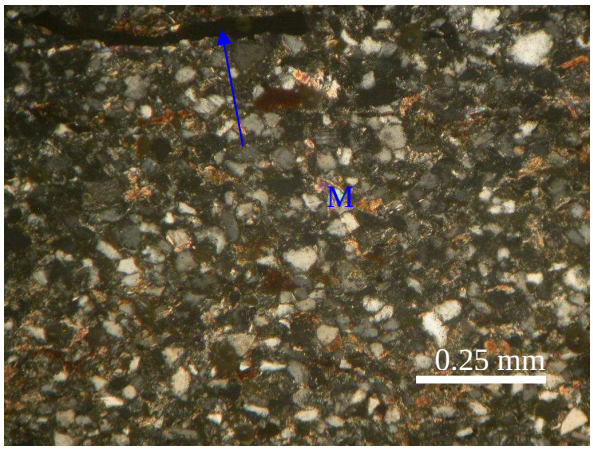

A_U1 (2688.1m) XP

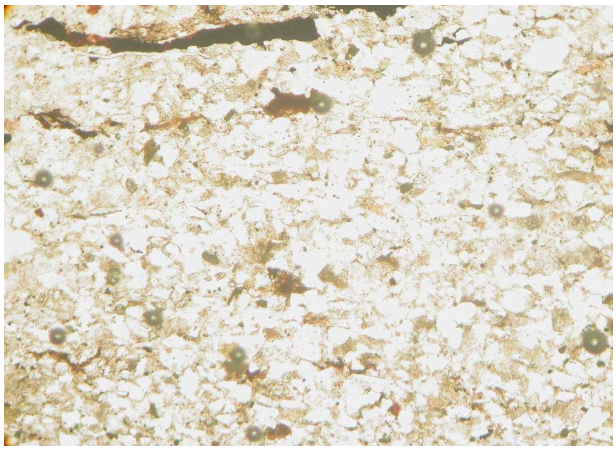

A_U1 (2688.1m) PPL

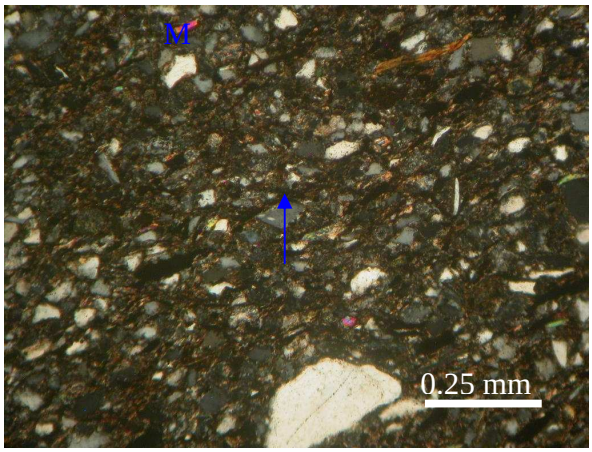

A_C2 (3246.32m) XP

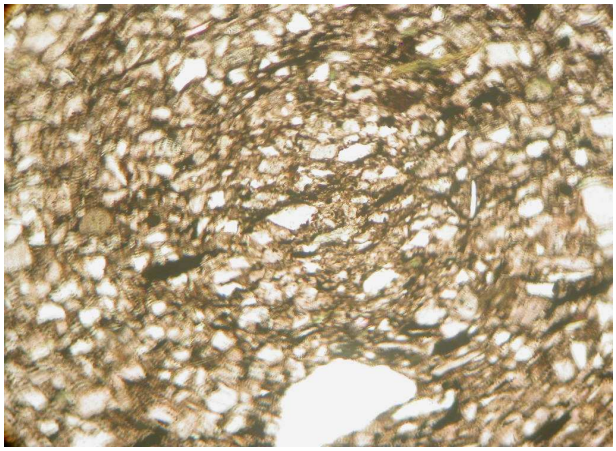

A_C2 (3246.32m) PPL

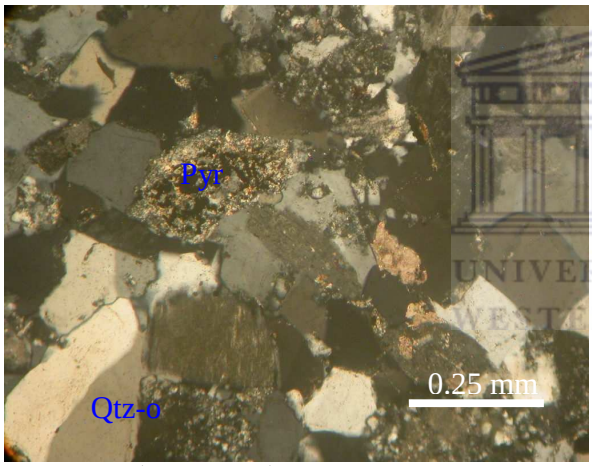

A_C2 (3245.16m) XP

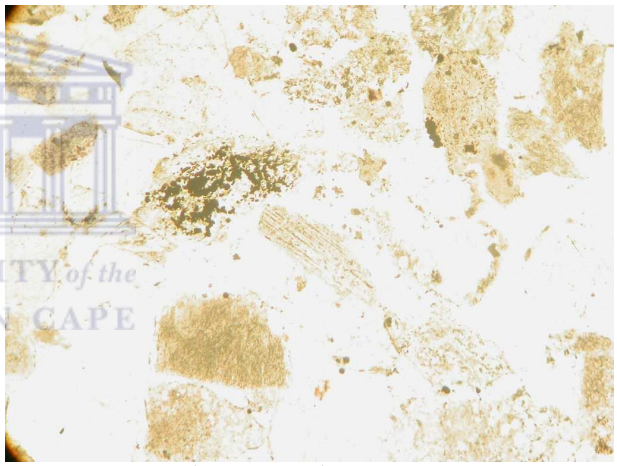

A_C2 (3245.16m) PPL

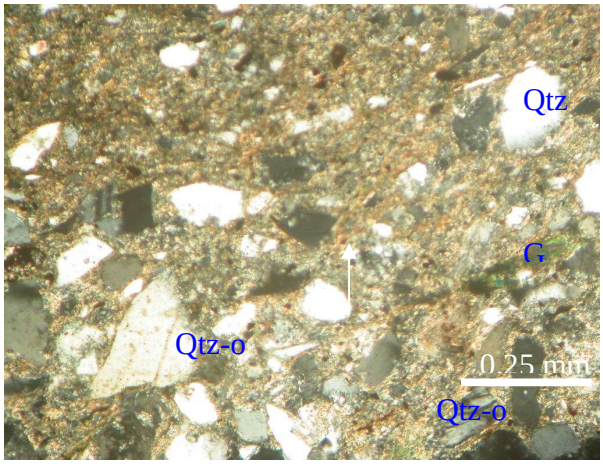

A_C3 (3675m) XP

A_C3 (3675m) PPL

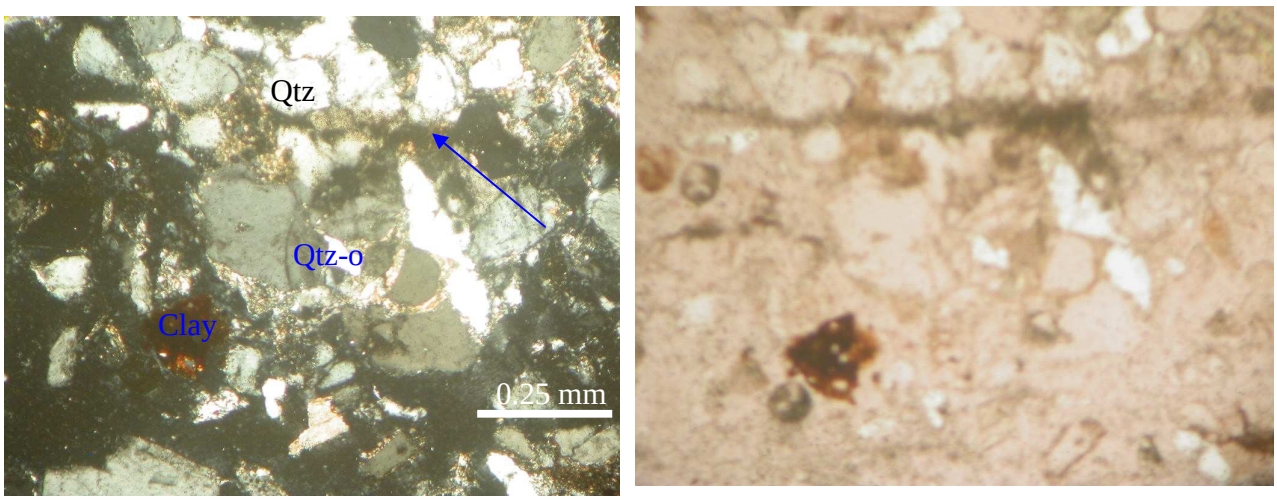

A_C3 (3670m) XP A_C3 (3670m) PPL

Fig. 4-7. The photomicrograph of samples collected within the TST showing different minerals both in plain (PPL) and cross polarised (XP): Micas (M), Quart (Qtz), Quartz overgrowth (Qtz-o), Pyrite (Pry), Chlorite (Chl), Clay and Glauconite (G). The arrows: blue showing evidence of fracturing and white showing dense micritic calcite cement.

HST

The oldest sample in well A_F1 (1180m) in the setting shows a complete cementation by calcite. The influence of calcite cements increase with depth. This is an attribute of a fluvial deposition. At depth 1180 m there is no trace of mica (Fig. 4-8). At 1179 m and 1178.5 m there are traces of elongated mica chips which might likely be as a result of compaction. There are also over growth of quartz within the setting. The well A_O1 at depths 3175m and 3242 m showed a lot of clay covering the detrital grains. There are also evidence of fracturing and precipitation of brown-reddish clays at the edges of the fractures. Glauconite droplets are seen in A_O1 (3175m) which may be due to alteration of mica by shallow marine diagenesis under a reducing condition. In well K_A2 at depth 2765 m, clay covers the entire detrital grains. At depth 1690 m of the same well, the detrital grains are very prominent, meaning that the influence of the clay increase with depth in the wells within the stratigraphic setting. In K_B1 at depth 1910 m there are evidences of fracturing whose intensity increase with depth. A clay ball was noticed in at depth 1950 m in well K_B1 which can be due to reworking of the sediments. Specs of glauconite also noticed in well K_B1 (1350m). K_D1 at greater depth, 3174 m shows

severe chloritization, its influence was reduced as depth 3652 m. In well A_C3 calcite mud (micrite) cover greater part of the detrital grains. Well O_A1 at depth 3874 m there is over growth of quartz and some flattened mica. The clay covers nearly all the detrital grains as seen at depths 3940 m and 3950 m in well O_A1. The influence of clay within HST is enormous. This must have been responsible for the poor quality of porosity and permeability in this stratigraphic setting.

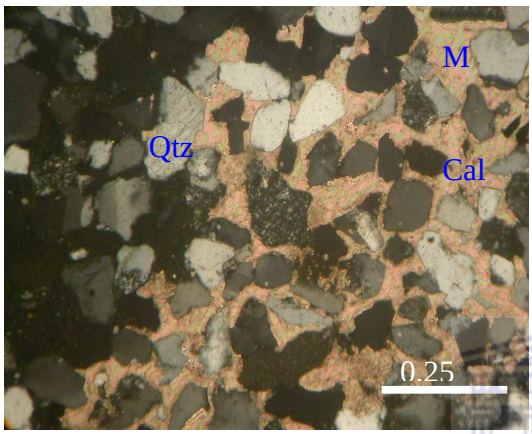

A_F1 (1180m) XP

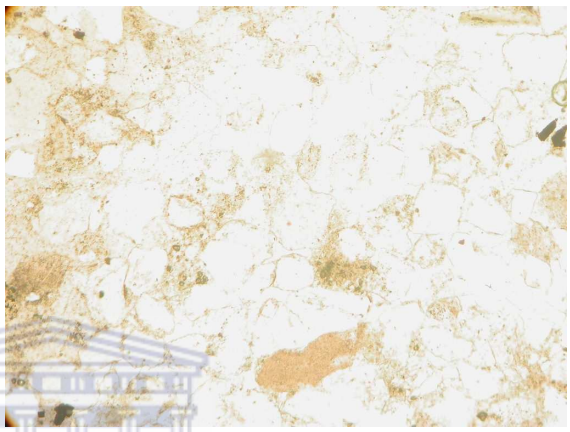

A_F1 (1180m) PPL

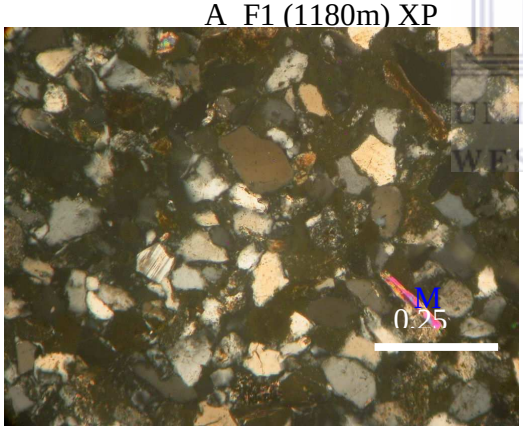

A_F1 (1179m) XP

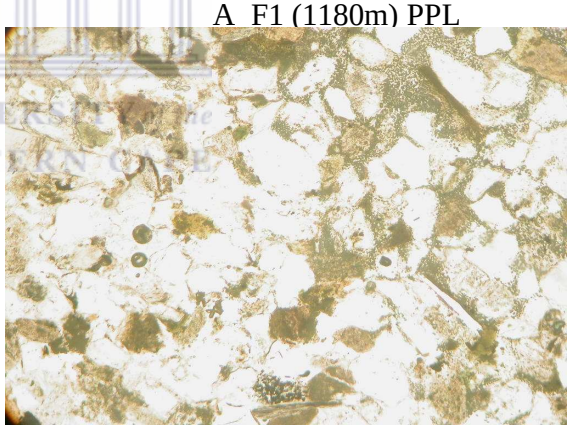

A_F1 (1179m) PPL

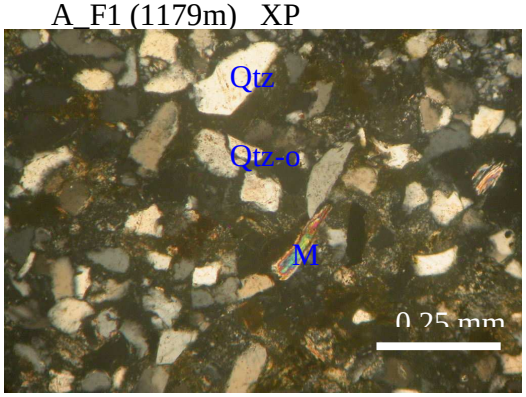

A_F1 (1178.5) XP

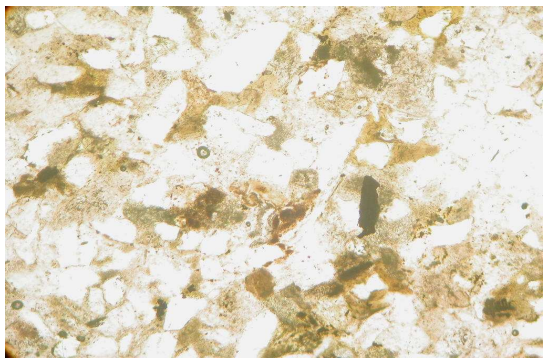

A_F1 (1178.5m) PPL

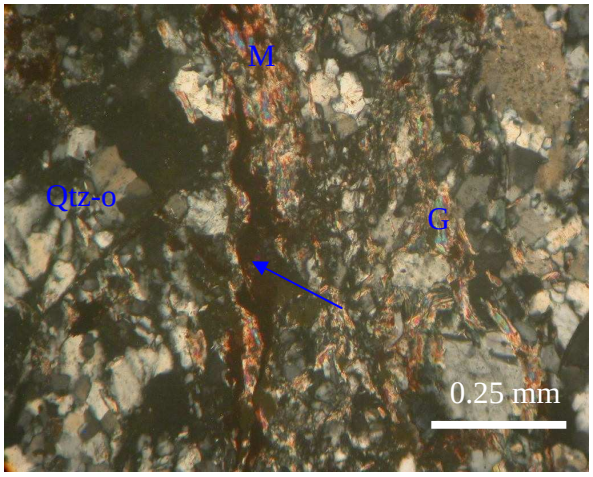

A_O1 (3175m) XP

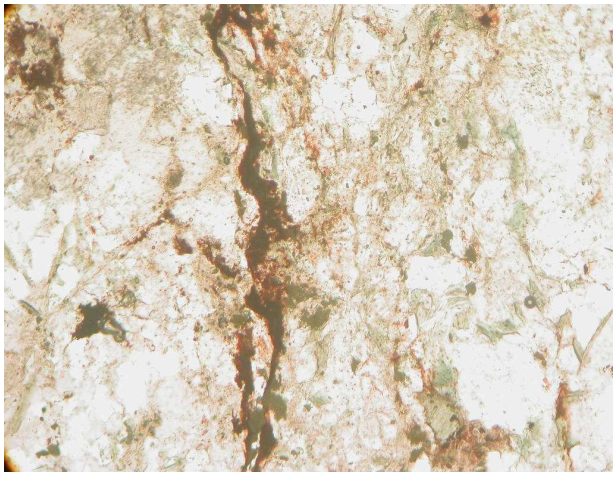

A_O1 (3175m) PPL

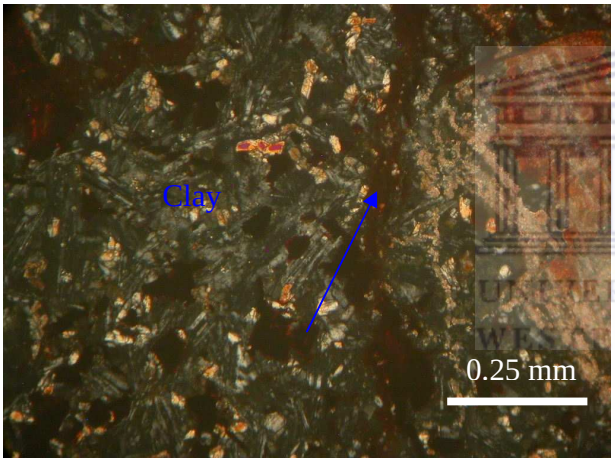

A_O1 (3242m) XP

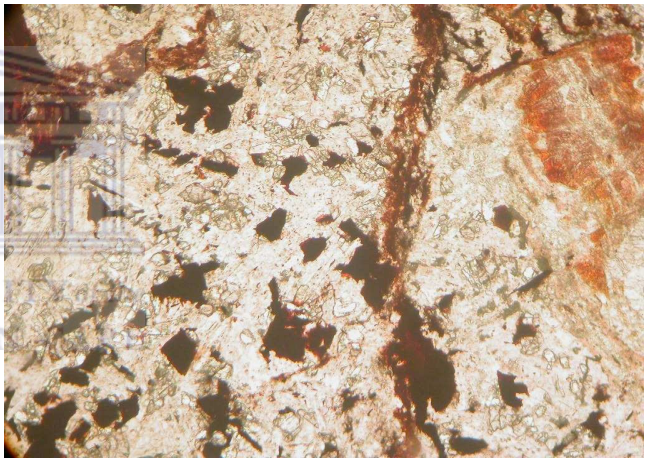

A_O1 (3242m) PPL

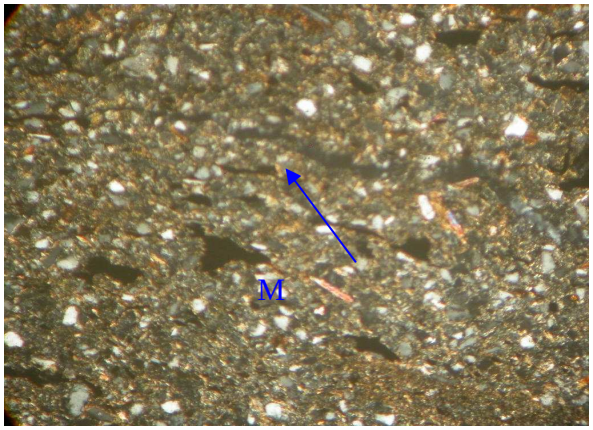

K_A2 (2765m) XP

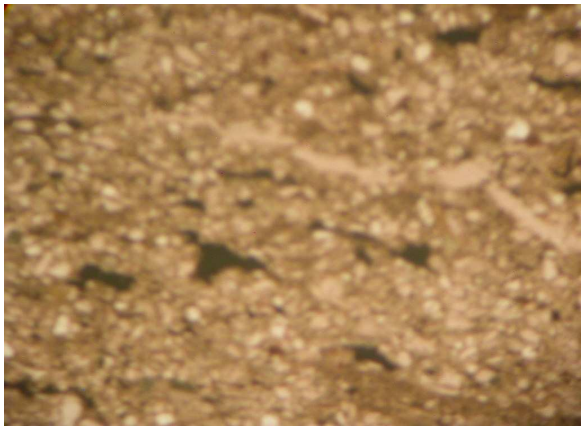

K_A2 (2765m) PPL

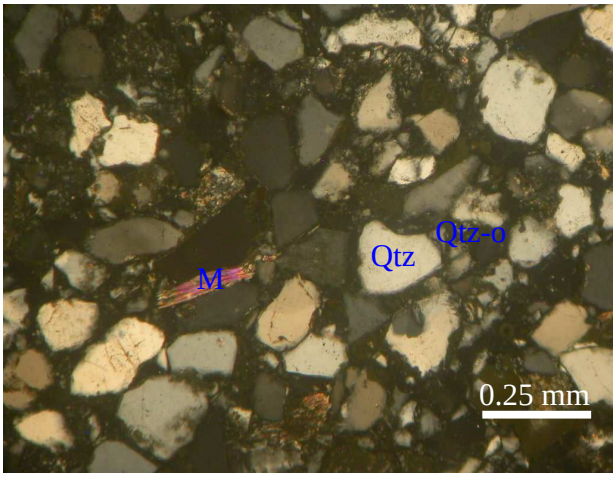

K_A2 (1690m) XP

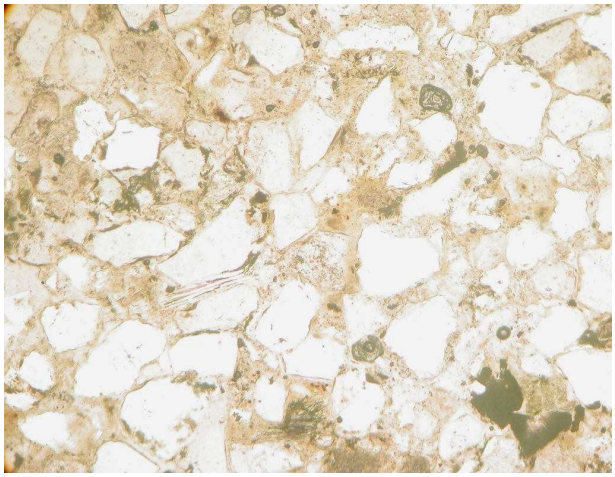

K_A2 (1690m) PPL

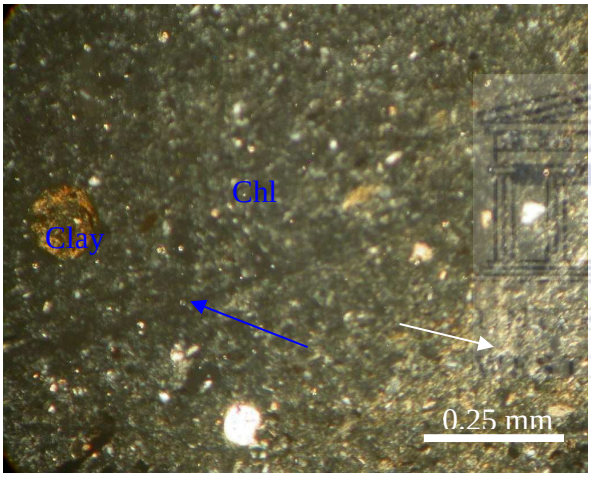

K_B1 (1950m) XP

K_B1 (1950m) PPL

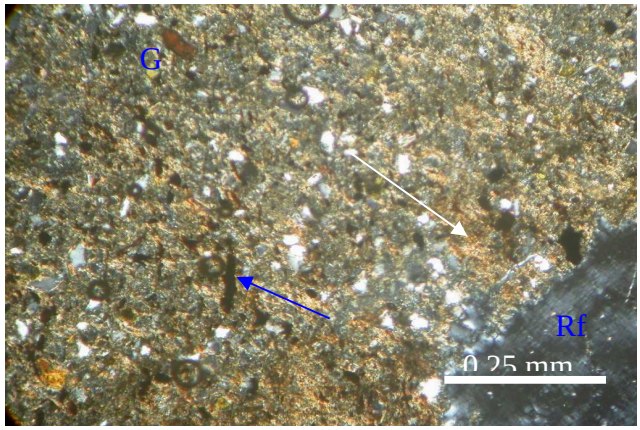

K_B1 (1350m) XP

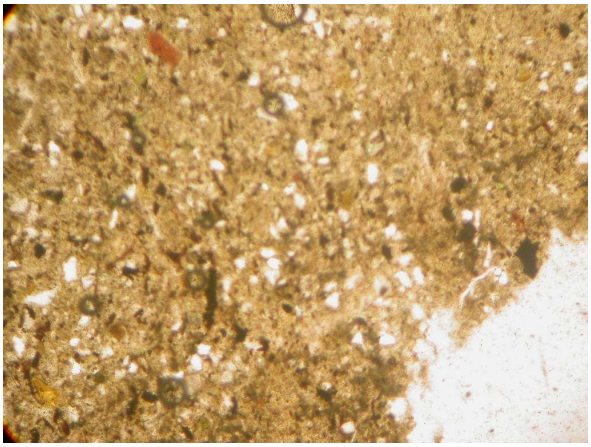

K_B1 (1350m) PPL

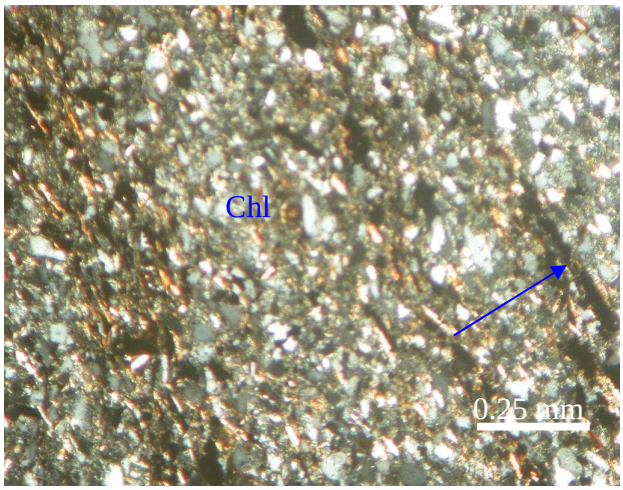

K_D1 (3174m) XP

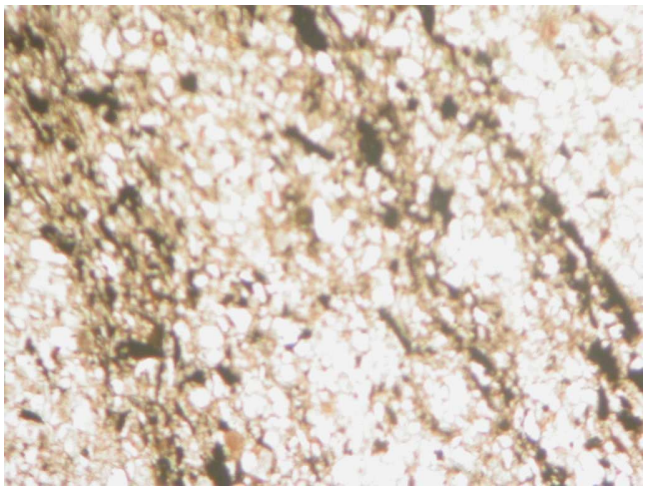

K_D1 (3174m) PPL

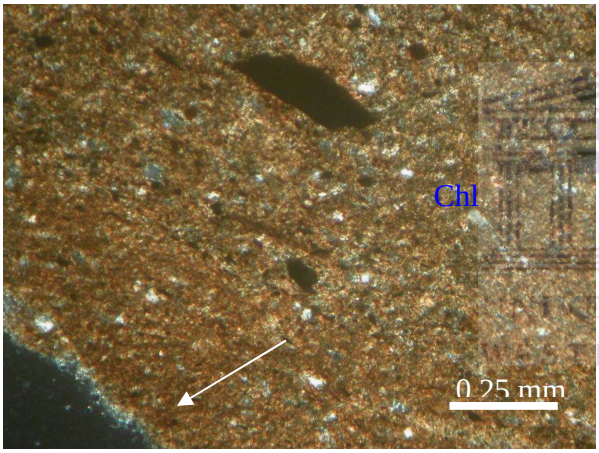

K_D1 (3652m) XP

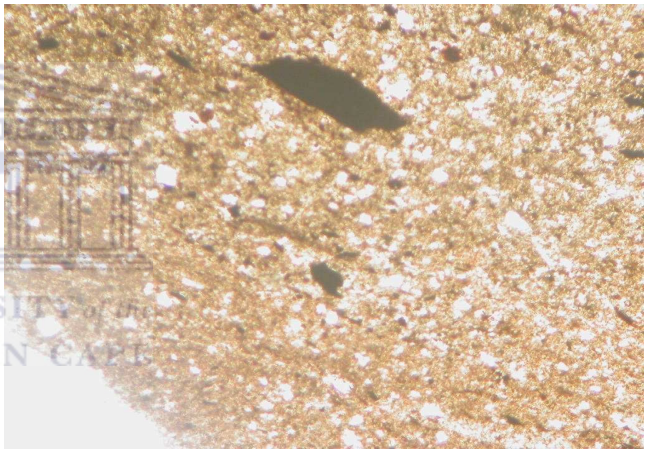

K_D1 (3652m) PPL

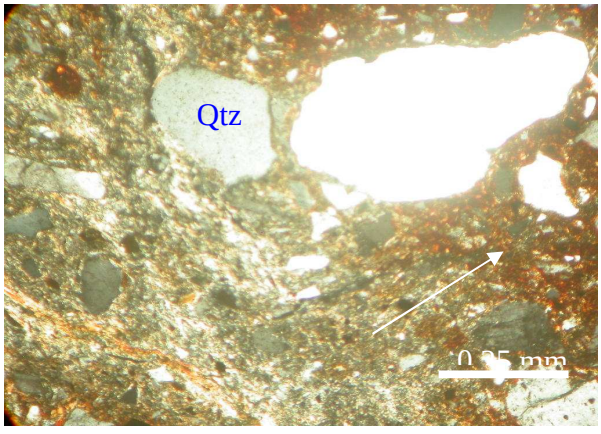

A_C3 (3727.5m) XP

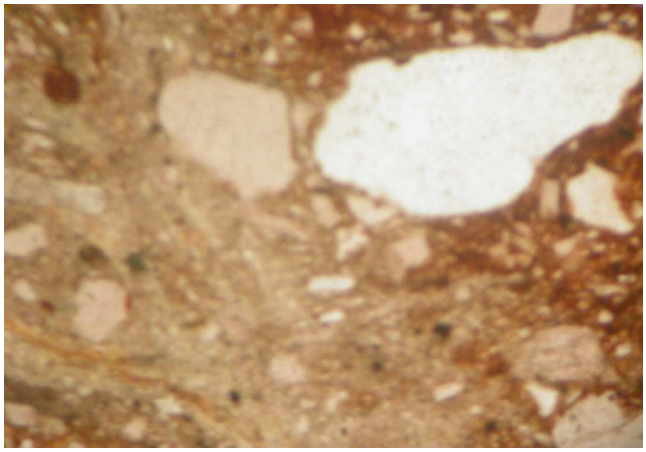

A_C3 (3727.5m) PPL

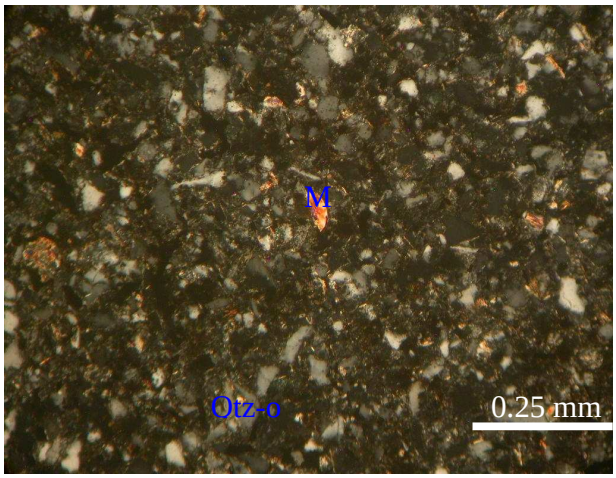

O_A1 (3940m) XP

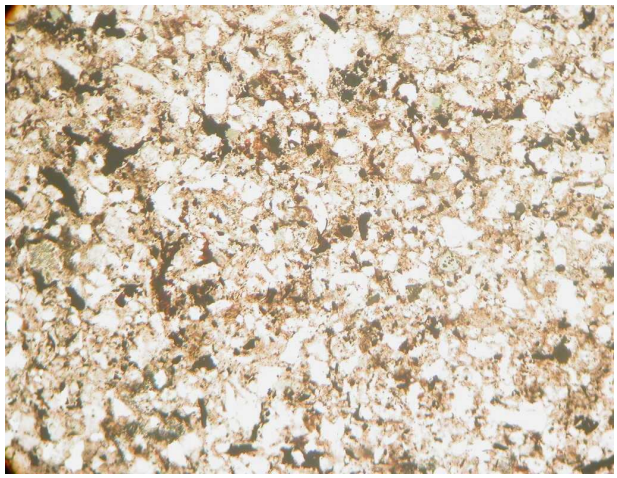

O_A1 (3940m) PPL

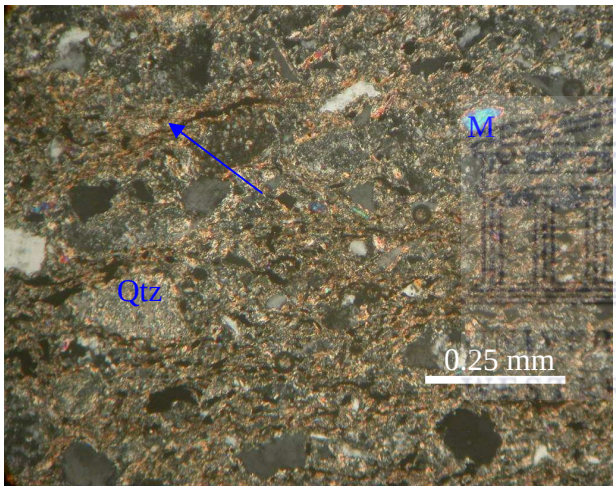

O_A1 (3950m) XP

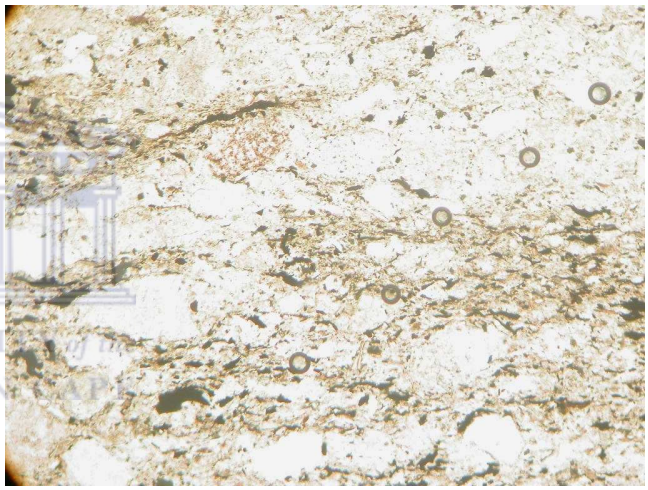

O_A1 (3950) PPL

Fig. 4-8. The photomicrograph of samples taken within HST showing different minerals both plain (PPL) and cross polarised (XP): Micas (M), Quart (Qtz), Quartz overgrowth (Qtz-o), Chlorite (Chl), Clay, Calcite cement (Cal) and Glauconite (G). The arrows: blue showing evidence of fracturing and white showing dense micritic calcite cement.

4.5 Mineralogical analyses results

4.5.1 The XRD interpretation

The sediments in Orange Basin from the XRD results show limited early diagenetic minerals. During early diagenesis the sandstones must have likely experienced severe compaction before cementation, which is likely to be due to predominance of compaction and precipitation of authigenic minerals which are common in all the stratigraphic sequences of the basin. Diagenetic reactions are those that transform unconsolidated sediments deposited at the earth's surface- sand, mud, carbonates and organic matter into coherent lithified rock of sandstone, shale, limestone and coal respectively as they are buried (De Ros, 1998).

Diagenetic events in Lowstand Systems Tract (LST)

The LST is defined an area bound by a sequence boundary below and transgressive surface above. It contains retrograding or aggrading parasequence sets. The LST deposits may be in incised valleys, shelf margin delta/lowstand shoreline system, lowstand fans or lowstand wedge.

Eight samples from various depths from 5 wells intersected this sequence stratigraphic setting (Fig. 4-9) which are A_O1 3601 m, 3679 m, K_A2 2795 m, K_B1 1950 m, 2060 m, K_D1 3692 m, 3272 m and A_C3 3597.5 m. The setting shows a good place for understanding of reducing environment because of the presence of pyrite.

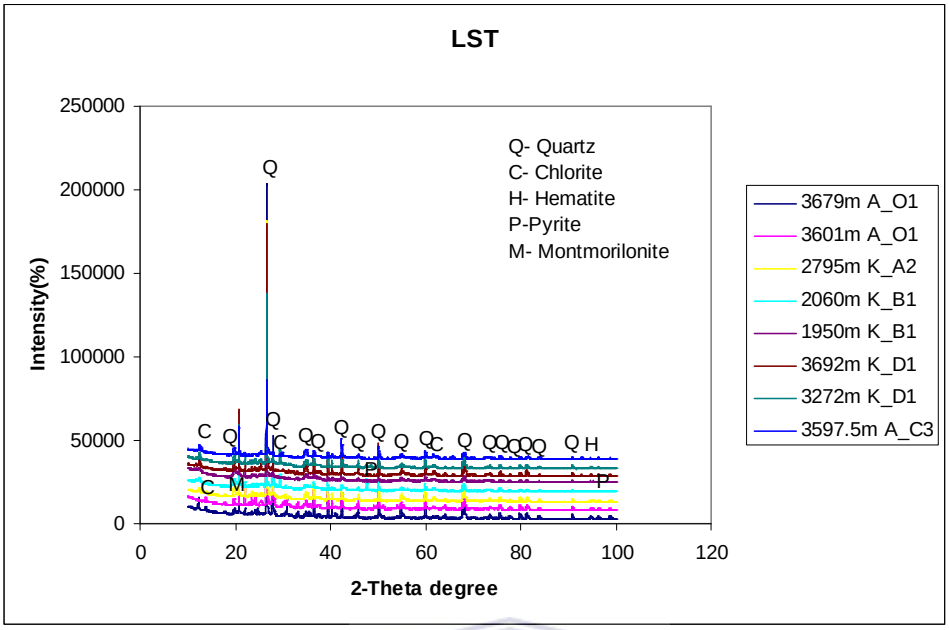

Fig. 4-9. XRD results showing mineral peaks within the Lowstand System Tract (LST) across the wells in this study.

Diagenetic events in Transgressive System Tract (TST)

The TST is defined as the area bound by transgressive surface below and maximum flooding surface above. It contains retrograding parasequence sets. Strata include shallow marine shelf systems, condensed slope/basin interval. Eleven samples from 5 of the wells intersected this systems tract and they are A_O1 3301 m, 3493 m, K_A2 1963 m, 2215 m, A_U1 2688.1 m, 2692.55 m, 2694 m, A_C2 3245.16 m, 3246.33 m, A_C3 3670 m, and 3675 m (Fig. 4-10). This systems tract is characterized by formation of (i) cement under oxic conditions at and immediately below seafloor, (ii) grain-coating, grain replacement from sub-oxic pore water, (iii) primary replacement of mica grains under weakly reducing condition (Curtis, 1987). The XRD results show more pyrite meaning that the setting is more reducing than oxidizing. This is supported by low amount of hematite which is found mainly in oxidizing environment. Pyrite formation is indicative of iron-reduction in the setting, an example of eogenetic alteration linked to sequence stratigraphy. This is formed as a result of maximum flooding event in the setting. There is relative abundance of chlorite in the setting because it is less extensively coated during late diagenetic events.

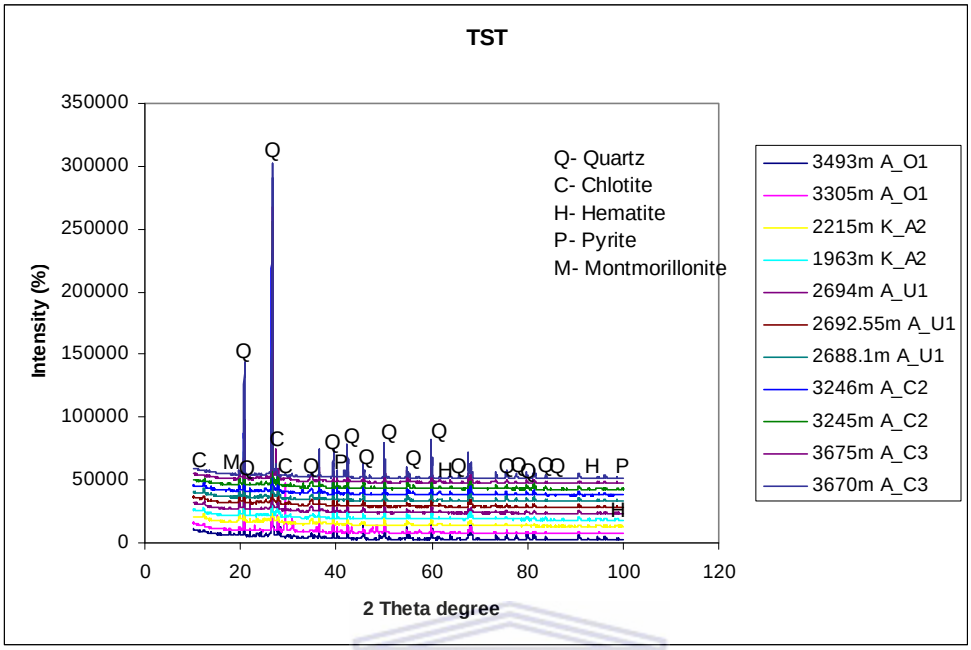

Fig. 4.10. XRD results showing mineral peaks within the Transgressive System Tract (TST) across the studied wells

Diagenetic events in Highstand System Tract (HST)

HST is defined as the area bound by maximum flooding surface below and sequence boundary above. It contains aggrading to prograding parasequence sets. Strata include outbudding shallow marine shelf system, minor slope/basin floor system.

7 wells of the well in this study intersect the HST and they are A_F1 1178 m, 1179 m, 1180 m, A_O1 3242 m, 3175 m, K_A2 1690 m, 2765, K_B1 1910 m, 1350 m, K_D1 3174 m, 3652 m, A_C3 3727.5 m, O_A1 3940 m, and 3950 m (Fig 4-11).

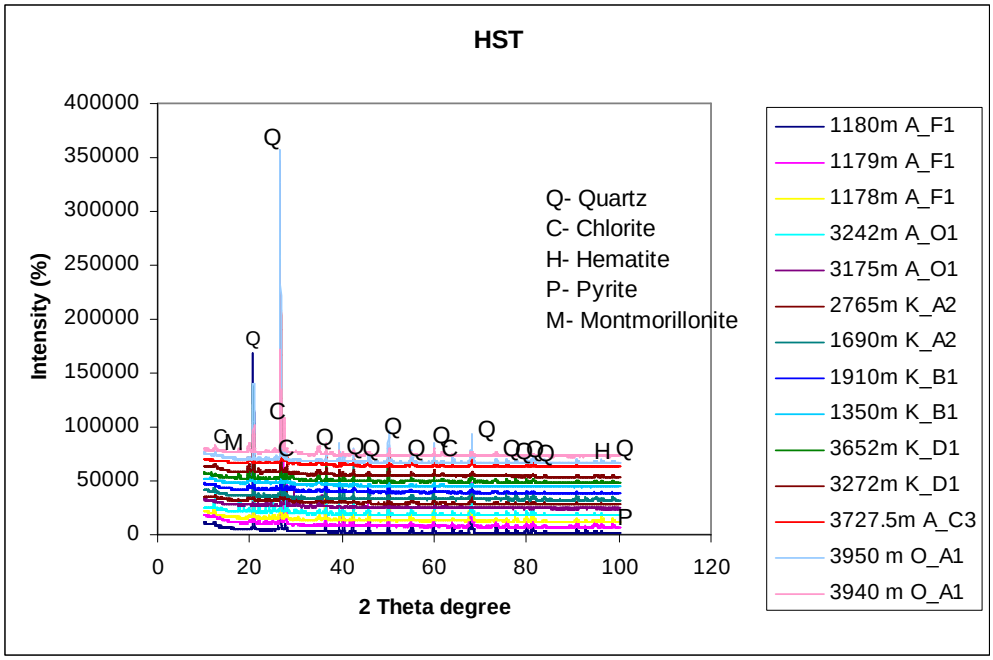

Fig. 4-11. XRD results showing mineral peaks within the High System Tract (HST) across the studied wells

Diagenetic alterations in the HST sandstones are similar to those in the TST sandstones except for the extensive and wide conversion of early authigenic clays such as kaolinite to chlorite and formation of considerable amount of quart in the HST sandstones. The silica needed for the formation of quartz is presumably derived internally from the intergranular dissolution of quartz grains in the sandstone (Ehrenberg, 1993, Bloch et al; 2002, Walderhaug, 1994, Walderhaug and Bjorkum, 2003).

The results of XRD show more quartz which is likely to be achieved as a result progradation and aggradation in HST (Posamentier et al., 1988). This is supported by the presence of hematite which is formed in oxidizing environments. There is limited grain coating which is responsible for the abundance of quartz in the setting. There is a possibility of feldspar conversion to montmorillonite and montmorillonite conversion to chlorite. There is presence of large amount of clay in the setting, which is a product of mesogenetic alteration (Morad et al., 2000) as a result of dissolution in the setting. Many investigators believe chlorites are formed directly from montmorillonite and Mg-rich solution. This is because kaolinite grades to montmorillonite and montmorillonite to chlorite. Kaolinite can also be converted to chlorite directly from the reaction of kaolinite

with quartz and availability of Mg^{2+} and Fe^{2+} in solution. For the Mg end member chlorite, the reaction would be:

$7H_2O+Al_2Si_2O_5(OH)_4+5Mg^{2+}+SiO_2$----- $Mg_5\ Al(AlSi_3)O_{10}(OH)_8+10H^+$

Kaolinite Quartz Clinochlore

K^+, Al^{3+}, Si^{4+} are needed for the formation of early diagenetic K-feldspar which was not detected in any of the samples in this study. K^+ is believed to be derived from sea water, on the other hand K^+, Al^{3+}, and Si^{4+} could also be derived from partial dissolution of mica and K-feldspar grains (De Ros, 1998). The abundance of silica (quartz) across the the systems tracts is an evidence of late (deeper) diagenetic events in the basin

4.5.2 The SEM interpretation

LST

The SEM imagery was done using magnification of 20, energy of 20 kV, probed to 50pA. Within the LST there is abundance of quartz and some overgrowth of quartz as a result of diagenesis (Fig. 4-12). There are framboidal, nodular and flattened pyrite in the samples, A_O1 (3679 m), A_O1 (3601 m), and K_B1 (2060 m). This is indicative of a marine reducing condition (Greensmith, 1989). Pyrite mineralization often take places along fractures, it may have been precipitated from diagenetic fluids that were passing through the reducing environment. The entire samples in the setting show few montmorillonite and more chlorite. The montmorillonite exists as flakes, while the chlorite is found around quartz and other framework grains. The montmorillonite found in few samples A_O1 (3679 m) and K_B1, and chlorite found in all the samples in this setting may be as a result of clay conversion. There is possibility of one clay mineal transforming into another under a favourable time and temperature (Zhang et al., 2008). The authigenic clay minerals must have been responsible for the poor porosity and permeability within the setting. The infiltrated clays in the LST are probably attributed to high initial depositional permeability (Moraes and De Ros, 1992). The grain-coating chlorite appear to have preserved some porosity by restricting subsequent quartz cementation during burial at higher temperature (Wilson and Pittman, 1977; Moraes and De Ros, 1989;

Storvol et al., 2002; Primmer et al., 1997; and Imam, 1986) as seen in samples K_B1 (1910 m) and A_C3 (3597.5 m). The sample A_O1 (3679 m) shows very tight grain contact making porosity to be very low. The presence of fewer hematites in samples K_A2 (2795 m), K_B1 (1950 m) and K_B1 (2060 m) must have been as a result of exposure to groundwater with dissolved oxygen or water that has been exposed to atmosphere.

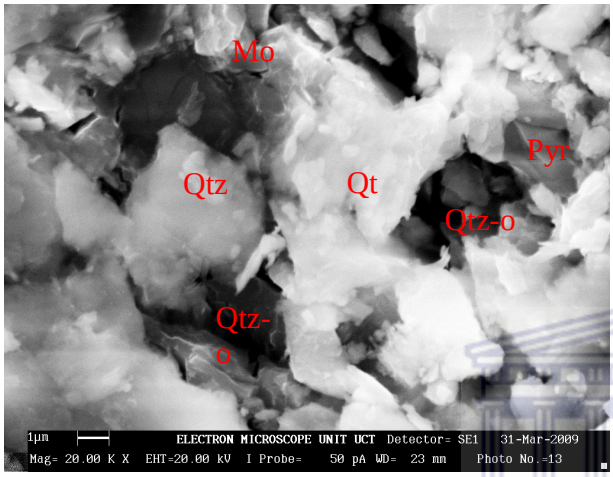

A_O1 (3679m)

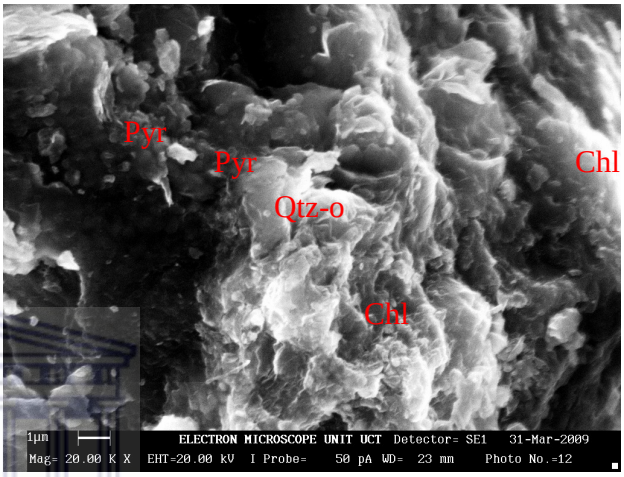

A_O1 (3601m)

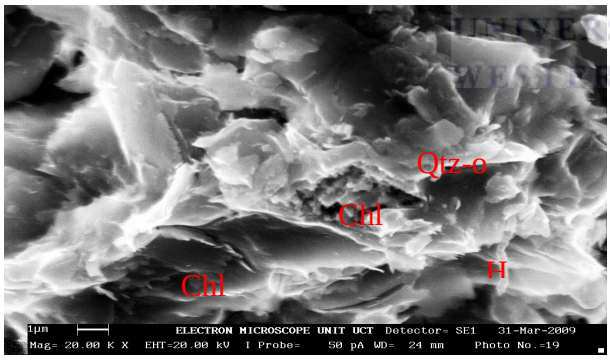

K_A2 (2795m)

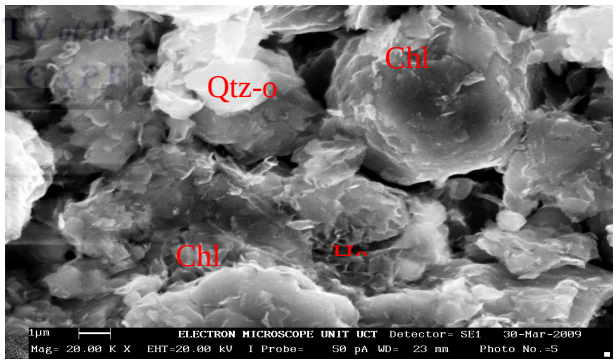

K_B1 (1950m)

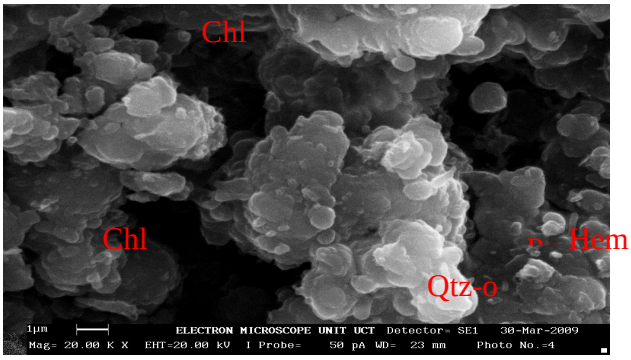

K_B1 (2060m)

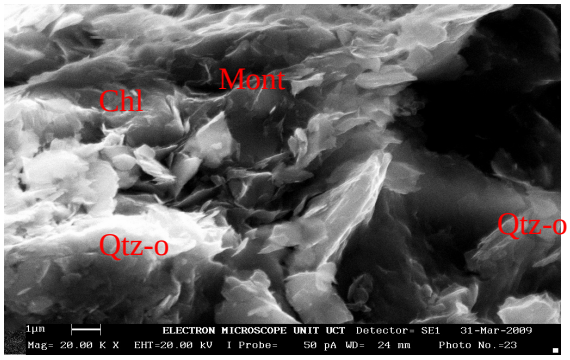

K_D1 (3272m)

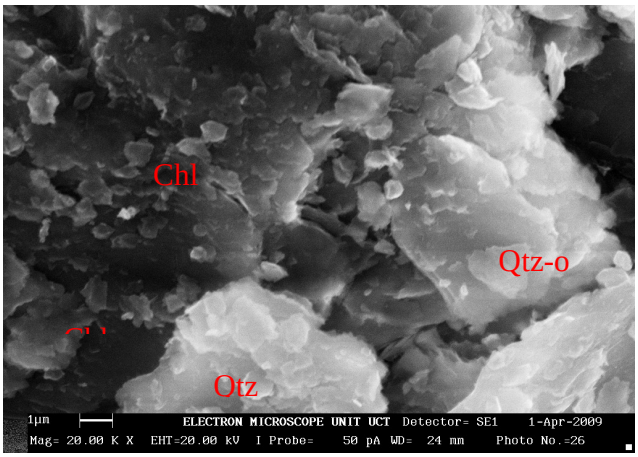

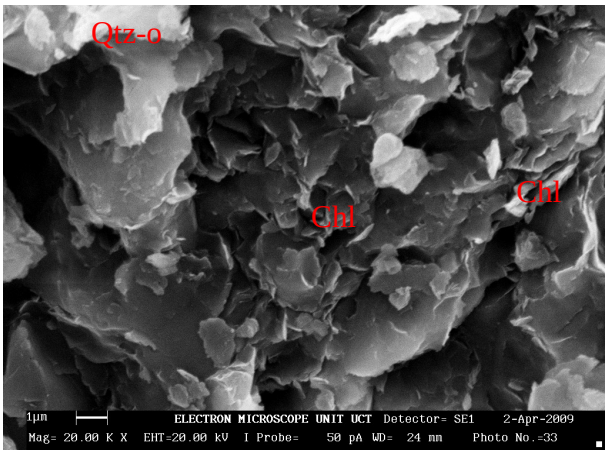

K_D1 (3692m) A_C3 (3597.5m)

Fig. 4-12. SEM imageries of samples within LST showing massive quartz overgrowth (Qtz-o), authigenic minerals montmorillonite (Mont) and chlorite (Chl) coating detrital grains, with some nodular pyrite and flattened/ fibre like hematite

TST

The TST is formed by progradtional event, with the transgressive surface below and maximum flooding surface on top. There is overgrowth of quartz across the setting. The overgrowth of quartz is an evidence of mesodiagenetic event in this system tract (Zhang et al., 2008). Quartz has significant presence; authigenic montmorillonite and chlorite are also present with trace of hematite and pyrite. Pyrite is most common in this package than in the retrogradational setting. The pyrite occurs as framboidal A_O1 (3305 m), A_O1 (3493 m), A_C2 (3245.5 m), A_C2 (3246.32 m) and A_C3 (3670 m) (Fig. 4-13). Silica that was used for the formation of quartz overgrowth must have been derived internally from the intergranular dissolution of quartz grains in the sandstones (Giles et al., 1992). In well A_O1, the effect of authigenic clay minerals at depths 3493 m and 3305 m is similar. The clay covers nearly all the pore spaces in the well making porosity to be poor. In well A_U1 (2697.55 m), the overgrowth of quartz is nodular, which may enhance secondary porosity. The initial porosity was obliterated by quartz overgrowth and authigenic clay deposits. The TST show early, near-surface grain-coating by authigenic clays, pyrite and grain-coating of micro-quartz. These are seen throughout the setting. The TST shows a place for understanding redox condition. This is established by the

presence of pyrite and hematite (Fig. 4-13 in A_C2 (3245.5m). Pyrite is more in abundance than hematite meaning it is more reducing than oxidizing. Pyrite is known to be formed under a marine reducing condition and hematite in oxidizing condition, A_O1 (3493 m) and A_C2 (3245.5 m). There is relatively high abundance of chlorite in this genetically related package because chlorites are less extensively coated during late diagenetic events, an attribute of physical weathering of rock formed under cold and dry climate (Ehrmann et al., 1992; Ehrmann and Mackensen, 1992).

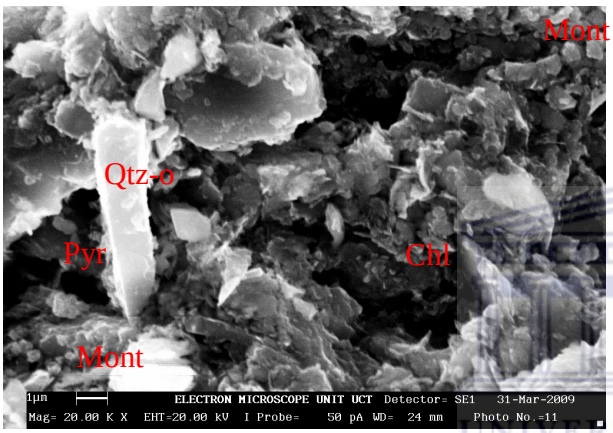

A_O1 (3305m)

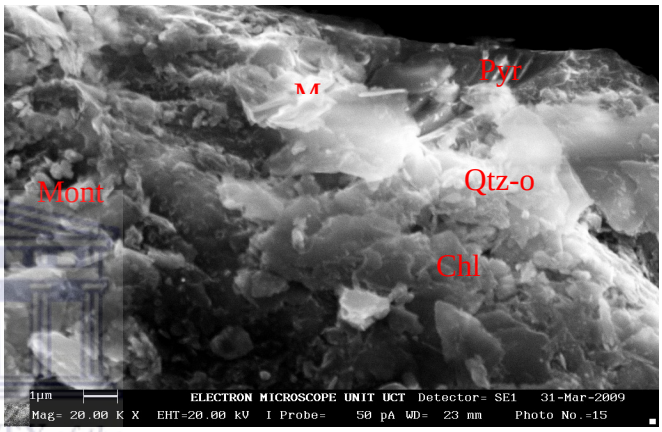

A_O1 (3493m)

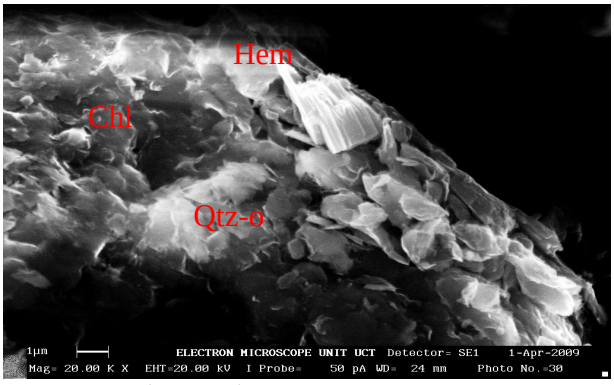

K_A2 (1963m)

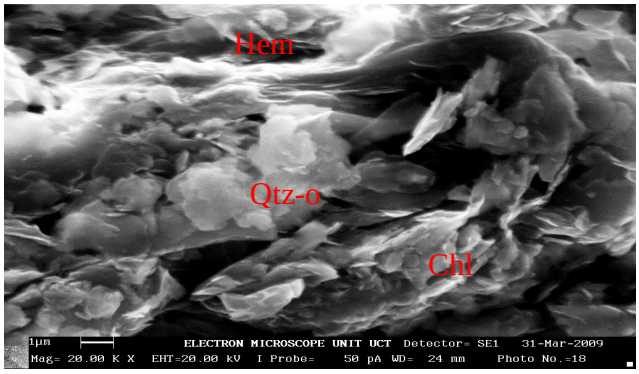

K_A2 (2215m

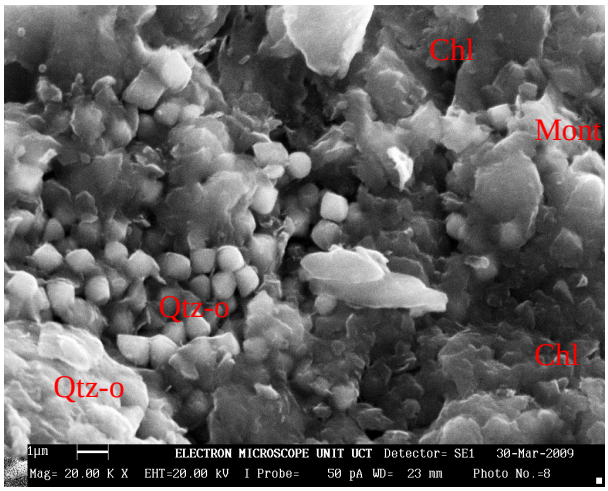

A_U1 (2697.55m)

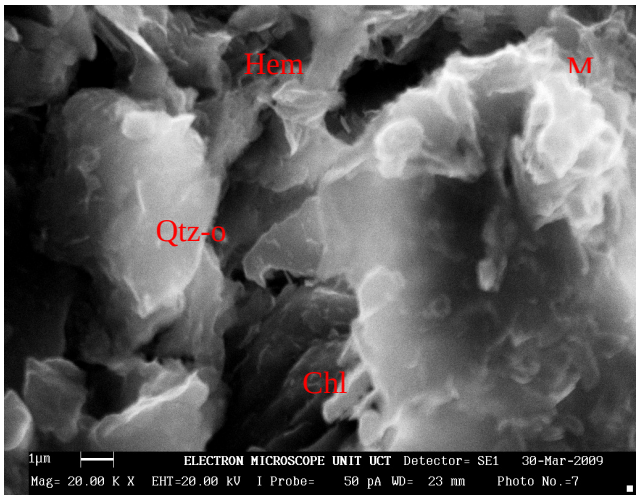

A_U1 (2688.10m)

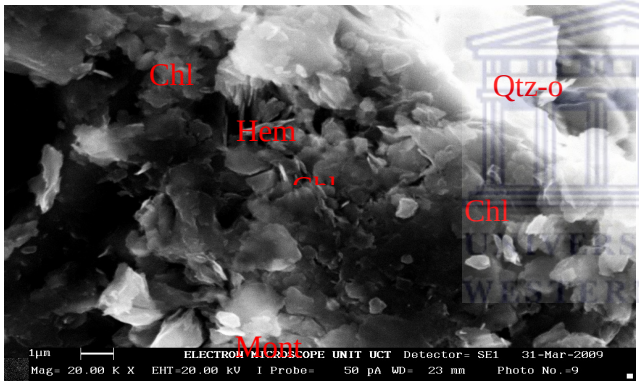

A_U1 (2694.05m)

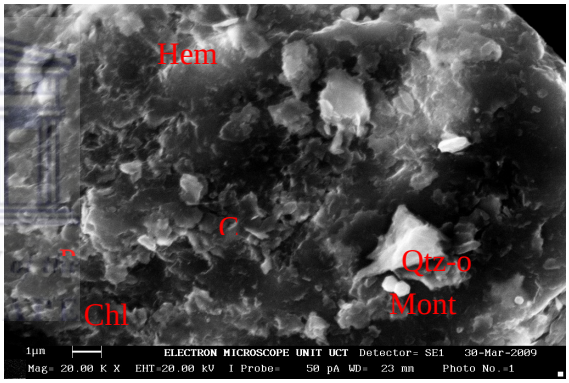

A_C2 (3245.5m)

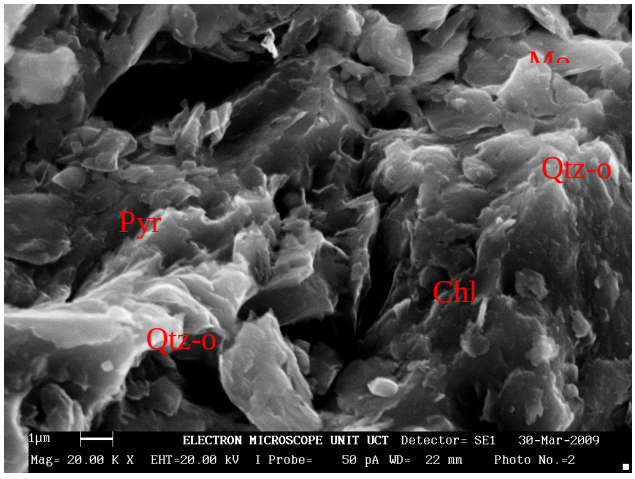

A_C2 (3246.32m)

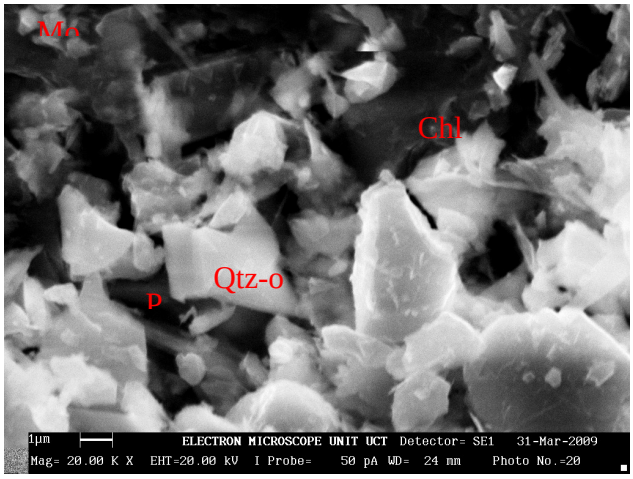

A_C3 (3670m)

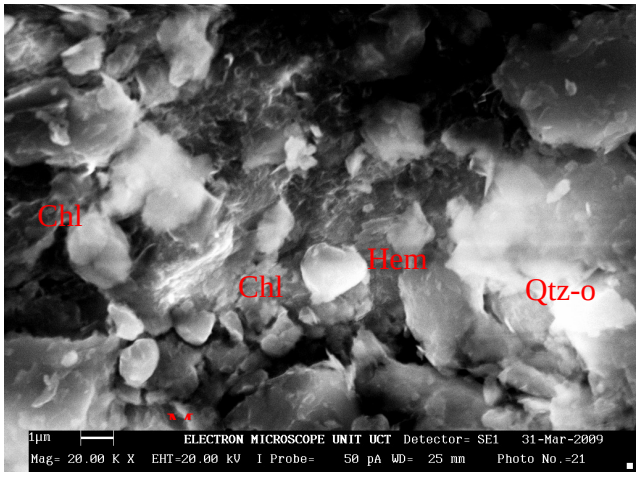

A_C3 (3675m)

Fig. 4-13. SEM imageries of samples within TST showing massive quartz overgrowth (Qtz-o), authigenic minerals montmorillonite (Mont) and chlorite (Chl) coating detrital grains, with some nodular pyrite and flattened/ fibre like hematite

HST

Diagenetic alterations of the HST sandstones are similar to those of the TST sandstones except for the extensive and wide conversion of early authigenic clays such as montmorillonite to chlorite and formation of considerable amount of quartz overgrowth in the former sandstone. The silica needed for the formation of quartz overgrowth is presumably derived internally from the intergranular dissolution of quartz grains in the sandstone (Ehrenberg, 1993; Bloch et al., 2002; Walderhaug, 1994; Walderhaug and Bjorkum, 2003). The abundance of quartz in the setting was as a result of progradation and aggradation in HST (Fig. 4-14). This is supported by more hematite which is formed in oxidizing environment. The hematite formation is due to exposure to oxidizing conditions during the period immediately following burial. The stratigraphic setting shows limited grain coating compared with other settings which might be responsible for the abundance quartz in the setting. The bent needle-like chlorite as seen in A_F1 (1179 m) (Fig. 4-14) might have been as a result of mechanical compaction. Across this setting there is grain coating by authigenic clay minerals. The chloritization in the systems tract may be due to clay conversion (De Ros, 1998). There is a wide range conversion of

montmorillonite to chlorite in the setting making the chlorite to be more abundant (Ehrenberg, 1993). Mechanical and chemical compaction in most sandstone is of more importance than cementation in the destruction of intergranular porosity (Morad and De Ros, 1994; Morad et el., 2000). The evidence of chemical compaction is the squeezing of the authigenic clay within the mass of the sample across this systems tract.

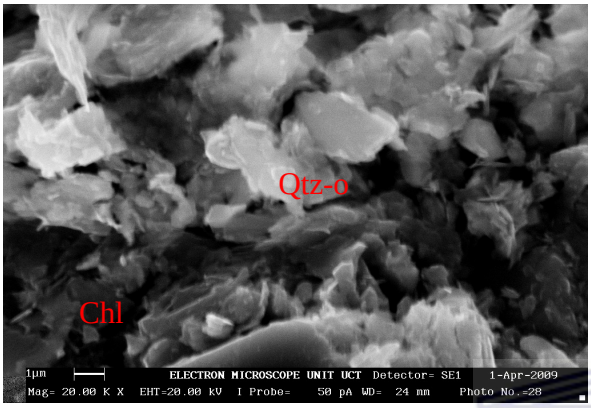

A_F1 (1180m)

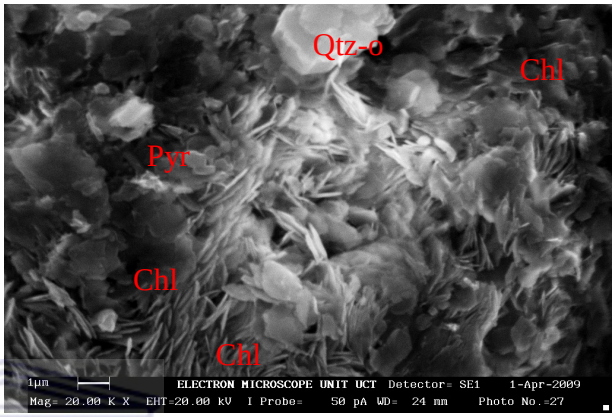

A_F1 (1179m)

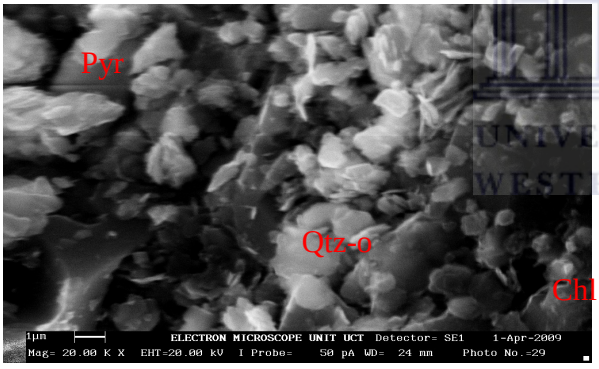

A_F1 (1178.5m)

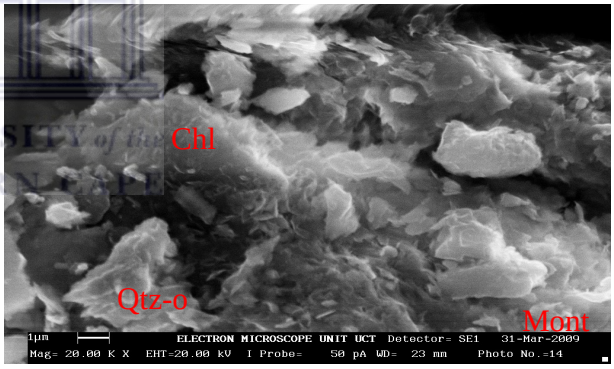

A_O1 (3242m)

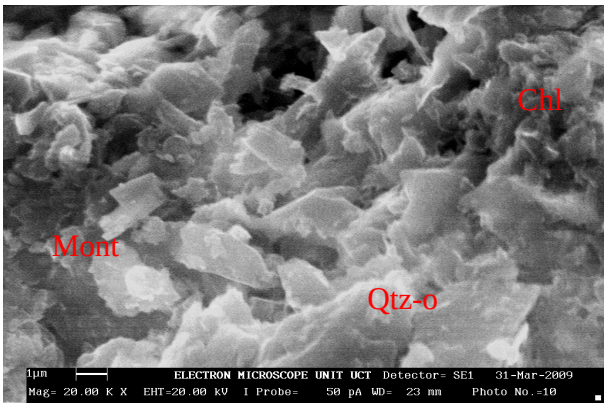

K_A2 (1690m)

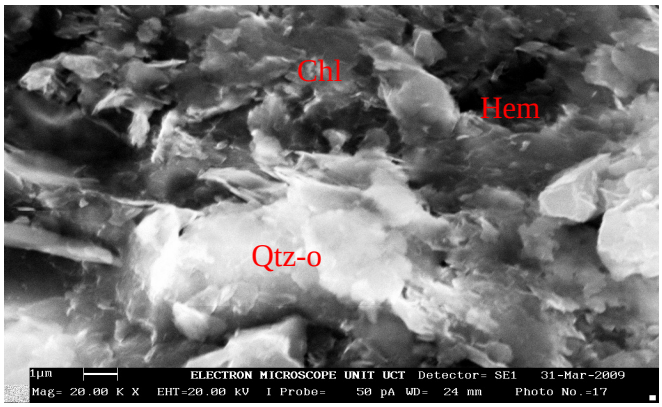

A_O1 (3175m)

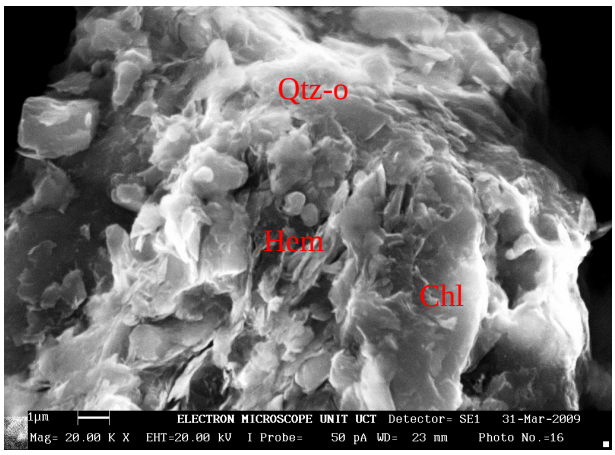

K_A2 (2765m)

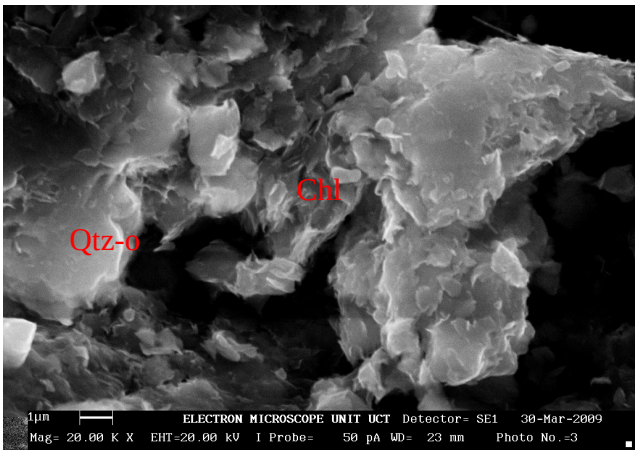

K_B1 (1350m)

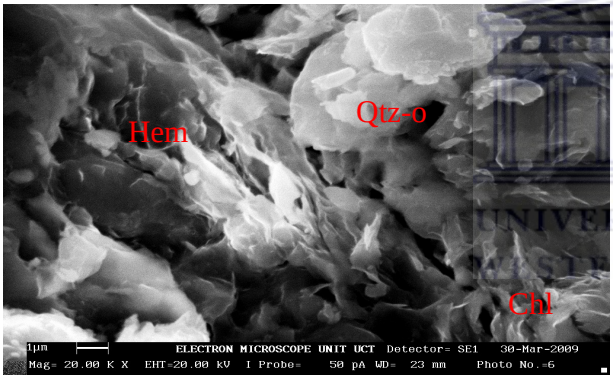

K_B1 (1910m)

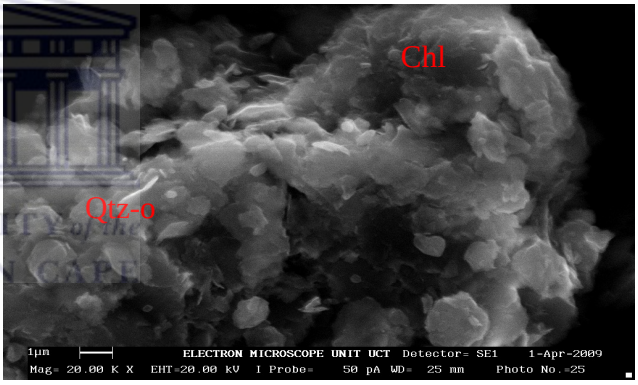

K_D1 (3652m)

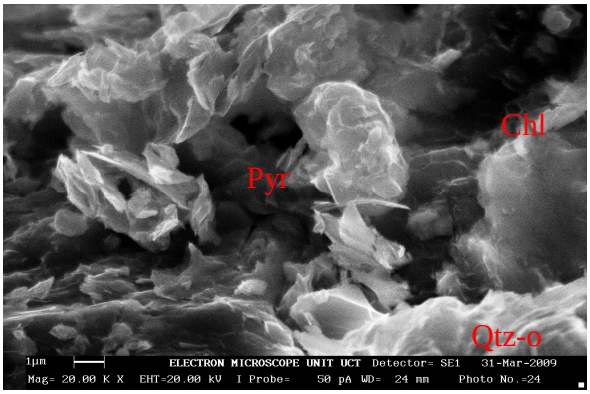

K_D1 (3174m)

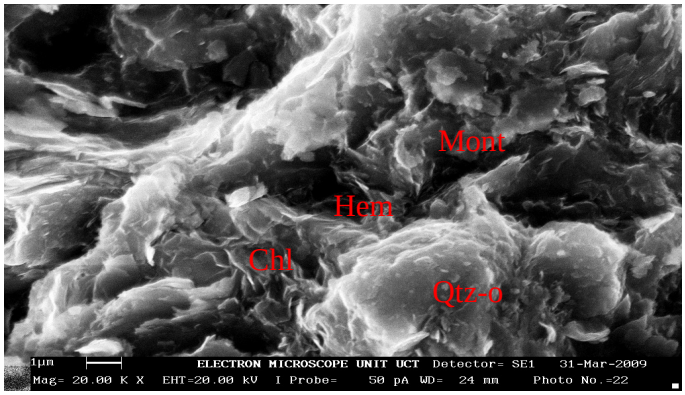

A_C3 (3727.5m)

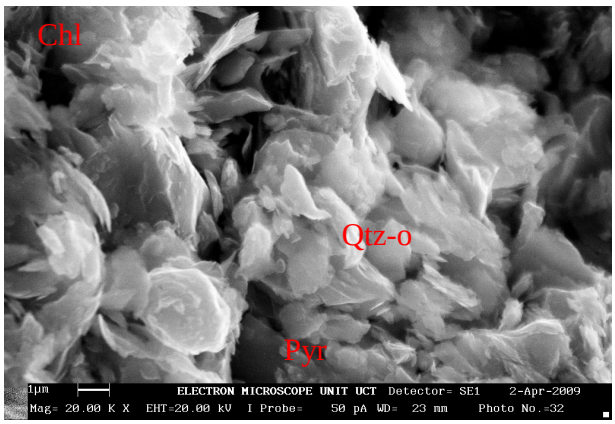

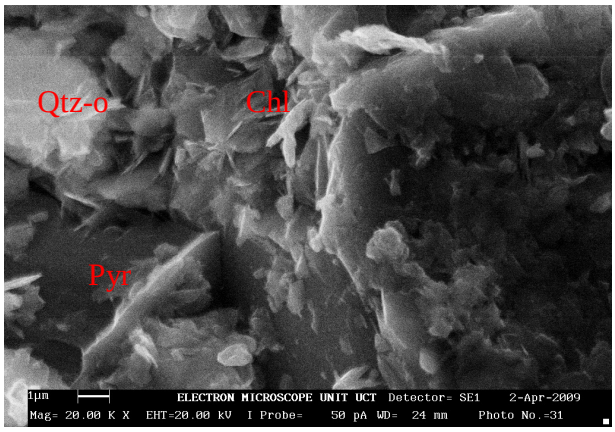

O_A1 (3940 m) O_A1 (3950 m)

Fig. 4-14. SEM imageries of samples within HST showing massive quartz overgrowth (Qtz-o), authigenic minerals montmorillonite (Mont) and chlorite (Chl) coating detrital grains, with some nodular/framboidal pyrite and flattened/ fibre like hematite

4.5.3 The EDS interpretation

LST

The results of EDS are presented graphically and in tabular form, with the plot of energy (keV) against the Intensity (%) (Fig. 4-15). Within the LST, intensity of the elemental composition varies from samples to samples. Silicon has the highest intensity ranging between 950 (%) and 2000 (%) with energy of about 200 keV. Elements distribution within this systems tract shows the presence of O, Mg, Al, Si, S, Cl, K, Ca, Ti, Fe, and Ni, which are presented % weight of elemental composition and % atomic composition, respectively (Tables 4.3a and 4.3b).

Table 4.3a Weight elemental composition from EDS analysis within LST (%)

Well	Depth (m)	O	Mg	Al	Si	P	S	Cl	Cr	K	Ca	Ti	Fe	Ni
A_O1	3601	12.72	0.47	9.62	42.07	na	na	1.57	na	14.52	3.46	2.56	13.02	na
A_O1	3679	12.04	0.27	4.92	59.62	na	na	0.75	na	8.82	0.74	na	12.84	na
K_A2	2795	12.84	0.76	11.97	43.61	na	na	na	na	12.11	na	1.69	17.03	na
K_B1	1950	12.32	0.9	11.37	43.92	na	2.13	na	na	6.37	1.57	3.02	18.4	na
K_B1	2060	na	na	na	na	na	na	1.38	11.32	na	na	na	76.09	11.21
K_D1	3272	16.35	0.34	9.95	38.97	na	na	na	na	8.8	11.87	0.97	12.74	na
K_D1	3692	8.39	0.88	12.5	38.71	na	0.86	na	na	12.65	na	1.59	24.42	na
A_C3	3597	8.24	na	12.3	44.33	0.9	na	na	na	17.15	na	1.98	15.1	na

Table 4.3b Atomic elemental composition from EDS analysis within LST (%)

Well	Depth (m)	O	Mg	Al	Si	P	S	Cl	Cr	K	Ca	Ti	Fe	Ni
A_O1	3601	23	0.56	10.32	43.32	na	na	1.28	na	10.74	2.5	1.55	6.74	na
A_O1	3679	21.12	0.31	5.11	59.56	na	na	0.6	na	6.33	0.52	na	6.45	na
K_A2	2795	23.06	0.89	12.74	44.62	na	na	na	na	8.9	na	1.01	8.76	na
K_B1	1950	22.3	1.07	12.2	45.28	na	1.92	na	na	4.72	1.13	1.83	9.54	na
K_B1	2060	na	na	na	na	na	na	2.15	12.02	na	na	na	75.28	10.55
K_D1	3272	28.69	0.39	10.35	38.96	na	na	na	na	6.32	8.32	0.57	6.4	na
K_D1	3692	16.26	1.12	14.38	42.77	na	0.83	na	na	10.04	na	1.03	13.57	na
A_C3	3597	15.46	na	13.7	47.42	0.87	na	na	na	13.18	na	1.24	8.13	na

Note:
O- Oxygen, Mg- Magnesium, Al- Aluminium, Si- Silicon, P- Phosphorous, S- Sulphur, Cl- Chlorine, Cr- Chromium, K- Potasium, Ca- Calcium, Ti- Titanium, Fe- Iron and Ni- Nickel.

The presence of Ni and Cr in the sample K_B1 (2060 m) suggests marine influence (Garver et al., 1996). In the same sample there is complete replacement of aluminium by chromium. Iron also replaced silicon showing high intensity. The presence of chlorine in A_O1 (3601 m) and A_O1 (3679 m) in the setting is an indication of sea water influence. The soluble elements Mg, Ca, and K show low intensity except K which may be due to concentration of its bearing salts. The less soluble Si, Al, and Fe show more intensities and more relatively high abundance. The sulphur presence in sample K_B1 and K_D1 (3692 m) is an indication of volcanic (basaltic) deposit source of the sediment making up the sandstone (Rickwood, 1981). Titanium is found in all the samples in this setting except in A_O1 (3679 m) and K_B1 (2060 m), the presence of this element is an indication of the source of the sandstone because they are found associated with granitic silicate rocks (Choo et al., 2002). The presence of these elements confirms the minerals found in this setting: quartz, montmorillonite, pyrite, hematite, and chlorite in XRD result. In sample K_B1 (2060 m), the presence of nickel and iron supports the formation of nimite a nickel-rich chlorite and chamosite, iron-rich chlorite. The phosphorus presence in well A_C3 (3597.5 m) may be due to input from the shell of marine invertebrate confirming the marine deposition environment (Garver et al., 1996).

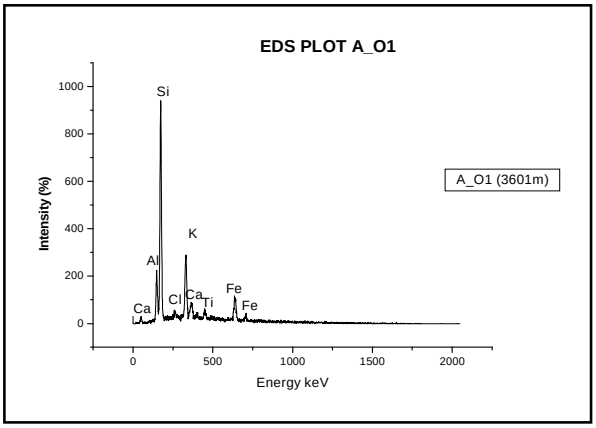

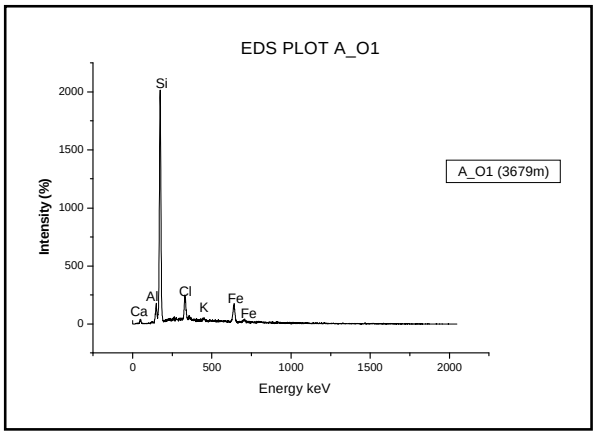

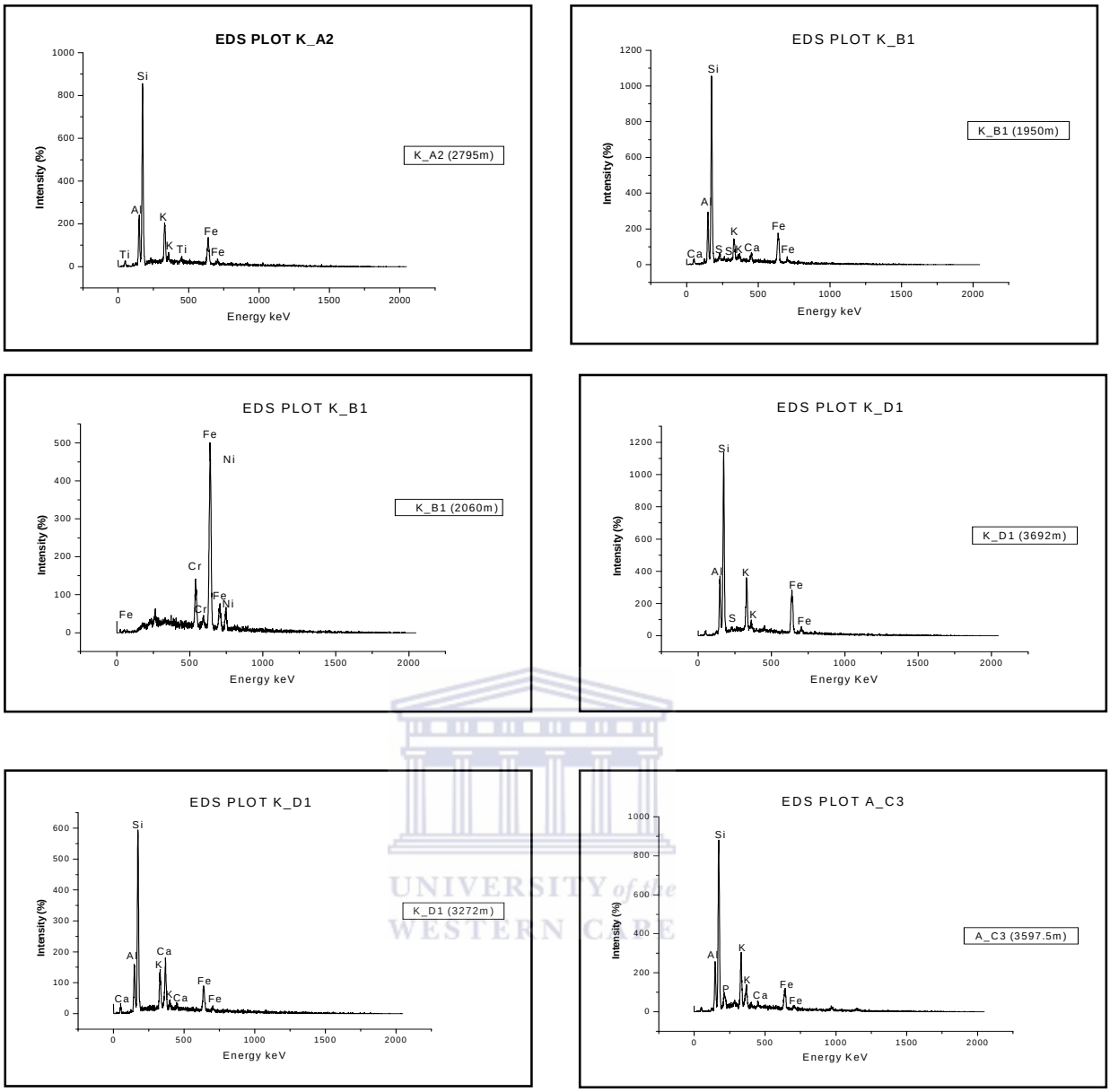

Fig. 4-15. EDS elemental distribution of samples within LST

TST

The elemental distributions within the TST are: O, Mg, Al, Si, S, Cl, K, Ca, Ti, and Fe. Tables 4.4a and 4.4b are presented in % weight of elemental composition and % atomic composition, respectively.

Table 4.4a Weight elemental composition from EDS analysis within TST (%)

Well	Depth (m)	O	Mg	Al	Si	S	Cl	K	Ca	Ti	Fe
A_O1	3305	11.96	0.78	4.53	19.42	na	1.83	5.35	32.22	na	23.91
A_O1	3493	11.39	0.23	4.58	68.08	na	1	5.9	0.54	0.43	7.85
K_A2	1963	12.8	0.34	7.29	59.39	na	0.64	3.9	na	1.52	14.12
K_A2	2215	14.52	0.29	9.11	57.68	na	na	7.16	na	2.47	8.77
A_U1	2688	14.51	0.35	8.66	55.57	1.17	na	6.89	0.96	1.17	10.72
A_U1	2694	11.21	0.29	12.49	41.67	0.48	na	13.91	1.49	4.03	14.41
A_U1	2697	15.92	0.21	12.36	54.52	1.87	na	6.01	1.25	0.82	7.04
A_C2	3245	16.99	na	4.3	73.93	*na*	*na*	4.78	na	na	na
A_C2	3246	11.27	na	9.93	40.32	na	3.48	14	1.63	1.57	17.8
A_C3	3670	7.51	0.18	9.33	47.04	na	1.55	32.06	na	0.65	1.68
A_C3	3675	13.42	na	10.58	57.5	na	na	10.91	na	na	7.59

Table 4.4b Atomic elemental composition from EDS analysis within TST (%)

Well	Depth (m)	O	Mg	Al	Si	S	Cl	K	Ca	Ti	Fe
A_O1	3305	24.43	1.05	5.48	22.6	na	1.68	4.48	26.28	na	13.99
A_O1	3493	19.47	0.26	4.64	66.27	na	0.77	4.13	0.37	0.24	3.84
K_A2	1963	22.22	0.39	7.5	58.72	na	0.5	2.77	na	0.88	7.02
K_A2	2215	24.51	0.33	9.12	55.47	na	na	4.95	na	1.39	4.24
A_U1	2688	24.69	0.39	8.73	53.86	0.99	na	4.79	0.65	0.66	5.22
A_U1	2694	20.55	0.35	13.57	43.51	0.44	na	10.43	1.09	2.47	7.57
A_U1	2697	26.26	0.23	12.09	51.22	1.54	na	4.05	0.82	0.45	3.33
A_C2	3245	26.72	na	4	66.2	na	na	3.08	na	na	na
A_C2	3246	20.92	na	10.93	42.65	na	3.22	10.63	1.21	0.97	9.47
A_C3	3670	13.79	0.21	10.16	49.2	na	1.28	24.08	na	0.4	0.88
A_C3	3675	22.72	0	10.62	55.43	na	na	7.56	na	na	3.68

Note:
O- Oxygen, Mg- Magnesium, Al- Aluminium, Si- Silicon, P- Phosphorous, S- Sulphur, Cl- Chlorine, Cr- Chromium, K- Potasium, Ca- Calcium, Ti- Titanium, Fe- Iron and Ni- Nickel.

The EDS graphs (Fig. 4-16) showed silicon as the element with highest intensity ranging between 800 and 4,500 (%). This confirms the samples to be siliciclastic. Aluminium and potassium shows high intensity in all the samples of the setting. Calcium shows an exceptional high intensity in sample A_O1 (3303 m) being a soluble metal and with the intensity, which suggests presence of high content of calcium salts in the sediment. The presence of chlorine in samples A_O1 (3304 m), A_O1 (3493 m), K_A2 (1963 m), A_C2 (3246.32 m) and A_C3 (3670 m) indicates sea water influence within the setting (Mitchell, 1997). Sulphur is found localised in the well A_U1 at depths 2688.2 m and 2694.05 m, titanium is found in samples A_O1 (3493 m), K_A2 (1690 m), K-A2 (2215 m), A_C2 (3246.32 m) and A_C3 (3670 m). The sulphur and titanium are indication of the source of the sediment. The presence of sulphur and titanium in sample A_U1 (2688.1 m) and A_U1 (2694.05 m) is an indication of two different sources. Sulphur presence is an indication of volcanic (basaltic) deposit source while titanium is an indication of granitic silicate source (Choo et al., 2002; Rickwood, 1981). The elemental distribution supports the distribution of different minerals found in the setting by the XRD analysis which are: chlorite, montmorillonite, pyrite, quartz and hematite.

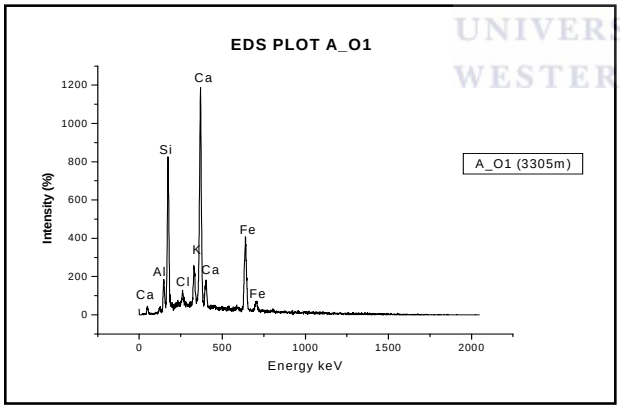

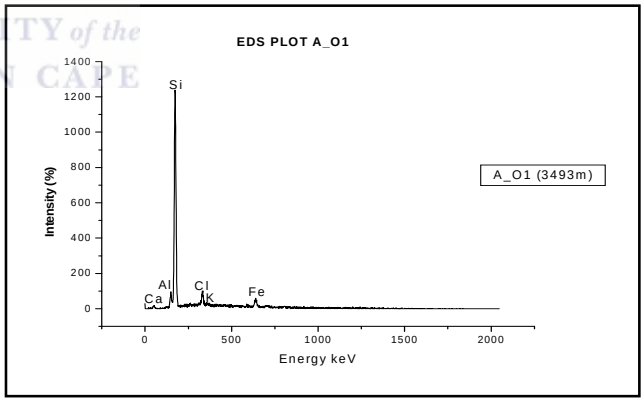

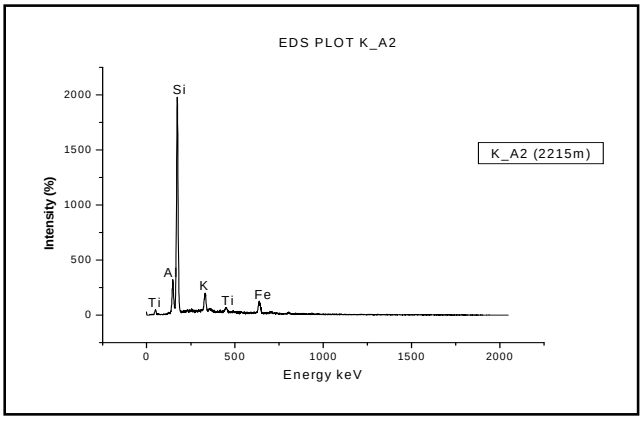

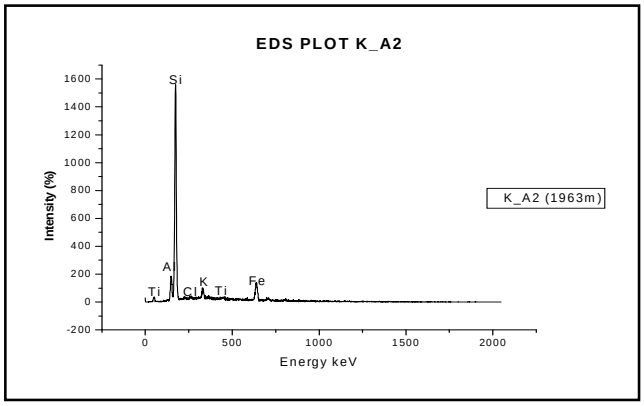

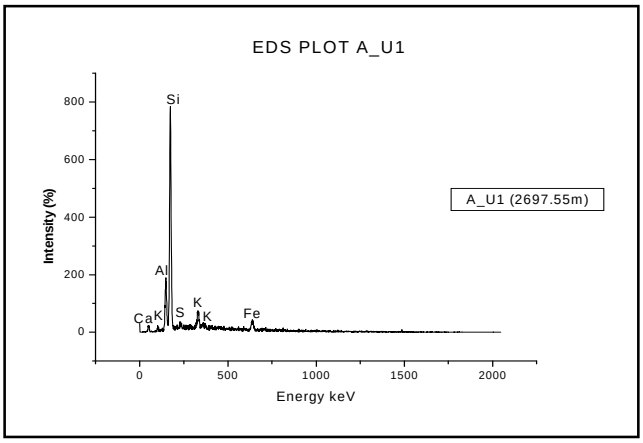

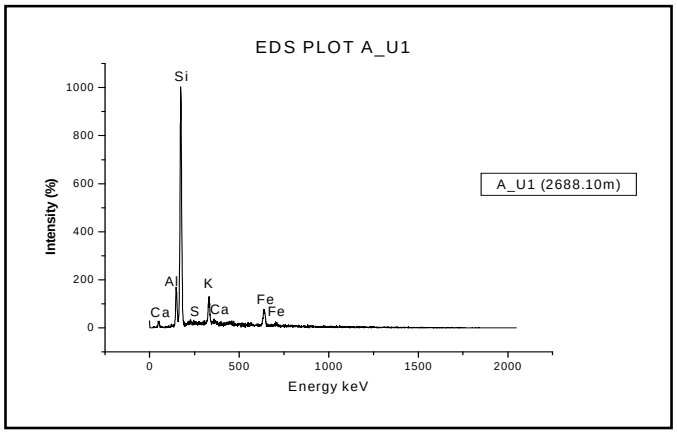

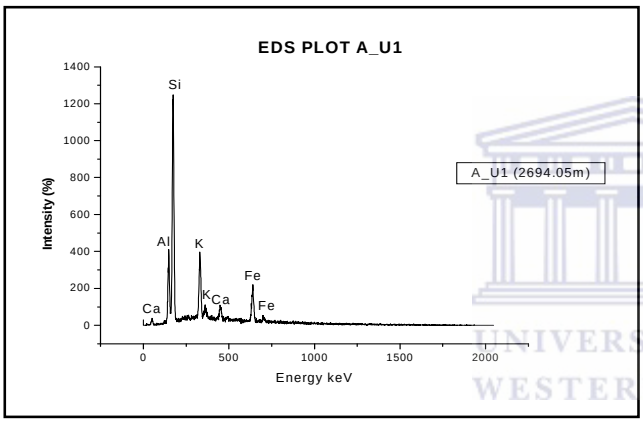

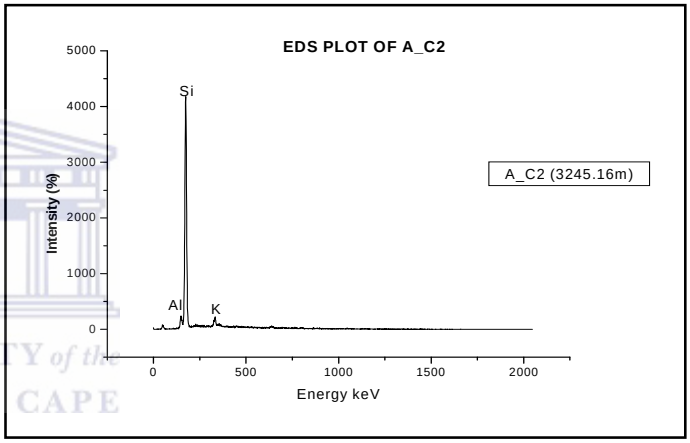

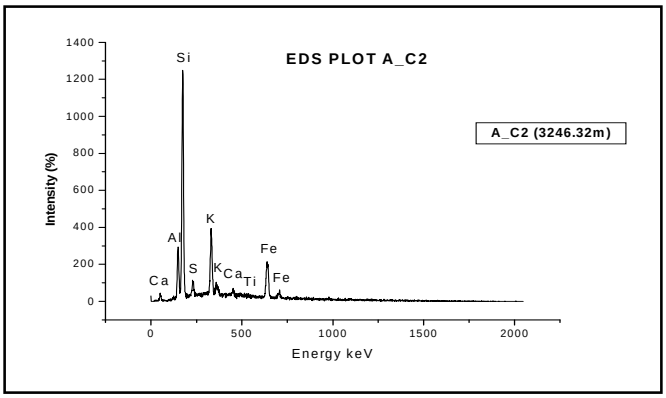

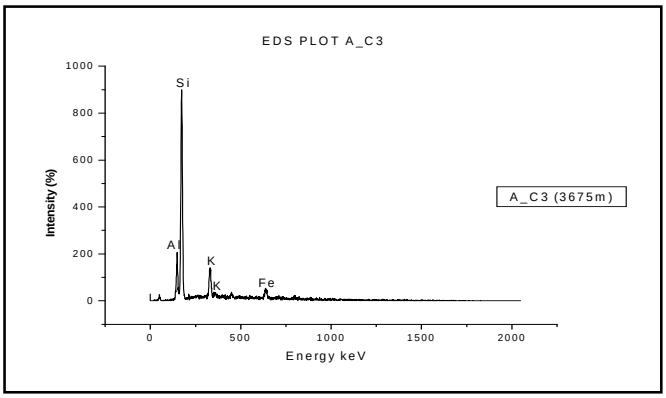

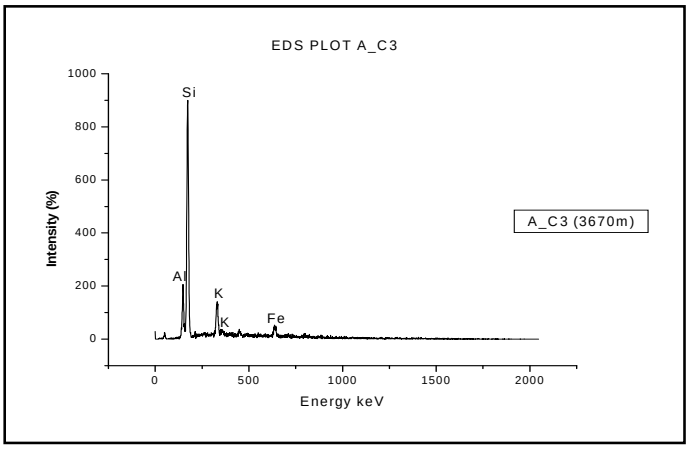

Fig. 4-16. EDS elemental distribution of samples within TST

HST

The elemental distributions within the HST are: O, Mg, Al, Si, Cl, K, Ca, Ti, and Fe (Fig. 4-17). Silicon has the element with the highest intensity in this setting which ranges between 450 and 2,250 (%). The results of their % weight and % atomic compositions are presented in table 4.5a and 4.5b respectively.

Table 4.5a Weight elemental composition from EDS analysis within HST (%)

Well	Depth (m)	O	Mg	Al	Si	P	S	Cl	Cr	K	Ca	Ti	Fe	Ni
A_F1	1178	14.58	0.25	10.2	62.24	na	na	0.56	na	2.66	na	0.83	8.69	na
A_F1	1179	11.54	0.88	11.99	44.99	na	na	1.24	na	4.26	na	na	25.1	na
A_F1	1180	12.23	0.62	11	51.02	na	na	1.64	na	4.42	na	1.11	17.96	na
A_O1	3242	11.21	6.65	9.6	34.59	na	na	2.91	na	7.03	1.52	0.62	25.86	na
A_O1	3175	12.24	0.63	6.99	48.49	na	0.79	na	na	8.41	1.1	2.36	18.98	na
K_A2	1690	11.38	1.41	13.03	43.54	na	na	2.17	na	2.64	na	na	25.83	na
K_A2	2765	12.84	0.76	11.97	43.61	na	na	na	na	12.11	na	1.69	17.03	na
K_B1	1350	12	1.05	10.69	45.63	na	1.04	na	na	5.76	2.09	2.68	19.04	na
K_B1	1910	15.75	0.57	9.62	44.31	na	1.7	na	na	6.26	3.46	2.3	16.03	na
K_D1	3652	10.54	0.47	12.27	47.14	na	1.45	na	na	11.5	na	1.36	15.27	na
K_D1	3174	12.77	0.16	7.65	50.78	na	5.64	na	na	8.4	na	4.4	10.2	na
A_C3	3727	11.81	0.25	13.68	41.4	na	na	na	na	15.22	na	1.21	16.43	na
O_A1	3940	14.08	na	13.44	39.85	na	na	na	na	20.4	na	2.63	9.59	na
O_A1	3950	11.19	na	6.38	53.18	na	na	na	na	15.43	na	na	13.82	na

Table 4.5b. Atomic elemental composition from EDS analysis within HST (%)

Well	Depth (m)	O	Mg	Al	Si	P	S	Cl	Cr	K	Ca	Ti	Fe	Ni
A_F1	1178	24.16	0.27	10.02	58.74	na	na	0.42	na	1.8	na	0.46	4.12	na
A_F1	1179	21.24	1.06	13.08	47.15	na	na	1.03	na	3.21	na	na	13.23	na
A_F1	1180	21.72	0.72	11.59	51.64	na	na	1.31	na	3.21	na	0.66	9.14	na
A_O1	3242	20.98	8.19	10.66	36.9	na	na	2.46	na	5.39	1.14	0.39	13.87	na
A_O1	3175	22.28	0.75	7.55	50.29	na	0.72	na	na	6.27	0.8	1.44	9.9	na
K_A2	1690	20.96	1.71	14.23	45.69	na	na	1.8	na	1.99	na	na	13.63	na
K_A2	2765	23.06	0.89	12.74	44.62	na	na	na	na	8.9	na	1.01	8.76	na
K_B1	1350	21.79	1.25	11.5	47.18	na	0.94	na	na	4.28	1.52	1.63	9.9	na
K_B1	1910	27.52	0.65	9.97	44.11	na	1.48	na	na	4.48	2.42	1.34	8.02	na
K_D1	3652	19.08	0.56	13.18	48.61	na	1.31	na	na	8.52	na	0.82	7.92	na
K_D1	3174	22.41	0.18	7.96	50.77	na	4.94	na	na	6.03	na	2.58	5.13	na
A_C3	3727	21.48	0.3	14.74	42.87	na	na	na	na	11.32	na	0.74	8.56	na
O_A1	3940	24.82	na	14.05	40.02	na	na	na	na	14.71	na	1.55	4.84	na
O_A1	3950	20.15	na	6.81	54.54	na	na	na	na	11.37	na	na	7.13	na

Note:
O- Oxygen, Mg- Magnesium, Al- Aluminium, Si- Silicon, P- Phosphorous, S- Sulphur, Cl- Chlorine, Cr- Chromium, K- Potasium, Ca- Calcium, Ti- Titanium, Fe- Iron and Ni- Nickel.

Silicon has the highest % weight composition and % atomic composition across the setting. HST sediment is typical of high silica content, which is confirmed by the % weight and % atomic composition of silicon and oxygen. Aluminium and potassium shows almost equal intensity across the setting except in some few cases where the intensity of iron is more than that of Al and K: A_O1 (3242 m), A_F1 (1179 m) and A_F1 (1180 m). Within wells A_F1, K_A2, K_D1, A_C3 and O_A1 samples, Fe replaces Ca making formation of iron-rich chamosite chlorite possible. Chlorine is found in all A_F1 samples, A_O1 (3242 m) and K_A2 (1690 m) which indicates sea water influence in the setting. Sulphur is only found in samples A_O1 (3175 m), K_B1 (1350 m), K_B1 (1910 m), K_D1 (3652 m) and K_D1 (3174 m) indicating basaltic origin of the sediment. Titanium exists in the samples in the setting except A_F1 (1179 m), K_A2 (1690 m) and O_A1 (3950 m) which indicates granitic silicate source (Choo et al., 2002). The elemental composition supports the formation of various minerals seen in the XRD results in the setting which are: montmorillonite, chlorite, quartz, hematite and pyrite.

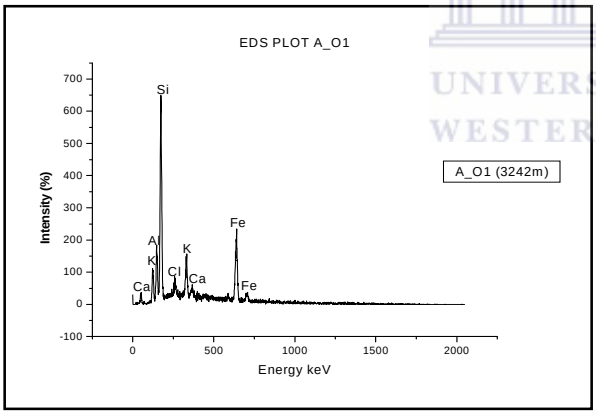

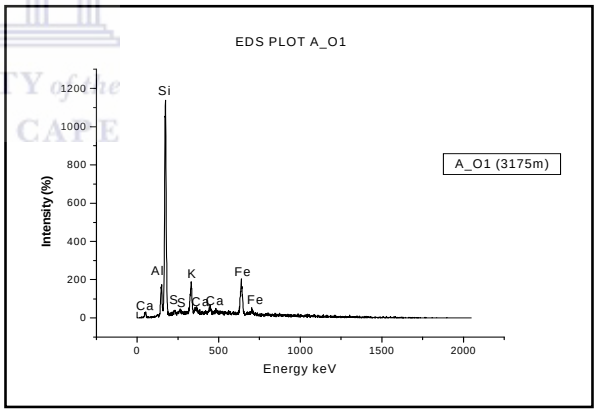

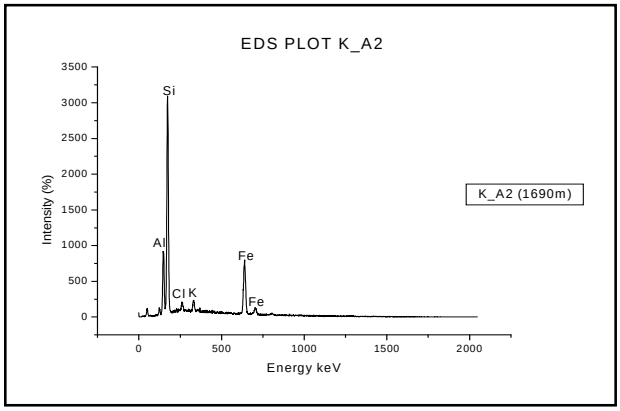

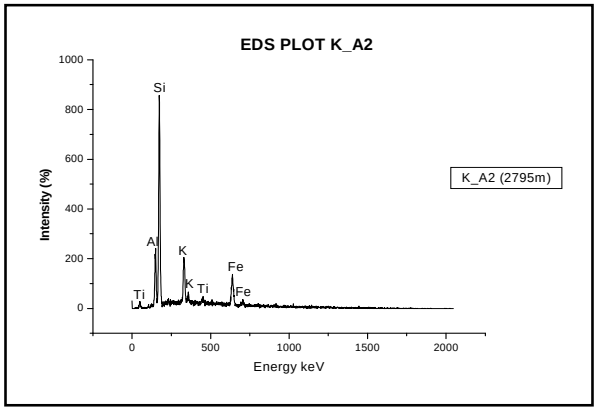

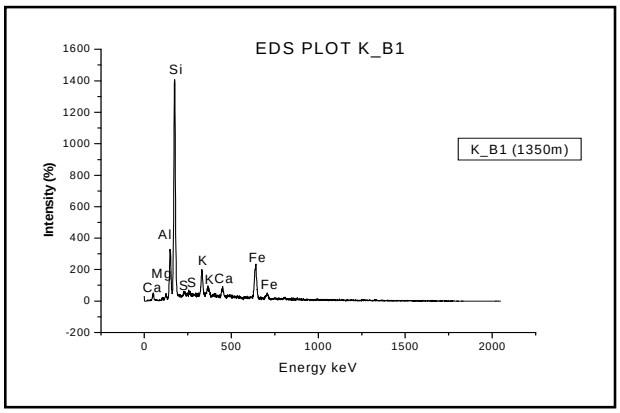

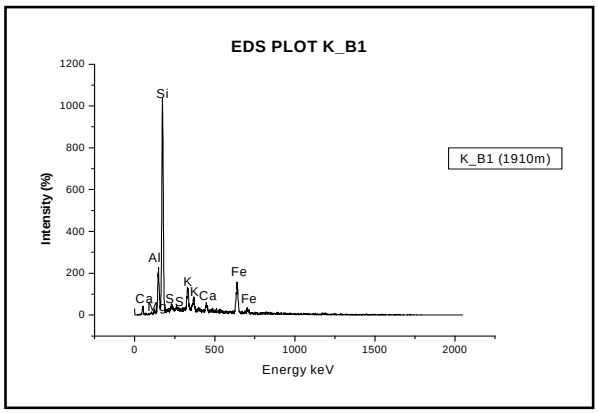

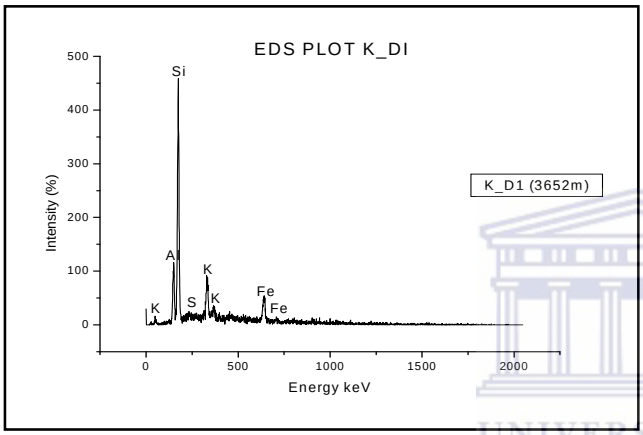

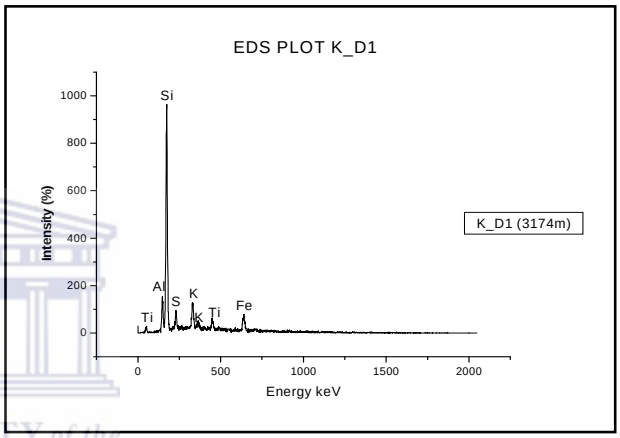

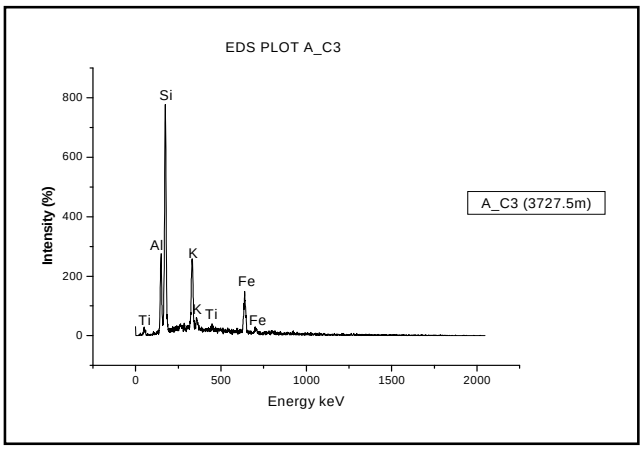

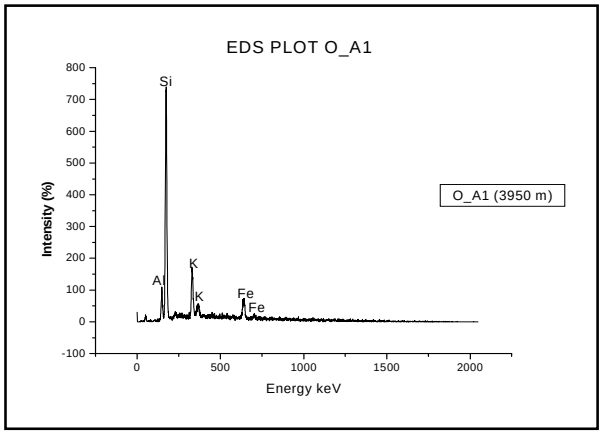

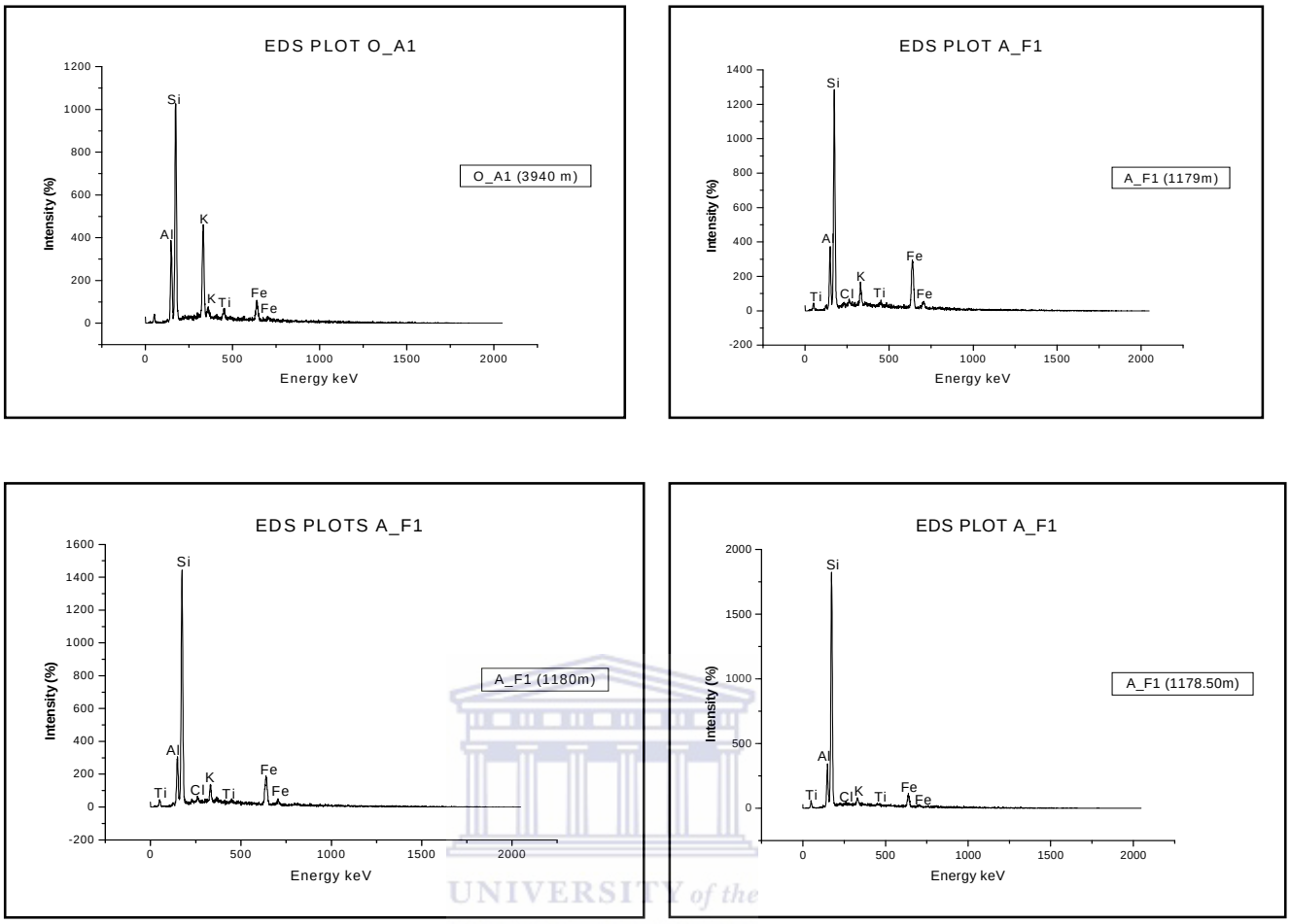

Fig. 4-17. EDS elemental distribution of samples within HST

4.5.6 Stable isotope analysis results

Carbon and oxygen isotope data were reported in the δ notation relative to the Vienna PeeDee Belemite (PBB) and standard mean ocean water (SMOW), respectively in tables 4.6 to 4.8.

The variations in $\delta^{13}C$ and $\delta^{18}O$ values in all the settings are illustrated in figure 4-18. The values of $\delta^{13}C$ and $\delta^{18}O$ increase with depth in all the wells except in well K_D1 within LST. The oxygen isotope data within LST shows a range of -1.648 to 10.054 vs SMOW with an average of 5.19 and $\delta^{13}C$, -25.667 to -12.44 vs PDB. The age of the samples in the LST range from Barremian - Santonian (Table 4.6). The TST shows similar trend of $\delta^{13}C$ and $\delta^{18}O$ except in well A_C2. The TST shows a range of -1.574 to

13.134 vs SMOW for oxygen and -27.862 to -6.954 vs PDB for carbon with the age ranging from Barremian - Turonian (Table 4.7). In the HST, the values of $\delta^{13}C$ increase with depth except in well K_D1. The $\delta^{18}O$ values increase with depth in all the wells except in wells K_D1 and K_A2, with the age ranging from Barremian - Campanian (Table 4.8).

Table 4.6. Geochemical results including pore water data and stable isotopes data of samples from the LST.

Well name	Depth (m)	Age	normalized Uδ13C vs. VPDB	normalized Uδ18O vs. VSMOW	pH	Ec	tds	eh
A_O1	3175	Barremian	-9.750	7.356	6.7	0.54	0.62	143
A_O1	3305	Barremian	-7.820	9.628	8.6	0.46	0.3	168
K_A2	2765	Lower Albian	-25.667	2.099	nd	nd	nd	nd
K_B1	1910	Santonian	-25.244	3.910	7.2	0.42	0.46	152
K_B1	1950	Santonian	-12.512	10.054	7.6	0.62	0.39	160
K_D1	3272	Albian	-14.954	7.155	nd	nd	nd	nd
K_D1	3652	Aptian	-23.018	4.956	nd	nd	nd	nd
A_C3	3597	Albian	-23.203	-1.648	nd	nd	nd	nd

Table 4.7. Geochemical results including pore water data and stable isotopes data of samples from the TST.

Well name	Depth (m)	Age	normalized Uδ13C vs. VPDB	normalized Uδ18O vs. VSMOW	pH	Ec	tds	eh
A_O1	3242	Barremian	-6.954	13.134	nd	nd	nd	nd
A_O1	3601	Barremian	-27.862	-0.162	nd	nd	nd	nd
K_A2	1690	Turonian	-23.224	7.376	7.8	0.56	0.44	169
K_A2	2215	Turonian	-24.142	2.961	7.62	0.61	0.3	132
A_U1	2688	Mid-Early Cenomanian	-23.839	2.345	8.15	0.44	0.25	178
A_U1	2694	Mid-Early Cenomanian	-23.239	0.924	nd	nd	nd	nd
A_U1	2697	Mid-Early Cenomanian	-20.657	3.969	nd	nd	nd	nd
A_C2	3245	Aptian	-22.089	-1.574	5.72	0.63	0.37	123
A_C2	3246	Aptian	-22.104	-1.169	nd	nd	nd	nd
A_C3	3670	Aptian	-23.149	3.705	nd	nd	nd	nd
A_C3	3675	Aptian	-24.502	1.567	nd	nd	nd	nd

Table 4.8. Geochemical results including pore water data and stable isotopes data of samples from the HST.

Well name	Depth (m)	Age	normalized Uδ13C vs. VPDB	normalized Uδ18O vs. VSMOW	pH	Ec	tds	eh
A_F1	1178	Turonian	-24.847	-0.267	6.79	1.36	0.78	185
A_F1	1179	Turonian	-24.841	0.482	nd	nd	nd	nd
A_F1	1180	Turonian	-21.307	16.180	nd	nd	nd	nd
A_O1	3493	Barremian	-19.935	2.233	nd	nd	nd	nd
A_O1	3679	Barremian	-27.407	0.685	nd	nd	nd	nd
K_A2	1963	Turonian	-27.009	1.919	nd	nd	nd	nd
K_A2	2795	Mid Albian	-25.057	1.634	nd	nd	nd	nd
K_B1	1350	Campanian	-21.963	4.026	nd	nd	nd	nd
K_B1	2060	Santonian	-20.569	6.883	nd	nd	nd	nd
K_D1	3174	Lower Albian	-22.064	3.920	nd	nd	nd	nd
K_D1	3692	Lower Albian	-24.381	2.227	8	0.52	0.46	142
A_C3	3727	Barremian	-25.904	-1.712	6.26	1.12	0.68	180
O_A1	3862	Barremian	-22.834	-2.644	nd	nd	nd	nd
O_A1	3874	Barremian	-22.636	-1.132	7.2	0.43	0.25	191

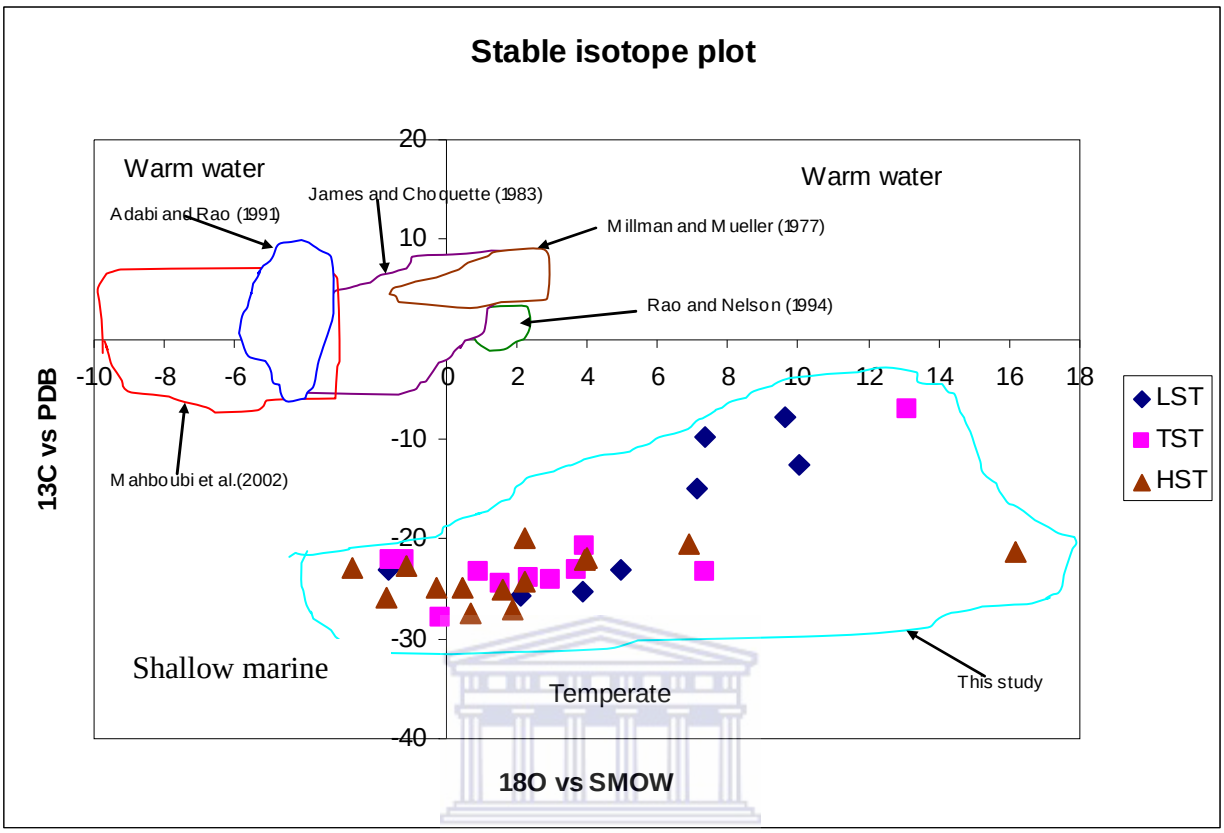

Fig. 4-18. Comparison of $\delta^{18}0$ and $\delta^{13}C$ values within generic packages (Systems tracts) of sandstone with published stable isotope data of other sandstone in the world.

LST isotopic interpretation

The oxygen isotope data within the LST show a range of -1.648 to 10.054 vs VSMOW with an average of 5.191 vs VSMOW (Table 4.6). This range falls within modern sea water and normal marine precipitated calcite cement (Shikazono and Utada, 1997; Scholle, 1978; Bellanca et al., 2005). The first marine input to the basin happened between Late Hauterivian and Early Aptian (112-117.5 Ma) just after the break-up unconformity at 117.5 Ma (Brown et al., 1996; Jungslanger, 1996; Soekor, 1994a, b). The age of the samples in this setting ranged from Lower Albian - Conaician. Rust and Summerfield, (1990) reported the increase in the rate of sedimentation near the mouth of Orange River in Late Cretaceous. This was substantiated by Gilchrist et al., (1994)

suggesting that breaching may have occurred at this time in the southwestern African margin. Some of the samples in this setting must have been deposited at this time as a result of filling the gap that was created.

There is oxygen enrichment with depth in wells A_O1 and K_B1 samples that intersected the LST setting. Well K_D1 samples show oxygen isotope depletion down the depth. This depletion may be as a result of re-crystallisation and meteoric water influence (Bellanca et al., 2005). 50 % of the samples in the setting fall within the range of mixture of detrital quartz which is put at between 6.4 to 20 % for $\delta^{18}0$ (Garlic and Epstein, 1967; Savin and Epstein, 1970; Clayton et al., 1972; Eslinger et al., 1973; Blatt, 1986 and Graham et al., 1996). The carbon isotope shows a range of -25.667 to -7.820 with an average of 17.565 vs VPDB. The moderately negative carbon isotope composition of 50 % of the samples indicates a normal marine signature likely modified by sedimentary organic matter decay (Bellanca et al., 2005). Comparison of the stable isotope data set from different parts of the world by Allan and Wiggins (1993) with the data of present study shows that the samples plot within relative low temperature zone which also confirms the thermal subsidence evidence in the basin between Albian and Cenomanian (Brown et al., 1996; Jungslanger, 1996; Seokor, 1994a, b).

TST isotopic interpretation

The TST setting shows a range of -1.574 to 13.134 vs VSMOW for $\delta^{18}O$ isotope and -27.862 to -6.954 vs VPDB for $\delta^{13}C$ (Table 4.7). The oldest sample was sourced from Barremian which is part of the first incursion of marine to the basin (Brown et al., 1996; Jungslanger, 1996; Seokor, 1994a, b). The oxygen isotope range falls within normal marine environment (Scholle, 1978; Bellanca et al., 2005). Two of the samples fall within sea water range of between -1.2 to -0.7 % VSMOW (Lavelle et al, 2001). Two of the samples in this systems tract (A_O1 3305 m; K_A2 1963 m) indicate mixture of detrital quartz grains using 6.4 to 20 vs VSMOW for $\delta^{18}O$ (Garlic and Epstein, 1967; Savin and Epstein, 1970; Clayton et al., 1972; Eslinger et al., 1973; Blatt, 1986 and Graham et al., 1996).

Approximately 10 % of the samples in this setting show moderately negative carbon isotope composition which may reflect normal marine signature slightly modified by variable contribution of CO_2 derived from sedimentary organic matter decay (Bellanca et al., 2005).

HST isotopic interpretation

The oxygen isotope data of samples from the HST show high values indicating a marine water precipitation (Scholles, 1978). Approximately 15 % of the samples fall within sea water field between -1.2 and -0.7 % VSMOW (Lavelle et al, 2001). 15 % of the samples also indicate mixture of detrital grains using 6.4 to 20 % for $\delta^{18}O$ (Garlic and Epstein, 1967; Savin and Epstein, 1970; Clayton et al., 1972; Eslinger et al., 1973; Blatt, 1986 and Graham et al., 1996). All the samples in the setting show extremely negative $\delta^{13}C$ values (between -27 and -20 %). The consistency in $\delta^{13}C$ occurrence across the stratigraphic sequences with exception of well A_O1 in the LST and one sample in the TST is an indication that the burial diagenesis has not shown significant effect on the abundance and geochemical significance of the $\delta^{13}C$ (Schmid et al., 2006).

As observed in the other systems tracts, all the samples in this setting show extremely negative $\delta^{13}C$ values, suggesting influence of terrestial organic matter decay (Bellanca et al., 2005).

4.6 Diagenetic alteration processes and reservoir environmental evolution in the basin

The combination of stable isotope data with petrographic data of the rock samples can be used to determine the geochemical environment of formation of authigenic minerals and thereby elucidate diagenetic mechanisms (Shikazono and Utada, 1997). The petrographic studies showed that the Orange Basin has had a complex diagenetic history (Fig. 4-19). These diagenetic processes include compaction, cementation /micritization, dissolution silicification, and fracturing.

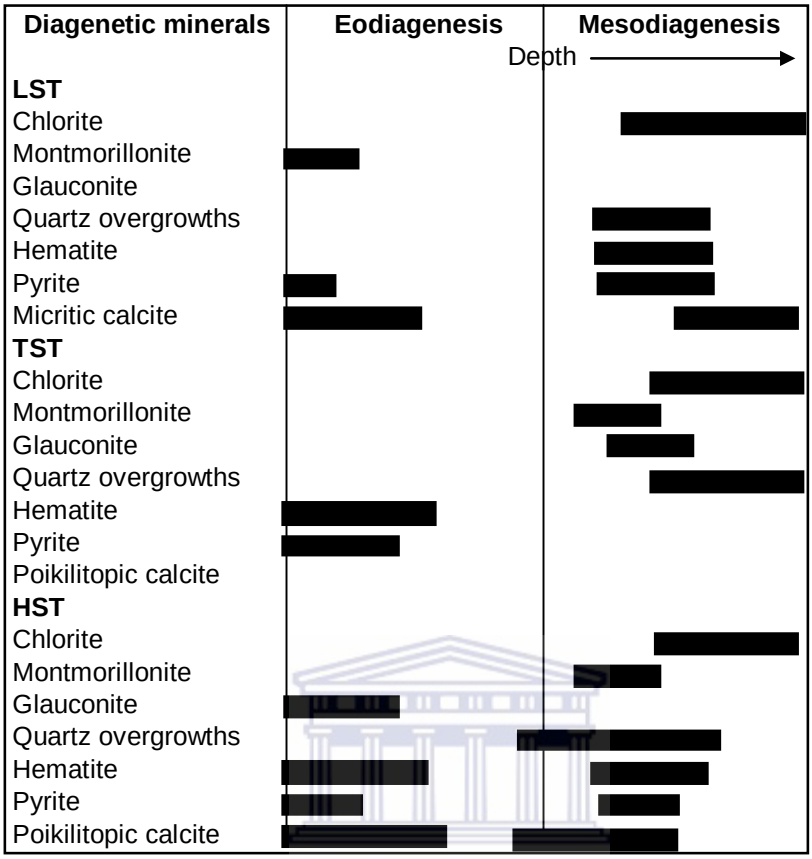

Fig. 4-19. Paragenetic sequence of the diagenetic alteration sandstones within the stratigraphic settings of Orange Basin using XRD and thin section results. The boundary between eodigenesis is < 2 km and mesodiagenesis is > 2 km according to Morad et al., (2000).

Compaction

The samples analysed for petrographic studies within HST shows evidence of tight packing, point grain contacts thereby reducing primary depositional porosity before cementation began (Fig. 4-6). As reported by Morad et al., (2000), eodiagenesis takes place at a depth less than 2 km and temperature less than 70 ° C. Samples from well K_A2 (1690 m) supports this postulation (Fig. 4-8). There was increase in the rate of sedimentation near the mouth of the Orange River during the Late Cretaceous (Rust and Summerfield, 1990) which led to breaching at this period in the southwestern Africa margin (Gilchrist et al., 1994). This must have imposed severe pressure on the sediments

thereby enhancing the constituent particles to be tightly packed. The grain contact in samples of TST and HST also support this (Figs. 4-7 and 4-8). Other evidence of compaction is the flattening of mica and rock fragment in K_B1 (2060 m) in LST even distal to the mouth of Orange River (Fig. 4-6 in K_B1 1950m and 2060 m) and HST samples (Fig. 4-8 A_C3 (3727.5 m).

Cementation/micitization

The different fabric displayed by the cements of the sandstone is suggesting that precipitation of the cements occur in different diagenetic environments, from marine through meteoric. The cement observed in samples in the LST is micritic calcite, completely filling the pore which is an evidence of marine diagenesis (El-ghali et al., 2009). The first marine incursion to the basin was during Barremian (Broad et al., 2006) in which the oldest sample in this study was deposited. The cementing conditions within TST and HST are not similar; this is suggesting different precipitation conditions within these systems tract. The cement type range from dense micritic calcite to grains embedded in poikilitopic calcite cement and also chlorite cement completely filling the pore spaces in TST, for example in sample A_C2 (3245.16 m) (Fig. 4-7). The cementation process really reduced the primary porosity because the pore spaces are severely blocked thereby contributing to the poor quality of reservoir rock in these wells.

Dissolution

The LST samples show an average pH value of 7.8 an alkaline condition (Table 4.7). The results of pore water analysis show that the pH condition within TST and HST is between weak acidic to slightly alkaline conditions (Tables 4.7 and 4.8). This should ordinarily aid leaching and generation of secondary porosity. This is not so in the wells studied because the pore spaces that might have been created through leaching are completely filled up by the process of cementation in all the stratigraphic as a result of the previling alkaline condition. The above conditions must have been responsible for the authigenic minerals and cementing materials found across the stratigraphic sequences. Chlorite and montmorrilonite which are the common authigenic minerals in the study are reported to be precipitated under weak acidic to alkaline conditions (Krumbein and Garrels 1952,

Shikazono and Utada 1997). The micritc calcite cement is also reported to be formed under these conditions. The authigenic kaolinite that is formed under strong acidic condition was not encountered in this study.

Silicification/quart growth

Well K_D1 samples at depths 3272 m and 3692 m (Fig. 4-6) within LST show evidence of silicification which affect the whole skeletal grains in the samples. This is also observed in K_B1 (1350 m) and A_C3 (3727. 5 m) samples in the HST (Fig. 4-8). Generally silica occurs in the form of chert and microcrystalline quartz. There is also an evidence of growth of quartz forming quartz overgrowth within TST and HST settings (Figs. 4-7 and 4-8).

Fracturing

The petrography of sandstones within LST reveals severe fracturing (Fig. 4-6). In some cases the fractures are healed up by new materials (Fig. 4-6 K_D1 1950 m), in some fracture still preserved (Fig. 4-6 K_B1 2060 m, K_D1 3693 and K_D1 3272 m). It was observerd in the samples within TST and HST that fractures are covered or filled up with secondary calcite cements (Figs. 4-7 and 4-8). Fracturing can enhance reservoir quality because when connected it improves permeability and transmisitivity. In the stratigraphic sequences under investigation the secondary mineral deposition severely impaired the reservoir quality of the sandstones, by covering every available space resulting in the poor quality of the reservoir rock (Fig. 4-6).

4.7 Diagenetic events within the depositional settings

The isotope results showed that the cementing materials were precipitated in temperate water, shallow marine condition (Fig. 4-18). A marine environment is characterised by slightly alkaline waters (sea water pH is 8.3). The LST deposition occurs as a response to fall and slow rise in relative sea level (Worden and Morad, 2003). The basin floor fan sediment of the LST setting must have bypassed the shelf through the incised valleys and deposited on the slope (Brown et al., 1996). Burial and mechanical compaction of the ductile interclast resulted in the formation of pseudomatrix as seen in

the thin sections. During the early to middle Aptian extensive drowning of the margin occurred and regional organic rich petroleum source shale was deposited (Van der Spuy, 2003). The setting shows carbon isotope range of -25.667 to -7.820 %. The extremely negative $\delta^{13}C$ values (between -25 and -16 %) of some samples may point to methane as a major source of the carbon (Bellanca et al., 2005). The moderately negative carbon isotope values indicate a normal marine signature which may be slightly modified by a variable contribution of CO_2 derived from sedimentary organic matter decay.

The authigenic calcite occurs in pores and fractures as micritic and coarsely crystalline or poikilitic calcite cements. Texturally the calcite was formed after chlorite and quartz overgrowth, because the calcites are seen covering all these authigenic minerals in all the settings. Within TST the micritic calcite cement was observed to continue to deeper depths (Fig. 4-7). The original depositional textures are obscured in the sandstone across the stratigraphic sequence of Orange Basin, in which calcite cements occur as grains replacement. The poikilitic calcite cement in HST samples in A_F1 (1180 m) was preserved and virtually outlines the grain contacts.

Chlorite precipitation implies basic pore solutions enriched in Fe^{2+} and Mg^{2+} (Small et al., 1992). A large volume basic water source is sea water which is typically buffered between pH 8.0 and 8.4 (Brownlow, 1979). The pore water analysis of samples across the basin shows a near similar condition. The LST shows average pH of 7.80, conductivity (Ec) average of 0.51 mS, and average redox potential (eh) 0.16 mV (Table 5.6).Within TST the average pH is 7.32, with conductivity (Ec) average of 0.56 mS and average oxidation-reduction potential (eh) of 0.15 mV (Table 4.7). The HST has average pH of 7.06, Ec of 0.86 mS and average eh of 0.74 mV (Table 4.8). These conditions support clay conversion (De Ros et al., 1994). The pH values within the stratigraphic settings exceed 7, thereby facilitating the reaction of HCO_3^- with dissolved Ca^{2+} to form calcite (Morse and Mackenzie, 1990; Schulz and Zabel, 2000). It is inferred that montmorillonite might have been converted to chlorite in the basin based on the XRD results and the dominance of chlorite over montmorillonite in the thin sections. The prevailing condition of the basin using chemical evaluation parameter discussed above satisfies Krumbein and Garrels, (1952) explanations for determination of origin of these authigenic minerals. Pyrite found in the basin my have been formed from precipitation in

alkaline condition. The silica requires weakly alkaline condition for its precipitation. The hematite that require oxidising condition for it precipitation can also persist in slightly reducing alkaline condition (Krumbein and Garrels, 1952).

Diagenetic alteration within different stratigraphic settings shows both eodiagenetic and mesodiagenetic events (Fig. 4-19). Within the LST the eodiagenesis event includes montmorillonite precipitation. The micritc calcite and the pyrite trend span from eodiagenesis to mesodiagenesis. Chlorite, quartz overgrowth and hematite formation are mainly mesodiagenetic event in the LST. Deposition of the LST occurs as a response to fall and slow rise in the relative sea level. The TST shows limited eodiagenesis events only in pyrite and hematite formations. This may be as a result of coarse grained sediments entrapped landward there by increasing the concentration of glauconite. This must have been the reason for the glauconite formation being pushed to the mesogenesis. The other mesodiagenetic events in the TST include chlorite, montmorillonite and quartz overgrowth formation. The main cementing materials in the settings are chlorite, micritic calcite and coarse crystalline calcite.

The HST shows more eodiagenesis events that span to mesodiagenesis with quartz overgrowth, hematite, pyrite and poikilitic calcite formations. The authigenic chlorite and montmorillonite are products of mesodiagenetic events. Deposition in the HST occurs in response to gradual sea level rise and later during initial stages of sea level fall. There was high influx of sediments in the Orange Basin during Late Cretaceous (Brown et el., 1990; Dingle and Hendry, 1984; Rust and Summerfield, 1990); this may thereby cause shoreline transgression to give way for regression and also increasing progradational stacking (Worden and Morad, 2003). This scenario may increase sand and mud ratio up the HST being accompanied by increase in the amount of authigenic glauconite, the reason for the eodiagenetic glauconite in HST. Landward top of HST is associated with widespread fluvial deposition (Posamentier et al., 1988). The fluvial deposit in well A_F1 within the HST maybe formed as a result of prevailing temperate climatic conditions which are subjected to clay infiltration pedogenesis or the formation of Mg-rich clay minerals in the setting.

4.8 Source Evaluation

4.8.1 Rock-Eval Pyrolysis

The results of Rock-Eval pyrolysis and Total Organic Carbon (TOC wt %) are presented based on the systems tract (LST, TST and HST) and the results are presented in Tables 4.9a to 4.11b.

4.8.1.1 Source Rock Potential within LST

The results of the LST samples which age range from Early Cretaceous to Late Cretaceous show most of the samples being marginally organic rich, a few samples are organic rich though (Table 4.9a). About 31% of the samples have good source rock potential, the remaining samples have poor source rock potential (Table 4.9b). The LST TOC values ranged from 0.15 to 4.03 wt % with an average of 1.44 wt %. The overall distribution of TOC is skewed towards values greater than 1.0, with approximately 77 % of the samples falling in the range of marginally organic rich to organic rich organic rocks, which could be potential source rocks if they are thermally mature and of good quality organic matter type (Peters and Cassa, 1994). This may be as a result of anoxic conditions which are possible within the LST parasequence set (Katz, 1994) that aided the preservation of the variable organic matter quality supplied. The LST prograding has some potential for organic matter development during aggradational phase and the few organic rich materials observed here may be restricted to incised valley (Emery et al., 1996).

The LST of the Orange Basin is found to contain incised valleys as seen on seismic and reported by Brown et al. (1996). The plot of TOC versus hydrocarbon potential (Fig. 4-20) shows that a preponderance of the samples is organic rich while a good number of the samples are organic lean. The hydrogen and oxygen indices as plotted on van Krevelen plot shows a variable organic matter type ranging from, marine Type II to mixed Type II/III, terrestrial Type III and inert Type IV (Fig. 4-21) (Tissot and Welte, 1984; Bordenave, 1993). S2/S3 values of these samples also indicate the kerogen type to range from Type II to mixed Type II/III, terrestrial Type III and inert Type IV (Table 4.9a). The S2 yield, liberated during pyrolysis is very useful to determine the generative potential of the source rock (Peters, 1986, Bordenave, 1993). A preponderance of the samples have S2 values less than 4.0 mgHC/g rock (Table 4.9a).

Pyrolysis S2 yields less than 4.0 mgHC/g rock is generally considered to be source rock with poor generative potential, yields greater than 4.0 mgHC/g rock are common in petroleum source rocks (Bordaenave, 1993). Therefore, only four samples, A_F1(1300 m), A_F1(1430 m), O_A1(3789 m), and O_A1(3792 m) can be considered to have good petroleum generative potential (Table 4.9a), the values of S1+S2 of these samples also support this. Sample A_C3 (3129 m) although displaying a TOC of 2.03 wt% and Tmax of 438 ^{o}C, could have been rated to be good to very good potential source rock but with the values of S2 of 1.34 mgHC/g rock, this suggest poor generative potential, and at best could yield gas. The maturity of the source rock samples were also determined using Tmax values, based on Peters and Cassa (1994) report, about 50 % of the samples are thermally immature with a few samples marginally mature (Table 4.9b, Fig. 4-22). The two samples that could be considered thermally mature have poor kerogen quality.

Table 4.9a Results of Rock-Eval analysis of samples sourced from wells within LST

Well name	Top Depth (m)	TOC (%)	S1 (mgHC/g rock)	S2 (mgHC/g rock)	S3($mgCO_2$/g rock)	Tmax (°C)	HI	OI	S2/S3
A_F1	1430	4.03	0.42	6.81	0.95	431	169	2.00	7.20
A_F1	1780	0.63	0.00	0.01	0.08	ND	100	14.00	0.70
A_K2	2540	1.02	0.32	0.63	0.85	433	116	9.00	1.00
A_K2	2545	0.76	0.37	1.18	1.23	433	46	12.00	0.10
K_A2	1855	0.15	0.03	0.35	3.88	428	7	60.00	0.10
K_D1	3447	1.11	0.16	0.70	1.89	430	63	8.00	0.40
A_U1	2210	1.37	0.24	0.77	1.23	430	56	7.00	0.60
A_U1	2220	1.27	0.23	0.39	1.98	438	31	7.00	0.20
A_C3	3129	2.03	0.62	1.34	1.25	438	66	4.00	1.10
O_A1	3741	1.69	0.38	0.77	2.55	429	46	5.00	0.30
O_A1	3789	3.07	3.06	4.68	0.28	433	152	3.00	16.70
O_A1	3792	3.08	2.64	5.08	1.20	429	165	3.00	4.20

Note: HI indicates hydrogen index, OI indicates oxygen index

HI = hydrogen index = S2 x 100 / TOC

OI = oxygen index = S3 x 100 / TOC

Table 4.9b Results of Rock-Eval analysis of samples sourced from wells within LST

Well name	Top Depth (m)	TI =(S1*100/TOC)	PI= (S1/S1+S2)	(S1+S2) (mgHC/g rock)	SRP	Maturation	Age
A_F1	1430	10.00	0.06	7.23	Good	Marginally mature	Turonian
A_F1	1780	51.00	0.34	0.01	Poor	Immature	Cenomanian
A_K2	2540	36.00	0.24	0.95	Poor	Immature	Cenomanian
A_K2	2545	4.00	0.08	1.55	Fair	Immature	Cenomanian
K_A2	1855	0.00	0.00	0.38	Poor	Immature	Turonian
K_D1	3447	14.00	0.19	0.86	Poor	Marginally mature	Late Aptian
A_U1	2210	18.00	0.24	1.01	Fair	Marginally mature	Late Cenomanian
A_U1	2220	18.00	0.37	0.62	Poor	Mature	Late Cenomanian
A_C3	3129	30.00	0.32	1.96	Fair	Mature	Late Aptian
O_A1	3741	22.00	0.33	1.15	Fair	Immature	Late Aptian
O_A1	3789	100.00	0.40	7.74	Good	Marginally mature	Early Aptian
O_A1	3792	86.00	0.34	7.72	Good	Immature	Early Aptian

Note: PI indicates production index, SRP indicates source rock potential

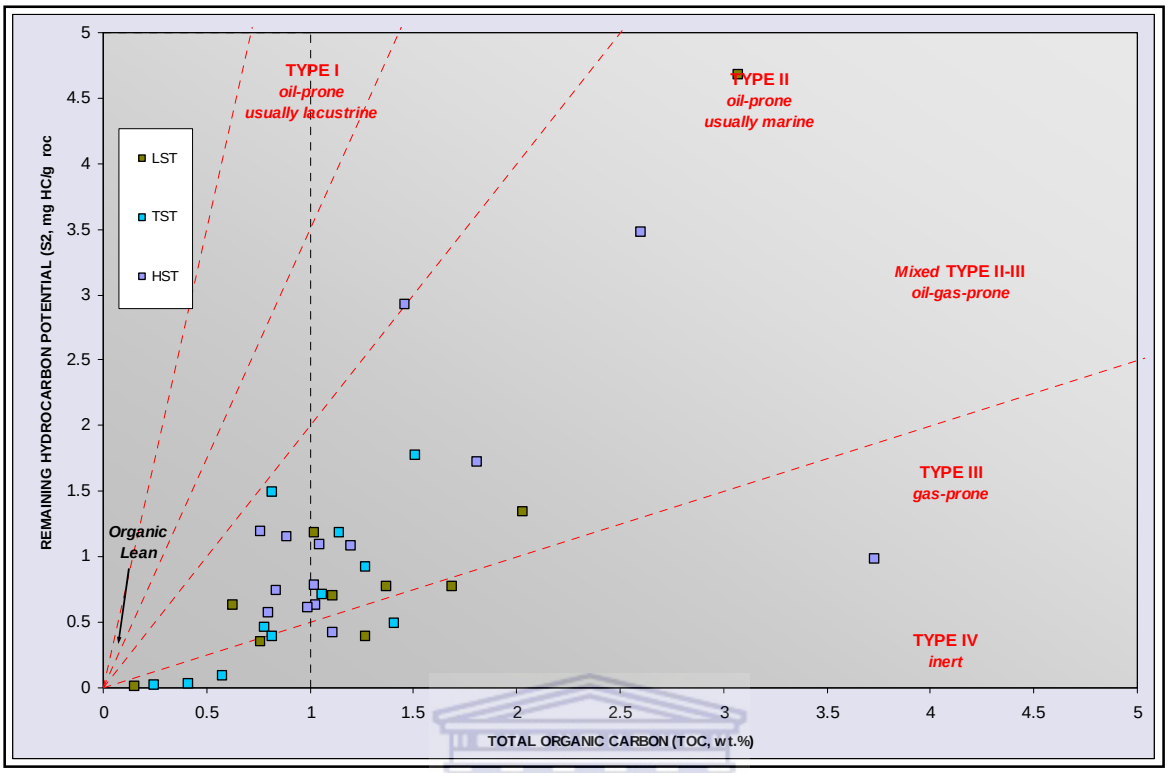

Fig 4-20 The Plot of Remaining hydrocarbon potential against total organic carbon

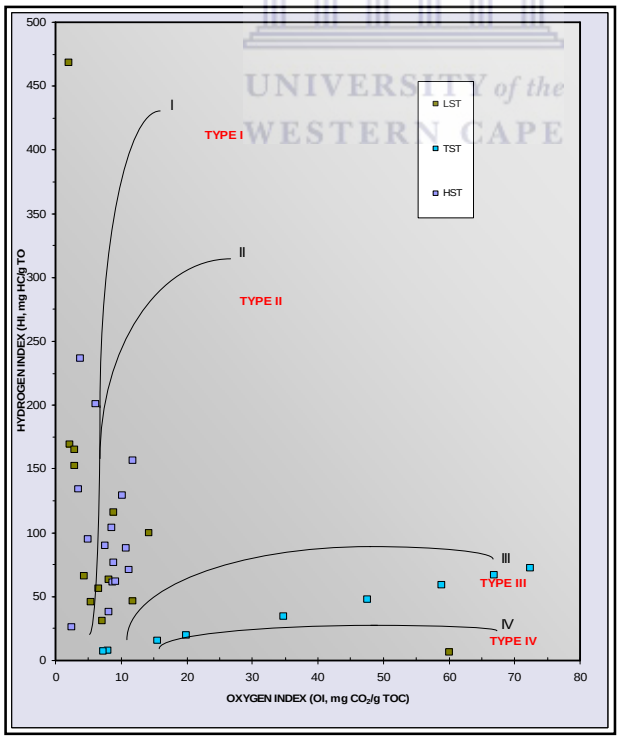

Fig 4-21. The Plot of hydrogen index against oxygen index

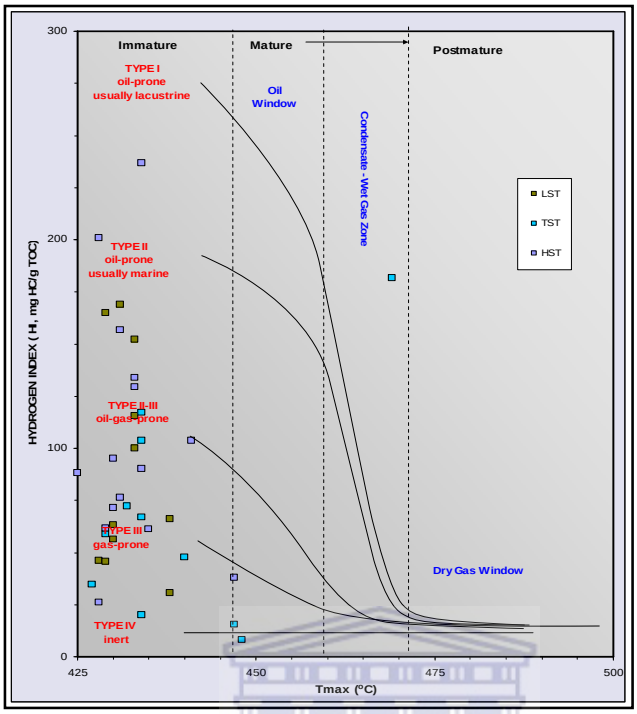

Fig 4-22. Plot of Hydrogen Index against Tmax

4.8.1.2 Source Rock Potential within TST

This is a parasequence set that is marked by transgressive surface below and maximum flooding surface above (Van Wagoner et al., 1990). 12 samples from 5 wells at TST intersections were collected for analyses. Many authors have reported that the TST setting shows good correlation between occurrence of organic matter and regional transgression (Demaison and Moore, 1980; Jenkyns, 1980; Loutit et al., 1988). This should have resulted in the development of marine oil-prone source rocks in this setting (Demaison and Moore, 1980; Jenkyns, 1980; Loutit et al., 1988). The TOC values of the samples indicate that only one sample is organic rich, a few samples are marginally organic rich and the remaining samples are organic lean (Table 4.10a). S2 values indicate only one sample to have good petroleum generation potential while the rest of the samples have poor petroleum generation potential (Table 4.10a). The cross plot of HI versus OI (Fig. 4-20) indicate that most of the samples are Type III while others are Type

IV. Thus, this indicates allochthonous organic matter input and the HI values of these samples do not suggest anoxic depositional environments. Therefore the results of the study do not support the development of marine prone source rocks in the TST. The Tmax values of the samples indicate that less than 30 % of the samples are thermally mature (Fig. 4-22, Table 4.10a), the thermally mature samples are of low organic matter quality (Table 4.10b).

The development of TST involves accommodation space becoming landward of backstepping shorelines and as a result of this the shelf becomes starved with sediments (Van Wagoner et al., 1988). The interval that results from this is called a condensed section. The condensed section leads to decrease in accumulation of the organic matter on the shelf due to bioturbation (Kosters et al., 2000). This was reported in the Orange Basin within TST by Brown et al. (1996). The Orange Basin is an ideal place for the understanding of passive continental margin (Macdonald et al., 2003; Reeves and Wit, 2000; Brown et al., 1996). The poor organic matter generative potential in the basin within TST may be as a result of oxygenation which is typical of passive continental margin (Emery et al., 1996).

Table 4.10a Results of Rock-Eval analysis of samples sourced from wells within TST

Well name	Top Depth (m)	TOC (%)	S1(mgHC/g rock)	S2(mgHC/g rock)	S3 ($mgCO_2$/g rock)	Tmax (^oC)	HI	OI	S2/S3
A_F1	1300	4.30	0.52	20.15	1.41	430	469	2.00	14.30
A_F1	1320	0.25	0.11	0.02	3.12	448	8.00	36.00	0.01
A_F1	1700	0.58	0.07	0.09	0.57	447	16.00	16.00	0.16
A_F1	1980	0.41	0.08	0.03	1.00	313	7.00	22.00	0.03
A_F1	1990	0.82	0.32	1.49	1.32	469	182.00	11.00	1.13
A_K2	2525	1.51	0.49	1.77	0.92	434	117.00	6.00	1.92
A_K2	2530	1.14	0.29	1.18	0.63	434	104.00	8.00	1.87
K_A2	2655	1.41	0.11	0.49	4.54	427	35.00	6.00	0.11
K_B1	1855	1.27	0.49	0.92	4.63	432	72.00	7.00	0.20
K_D1	2997	0.78	0.18	0.46	1.04	429	59.00	12.00	0.44
A_U1	3008	1.05	0.64	1.09	2.74	441	104.00	9.00	0.40
A_U1	3068	0.82	0.22	0.39	1.00	440	48.00	11.00	0.39

Note: HI indicates hydrogen index, OI indicates oxygen index,

HI = hydrogen index = S2 x 100 / TOC

OI = oxygen index = S3 x 100 / TOC

Table 4.10b Results of Rock-Eval analysis of samples sourced from wells within TST

Well name	Top Depth (m)	TI =(S1*100/TOC)	PI	(S1+S2) (mgHC/g rock)	SRP	Maturation	Age
A_F1	1300	12.00	0.03	20.67	Good	Mature	Turonian
A_F1	1320	44.00	0.85	0.13	Poor	Mature peak	Turonian
A_F1	1700	12.00	0.44	0.16	Poor	Mature peak	Cenomanian
A_F1	1980	20.00	0.73	0.11	Poor	Immature	Cenomanian
A_F1	1990	39.00	0.18	1.81	Poor	Mature late	Cenomanian
A_K2	2525	32.00	0.22	2.26	Poor	Maginally mature	Cenomanian
A_K2	2530	26.00	0.20	1.47	Fair	Immature	Cenomanian
K_A2	2655	8.00	0.18	0.60	Poor	Immature	Cenomanian
K_B1	1855	39.00	0.35	1.41	Fair	Immature	Campanian
K_D1	2997	23.00	0.28	0.64	Poor	Immature	Albian
A_U1	3008	61.00	0.37	1.73	Fair	Mature	Albian
A_U1	3068	26.00	0.36	0.61	Poor	Mature early	Albian

Note: PI indicates production index, SRP indicates source rock potential

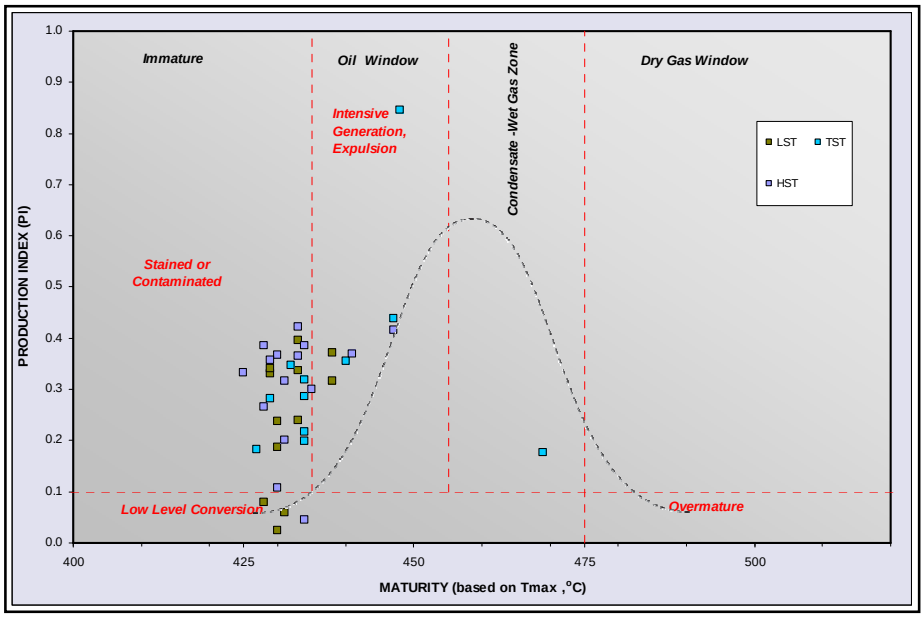

Fig 4-23. The plot of Production Index against Maturity

4.8.1.3 Source Rock Potential within HST

Marine dominated HST has the potential for high organic content if the rate of progradation is low and the organic matter are mixed with contribution from both terrestrial and marine organic matter particles (Emery, 1996). The HST is typified by maximum flooring surface below and sequence boundary above (Posamentier, 1988). In this setting organic matter is transported from continent to the ocean, the shelf functions as a trap for sediments and continent derived organic matter (Kosters et al., 2000). The trapping mechanism is only efficient when the shelf is relatively wide and the rivers contain abundant fine-grained sediments and organic matter, a condition mostly achieved during sea-level fall in HST (Kosters, et al., 2000).

Table 4.11a Results of Rock-Eval analysis of samples sourced from wells within HST

Well name	Top Depth (m)	TOC (%)	S1(mgHC/g rock)	S2(mgHC/g rock)	S3(mgCO_2/g rock)	Tmax (^oC)	HI	OI	S2/S3
A_F1	1270	2.37	0.26	5.61	0.13	434	237.00	2.00	43.20
A_F1	1290	5.91	0.24	7.36	1.30	424	124.53	22.00	5.66
A_K2	2405	0.76	0.30	1.19	3.40	431	157.00	12.00	0.30
K_A2	2572	1.81	0.21	1.72	0.44	430	95.00	5.00	3.90
K_B1	2084	0.84	0.37	0.74	2.74	425	88.00	11.00	0.30
K_B1	2423	3.73	0.49	1.90	0.38	426	50.94	10.19	5.00
K_B1	2718	0.80	0.33	0.57	2.74	430	71.00	11.00	0.20
K_B1	2721	1.02	0.36	0.78	3.12	431	76.00	9.00	0.30
K_B1	2742	1.06	0.33	0.71	1.10	434	67.00	8.00	0.65
K_B1	2808	0.89	0.66	1.15	3.02	433	129.00	10.00	0.40
K_D1	2947	1.03	0.27	0.63	2.55	435	61.00	9.00	0.20
K_D1	2979	0.99	0.34	0.61	1.04	429	62.00	9.00	0.60
K_D1	2988	1.11	0.30	0.42	3.21	447	38.00	8.00	0.10
O_A1	3741	1.20	0.38	0.77	2.55	429	90.00	8.00	0.20
O_A1	3756	1.46	0.68	1.08	5.29	434	201.00	6.00	2.20
O_A1	3771	2.60	1.84	2.93	1.32	428	134.00	3.00	0.90

Note: HI indicates hydrogen index, OI indicates oxygen index

HI = hydrogen index = S2 x 100 / TOC

OI = oxygen index = S3 x 100 / TOC

Table 4.11b Results of Rock-Eval analysis of samples sourced from wells within HST

Well name	Top Depth (m)	TI =(S1*100/TOC)	PI	(S1+S2) (mgHC/g rock	SRP	Maturation	Age
A_F1	1270	11.00	0.04	5.87	Good	Marginally matured	Turonian
A_F1	1290	0.10	0.04	7.60	Good	Immature	Turonian
A_K2	2405	39.00	0.20	1.49	Fair	Marginally matured	Cenomanian
K_A2	2572	12.00	0.11	1.93	fair	Marginally matured	Cenomanian
K_B1	2084	44.00	0.33	1.11	Fair	Immature	Santonian
K_B1	2423	44.05	0.04	2.39	Poor	Marginally mature	Santonian
K_B1	2718	41.00	0.04	0.90	Fair	Marginally matured	Coniacian
K_B1	2742	31.00	0.32	1.14	Fair	Immature	Coniacian
K_B1	2721	35.00	0.32	1.04	Fair	Marginally matured	Coniacian
K_B1	2808	74.00	0.36	1.81	Good	Immature	Coniacian
K_D1	2947	26.00	0.30	0.90	Poor	Mature	Albian
K_D1	2979	34.00	0.36	0.95	Poor	Immature	Albian
K_D1	2988	27.00	0.42	0.72	Poor	Mature	Albian
O_A1	3741	56.00	0.39	1.15	Fair	Marginally matured	Late Aptian
O_A1	3756	126.00	0.39	1.76	Fair	Immature	Late Aptian
O_A1	3771	97.00	0.42	4.77	Good	Immature	Late Aptian

Note: PI indicates production index, SRP indicates source rock potential

16 samples were collected for analyses in this setting and the results are presented in (Table 4.11a). The samples were obtained from 6 wells within the Early Cretaceous to Late Cretaceous (Table 4.11b). The TOC values ranged from 0.76 to 3.73 wt % with an average of 1.44 wt %. The TOC values indicate that about 70 % of the samples are fair to good potential source rocks while other samples have fair source rock potential (Table 4.11b). S2/S3 values also indicate prevalent of Type III and Type IV kerogen, although, one sample (A_F1, 1290 m) is suggested to be mixed Type II/III. Sample A_F1 (1290 m) that has good source rock potential is thermally immature.

The Tmax values of the samples indicate that most of the samples are immature to marginally mature while only a few samples are mature (Tissot and Welte, 1984). The cross plot of HI versus OI revealed that the samples are mainly Type III while two samples (A_F1, 1270m and O_A1, 3756 m) are mixed Type II/III with one Type IV kerogen. These results suggest contributions mainly from allochtonous organic matter with subordinate autochtomous organic matter. These results seem not to be in perfectly consistent with the Emery et al. (1996) and Kosters et al. (2000) assertion, although, there were contributions from both terrestrial organic matter and marine organic matter but the contribution from the terrestrial is pervasive. The kerogen conversion plot of the samples showed that samples are mainly immature with only a few samples in the oil window (Fig. 4-23). The only one sample (from well A_F1 at depth 1290 m) that was discriminated as marine Type II organic matter that has good source rock potential is not mature sufficiently for petroleum generation (Tables 4.11a and 4.11b).

4.8.2 Organic geochemical evaluation of the shale samples

4.8.2.1. Geochemical parameters from Rock-Eval pyrolysis, *n*-alkanes and isoprenoids

Geochemical parameters derived from gas chromatographic data of the rock extracts of the selected shale samples are presented in Tables 4.12 to 4.15. Values for the following parameters were calculated from GC data: pristane/phytane (Pr/Ph), pristane/*n*-heptadecan (Pr/nC_{17}), phytane/*n*-octadecan (Ph/nC_{18}), and carbon preference index (CPI)

of *n*-alkanes (nC_{25-33}-nC_{24-34}). The values of the Tmax, hydrogen index (HI), oxygen index (OI) and S2 (hydrocarbon generated from kerogen using pyrolysis)/S3 (released and trapped CO_2 during pyrolysis) ratio were obtained by Rock Eval pryolysis and were also listed in Table 4.15.

A representative gas chromatogram (sample O_A1 3792) for the shale sample extracts show *n*-alkanes ranging from *n*-C_{12} to *n*-C_{35} with a unimodal distribution and a maxima at *n*-C_{17} (Fig. 4-24a) indicating a typical *n*-alkane distribution for oil-derived hydrocarbons. The carbon number preference index (CPI) of the *n*-alkanes in the investigated sample set range from 0.97-1.96 (Table 4.15) and a bimodal distribution is not visible anymore in the chromatograms, thus, most samples already show an advanced level of maturity (Gulbay and Korkmaz, 2008). Samples of Aptian and Albian age and some of Cenomanian age show the highest maturity with CPI values close to one. CPI values higher than 1.5 is an indication of less mature source rocks. Based on their CPI values and compared to the other samples the Turonian and Campanian samples seem to indicate a lower maturity level (Table 4.15).

Pr/Ph values (Table 4.15) ranged from 1.21-6.30 suggesting suboxic to oxic depositional environments for most of the samples. With one exception (A_F1 1990 m depth) the Pr/Ph values of samples in all system tracts at ages between Cenomanian to Turonian are higher than 3 (Table 4.15), suggesting an input from terrestrial organic matter deposited under oxic depositional conditions (Powell, 1988). Samples of Aptian, Albian, Coniacian, Santonian and Campanian age in the wells studied show Pr/Ph ratios that ranged from 1.14-2.97 suggesting suboxic to oxic depositional conditions (Powell, 1988). The plot of carbon preference index (CPI) against Pr/Ph (Fig. 4-25; after Meyers and Snowdon, 1993) visualized that most of the samples fall into the field of more oxidizing depositional conditions with some marginal samples. However, it has to be kept in mind that the Pr/Ph ratio can be influenced by other source material than phytol from chlorophylls (ten Haven et al., 1987) and by maturity related alteration of the organic matter (Radke et al., 1980b; Dzou et al., 1995; Vu et al., 2009).

Further geochemical plots were constructed from the biomarker ratios to understand the geochemical trends in the Orange Basin. Pr/nC_{17} and Ph/nC_{18} values

ranged from 0.06-4.13 and 0.05-1.11, respectively (Table 4.15). The cross plot of these parameters (Fig. 4-26) after Peters et al. (1999) suggests three organic matter types: mainly terrigenous organic matter Type III (Tissot and Welte, 1984, Peters and Cassa, 1994, Peters et al., 1999) deposited under oxidizing conditions, mixed Type II/III organic matter (Table 4.15) (Tissot and Welte, 1984, Peters and Cassa, 1994, Peters et al., 1999) and few marine algal Type II in Late Aptian and Campanian samples. The results from the Peters et al. (1999) plot does not match in some case with the results of the kerogen typ analysis (Table 4.15) deduced from comparing the oxygen index (OI), hydrogen index (HI) and S2/S3 ratios (Table 4.15) (Tissot and Welte, 1984). However, also these data indicate mainly mixed Type III and partly Type II/III kerogen. The Aptian (Early and Late), Albian, Cenomanian, Coniacian, Santonian and Campanian samples are mainly terrestrial organic matter Type III, marine Typ II and mixed Type II/III organic matter occur in the Turonian (Table 4.15).

Information about the type and the quality of the organic matter present in the source rock was obtained from the ratio of S2 (hydrocarbon generated from kerogen using pyrolysis) to S3 (released and trapped CO_2 during pyrolysis) (Table 4.15). Peters and Cassa (1994) stated that S2/S3 less than 1 cannot generate any products. Bulk of the samples from the Campanian, Santonian, Coniacian, Cenomanian, Albian and Aptian showed S2/S3 values less than 1. Exception are sample K_B1 2423 m from the Coniacian, A_F1 1990 m, A_K2 2525 m and A_K2 2530 m from the Cenomanian as well as O_A1 3756 m and A_C3 3129 m from the late Aptian. The Early Aptian and Turonian samples (with exception of A_F1 1320 m) reveal higher S2/S3 ratios ranging from 4.2 to 43.2. This is an indication of extinite, extinite/vitrinite or vitrinite kerogen composition (Peters and Cassa, 1994) (Table 4.15). In most cases, these samples also show higher HI values indicating their hydrocarbon generation potential (Table 4.15).

Generally, samples deposited under different systems tracts (LST, TST and HST) show mainly terrestrial organic matter typified by kerogen Type III (Table 4.15). An exception form some samples of Turonian age showing marine Typ II and Typ II/III transitional organic matters in the TST and HST samples A_F1 1300 and A_F1 1270, respectively (Table 4.15).

Table 4.12. Gas chromatographic data of Orange Basin sediments within LST

Well name	Top Depth (m)	Age	Pr/Ph	Pr/nC17	Ph/nC18	CPI	TAR
A_K2	2540	Cenomanian	5.21	1.47	0.33	1.08	0.68
A_K2	2545	Cenomanian	4.84	1.33	0.37	1.10	0.99
K_D1	3447	Late Aptian	1.22	0.21	0.30	1.04	0.09
A_U1	2210	Late Cenomanian	5.37	3.75	0.89	1.29	1.65
A_U1	2220	Late Cenomanian	4.92	4.13	1.11	1.29	1.37
A_C3	3129	Late Aptian	1.51	0.14	0.14	1.08	0.09
O_A1	3789	Early Aptian	1.72	0.71	0.46	0.97	0.29
O_A1	3792	Early Aptian	1.70	0.70	0.46	1.01	0.28

Table 4.13. Gas chromatographic data of Orange Basin sediments within TST

Well name	Top Depth (m)	Age	Pr/Ph	Pr/nC17	Ph/nC18	CPI	TAR
A_F1	1300	Turonian	5.13	2.86	0.60	1.9	6.05
A_F1	1320	Turonian	4.18	1.91	0.57	1.74	5.14
A_F1	1990	Cenomanian	1.76	0.80	0.51	1.09	1.31
A_K2	2525	Cenomanian	4.88	1.38	0.39	1.12	0.98
A_K2	2530	Cenomanian	5.35	1.35	0.33	1.20	0.77
K_B1	1855	Campanian	1.52	0.42	0.43	1.90	0.64
A_U1	3008	Albian	2.47	0.53	0.26	1.05	0.27
A_U1	3068	Albian	2.67	0.46	0.2	1.02	0.21

Table 4.14. Gas chromatographic data of Orange Basin sediments within HST

Well name	Top Depth (m)	Age	Pr/Ph	Pr/nC17	Ph/nC18	CPI	TAR
A_F1	1270	Turonian	6.39	3.76	0.6	1.96	8.53
A_F1	1290	Turonian	5.78	3.62	0.65	1.86	7.17
A_K2	2405	Cenomanian	4.86	1.88	0.47	1.12	1.1
K_B1	2084	Santonian	1.14	0.74	0.65	1.24	0.43
K_B1	2423	Coniacian	1.47	0.85	0.71	1.18	0.42
K_B1	2718	Coniacian	2.64	1.27	0.58	1.15	0.59
K_B1	2721	Coniacian	2.03	0.98	0.59	1.13	0.46
K_B1	2742	Coniacian	2.02	0.98	0.65	1.13	0.61
K_B1	2808	Coniacian	2.88	1.27	0.55	1.15	0.04
K_D1	2947	Albian	1.64	0.09	0.10	1.09	0.06
K_D1	2979	Albian	1.96	0.10	0.10	1.01	0.07
K_D1	2997	Albian	2.06	0.06	0.06	1.02	0.04
K_D1	2998	Albian	2.09	0.06	0.05	0.99	0.25
O_A1	3741	Late Aptian	1.76	0.75	0.46	0.99	0.28
O_A1	3756	Late Aptian	2.04	0.84	0.45	0.99	0.27
O_A1	3771	Late Aptian	2.97	1.11	0.50	1.09	0.37

Pr= Pristane, Ph= Phytane, CPI= Carbon Preference Ratio, TAR= Terrigeneous Aquatic Ratio.

Table 4.15 Re-ordered gas chromatographic and rock eval pyrolysis results of samples collected based on wells, ages and sequences in Orange Basin

Well name	Top Depth (m)	Age	Sequence	TOC (wt %)	HI (mgHC/gTOC)	OI (mgHC/gTOC)	S2/S3	Kerogen type	Tmax (°C)	Pr/Ph	Pr/*n*C17	Ph/*n*C18	CPI
K_B1	1855	Campanian	TST	1.27	72	7	0.2	Type III	432	1.52	0.42	0.43	1.9
K_B1	2084	Santonian	HST	0.84	88	11	0.3	Type III	425	1.14	0.74	0.65	1.24
K_B1	2423	Coniacian	HST	0.8	51	10	5	Type III	430	1.47	0.85	0.71	1.18
K_B1	2718	Coniacian	HST	1.02	71	11	0.2	Type III	431	2.64	1.27	0.58	1.15
K_B1	2721	Coniacian	HST	0.89	76	9	0.3	Type III	433	2.03	0.98	0.59	1.13
K_B1	2742	Coniacian	HST	1.06	67	8	0.65	Type III	434	2.02	0.98	0.65	1.13
K_B1	2808	Coniacian	HST	3.73	129	10	0.4	Type III	426	2.88	1.27	0.55	1.15
A_F1	1290	Turonian	HST	5.91	125	22	5.66	Type III	424	5.78	3.62	0.65	1.86
A_F1	1270	Turonian	HST	2.37	237	2	43.2	Type II/III	434	6.39	3.76	0.6	1.96
A_F1	1300	Turonian	TST	4.3	469	2	14.3	Type II	430	5.13	2.86	0.6	1.9
A_F1	1320	Turonian	TST	0.25	8	36	0.01	Type IV	448	4.18	1.91	0.57	1.74
A_F1	1990	Cenomanian	TST	0.82	182	11	1.13	Type III	469	1.76	0.8	0.51	1.09
A_K2	2405	Cenomanian	HST	0.76	157	12	0.3	Type III	431	4.86	1.88	0.47	1.12
A_K2	2525	Cenomanian	TST	1.02	117	6	1.92	Type III	433	4.88	1.38	0.39	1.12
A_K2	2530	Cenomanian	TST	0.76	104	8	1.87	Type III	433	5.35	1.35	0.33	1.2
A_K2	2540	Cenomanian	LST	1.51	116	9	0.1	Type III	434	5.21	1.47	0.33	1.08
A_K2	2545	Cenomanian	LST	1.14	46	12	0.1	Type III	434	4.84	1.33	0.37	1.1

A_U1	2210	Cenomanian	LST	1.37	56	7	0.6	Type III	430	5.37	3.75	0.89	1.29
A_U1	2220	Cenomanian	LST	1.27	31	7	0.2	Type III	438	4.92	4.13	1.11	1.29
A_U1	3008	Albian	TST	1.05	104	9	0.4	Type III	441	2.47	0.53	0.26	1.05
A_U1	3068	Albian	TST	0.82	48	11	0.39	Type III	440	2.67	0.46	0.2	1.02
K_D1	2947	Albian	HST	1.03	61	9	0.2	Type III	435	1.64	0.09	0.1	1.09
K_D1	2979	Albian	HST	0.99	62	9	0.6	Type III	429	1.96	0.1	0.1	1.01
K_D1	2997	Albian	HST	0.78	59	12	0.44	Type III	429	2.06	0.06	0.06	1.02
K_D1	2988	Albian	HST	1.11	38	8	0.1	Type III	447	2.09	0.06	0.05	0.99
K_D1	3447	Late Aptian	LST	1.11	63	8	0.4	Type III	430	1.22	0.21	0.3	1.04
O_A1	3741	Late Aptian	HST	1.69	90	8	0.2	Type III	429	1.76	0.75	0.46	0.99
O_A1	3756	Late Aptian	HST	1.46	201	6	2.2	Type III	434	2.04	0.84	0.45	0.99
O_A1	3771	Late Aptian	HST	2.6	134	3	0.9	Type III	428	2.97	1.11	0.5	1.09
A_C3	3129	Late Aptian	LST	2.03	66	4	1.1	Type III	438	1.51	0.14	0.14	1.08
O_A1	3789	Early Aptian	LST	3.07	152	3	16.7	Type III	433	1.72	0.71	0.46	0.97
O_A1	3792	Early Aptian	LST	3.08	165	3	4.2	Type III	429	1.7	0.7	0.46	1.01

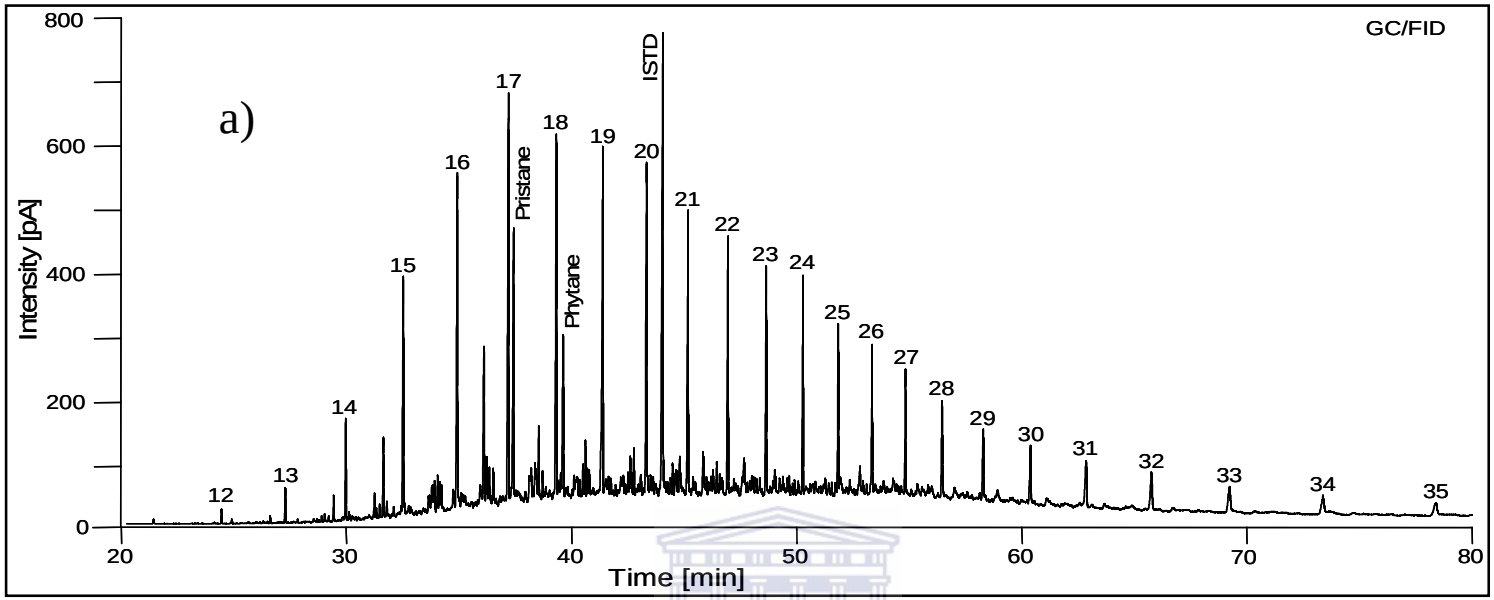

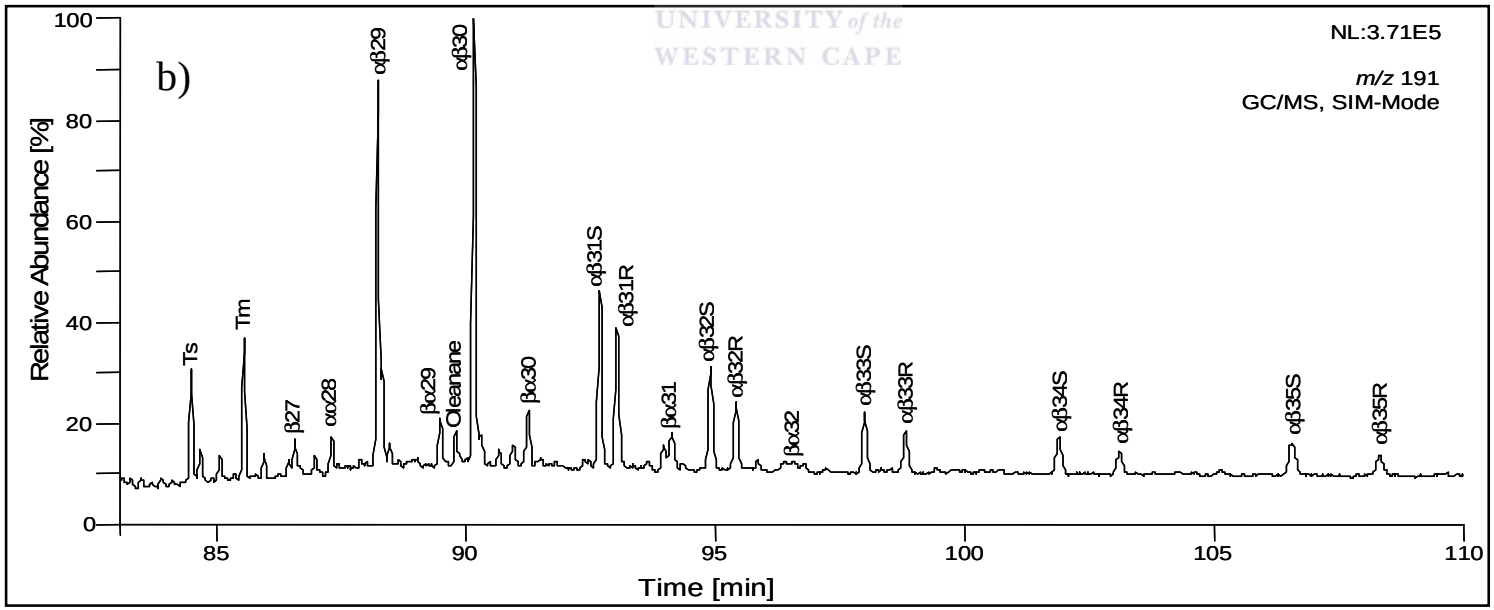

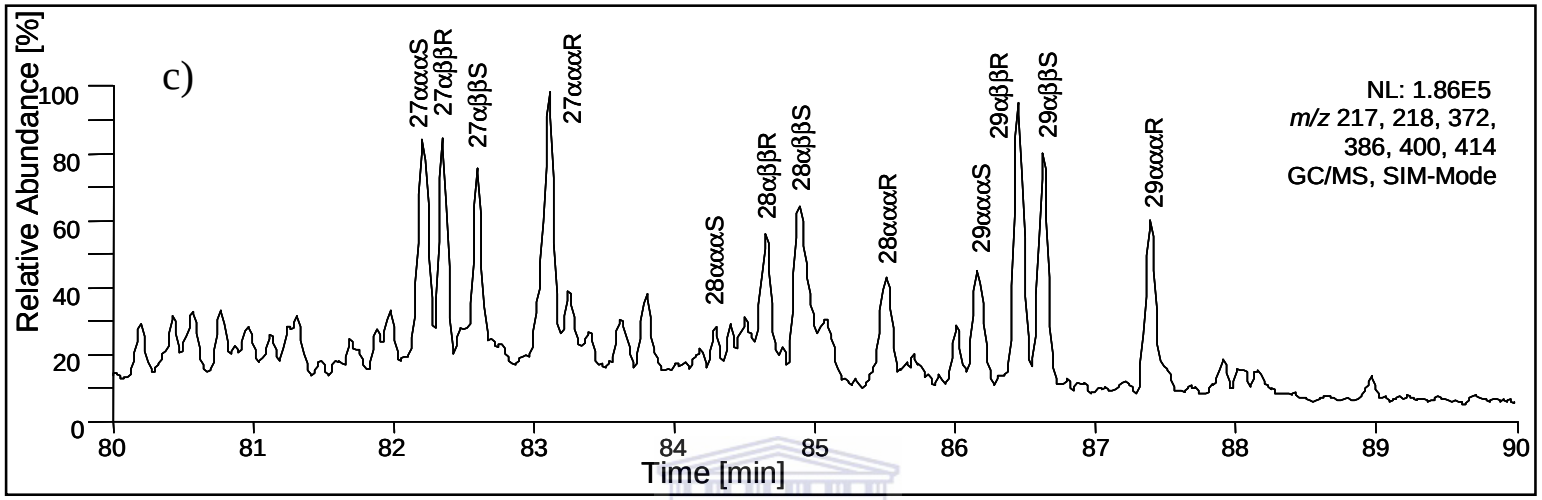

Fig. 4-24. (a) A representative gas chromatogram of rock extracts of samples from the Orange Basin
(b) A typical mass fragmentogram (m/z = 191) terpanes in rock extracts of samples from the Orange Basin
(c) A typical mass fragmentogram (m/z = 217) of steranes in rock extracts of samples from the Orange Basin

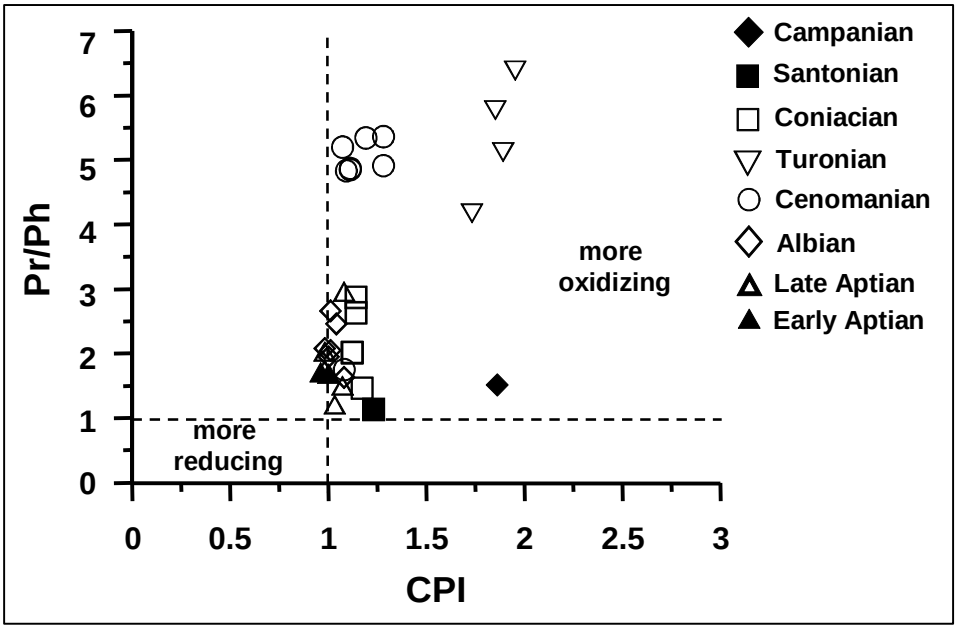

Fig. 4-25. The plot of CPI against Pr/Ph of shale samples from stratigraphic sequences of Orange Basin

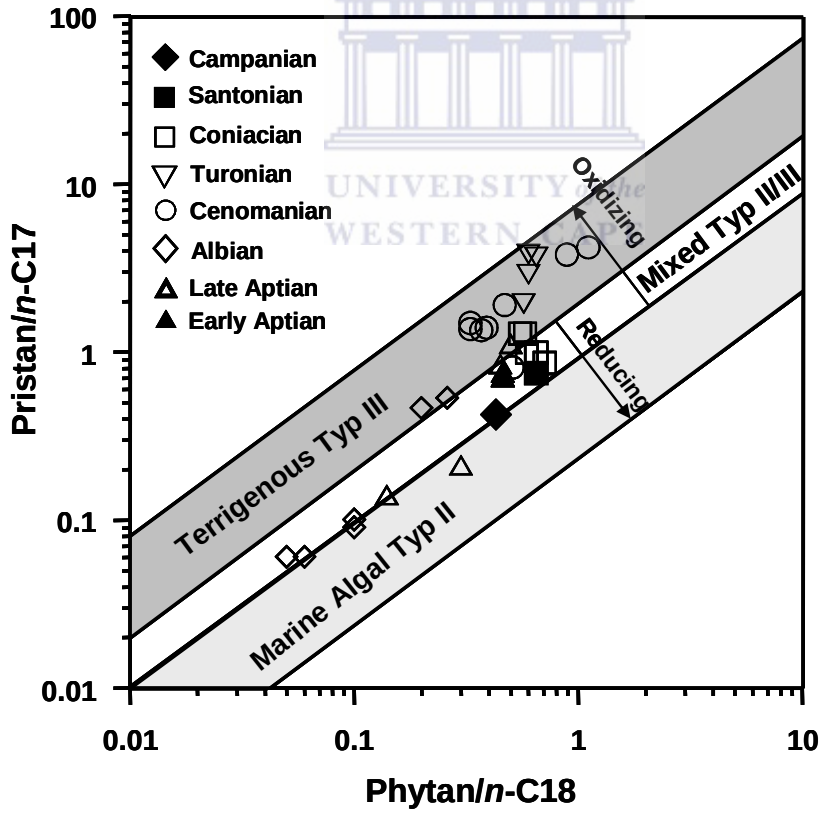

Fig. 4-26. The plot of Pr/nC_{17} vs Ph/nC_{18} of source rock samples from stratigraphic sequences of Orange Basin using Peters et al. 1999.

4.8.2.2 Biomarker geochemistry

Origin of the organic matter

The investigated samples contain pentacyclic triterpanes with both oleanane and hopane skeletons as well as steranes. Source and thermal maturity dependent parameters were calculated from these biomarker distributions.

The presence of 18α(H)-oleanane, a biomarker for angiosperms, in some of the samples across the basin (Table 4.19, Fig. 4-24b) is an indication of terrestrial organic matter supply and that these rock samples have organic matter of Cretaceous to younger as a result of the first occurrence of angiosperm land plant during the Cretaceous (Philp and Gilbert, 1986; Rival et al., 1988; Ekwezor and Udo, 1988; Waples and Machihara, 1991; Peters and Moldowan, 1993; Moldowan et al., 1994; Hunts, 1995; Lopez et al., 1998; Peters et al., 2004). The samples analysed across the stratigraphic sequences of Orange Basin from Upper Cretaceous showed the presence of oleanane in all shales of the Campanian, Santonian and Coniacian. In the samples from the Turonian oleanane was not detected. However, in some of the Cenomanian samples it was measured again (Table 4.19). In the Lower Cretaceous oleanane was detected in three Albian shales and only one shale sample from the Late Aptian (Table 4.19). The relatively wide spread presence of oleanane, although very low in abundance in some ages, is an indication of terrestrial organic matter input to the basin. If compared to the kerogen typ data in table 4.15 the absence of 18α(H)-oleanane in some of the samples may not indicate insignificant contribution of terrestrial organic matter to those samples. However, the lack of oleanane in some of the Turonian samples might be the result of a higher marine influence (Table 4.19).

Steranes or their sterol precursors inherited directly from higher plants, animals and algae. Although an unambiguously assignment of sterols to precursor organisms is difficult, a rough classification of steroid biomarkers into marine and terrestrial biomarkers is tentatively possible. C_{27}- and C_{28}-sterols are mainly from marine phytoplanctonic material, whereas zooplankton contains more C_{27}- and phytoplankton more C_{28}-sterols. Terrestrial biomass is thought to contain more C_{29}-sterols (Huang and Meinschein, 1976 and 1979; Volkman, 1986; Volkman et al., 1998). However, due to the

fact that also marine organisms appear to contain C_{29}-sterols (Volkman, 1986; Volkman et al., 1998) interpretation must be drawn with caution and the location and depositional conditions have to be reviewed whether a terrestrial supply of organic matter is plausible. In a ternary diagram the geochemical degradation products of the sterols the 20R epimers of C_{27}-, C_{28}- and C_{29}-steranes (Fig. 4.24c) (Peters and Moldowan 1993) plot predominantly in the centre indicating a mixture of marine and terrestrial biomass, which is typical for a depositional system along a continental margin (Fig 4-27). The data show a slight dominance of % C_{28} 20R in ages between Cenomanian and Coniacian over % C_{27} 20R and % C_{29} 20R. There is significantly higher proportion of C_{27} 20R in the basin in the ages from Early and Late Aptian. In general, there is no definite pattern of the steranes distribution across the stratigraphic sequences of the basin. The higher proportion of C_{28} steranes may be related to the increase diversification of phytoplanktonic assemblages, including diatoms, coccolithophores and dinoflagellates during their deposition in the Cretaceous period (Grantham and Wakefield, 1988). The proportion of C_{29} sterane is higher in the Campanian (Fig. 4-27; Table 4.19). This might be an indication of an above-average relative supply of terrestrial organic matter during that time in this basin. In spite of the fact that for most samples the organic matter was classified to be kerogen Type III, the sterane data suggest also a supply of marine organic material to the total organic matrix. Something, which can be expected at a continental margin.

Table 4.16 Biomarkers of data within the LST of Orange Basin sediments

Well name	Top Depth (m)	Ole/C30H	Ts/(Ts+Tm)	% C27 20R	% C28 20R	% C29 20R	C29 20S/ C29 20R	C29 20S/S+R	C29αββ20R/(αββR+ ααaR)	βα30/C30H (Mor/Hop)
A_K2	2540	0.1	0.31	28.98	44.97	26.05	0.85	0.46	0.55	0.42
A_K2	2545	0.10	0.22	33.96	41.21	24.84	0.66	0.40	0.52	0.4
K_D1	3447	0.23	0.34	40.65	36.01	23.34	0.66	0.40	0.61	0.31
A_U1	2210	ND	0.16	26.87	44.87	28.26	0.38	0.28	0.39	0.58
A_U1	2220	0.11	0.23	33.11	39.61	27.28	0.34	0.25	0.42	0.49
A_C3	3129	ND	0.42	42.66	33.09	24.25	0.81	0.45	0.63	0.14
O_A1	3789	ND	0.51	61.77	20.86	17.38	1.05	0.51	0.67	0.05
O_A1	3792	ND	0.51	55.02	26.07	18.91	0.97	0.49	0.66	0.15

Table 4.17 Biomarkers of data within the TST of Orange Basin sediments

Well name	Top Depth (m)	Ole/C30H	Ts/(Ts+Tm)	% C27 20R	% C28 20R	% C29 20R	C29 20S/ C29 20R	C29 20S/S+R	C29αββ20R/(αββR+ ααaR)	βα30/C30H (Mor/Hop)
A_F1	1320	ND	0.21	29.26	41.56	29.18	0.36	0.26	0.52	0.46
A_F1	1990	ND	0.30	30.74	35.66	33.59	0.84	0.46	0.53	0.93
A_K2	2525	ND	0.29	37.94	40.01	22.05	1.55	0.61	0.63	0.72
A_K2	2530	ND	0.17	30.87	48.44	20.69	0.63	0.39	0.43	0.61
K_B1	1855	0.29	0.15	20.62	29.37	50.01	0.11	0.10	0.31	0.42
A_U1	3008	0.18	0.36	39.72	38.68	21.6	0.83	0.45	0.64	0.2
A_U1	3068	0.19	0.45	44.21	32.17	23.62	0.59	0.37	0.61	0.34

Table 4.18 Biomarkers of data within the HST of Orange Basin sediments

Well name	Top Depth (m)	Ole/C30H	Ts/(Ts+Tm)	% C27 20R	% C28 20R	% C29 20R	C29 20S/ C29 20R	C29 20S/S+R	C29αββ20R/(αββR+ ααR)	βα30/C30H (Mor/Hop)
A_F1	1290	ND	0.19	26.87	45.89	27.24	0.26	0.21	0.68	0.60
A_K2	2405	ND	0.32	30.67	46.41	22.93	0.78	0.44	0.53	0.57
K_B1	2084	0.2	0.27	28.47	35.74	35.79	0.3	0.23	0.42	0.35
K_B1	2423	0.11	0.23	27.41	43.93	28.65	0.59	0.37	0.43	0.36
K_B1	2718	0.1	0.25	25.98	44.91	29.10	0.58	0.37	0.45	0.41
K_B1	2721	0.11	0.30	30.93	41.65	27.42	0.65	0.39	0.5	0.35
K_B1	2742	0.41	0.34	30.51	32.97	36.52	0.61	0.38	0.29	0.62
K_B1	2808	0.11	0.24	28.31	42.58	29.12	0.67	0.40	0.46	0.33
K_D1	2947	0.10	0.25	28.89	47.7	23.41	0.49	0.33	0.48	0.36
K_D1	2979	ND	0.27	31.73	47.65	20.63	0.74	0.42	0.55	0.22
K_D1	2997	ND	0.29	33.36	43.44	23.2	0.59	0.37	0.51	0.27
K_D1	2998	ND	0.26	28.88	49.34	21.78	0.56	0.36	0.57	0.26
O_A1	3741	ND	0.55	64.38	17.97	17.65	0.82	0.45	0.70	0.26
O_A1	3756	ND	0.47	49.39	25.55	25.06	0.75	0.43	0.66	0.16
O_A1	3771	ND	0.33	36.08	36.15	27.77	0.86	0.46	0.64	0.26

ND- Not detected

Ole- Oloeanane

C30H- 17 α (H)-21 β((H)-hopane

Ts- 18α(H)-22,29,30-trinorneohopane

Tm- 17α(H)-22,29,30-trinorhopane

Table 4.19 Re-ordered biomarker results of samples collected based on wells, ages and sequences in Orange Basin

Well name	Top Depth (m)	Age	Sequence	Ole/ $C_{30}H$	Ts/ (Ts+Tm)	βα/αβ Mor/Hop C30H	αβ/(αβ+βα) C30H	22S/ (22S+22R) $C_{31}H$	C_{27} 20R (%)	C_{28} 20R (%)	C_{29} 20R (%)	20S/ (20S+20R) ααα-C_{29}	αββ/ (αββ+ααα) C_{29}20R
K_B1	1855	Campanian	TST	0.29	0.15	0.42	0.71	0.40	20.62	29.37	50.01	0.10	0.31
K_B1	2084	Santonian	HST	0.20	0.27	0.35	0.74	0.51	28.47	35.74	35.79	0.23	0.42
K_B1	2423	Coniacian	HST	0.11	0.23	0.36	0.74	0.55	27.41	43.93	28.65	0.37	0.43
K_B1	2718	Coniacian	HST	0.10	0.25	0.41	0.71	0.58	25.98	44.91	29.1	0.37	0.45
K_B1	2721	Coniacian	HST	0.11	0.30	0.35	0.74	0.56	30.93	41.65	27.42	0.39	0.50
K_B1	2742	Coniacian	HST	0.41	0.34	0.62	0.62	0.52	30.51	32.97	36.52	0.38	0.29
K_B1	2808	Coniacian	HST	0.11	0.24	0.33	0.75	0.55	28.31	42.58	29.12	0.4	0.46
A_F1	1270	Turonian	HST	ND	0.31	0.56	0.64	0.28	26.00	38.00	35.59	0.15	0.41
A_F1	1290	Turonian	HST	ND	0.19	0.6	0.62	0.28	26.87	45.89	27.24	0.21	0.68
A_F1	1300	Turonian	TST	ND	0.19	0.44	0.69	0.27	27.27	43.63	29.11	0.23	0.58
A_F1	1320	Turonian	TST	ND	0.21	0.46	0.68	0.35	29.26	41.56	29.18	0.26	0.52
A_F1	1990	Cenomanian	TST	ND	0.30	0.93	0.52	0.60	30.74	35.66	33.59	0.46	0.53
A_K2	2405	Cenomanian	HST	ND	0.32	0.57	0.64	0.60	30.67	46.41	22.93	0.44	0.53
A_K2	2525	Cenomanian	TST	ND	0.29	0.72	0.58	0.62	37.94	40.01	22.05	0.53	0.63
A_K2	2530	Cenomanian	TST	ND	0.17	0.61	0.62	0.55	30.87	48.44	20.69	0.39	0.43
A_K2	2540	Cenomanian	LST	0.10	0.31	0.42	0.71	0.57	28.98	44.97	26.05	0.46	0.55
A_K2	2545	Cenomanian	LST	0.10	0.22	0.40	0.71	0.55	33.96	41.21	24.84	0.40	0.52
A_U1	2210	Cenomanian	LST	ND	0.16	0.58	0.63	0.53	26.87	44.87	28.26	0.28	0.39
A_U1	2220	Cenomanian	LST	0.11	0.23	0.49	0.67	0.61	33.11	39.61	27.28	0.25	0.42
A_U1	3008	Albian	TST	0.18	0.36	0.2	0.83	0.52	39.72	38.68	21.6	0.45	0.64
A_U1	3068	Albian	TST	0.19	0.45	0.34	0.75	0.47	44.21	32.17	23.62	0.37	0.61
K_D1	2947	Albian	HST	0.10	0.25	0.36	0.74	0.55	28.89	47.7	23.41	0.33	0.48
K_D1	2979	Albian	HST	ND	0.27	0.22	0.82	0.54	31.73	47.65	20.63	0.42	0.55

K_D1	2988	Albian	HST	ND	0.26	0.26	0.80	0.51	28.88	49.34	21.78	0.36	0.57
K_D1	2997	Albian	HST	ND	0.29	0.27	0.79	0.55	33.36	43.44	23.2	0.37	0.51
K_D1	3447	Late Aptian	LST	0.23	0.34	0.31	0.76	0.57	40.65	36.01	23.34	0.40	0.61
O_A1	3741	Late Aptian	HST	ND	0.55	0.26	0.79	0.46	64.38	17.97	17.65	0.45	0.70
O_A1	3756	Late Aptian	HST	ND	0.47	0.16	0.86	0.52	49.39	25.55	25.06	0.43	0.66
O_A1	3771	Late Aptian	HST	ND	0.33	0.26	0.79	0.54	36.08	36.15	27.77	0.46	0.64
O_A1	3789	Early Aptian	LST	ND	0.51	0.05	0.95	0.52	61.77	20.86	17.38	0.51	0.67
O_A1	3792	Early Aptian	LST	ND	0.51	0.15	0.87	0.50	55.02	26.07	18.91	0.49	0.66
A_C3	3129	Late Aptian	LST	ND	0.42	0.14	0.88	0.54	42.66	33.09	24.25	0.45	0.63

Note:
ND- Not detected
Ole = Oleanane
$C_{30}H$ = 17 α (H), 21β(H)-hopane
Ts = 22,29,30-*trisnor*-18α(H)- neohopane

Tm = 22,29,30-trisnor-17α(H)-hopane;

βα/αβ $C_{30}H$ (Mor/Hop) and αβ/(αβ+βα)$C_{30}H$ (Mor/Hop) = ratios of the 17α (H),21β (H)-hopane and 17β(H), 21α(H)-hopane (Moretane) ,

22S/(22S+22R) $C_{31}H$ = 22S and 22R epimer ratio of 29-*homo*-17 α(H)-21β(H)-hopane

C_{27} 20R = (20R)-5α (H),14α (H),17α (H)-cholestane

C_{28} 20R = (20R)-5α (H),14α (H),17α (H)-methylcholestane

C_{29} 20R = (20R)-5α (H),14α (H),17α (H)-ethylcholestane

20S/(20S+20R) ααα-C_{29} = 20S and 20R epimer ratio of the 5 α(H),14α(H),17α(H)-ethylcholestane

αββ /(αββ +ααα)C_{29}20R = ratio of the (20R)-5α (H),14β (H),17β (H)- and (20S)-5 α (H),14β (H),17β (H)-ethylcholestane

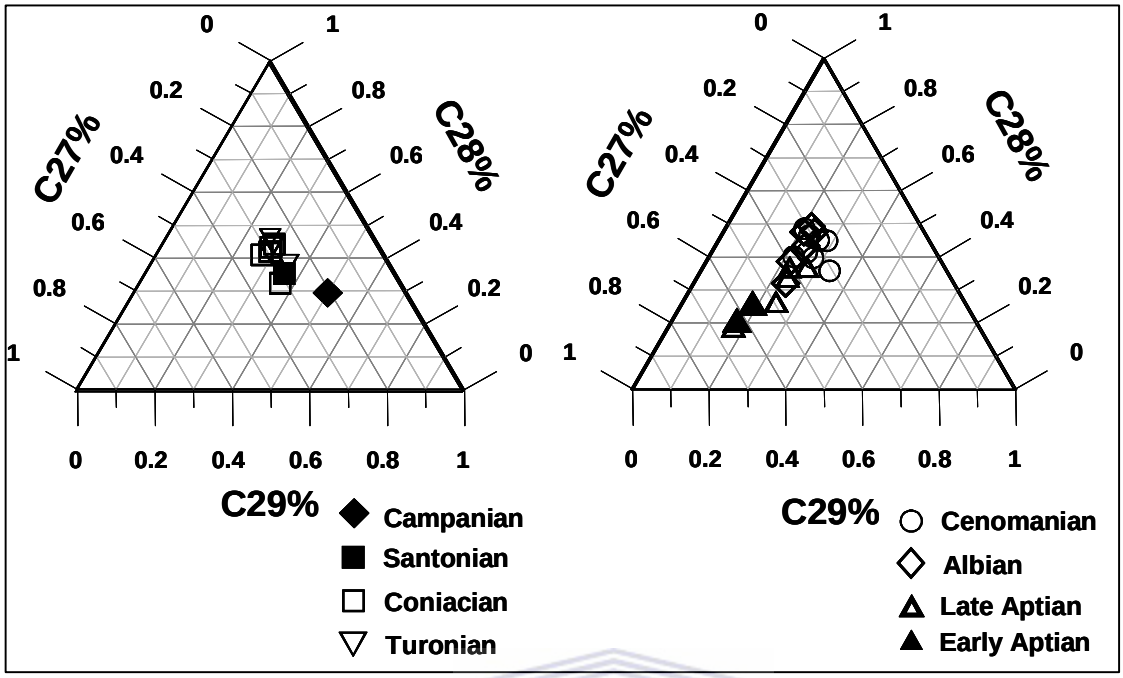

Fig. 4-27. The ternary plot of steranes inherited directly from higher plants, animals and algae the 20R epimers of C_{27}, C_{28} and C_{29} steranes (Peters and Moldowan, 1993), all values in the axes per 100.

4.8.3 Thermal maturity of the organic matter

Thermal maturity of the organic matter was assessed based on parameters calculated from the terpane and sterane distributions in the rock extracts. During maturation the 18α(H)-*trisnor*-neohopane (Ts) is less stable relative to 17α(H)-*trisnor*-hopane (Tm) (Table 4.19). Therefore, the Ts/(Ts+Tm) ratio increases with increasing thermal maturity (Seifert and Moldowan, 1978; Hunt, 1995). In contrast, the moretane/hopane ratio (17β(H),21α(H)-/(17α(H),21β(H)-hopane) decreases with maturity (Seifert and Moldowan, 1980; Grantham, 1986; Kvenvolden and Simoneit, 1990) due to the higher thermal stability of the α,β-configurated hopane.

In the current study the Ts/(Ts+Tm) ratio shows highest values (0.42 to 0.55) in the oldest samples from the Early and Late Aptian. The lowest value was determined in the youngest samples from the Campanian with 0.15. Sample from Santonian to Albian age show varying values between 0.16 and 0.45.

Moretane/hopane ratios higher than 0.8 are an indication of immature source rocks, ratios between 0.8 and 0.15 indicate mature and less than 0.15 highly mature source rocks (Peters and Moldowan, 1993). In the samples analysed the ratios of moretane/hopane range between 0.05-0.93 (Table 4.19). Almost all samples investigated fall within the range indicating early mature to mature source rocks (Seifert and Moldowan, 1986; Peters and Moldowan, 1993). Lowest values, indicating a higher maturity level, are indicated for the Albian, Late and Early Aptian samples.

The isomerisation of C_{31} homohopane commonly equilibrates at a ratio around 0.58 to 0.62 at vitrinite reflectance (Ro) > 0.6% (Peters and Moldowan 1993). It is believed that the approach to equilibrium of C_{31}-hopane 22S/(22S+22R) ratios in the range of 0.5 to 0.54 may indicate the onset of oil generation while the attainment of equilibrium in the range of 0.57 to 0.62 indicates that the main phase of oil generation has been reached or surpassed (Peters and Moldowan 1993). Observation from this study showed that most C_{31}-hopane 22S/(22S+22R) values are in the range of the early to main oil window. However, the Campanian and some Turonian samples appear to have significantly lower parameter values (Table 4.19).

The 17α,21β/(17α,21β + 17β,21α) C_{30}-hopane parameter (Fig. 4-28a) usually range between a variable value and 0.9 (Seifert and Moldowan, 1980) covering the maturity transition from early catagenesis to the main oil window. Most values are higher than 0.6 and highest values are again determined for the oldest samples from Albian, Late and Early Aptian age. In the cross plot of the two hopane parameters (Fig. 4-28a) most samples are plotting in the upper right corner of the diagram showing that most samples already reached a maturity level being at the end indicated by the hopanes parameters. The Campanian and some Turonian samples show lower maturities.

Steranes cover a higher maturity range. The C_{29}-5α,14β,17β-20R/(αββ+ααα) and the C_{29}-5α,14α,17α-20S/(20S+20R) sterane parameters of the investigated shales, both increasing with thermal maturity, show values ranging from 0.29-0.70 and 0.10-0.51, respectively (Tables 4.19, Fig. 4-28b). Highly mature sediments are expected to reach about 70 % for C_{29}-αββ-20R/(αββ + ααα) and about 50 % for the C_{29}-ααα-20S/(20S+20R) (Seifert and Moldowan, 1986). In general for the samples both parameters show a consistent maturity trend as indicated by the diagonal distribution of

the data points in the cross plot (Fig. 4-28b). There are some deviations from this trend in the Turonian and Coniacian sample set. The cross-plot of these parameters show a higher thermal maturity for the older sediments of Aptian, Albian and Cenomanian age (Fig. 4-28a and 4-28b). The younger sediments of Turonian, Santonian and especially Campanian age show, in general, parameter values indicating a lower maturity level. The Coniacian samples plot in between both sample sets. The sterane parameter values of these rock samples suggest that some of the samples must have undergone complete sterane isomerization (Grantham, 1986), which could be the result of favourable time/temperature conditions on the organic matter.

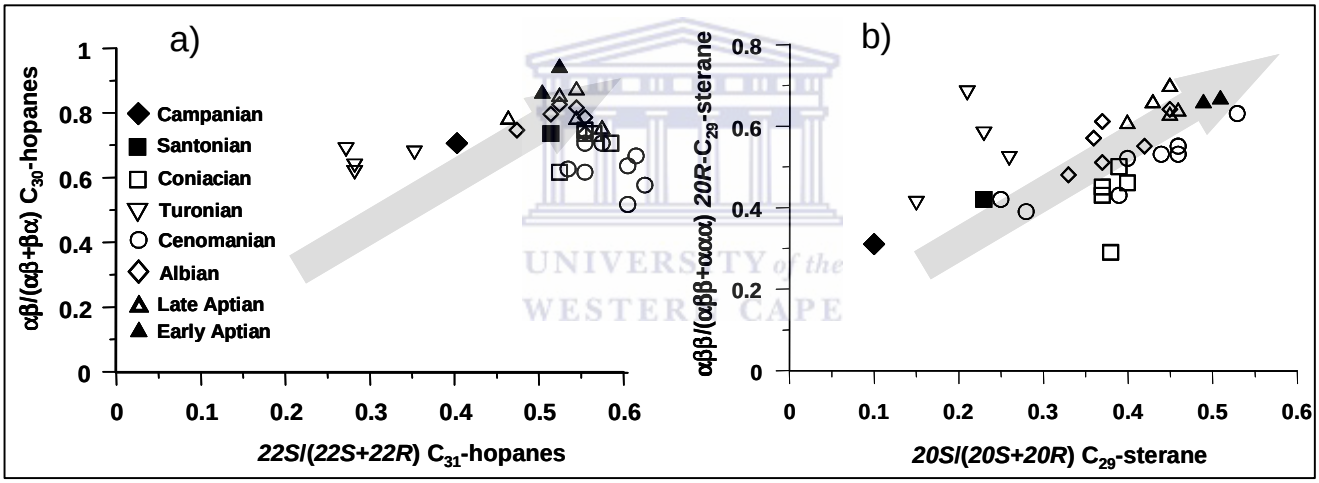

Fig. 4-27. Cross plot of $C_{29\alpha\beta\beta 20}/(_{\alpha\beta\beta\,+\,\alpha\alpha\alpha})$ vs $C_{29\alpha\alpha\alpha 20S}/(_{S}{+}_{R})$ steranes, the arrow indicating increasing thermal maturity (Seifert and Moldowan, 1986).

Chapter Five

5.0 Conclusions and Recommendations

An integrated approach was adopted in this study to investigate some elements of petroleum system of the Orange Basin, South Africa, with a particular emphasis on reservoir rocks and source rocks.

The seismic reflection (2D) comprising – inlines and crosslines were utilized in structural (faults) identification, depositional sequence delineation, as well as recognition of the constituent systems tracts. Growth fault that are listric and normal were found localized in the basin. The faults are flank faults, crestal faults as well as antithetic faults. The wireline logs provided were used for lithostratigraphic studies and identification of sequences and systems tracts. 8 depositional cycles were identified from the wireline logs, from which the sandstone and shale samples were collected.

The EDS results show the presence of sulphur and titanium that suggests evidence of two provenance of the sandstone samples investigated; volcanic and granitic, respectively. The presence of glauconite and frameboidal pyrite across the stratigraphic sequences is an indication of deposition of sediments in continental shelf marine environment.

This study revealed a complex diagenetic history of sandstones of the Orange Basin in which compaction, cementation/micritization, dissolution, silicification/overgrowth of quartz and fracturing were observed. The cements precipitation occurs in different environments. The LST has micritic cement which is an evidence of marine diagenesis. The TST and HST have micritic and poikilitopic calcite cements and evidence of different conditions of precipitation. The micritic morphology and coarse crystalline nature of the cementing materials strongly suggest autochtonous and allochtonous origin of the cementing materials, respectively. 50 % of the LST

samples show possibility of mixture of detrital quartz grains based on the oxygen isotope data. The detrital quartz mixture decreases from LST to TST and HST.

The Eh-pH conditions in the basin show that the authigenic minerals were precipitated in slightly alkaline conditions, in which the TST is slightly more alkaline than HST, thereby causing more authigenic clay precipitation in the TST. This alkaline condition also supports clay conversion in the basin under a low relative temperature condition as a result of thermal subsidence in the basin between Aptian and Cenomanian in which some of these samples were deposited.

The sandstones across the basin have pseudomatrix rich in authigenic chlorite, montmorillonite, quartz and calcite. These minerals cemented the pores thereby reducing porosity. The continued burial compaction disrupted the depositional texture which in turn impaired secondary porosity development.

The organic geochemical characterisation of the shale intervals within the stratigraphic settings of the Orange Basin indicates marginal gas generation potential.

Marginally organic rich rocks with a very few organic rich rocks were identified in the LST setting, with variable kerogen types ranging from Type II to Type IV. Four samples from wells A_F1 and O_A1 show indications of good petroleum potential but are not mature sufficiently for petroleum generation, while a few samples that are thermally mature have low organic matter quality.

Only one organic rich rock and a few marginally organic rich rocks were identified in the TST setting, the rest of the samples in this setting are organic lean. Most of the samples have poor petroleum generation potential with only one sample showing indications of petroleum generation potential. The results showed that the samples are mainly Type III kerogen with a few Type IV kerogen. Most of the samples are thermally immature; the few thermally mature samples have low organic matter quality.

The shale samples in the HST setting are mainly marginally organic rich with predominance of Type III and presence of very few mixed Type II/III kerogen. Most of the samples in this setting are thermally immature to marginally mature with a few mature samples that are in the oil window. The results show prevalent of allochthonous organic matter with subordinate autochthonous organic matter.

Generally, LST setting has the best petroleum prospect followed by HST and TST setting has the least petroleum generation potential. The results of this study reveal that a very limited petroleum source rock exists in the basin. The limited potential source rocks present are further limited by low levels of thermal maturity.

Source rock samples ranging from Early Aptian to Campanian age and gathered from the 7 different locations along the southwest African continental margin in the Orange Basin were analyzed to characterize the source organic matter, depositional environment, level of geothermal maturity and hydrocarbon potential.

Hydrogen (HI) and oxygen index (OI) data, the Oleanane/C_{30}-hopane ratio, proportions of C_{27}-, C_{28}- and C_{29}-steranes and the cross plot of Pristane/*n*-C_{17}-alkane vs. Phytane/*n*-C_{18}-alkane indicate that the organic matter type across the basin is mainly Typ III indicating predominantly terrestrial organic matter. Some samples of Turonian age are Typ II/III or Typ II indicating an enhanced proportion of marine organic matter.

Pristane/Phytane ratio values higher than 1 in all samples analysed, carbon preference index (CPI) values of close to or above 1 and interpretation from the cross plot of Pr/*n*-C_{17} vs. Ph/*n*-C_{18} point to suboxic to oxic environmental condition during time of sediment deposition.

In general, the thermal maturity of the selected samples coincides with the sample ages. Samples with the highest maturity are of Aptian, Albian and Cennomanian age as indicated by the *n*-alkane distribution, CPI and Tmax values, as well as hopane and

sterane maturity parameters. Most samples show a maturity at the initial oil window with some samples being slightly more mature.

S2/S3 ratio as well as OI and HI values assign only a low hydrocarbon generation potential to most of the samples investigated in the current study from Early Aptian to Campanian, exceptions are samples from Turonian and Aptian age

5.1 Main scientific contribution of the dissertation

Information about the petroleum system(s) of Orange Basin is relatively scarce. Where available they remain in the purview of the companies that owns them, which are considered as classified documents.

This dissertation presents a holistically look at the petroleum system of the basin, looking at the depositional sequence, structure, reservoir and source rocks. Results of some of the finding have been presented in international conferences, some already accepted for publications in reputable international journals and some under review. This study has generated data on petroleum system of the basin on a regional scale using integrated approach. The results obtained from each systems tract are identical thereby making the regional outlook possible.

The study also provided information on diagenetic history of the reservoir rock, depositional history and thermal maturity of the organic matter in the Orange Basin. This can be used as a tool for exploration and exploitation activities in the future.

Some of these findings will continue to generate debate in years to come thereby increasing interest in once abandoned basin. The hope for gas generation is higher than oil as concluded by this study because of abundance of Type II/III and Type III organic matters. The demand for gas now is on the increase across the globe and the basin in some years to come might be a player in gas production.

5.2 Recommendation for future work

We strongly recommend that effort should be geared toward exploration in the horizon with age older than the Cretaceous for possible discovery of oil and gas. Klemme and Ulmishek, 1991 reported that Upper Jurassic account for more than 25 % of the world recoverable oil and gas. With the LST showing more prospect than other systems tracts, there might be prospect beneath the Cretaceous of Orange Basin, this coupled with production in Jurassic in Southern America basins which happen to be lateral equivalent as a result of Gondwana break up.

References

Adabi, M.H., Rao, C.P., 1991. Petrographic and geochemical evidence for original aragonite mineralogy of Upper Jurassic carbonate (Mozduran Formation), Sarakhs area, Iran. Sedimentary Geology, **72**, 253-267.

Akinlua, A., Ajayi, T.R., 2009. Geochemical Characterization of Central Niger Delta oils. Journal of Petroleum Geology, vol. 34 (4), 373-382pp.

Akinlua, A., Smith, R.M., 2009. High Temperature Steam Extraction for the Determination of Alphatic Hydrocarbon in Petroleum Source Rock. Chromatographia, vol. 69, no. 11-12, 1-7.

Akinlua, A., Ajayi, T.R., Adeleke, B.B., 2007. Organic and inorganic geochemistry of northwestern Niger Delta oils. Geochemical Journal, vol. 41, 271-281pp.

Akinlua, A., Ajayi, T.R., Jarvie, D.M., Adeleke, B.B., 2005. A Re-Appraisal of the Application of Rock-Eval Pyrolysis to Source Rock Studies in the Niger Delta. Journal of Petroleum Geology, vol. 28 (1), 39-48

Allan, J.R., Wiggins, W.D., 1993. Dolomite Reservoirs: Geochemical Techniques and Evaluating Origin and Distribution. AAPG Continuing Education Course Note Series 36, 129pp.

Al-Ramadan, K., Morad, S., Proust, J.N., Al-Asam, I. 2005. Distribution of diagenetic alterations in siliciclastic shoreface deposits within a sequence stratigraphic framework: evidence from the Upper Jurassic, Boulonnais, NW France. Journal of Sedimentary Research, 75, 943-959.

Amorosi, A., 1995. Glaucony and sequence stratigraphy: a conceptual framework of distribution in siliciclastic sequences. Journal of Sedimentary Research, B65, 419-425.

Arditto, P.A., 1991. A sequence Stratigraphic analysis of the Late Permian succession in the South Coalfield, Sydney Basin, New South Wales, Australian Journal of Earth Sciences, 38, 125-137

Bellanca, A., Aghib, F., Neri, R., Sabatino, N., 2005. Bulk carbonate isotope stratigraphy from CRP-3 core (Victoria Land Basin, Antarctica): evidence for Eocene-Oligocene paleoclimatic evolution. Global and Planetary Change 45, 237-247.

Ben-Avraham, Z., Smith, G., Reshef, M., Jungslager, E., 2002. Gas hydrate and mud volcanoes of the southwest Africa continental margin of South Africa. Geology (Boulder) 30 (10), 927-930pp

Blatt, H., 1986. Oxygen isotopes and the origin of quartz. Journal of Sedimentary Petrology 57 (2), 373-377.

Bloch, S., Lander, R.H., Bonnell, L., 2002. Anomalously high porosity and permeability in deeply buried sandstone reservoirs: origin and predictability. American Association of Petroleum Geologists Bulletin, 86, 301-328.

Bohacs, K.M., Isaksen. G.H., 1991. Source quality variation tied to sequence development: integration of physical and chemical aspects, Lower to Middle Triassic, western Barrents Sea. Bulletin of the American Association of Petroleum Geologist, 75, 544.

Bohacs, K., Suter, J.R., 1997. Sequence stratigraphic distribution of coaly rocks: fundamental controls and paralic examples. American Association of Petroleum Geologists Bulletin 81; issue 10, 1612–1639.

Bordenave, M.L., 1993. Applied Petroleum Geochemistry. Editions Technip, Paris.

Broad, D. 2004. South Africa Activities and Opportunities. An Unpublished Power Point Presentation to PetroChina

Broad, D.S., Jungslager, E.HA., Mclachlan, I.R., Roux, J., 2006. Offshore Mesozoic Basins. In: Johson, M.R., Anhaeusser, C.R., Thomas, R.J. (eds). The Geology of Southern Africa. Geological Society of South Africa., Johannesburg. Council for Geoscience Pretoria, 553-571.

Brown, L.F., Brown, L.F, Jr., Benson, J.M., Brink, G.J., Doherty, S., Jollands, A., Jungslager, E.H.A., Keenan, J.H.G., Muntingh, A., Van Wyk, N.J.S., 1996. Sequence stratigraphy in offshore South Africa divergent basins. An atlas on exploration for cretaceous lowstand traps by SQEKOR (Pty) Ltd. Am. Ass. Petro. Geol. Stud. in Geology. 41, 184pp.

Brown, L.F., Fisher, W.L, 1977. Seismic stratigraphy interpretation of depositional system: examples from Brazilian Rift and Pull-Apart Basin; In Payton, C.E. ed; Seismic stratigraphy Application to hydrocarbon Exploration, American Association of Petroleum Geologist Bulletin, memoir 26, p. 213-248.

Brownlow, A.H., 1979. Geochemistry. Prentice-Hall, Englewood Cliffs, NJ, 498 pp.

Burley, S.D., Leeson, T.H., Worden, R.H., 1985. Sandstone Diagenesis the evolution of sand in sandstone. In sandstone Diagenesis Recent and Ancient, Burley, S.D; and Worden, R.H, (eds) Blackwell Publishing. vol. 4. 656pp.

Catuneanu, O., Erikson, P.G., 2007. Sequence stratigraphy of the Precambrian. International Association of Gondwana Research. Elsevier B.V. pp. 560-565

Choo, O.C., Young, S.S., In Seok, K., 2002. Mineralogical evidence for red coloration of sandstones at Chilgok Formation of the Cretaceous Hayang Group, Southestern Korea, Geosciences Journal, vol.6, No. 2. 141-148.

Clayton, R.N., O'Neil, J.R., Mayeda, T.K., 1972. Oxygen isotopic exchange between quartz and water. Journal of Physical Research 77 (17), 3057-3067.

Clemson, J., Cartwright, J., Booth, J., 1997. Structural segmentation and influence of basement structure on the Namibian passive margin. Journal of the Geological Society of London. 154, 447-482.

Clemson, J., Cartwright, J., Zwart, R., 1999. The Namibia Rift: a rift system of possible Karro age, offshore Namibia. In: Cameron, N.R; Bate, R.H; Clure, V.S ;(eds). The oil and gas habitat of South Atlantic. Geological Society of London. 381-402pp

Creaney, S., Passey, Q.R., Allan, J., 1991. Use of well logs and core data to assess the sequence stratigraphic distribution of organic-rich rocks. Bulletin of the American Association of Petroleum Geologist, 75, 557.

Cross, T.A., 1988. Controls on coal distribution in trangressive-regressive cycles, Upper Cretaceous, Western Interior, USA. In: Wilgus, C.K., Posamentier, H.W., Ross, C.A., Kendall, C.G. St. C (Eds), Sea-Level Changes, an Integrated Approach. SEPM Special Publication no. 42, 371-380.

Curtis, C.D., 1987. Mineralogical consequences of organic matter degradation in sediments: Inorganic/organic diagenesis. In: J.K. Leggett and G.G. Zuffa (Eds.), Marine Clastic Sedimentology. Graham and Trotman, London, pp. 108-123.

Curtis, D.C., 1978. Probable links between sandstone diagenesis and depth-related geochemical reactions occurring in enclosing mudstones Q.J. Geol. Society of London, vol. 135. p. 1-11.

De Ros, L.F., 1998. Heterogeneous generation and evolution of diagenetic quartz-arenites in the Silurian-Devonian Furnas Formation of the Panama Basin, Southern Brazil. Sedimentary Geology. 11. 99-128.

De Ros, L.F., Sgarbi, G.N.C., Morad, S. 1994. Multiple authigenesis of K-feldspar in sandstones: evidence from the Cretaceous Areado Formation, Sao Francisco Basin, central Brazil. Journal of Sedimentary Research, A64, 778-787.

Demaison, G.J., Moore, G.T., 1980. Anoxic environments and oil source bed genesis. American Association of Petroleum Geologist Bulletin, v 64, no 8, 1179-1209.

Dingle, R.V., Hendy, Q.B., 1984. Late Mesozoic and Tertiary sediment supply to the eastern Cape Basin (SE Atlantic) and palaeo-drainage systems in southwestern Africa. Marine Geology, 56, 13-26.

Doust, H., Omatsola, E., 1990. Niger Delta. Divergent/Passive Margin Basins. Edwards, J. D. and Santogrossi, P. A., (eds.), AAPG Bull. 48, 201–238pp.

Durand, J., 1995. High-resolution sequence stratigraphy (Genetic stratigraphy) in reservoir sedimentary. Example from Niger Delta: Nigerian Association of Petroleum Explorationists. Bulletin, vol.10/01, p.65-73.

Dutton, S.P., 2008. Calcite cement in Permian deep water sandstones, Delware Basin, West Texas. Origin, distribution and the effect of the reservoir properties. AAPG Bulletin, v.92; no. 6, 765-787.

Dzou, L.I.P., Noble, R.A., Senftle, J.T., 1995. Maturation effects on absolute biomarker concentration in a suite of coals and associated vitrinite concentrates. Organic Geochemistry 23, 681–697.

Ehrenberg, S.N. 1993. Preservation of anomalously high porosity in deeply buried sandstones by grain-coating chlorite: examples from the Norwegian continental shelf. American Association of Petroleum Geologists, 77, pp. 1260-1286.

Ehrmann, W.U., Mackensen, A., 1992. Sedimentological evidence for formation of the East Antarctic ice sheet in Eocene-Oligocene time. Paleogeography, Paleoclimatology, Paleoecology 93, 85-112.

Ehrmann, W.U., Melles, M., Kuhn, G., Grobe, H., 1992. Significance of clay mineral assemblages in the Antarctic Ocean. Marine Geology 107, 249-273.

Ekweozor, C, M., Okogun, J. I., Ekong, D. U. E., Maxwell, J. R., 1979. Preliminary organic geochemical studies of samples from the Niger Delta, Nigeria. Part 1: Analysis of oils for triterpanes. Chem. Geol., 27, 11–28pp.

Ekweozor, C.M., Udo, O.T., 1988. The oleanane: Origin, maturation and limits of occurrence in southern Nigeria sedimentary basins. Advances in Organic Geochemistry. L. Mattavelli, L. Novelli. (eds). Oxford: pergamon Press. 131-140pp.

El-Ghali, M.A. K., Morad, S., Mansurbeg, H., Caja, M.A., Ajdanlijsky, G., Ogle, N, Al-Aasm, I., Sirat, M., 2009. Distribution of diagenetic alterations within depositional facies and sequence stratigraphic framework of fluvial sandstones: Evidence from the Petrohan Terrigenous Group, Lower Triassic, NW Bulgaria. Marine and Petroleum Geology 26, 1212–1227

El-Ghali, M.A. K., Morad, S., Mansurbeg, H., Caja, M.A., Sirat, M., Ogle, N,, 2008. Diagenetic alterations related to marine transgression and regression in fluvial and shallow marine sandstones of the Triassic Buntsandstein and Keuper sequence, the Paris Basin, France. Maine and Petroleum Geology, 26, 298-309.

Emery, D., Meyers, K.J., Berlam, G.T., 1996. Sequence Stratigraphy. In: Emery, D., Meyers, K.J (Eds) Wiley-Blackwell Synergy Publisher. 267pp.

Emery, E., Myers, K.J., 1996. Sequence Stratigraphy, Blackwell Science Ltd; London**,** 297pp.

Eslinger, E., Mayer, L.M., Durst, T.L., Hower, J., Savin, S.M., 1973. An X-ray technique for distinguishing between detrital and secondary quartz in the fine-grained fraction of sedimentary rocks. Journal of Sedimentary Petrology 43 (2), 540-543.

Fairbridge, R.W., 1961. Eustatic changes in sealevel; Phys. Chem. Earth, 4, p. 99-164.

Folk, R.L., 1965. Some aspects of recrystallization in ancient limestone. In Pray, L.C; and Murray, R.C. (eds). Dolomitization and limestone diagenesis. Soc. Econ. Paleon. Mineral. Spec. Pub**.** v 13, p. 14-48.

Garlick, G.D., Epstein, S., 1967. Oxygen isotope ratios in coexisting minerals of regionally metamorphosed rocks. Geochimica et Cosmochimica Acta 31, 181-214.

Garver, J.I., Royce, P.R., Smick, T.A., 1996. Chromium and Nickel on shale of the Traconic Foreland: A case study of the Provenance of Fine-Grained sediment with an ultramafic Source. Journal of Sedimentary Research. Vol. 66, 100-106.

Garzanti, E., 1991. Non-carbonate intrabasinal grains in arenites: their recognition, significance, and relationship to eustatic cycles and tectonic setting. Journal of Sedimentary Petrology, 61, 959-975.

Gerrard, I., Smith, G.C., 1982. Post-Palaeozoic succession and structure of Southwestern African Continental Margin In: Watkins, J.S; Drake, C.L. (Eds), Studies in Continental Margin Geology, American Association of Petroleum Geologists**.** 49-76pp

Gilchrist, A.R., Kooi, H., Beaumont, C. 1994. Post-Gondwana geometric evolution of southwestern Africa: Implications for the controls of landscape development for observations and numerical experiments. Journal of Geophysical Research. Vol. 99. B6. 211-228.

Giles, M.R., Stevenson, S., Martin, S.V., 1992. The reservoir properties and diagenesis of the Brent Group: a regional perspective. In: Morton, A.C; Haszeldine, R.S; Giles, M.R; Brown, S. (Eds), Geology of the Brent Group. Special Publication of the Geological Society of London, vol 61, 289-327.

Graham, C.M., Valley, J.W., Winter, B.L., 1996. Ion microprobe analysis of $O^{18}/^{16}O$ in authigenic and detrital quartz in the St. Peter Sandstone, Michigan Basin and Wisconsin Arch, USA: contrasting diagenetic histories. Geochimica et Cosmochimica Acta 60-24, 5101-5116.

Grantham, P. J., 1986. Sterane isomerisation and moretane/hopane ratios in crude oils derived from Tertiary source rocks. Org. Geochem. Vol. 9, No. 6. 293-304pp.

Grantham, P.J., Wakefield, L.L., 1988. Variations in the sterane carbonnumber distributions in main source rock derived crude oil through geological time. Organic Geochemistry, vol. 12, no. 1. 61-73pp

Greensmith, J.T. 1989. Petrology of the Sedimentary Rocks 7th edition Unwin Hijman Ltd.

Gulbay, R.K., Korkmaz, S., 2008. Organic geochemistry, depositional environment and hydrocarbon potential of the Tertiary Oil Shale Deposit in NW Anatolia, Turkey. Oil Shale, vol. 25; Issue 4, 444-464pp.

Haq, B.U., Hardenbol, J., Vail, P.R., 1987. Chronology of fluctuating sea levels since the Triassic; Science, vol. 235, p. 1156-1167.

Haq, B.U., Hardenbol, J., Vail, P.R., 1988. Mesozoic and Cenozoic chronostratigraphy and cycle of sea level change. In: sea level change: an integrated approach (eds C.K; Wilgus et al), Society of Economic Paleontologist and Mineralogists, special publication, 42, p. 71-108

Hart, G.F., Pasley, M.A., Gregory, W.A., 1994. Particulate organic matter, maceral facies models and application to sequence stratigraphy. In: Transverse, A. (Ed), Sedimentation of Organic Particulates. Cambridge Univ. Press, Cambridge, UK, 337-391

Hendry, J.P., Trewin, N.H., Fallick, A.E., 1996. Low-Mg Calcite marine cement in Cretaceous turbidites: origin, spatial distribution and relationship to seawater chemistry. Sedimentology. vol. 43. p. 877-900.

Hirsch, K., Scheck-Wendroth, M., Paton, D., Horsfield, B., di Primio, R., Bauer, K., 2006. 3D Gravity modelling and subsidence analysis in the Orange Basin, Southwest African continental margin. Poster PhD Day.

Http://srata.geol.sc.edu/index.html., 2005

Huang, W.Y., Meinschein, W.G., 1976. Sterols as source indicators of organic materials in sediments. Geochimica et Cosmochimica Acta 40, 323-330.

Huang, W.Y., Meinschein, W.G., 1979. Sterols as ecological indicators. Geochimica et Cosmochimica Acta 43, 739-745.

Huang, H., Bowler, B. F. J., Oldenburg, T. B. P., Larter, S. R., 2004. The effect of biodegradation on polycyclic aromatic hydrocarbons in reservoired oils from the Liaohe basin, NE China. Org. Geochem., 35(11-12), 1619–1634.

Hunt, J. M., 1995. Petroleum Geochemistry and Geology.--New York: W. H.Freeman and Company, 617pp.

In-Chang Ryu., Alan R. Niem., 1999. Sandstone diagenesis reservoir potential, and sequence stratigraphy of the Eocene Tyee Basin Oregon; Journal of Sedimentary Research; vol. 69;no. 2, pp. 384-393.

Imam, B., 1986. Scanning electron microscopy study of the quartz overgrowths within Neogene sandstones of Bengal Basin, Bangladesh. Journal Geological Society of India. 28, 407-413.

James, N.P., Choquette, P.W., 1983. Diagenesis 9. Limestones the sea-floor diagenetic environment. Geosciences Canada, v. 10, 162-179.

Jenkyns, H.C., 1980. Tethys: past and present. Proceedings of Geologists' Association. vol. 91. iss. 1-2, 107-118.

Jervey, M., 1988. Qualitative geological modelling of siliciclastic rock sequences and their seismic expression. In: Wiligus, C.K. et. al. (eds.) sea-level changes: An integrated approach special publication, American Association of Petroleum Geologists Bulletin, v.42.

Jungslager, E.H.A., 1999 Petroleum habitat of the Atlantic margin of South Africa. In: Cameron, N.R; Bate, R.H; Clure, V.S; (Eds). The oil and gas habitat of South Atlantic. Geological Society of London. 153-168pp

Karlsen, D. A., Nyland, B., Flood, B., Ohm, S. E., Brekke, T., Olsen, S., Backer-Owe, K., 1995. Petroleum geochemistry of the Haltenbanken, Norwegian continental shelf. The Geochemistry of Reservoirs. Cubitt, J. M. and England, W. A., (eds.), Geol. Soc. Special Publication 86, 203–256pp.

Katz, B.J., 1994. An introductory overview. In: Katz, B.J. (Ed). Petroleum Source Rocks. Springer Verlag, New York. 327pp

Ketzer, J.M., 2002. Diagenesis and sequence stratigraphy: An Integrated Approach to constrain Evolution of Reservoir Quality in Sandstone. Dissertation for the Degree of Doctor of Philosophy in Mineral Chemistry, Petrology and Tectonics at the Department of Earth Sciences, Uppsala University. Sweden.

Ketzer, J.M., Holz, M., Morad, S., Al-Aasm, I.S., 2003a. Sequence stratigraphic distribution of diagenetic alterations in coal bearing, paralic sandstones: Evidence from the Rio Bonito Formation (early Permian), southern Brazil. Sedimentology, 50, 855-877.

Ketzer, J.M., Morad, S., Amorosi, A., 2003b. Predictive diagenetic clay mineral distribution in Siliciclastic rocks within a sequence stratigraphic framework. In: Clay Mineral Cements in Sandstones. R.H. Worden and S. Morad (Eds), Blackwell. Oxford, International Association of Sedimentologists, Special Publication, 34, 42-59.

Ketzer, J.M., Morad, S., Evans, R., Al-Aasm, I.S., 2002. Distribution of diagenetic alterations in fluvial, deltaic, and shallow marine sandstones within a sequence stratigraphic framework: Evidence from the Mullaghmore Formation (Carboniferous), NW Ireland. Journal of Sedimentary Research, 72, 760-774.

Klemme, H.D., Ulmishek, G.F., 1991. Effective Petroleum Source Rock of the World: Stratigraphic Distribution and Controlling Depositional Factors. AAPG Bulletin, v.75, 1809-1851.

Kosters, E.C., Suter, J.R., 1993. Facies relationships and the system tracts in the Late Holocene Mississippi Delta Plain. Journal of Sedimentary Petrology 63 (4), 727-733

Kosters, E.C., VanderZwaan, G.J., Jorrissen, F.J., 2000. Production, preservation and prediction of source-rock facies in deltaic settings. International Journal of Coal Geology, 43, 13-26.

Krumbein, W.C., Garrels, R.M, 1952. Origin and classification of chemical sediments in terms of Eh and oxidation-reduction potentials. Journal of Geology. 60, 1-33.

Kuhlmann, G., Adams, S., Campher, C., van der Spuy, D., di Primio, R., Horsfield, B., 2010. Passive Margin Evolution and its Controls On Natural Gas Leakage In the Southern Orange Basin, Blocks 3/4, Offshore South Africa. Marine and petroleum Geology. vol. 27, issue 4, 973-992.

Kvenvolden, K. A., Simoneit, B. R. T., 1990. Hydrothermally derived petroleum examples from Guaymas Basin, Gulf of California, and Escanaba Trough, northeast Pacific Ocean. AAPG Bulletin. Vol. 74. 223-237pp.

Larter, S. R., Aplin, A. C., 1995. Reservoir geochemistry: Methods, Applications and Opportunities. The Geochemistry of Reservoirs. Cubitt, J. M. and England, W. A., eds.), Geol. Soc. Special Publication 86, 5–32pp.

Lavelle, M., Fielding, C.R., Hall, M.A., Thomson, M.R.A., 2001. Molluscan stable isotope temperature estimates of the southwestern Ross Sea during early Oligocene and early Miocene, CRP-2/2A and CRP-3, Victoria Land Basin, Antarctica. Terra Antarctica 8, 439-444.

Light, M.P.R., Maslanyj, M.P., Greenwood, R.J., Banks, N.L., 1993. Seismic sequence stratigraphy and tectonic offshore Namibia. In: Williams, G.D; Dobbo, A. (Eds), Salt Tectonic and seismic sequence stratigraph. Geol.soc. London, 163-191pp

Loomis, J.L., Crossey, L.J., 1996. Diagenesis in a cyclic, regressive siliciclastic sequence: the Point Lookout Sandstone, San Juan Basin, Colorado. In: Crossey, L.J., Loucks, R., and Totten, M.W. (eds.), Siliciclastic diagenesis and fluid flow: concepts and applications, SEPM Society for Sedimentary Geology Special Publication, 55, 23-36.

Lopez, L., LO Monaco, S., Richardson, M., 1998. Use of molecular parameters and trace elements in oil-oil correlation studies, Barinas sub-basin, Venezuela. Organic Geochemistry. Vol. 29. No. 1-3. 613-629pp.

Loseth, H., Gading, M., Wensaas, L., 2009. Hydrocarbon leakages interpreted on Seismic data. Marine and Petroleum Geology, 26, 1304-1319.

Loutit, T.S., Hardenbol, J., Vail, P.R., 1988. Condensed sections: the key to age determination and correlation of continental margin sequences. In: C.K. Wilgus; B.S. Hasting; C.G.St.C. Kendall; H.W.Posamentier; C.A. Ross; J.C. van Wagoner (Eds), Sea-Level Changes: An Integrated Approach. Soc. Econ. Paleaontol. Mineral, 42. 183-213.

Macdonald, D., Gomez-Perez, I., Franzese, J., Spalletti, L., Lawver, L., Gahangan, L., Dalziel, I., Thomas, C., Trewin, N., Hole, M., Paton, D., 2003 Mesozoic break up of SW Gondwana: implications for regional hydrocarbon potential of southern South Atlantic Marine. Petroleum Geology 20, 287-308pp

Maslanyj, M.P., Light, M.P.R., Greenwood, R.J., Banks, N.L., 1982. Extension tectonic offshore Namibia and evidence of passive rifting in the South Atlantic. Marine and Petroleum Geology 9. 590-601.

McKay, J.L., Longstaffe, F.J., Plint, A.G., 1995. Early diagenesis and its relationship to depositional environment and relative sealevel fluctuations (Upper Cretaceous Marshybank Formation, Alberta and British Columbia). *Sedimentology*, 42, 161-190.

McKirdy, D.M., Kantsler, A.J., Emmett, J.K. and Aldridge, A.K., 1984. Hydrocarbon genesis and organic facies in Cambrian carbonates of the Eastern Officer Basin, South Australia. In: Palacas, J.G., (Editor), Petroleum Geochemistry and Source Rock Potential of Carbonate Rocks AAPG studies in Geology, no. 18, Tulsa, Oklahoma . 13–31pp

Meyers, P.A., Snowdon, L.R., 1993. Types and maturity of organic matter accumulated during Early Cretaceous subsidence of the Ex-mouth Plateau, Northwest Australia margin. AAPG studies in geology, 37. 119-130.

Milliman, J.D., Muller, J., 1977. Characteristics and genesis of shallow water and deep-water limestone. In: N.R. Anderson and A. Malahoff (Eds.), The Fate of Fossil Fuel CO_2 in the Oceans. Plenum Press, New York, pp. 655-672.

Mitchell, M.M., 1997. Identification of multiple detrital sources for Otway Supergroup sedimentary rocks: implications for basin models and chronostratigraphic correlation. Journal of earth Science, vol. 44, iss. 6, 743-750.

Mitchum, R.M., Vail, P.R., Thompson, S. 1977. Seismic stratigraphy and global changes of sea level, part 2: the depositional sequence as a basin unit for stratigraphic analysis. In C.E. Payton ed; Seismic stratigraphy- Application to Hydrocarbon Exploration; American Association of Petroleum Geologist*s*, memoir 26. p. 53-63.

Mitchum, R.M., van Wagoner, J.C., 1991. High frequency sequence and their stacking patterns-sequence stratigraphic evidence of high frequency eustatic cycle; sedimentary Geology, 70, p. 131-160.

Moldowan, J.M., Dahl, J., Huizngа, B.J., Fago, F.J., Hickey, L.J., Peakman, T.M., Taylor, D.W., 1994. The molecular fossil record of oleanane and its relation to angiosperms, science 256, 768-771

Morad, S., Al-Aasm, I.S., Ramseyer, K., Marfil, R., Aldahan, A.A., 1990. Diagenesis of carbonate cements in Permo-Triassic sandstones from the Iberian Range, Spain: evidence from chemical composition and stable isotopes. Sedimentary Geology 67, 281– 295.

Morad, S., De Ros, L.F., 1994. Geochemistry and diagenesis of stratabound calcite cement layers within the Ranoch Formation of the Brent Group, Murchison Field, North Viking Graben (northern North Sea). Sedimentary Geology, 93, 135-141.

Morad, S., Ketzer, J.M., De Rod, L.F., 2000. Spatial and temporal distribution of diagenetic alteration in Siliciclastic rocks: implications for mass transfer in sedimentary basins. Sedimentology, 47, 95-120.

Moraes, M.A.S., De Ros, L., 1989. Infilterated clays in fluvial Jurassic sandstones of Reconcavo Basin, Northeastern Brazil. Journal of Sedimentary Petrology 60 (6), 809-819.

Moraes, M.A.S., De Ros, L.F., 1992 Depositional infiltrated and authigenic clays in fluvial sandstones of the Jurassic Sergi Formation, Reconcavo Basin, north-eastern Brazil. In: Houseknecht, D.W; Pittman, D.E. (Eds), Origin, Diagenesis and Petrophysics of clay minerals in sandstones. Tulsa, OK, United States, SEPM, Society for Sedimentary Geology, vol. 47, 197-208.

Morse, J.W, Mackenzie, F.T., 1990. Geochemistry of Sedimentary Carbonates. Developments in Sedimentology, 48, Elsevier, New York, 707pp.

Moss, S.J., Tucker, M.E., 1995. Diagenesis of Barremian-Aptian platform carbonates (the Urgonian Limestone Formation of SE France): near-surface and shallow-burial diagenesis. Sedimentology, v. 42, pp. 853-874

Muntingh, J.K., Robson, S., Jungslanger, E., Paton, D.A., Strauss, P., 1991. Integration of borehole data with the regional seismic/sequence stratigraphic framework of the western offshore, South Africa. AAPG Bulletin, vol. 75. Issue 3.

Murray, A.P., Sosrowidjojo, I.M., Alexander, R., Kagi, R.I., Norgate, C.M., Summons, R.E., 1997. Oleananes in soils and sediments: evidence of marine influence during early diagenesis. Organic Geochemistry, 61, 1261-1276pp.

Odin, G.S., Matter, A., 1981. De glauconiarum origine. Sedimentology, In: Banerjee, S; Jeevankumar, S. and Eriksson, P.G. Mg-rich Ferric illite in marine trangressive and highstand system tracts: Example for Paleoproterozoic Semri Group, central India. Precambrian Research 162 (2008), 212-226.

Onuoha, K.M., 2000. Technology and the Challenges of Oil and Gas Exploration in the 21st Century. Nigerian Academy of Science. Lagos (Public lecture). 1-61pp

Ozcelik, O., Atunsoy, M., 2005. Organic Geochemical Characteristic of Miocene Bituminous unit of the Beypazari Basin, Central Anatolia, Turkey. The Arabian Journal for Science and Engineering. vol. 30. no 2A, 181-194pp

Pan, C., Zhang, M., Peng, D., Yu, L., Liu, J., Sheng, G., Fu, J., 2009. Confined Pyrolysis of Tertiary Lacustrine Source Rocks in the Western Qaidam Basin, Northwest China: Implications of Generative Potential and Oil Maturity Evaluation. Applied Geochemistry, doi: 10.1016/j.apgeochem.2009.11.013.

Parrish, J.T., Ziegler, A.M., Scotese, C.R., 1982. rainfall patterns and the distribution of coals and evaporates in the Mesozoic and Cenozoic. Paleogeography, Palaeclimatology, Palaeoecology, 40. 67-101.

PASA., 2003a. Exploration Opportunities in the Deepwater Orange Basin, off the West Coast of South Africa. Petroleum Agency of South Africa. www.petroleumagencysa.com

PASA., 2003b. Southern Orange Basin Exploration opportunities offshore South Africa's West Coast. Petroleum Agency of South Africa. www.petroleumagencysa.com

Pasley, M.A., Hazel, J.E., 1990. Use of organic petrology and graphic correlation of biostratigraphic data in sequence stratigraphic interpretations: example from Eocene-Oligocene boundary section. St Stephens Quarry, Alabama. Gulf Coast Association of Geological Societies Transaction, 40, 661-683.

Pasley, M.A., 1991. Organic matter variations in a deposition sequence: implication for use of source rock data in sequence stratigraphy. Bulletin of the American Association of Petroleum Geologist, 75, 650.

Pasley, M.A., Riley., G.W., Nummedal, D., 1993. Sequence stratigraphic significance of organic matter variations: example from the Upper Cretaceous Mancos shale of the San Juan Basin, New Mexico. In: Katz, B.J., Pratt, L.M., (Eds), Source Rocks in a Sequence Stratigraphic Framework, American Association of Petroleum Geologists, Studies in Geology, no 37, 221-242

Patch, J.A., Beard, J.H., Shafer, B.L., 1990. Sequence stratigraphy of the Plio- Pleistocene depositional facies in the offshore Louisiana South additions. Trans Gulf Coast Association Geological Society, p. 643-659.

Paton, D.A., di Primio, R., Kuhlmann, G., van der Spuy, D., Horsfield, B., 2007. Insights into the petroleum system evolution of the Southern Orange Basin South Africa. South African Journal of Geology; vol. 110; no 2-3; 261-274

Paton, D.A., ver der Spuy, D., di Primio, R., Horsfield, B., 2008 Tectonically induced adjustment of passive-margin accommodation space; influence on the hydrocarbon potential of the Orange Basin, South Africa. American Association of Petroleum Geologists Bulletin, v.92. No.5. 589-609.

Peters, K.E., 1986. Guidelines for evaluating petroleum source rock using programmed pyrolysis. American Association of Petroleum Geologists Bulletin 70, 318–329.

Peters, K. E., Moldowan, J. M., 1993. The Biomarker Guide: Interpreting Molecular Fossils in Petroleum and Ancient Sediments.--New Jersey: Prentice-Hall, 483-664pp.

Peters, K.E., Cassa, M.R., 1994. Applied source rock geochemistry. In: Magoon, L.B., Dow, W.G., (Eds). The Petroleum Systems from source to trap. The American Association of Petroleum Geologists. Memoir 60, 93-120.

Peters, K.E., Fraser, T.H., Amris, W., Rustanto, B., Hermanto, E., 1999. Geochemistry of crude oil from eastern Indonesia. American Association of Petroleum Geologists Bulletin, vol. 83. no. 12, 1927-1942.

Peters, K. E., Walters, C. C., Moldowan, J. M., 2004. The Biomarker Guide. Vol. 2: Biomarkers and Isotopes in Petroleum Exploration and Earth History. 2rd ed. – Cambridge.475-1155pp.

Petersen, H.I., Bojesen-Koefoed, J.A., Nytoft, H.P., Surlyk, F., Therkelsen, J., Therkelsen, J., Vosgerau, H., 1998. Relative sea level changes recorded by paralic liptinite-enriched coal facies cycle, middle Muslingebjerg Formation, Hochestetter Foreland, Northeast Greenland. International Journal of Coal Geology 36, 1-30.

Philp, R. P., Gilbert, T. D., 1986. Biomarkers distribution in Australian oils predominantly derived from terrigenous source materials. In: Leythacusor, D. and Rullkotter, J. (Eds), Advances in Organic Geochemistry, Pergamon Press, Oxford. 78–84pp.

Posamentier, H.W., Jervey, M.T., Vail, P.R., 1988. Eustatic control on clastic deposition 1-conceptual framework: In C.K. Wilgus; B.S. Hastings; C.G. St. C. Kendall; H.W. Posamentier; C.A. Ross and J.C. van Wagoner, eds. Sea level change. An approach*:* *SEPM* special publication, 42, p. 110-124.

Powell, T.G., 1988, Pristane/Phytane ratio as environmental indicator. Scientific Correspondence. Nature, vol. 33. 604pp

Primmer, T.J., Cade, C.A., Evans, J., Gluyas, J.G., Hopkins, M.S., Oxitoby, N.H., Smalley, P.C., Warren, E.A., Worden, R.H.,1997. Global patterns in sandstones diagenesis: their application to reservoir quality prediction for petroleum exploration. American Association of Petroleum Geologists Memoir 69, 61-77.

Purvis, K., 1995. Diagenesis of Lower Jurassic sandstones, Block 211/13 (Penguin Area, UK northern North Sea. Marine and Petroleun Geology 12, 219-228

Radke, M., Willsch, H., Welte, D.H., 1980a. Preparative hydrocarbon group type determination by automated medium pressure liquid chromatography. Analytical Chemistry, 52, 406-411.

Radke, M., Schaefer, R.G., Leythaeuser, D., 1980b. Composition of soluble organic matter in coals: relation to ranks and liptinite fluorescence. Geochimica et Cosmochimica Acta 44, 1787–1800

Radke, M., Welte, D. H., Willsch, H. 1986. Maturity parameters based on aromatic hydrocarbons: Influence of the organic matter type. Org. Geochem., 10, 51 – 63

Rao, C.P., Nelson, C.S., 1992. Oxygen and carbon isotope field for temperature shelf carbonates from Tasmania and New Zealand. Marine Geology**,** 103, 273-286.

Read, J.F., Horbury, A.D., 1993. Eustatic and tectonic controls on porosity evolution beneath sequence-bounding unconformities and parasequences disconformities on carbonate platforms. In: Horbury, A.D., and Robinson, A.G. (eds.), Diagenesis and basin development, American Association of Petroleum Geologists Studies in Geology #36, p. 155-197.

Reeves, C., de Wit, M., 2000. Making ends meet in Gondwana: retracing the transforms of the Indian Ocean and reconnecting continental shear zones. Terra Nova, 12, 272-280.

Reistroffer, J., 2001. PhD Dissertation submitted to Geology Department University South Carolina. http://srata.geol.sc.edu/index.html.

Rickwood, P.C., 1981. The largest crystals. American Mineralogist. vol. 66, 885-907.

Riva, A., Caccialanza, P. G., Quagliaroli, F., 1988. Recognition of 18[beta](H) oleanane in several crudes and Tertiary-upper Cretaceous sediments. Definition of new maturity parameters. Advances in Organic Geochemistry. L. Mattavelli, L. Novelli (eds.). Oxford: Pergamon Press, 671-675pp.

Rust, D.J., Summerfield, M.A. 1990. Isopach and borehole data as indicator of rifted margin evolution in southwestern Africa. Marine and Petroleum Geology. 7. 277-287.

Ryu, I., Niem, A.R., 1999. Sandstone diagenesis, reservoir potential, and sequence stratigraphy of the Eocene tyee Basin, Oregon, J. sed Res. 69, 384-393.

Ryu, I. 2008. Source rock characterization of petroleum systems of Eocene Tyee Basin, southern Oregon Coast Range, U.S.A. Organic Geochemistry 39: 75-90.

Sauer, R., Seifert, P., Wessely, G., 1982. Guidebook to excursions in the Vienna Basin and the adjacent Alpine-Carpathian thrust belt in Australia. Milleilungen der Osterrichischen Geologischen Gesel 85, 1-126.

Savin, S.M., Epstein, S., 1970. The oxygen isotopic compositions if coarse grained sedimentary rocks and minerals. Geochimica et Cosmochimica Acta 34, 323-329.

Schlumberger, 2005. Schlumberger Oil Field Glossary: Where the Oil Field Meets the Dictionary. URL: http://www.glossary.oilfield.slb.com.

Schmid, S., Worden, R.H., Fisher, Q.J., 2006. Carbon isotope stratigraphy using carbonate cements in the Triassic Sherwood Sandstone Group: Corrib Field, west of Ireland. Chemical Geology 225; 137– 155

Scholle, P.A., 1978. A Colour Illustrated Guide to Carbonate Rocks Constituents, Textures, Cement and Porosity. AAPG Memoir 27 Tulsa. 129-168.

Schulz, H.D., Zabel, M., 2000. Marine Geochemistry. Velarg, Berlin, Heidelberg. 455pp.

Seifert, W. K., Moldowan, J. M., 1978. Applications of steranes, terpanes, and monoaromatics to the maturation, migration, and source of crude oils. Geochim. Cosmochim.Acta.Vol.42,No.1.77-95pp.

Seifert, W. K., Moldowan, J. M., 1980. The effect of thermal stress on source rock quality as measured by hopane stereochemistry. Advances in Organic Geochemistry. A. G. Douglas, J. R. Maxwell (eds.).--Oxford: Pergamon Press, 229-237pp.

Seifert, W. K., Moldowan, J. M., 1986. Use of biological markers in petroleum exploration. Methods in Geochemistry and Geophysics. Vol. 24 / P. B. Johns (ed.). 261-290pp.

Seifert, W.K., Moldowan, J.M., 1981. Paleoreconstruction by Biological Markers, Geochemica et Cosmochimica Acta, 45, 783–794pp.

Seranne, M., Anka, Z., 2005. South Atlantic continental margins of Africa; A comparison of the tectonic vs. climate interplay on the evolution of equatorial West Africa and SW Africa margins. Journal of African Earth Sciences 43, 283-300pp.

Shikazono, N., Utada, M., 1997. Stable isotope geochemistry and diagenetic mineralization associated with Tono sandstone-type uranium deposit in Japan. Mineralium Deposita, 32, 596-606.

Sloss, L.L., 1963. Sequences in the cratonic interior of North America; Geological Society of America Buttetin, v. 74. p. 93-113.

Sloss, L.L., Krumbein, W.C., Dapples, E.C., 1949. Integrated facies analysis; Geological Society of America, Memoir 39. p. 91-124.

Small, J.S., Hamilton, D.L., Habesch, S., 1992. Experimental simulation of clay precipitation within reservoir sandstones, 1. Techniques and examples. J. Sediment. Petrol. 62, 520–529

Soekor, 1994a. Orange Basin. Report of South Africa Licensing Round Information Brochure, 18pp.

Soekor, 1994b. Outeniqua Basin. Report of South Africa Licensing Round Information Brochure, 52pp.

Sonibare, O. O., Ekweozor, C. M., 2001. Distribution of pentacyclic triterpanes and steranes in relation to the origin and thermal maturity of crudes from the Niger Delta, Nigeria. J. Mining Geol., 37, 37 – 43.

South, D.L., Talbot, M.R., 2000. The sequence stratigraphic framework of carbonate diagenesis within transgressive fan-delta deposits, Saint Llorenc Del Munt fan-delta complex, SE Ebro Basin, NE Spain. Sedimentary Geology, 183, 179-198

Storvol, V., Bjorlykke, K., Karlsen, D., Sagial, G., 2002. Porosity preservation in 357 reservoir sandstones due to grain coating illite: a study of the Jurassic Gam Formation from the Krsitin and Lavrans Fields, offshore Mid-Norway. Marine and Petroleum Geology 19, 767-781

Taylor, K.G., Gawthorpe, R.L., Curtis, C.D., Marshall, J.D., Awwiller, D.N., 2000. Carbonate cementation in a sequence stratigraphic framework: Upper Cretaceous sandstones, Book Cliffs, Utah-Colorado. Journal of Sedimentary Research, 70, 360-372.

Taylor, K.G., Gawthorpe, R.L., Van Wagoner, J.C., 1995. Stratigraphic control on laterally persistent cementation, Book Cliffs, Utah. Journal of Geological Society of London, 152, 225-228.

ten Haven, H.L., de Leeuw, J.W., Rullkötter, J., Sinnighe Damste, J.S., 1987. Restricted utility of the pristane/phytane ratio as a paleoenvironmental indicator. Nature 330, 641-643.

Tissot, B.P., Pelet, R., Ungerer, P.H., 1987. Thermal history of sedimentary basins, maturation indices, and kinetics of oil and gas generation. American Association of Petroleum Geologists Bulletin 71, 1445–1466.

Tissot, B.P., Welte, D.H., 1978. Petroleum Formation and Occurrence. Springer, New York.

Tissot, B.P., Welte, D.H., 1984. Petroleum Formation and Occurrence, second ed. Springer, New York. 699.

Tucker, M.E., 1993. Carbonate Diagenesis and Sequence Stratigraphy. Sedimentology Reviews **1,** pp. 51-72.

Tyson, P.D., 1986. Climatic Change and Variability in Southern Africa. Oxford University Press, New York.

Vail, P.R., 1987. Seismic stratigraphy using sequence stratigraphy, Part 1: Seismic stratigraphy interpretation procedure, in A.W. Bally, (ed); Atlas of seismic stratigraphy: American Association of Petroleum Geologists, studies in Geology 27, v. 1; p. 1-10.

Vail, P.R., Audemard, F., Bowman, S.A., Eisner, P.N., Perez-cruz, G., 1991. The stratigraphic signatures of tectonic, eustasy and sedimentology an overview. In G. Einsele, W.Ricken, and A. Seilader, eds, sequence stratigraphy of foreland basin deposit; American Association of Petroleum Geologists, memoir 64, p. 137-223.

Vail, P.R., Mitchum, R.M., Todd, R.G., Widmier, J.M., Thompson, S., Sangree, J.B., Bubb, J.N., Hatlied, W.G., 1977. Seismic stratigraphy and global changes in Sea level. Part 2. In seismic stratigraphy- Application to Hydrocarbon Exploration (ed. by C.E. Payton); American Association Petroleum Geologists, Tulsa, memoir 26, p. 49-62

Vail, P.R., Wornardt, W.W., 1990. Well log seismic sequence stratigraphy: An integrated tool for the 90's: Gulf coast section Society of Economic Paleontologists and Mining Foundation, Eleventh Annual Research program and extended abstract, p. 379-388.

Vail, P.R., Wornardt, W.W., 1991. An integrated approach to exploration and development in the 90's: Well log seismic sequence stratigraphy analysis, Gulf Coast Association of Geological Society Transaction, 41, p. 430-650.

van Aarssen, B. G K., Fishers, S.J., Bastow, T. P., 2004. Reconstructing the original composition of biodegraded oils using aromatic hydrocarbons. Abstract, Biodegradation in reservoirs. AAPGeologists Annual Meeting, 2004.

Van Der Spuy, D., 2003. Aptian source rocks in some South African Cretaceous basins. Geological Society of London Special Publications, v. 207. p. 185-202.

Van Wagoner, J.C., Mitchum, R.M., Posamentier, H.W., Vail, P.R., 1987. Seismic stratigraphy interpretation procedure using sequence stratigraphy, part II: Key definitions of sequence stratigraphy. In: Bally, A.W. (Eds), Atlas of Seismic Stratigraphy, I. Amer. Assoc. Petro. Geol. Stud. Geol; 27, 11-14.

Van Wagoner, J.C., Posamentier, H.W., Mitchum, R.M.JR., Vail, P.R., Sarg, J.F., Loutit, T.S., Hardenbol, J.C.1988. An overview of the fundamentals of sequence stratigraphy and key definitions, in C.K. Wilgus; B.S. Hastings; C.G. St. C. Kendell; H.W. Posamentier; C.A. Ross; and J.C. van Wagoner, eds; sea level change an integrated approach*; SEMP* special edition 42

Van Wagoner., Mitchum, R.M., Rahaman, V.D., 1990. Siliciclastic sequence stratigraphy in well logs core and outcrops; American Association of Petroleum Geologist, methods in exploration series, No 7, 55p.

Volkman, J.K., 1986. A review of sterol markers for marine and terrigenous organic matter. Organic Geochemistry 9, 83-99.

Volkman, J.K., Barrett, S.M., Blackburn, S.I., Mansour, M.P., Sikes, E.L., Gelin, F., 1998. Microalgal biomarkers: A review of recent research developments. Organic Geochemistry 29, 1163-1179.

Vu, T.T.A., Zink, K.-G., Mangelsdorf, K., Sykes, R., Wilkes, H., Horsfield, B., 2009. Changes in bulk properties and molecular compositions within New Zealand Coal Band solvent extracts from early diagenetic to catagenetic maturity levels. Organic Geochemistry 40, 963-977.

Walderhaug, O. 1994. Temperature of quartz cementation in Jurassic sandstones from the Norwegian continental shelf-evidence from fluid inclusions. Journal of Sedimentary Research, A64, pp. 311-323.

Walderhaug, O., Bjorkum, P.A**.,** 2003. The effect of stylolite spacing on quartz cementation in the Lower Jurassic Sto Formation, southern Barents Sea. Journal of sedimentary Research, 73, pp. 146-156.

Wanas, H.A., 2008. Calcite-cemented concretions in shallow marine and fluvial sandstones of the Birket Qarun Formation (Late Eocene), El-Faiyum depression, Egypt: Field, petrographic and geochemical studies: Implications for formation conditions. Sedimentary Geology. 40–48.

Wang, H.D., Philp, R.P., 1997. Geochemical study of potential source rocks and crude oil in the Anadorka Basin, Oklahoma. AAPG Bulletin, vol. 81. 249-275pp.

Wang, F.C., Walters., C.C., 2007. Pyrolysis comprehensive two-dimensional gas chromatography study of petroleum source rock. Analytical chemistry, vol. 79, no. 15, 5642-5650.

Waples, D. W., Machihara., T., 1991. Biomarkers for Geologists: A Pratical Guide to the Application of Steranes and Triterpanes in Petroleum Geology.--AAPG Methods inExploration,No.9,91pp.

Ward, J.D., Seely, M.K., Lancaster, N., 1983. On the antiquity of the Namabia. South Africa Journal of Science, 79. 175-183.

Wheeler, H.E., 1958. Time stratigraphy. AAPG Bulletin, vol. 42, 1047-1063.

Wilkinson, M., 1989. Discussion: Evidence for surface reaction controlled growth of carbonate concretions in shales. Sedimentology, 36, 951-953.

Wilson, M.W., Pittman, E.D., 1977. Authigenic clays sandstones recognition and influence on reservoir properties and paleoenvironmental analysis. Journal of Sedimentary Petrology 47 (1), 3-31.

Worden, R.H., Morad, S., 2003. Clay mineralisation in sandstone: Controls on formation, distribution and evolution. In: Worden, R.H., Morad, S. (Eds). Clay mineral cements in sandstones. International Association of Sedimentologists. Wiley-Blackwell, 3-42.

www.parks.tas.gov.au., 2003. Gondwana the great supercontinent. Geodiversity. Parks and Wildlife Services Tasmania. Department of Tourism, Parks heritage and the Arts.

Yancey, T.E., 1997. Depositional environments of Late Eocene lignite-bearing strata, east-central Texas. International Journal of Coal Geology, 34, 261-275

Zhang, J., Qin, L., Zhang, Z., 2008. Depositional facies, diagenesis and their impact on the reservoir of Silurian sandstones from Tazhong area in central Tarim Basin, western China. Journal of Asian Earth Sciences 33, 42-60.

Zuffa, G.G., Cibin, U., Di Giulio, A. 1995. Arenite petrography in sequence stratigraphy. The Journal of Geology, 103, 451-459